ADVANCED TECHNOLOGY LABORATORIES

DESIGN CRITERIA FOR ZERO LEAKAGE CONNECTORS FOR LAUNCH VEHICLES

FINAL REPORT FOR SECOND CONTRACT PERIOD

Fundamental Seal Interface Studies and Design and Testing of Tube and Duct Separable Connectors

EDITED BY
F.O. RATHBUN, JR.

Contract NAS 8-4012

JUNE 1, 1964

GENERAL ELECTRIC

FINAL REPORT FOR SECOND CONTRACT PERIOD

(March 1963 through December 1963)

DESIGN CRITERIA FOR ZERO LEAKAGE CONNECTORS FOR LAUNCH VEHICLES

Contract NAS 8-4012

FUNDAMENTAL SEAL INTERFACE STUDIES AND DESIGN AND TESTING OF TUBE AND DUCT SEPARABLE CONNECTORS

Edited by

F. O. Rathbun, Jr.

June 1, 1964

PREPARED FOR: Propulsion and Vehicle Engineering Division
George C. Marshall Space Flight Center
National Aeronautics and Space Administration
Huntsville, Alabama

PREPARED BY: Advanced Technology Laboratories
General Electric Company
Schenectady, New York

SPONSORED BY: Missile and Space Division
General Electric Company
Philadelphia, Pennsylvania

NASA TECHNICAL MANAGER: C. C. Wood (M-P&VE-PT)

CONTENTS

CONTENTS (CONT'D)

1. PROJECT SCOPE

by

F.O. Rathbun, Jr.

1.0 Introduction

The goals of this investigation are to gain additional understanding of the effect of gasket material properties and geometry on leakage flow and to "prove by testing" the validity of the design principles gained under the previous phase of this contract.

The first phase of this contract had as its goal "the establishment of fundamental design criteria that will provide for zero leakage in separable connectors used in launch vehicles." In the first investigation, the approach was taken to regard the separable connector as an interface between two surfaces, backed up by a supporting structure, designed to withstand a variety of environmental conditions.

The principle results from that investigation were:

1. Substantial plastic flow of at least one of the materials at the seal interface is necessary for zero leakage.

2. The plastic flow required for zero leakage can never be achieved in a conventional flared fitting with metal-to-metal contact, because the fitting will fail by hoop compression before the plastic stress range is reached at the seal interface.

3. To reduce the effect of flange rolling in the larger sizes of bolted flanged connectors, efficient lightweight designs can often be obtained by having the flanges in contact outside the bolt circle.

4. The many interacting factors in connector design can best be evaluated by building and testing connectors for specific applications.

The results of the first investigation have been published in six volumes, dated March 15, 1963:

Volume I	"Summary Conclusions and Design Examples," edited by T.P. Goodman, N63-18390, NASA-CR-50557.
Volume II	"Leakage Flow," edited by T.P. Goodman, N63-18493, NASA-CR-50558.
Volume III	"Sealing Action at the Seal Interface," edited by F.O. Rathbun, Jr., N63-18159, NASA-CR-50559.
Volume IV	"Design of Connectors," edited by S. Levy, N63-18494, NASA-CR-50560.
Volume V	"Pressure Energized Seals," edited by B.T. Fang, N63-18391, NASA-CR-50561.
Volume VI	"Environmental Effects," edited by S. Levy, N63-18323, NASA-CR-50562.

The present investigation has been divided into two parts:

1. A continuation of the experimental investigations begun during the first phase of the interface leakage phenomenon, and

2. the design, fabrication, assembly and testing of three different types of separable fluid connectors.

A Tentative Separable Connector Design Handbook has been written under this contract (separate volume).

1.1 Conclusions

The principal conclusions from this investigation are:

1. The cold-flow of plastic gaskets can be reduced to a negligible rate by the reduction of the gasket height to width ratio to the point where the sealing surface asperities effectively contain the plastic.

2. A solid soft metal O-ring, compressed between two sealing surfaces having semi-circular grooves provides an excellent low-load gasket system.

3. The analytic design procedure established for large flanged connectors was verified by test.

4. A tube connector which utilized knife edges and a soft metal replaceable gasket was tested and shown to be adequate at -300°F, 70°F, and 500°F (with an internal pressure of 1500 psi).

5. The use of soft metal crush washers with stainless steel MC fitting reduces the leakage rate considerably; however their use with aluminum MC fittings does not appreciably affect the leakage rate.

1.2 Project Tasks

The completion of the first phase investigations is taken as a starting point, for the second phase investigation reported here. The five tasks outlined for the second phase investigation were:

I. Continuation of experimental investigation of effect of gasket material properties and geometry on leakage flow. This task included continuation of experimental tests to determine the relationship among surface finish, sealing pressure, internal pressure, and leakage for promising gasket materials, including several commercially available materials used in-proof-of-principle testing. In addition to flat mating surfaces, some examples of other geometries such as flat surfaces vs. curved surfaces and flat surfaces vs. knife-edge surfaces were tested.

II. Design of improved connectors employing design criteria of first-year program.

A. Tube connectors for high-pressure gases (using various techniques for obtaining adequate sealing pressure without overstressing connector parts).

B. Flange connectors for low-temperature liquid-oxygen and liquid-hydrogen service (using various principles of pressure self-energizing and temperature compensation).

C. Flange connectors for high-temperature, high-pressure service.

III. Fabrication and assembly of improved connectors designed in Part II.

IV. "Proof-of-principle" testing of improved connectors designed in Part II. These tests were conducted in Schenectady under simulated service conditions. They duplicated the internal pressures and static loading conditions to which connectors are subjected in service. Preliminary testing was done at room temperature, using gasket materials whose room-temperature behavior simulates the high-temperature and low-temperature behavior of actual gasket materials. Additional testing was done at operating temperatures, using liquid nitrogen in place of liquid oxygen. The effect of shock and vibration on the connecter system was represented for leakage tests by static and low-cycle loading on the connector itself. These tests were primarily intended to measure leakage to determine the effectiveness of the connector designs. Stress and deflection measurements were also made to verify the intermediate steps in the design calculations.

V. Analysis of results and preparation of a Handbook of Proven Connector Design Principles

A. Analysis of results, including correlation of design calculations with test results and revision of design methods as required.

B. Publication of a Handbook of Proven Connector Design Principles

1.3 Organization of Report

The final report is organized into six sections, the first dealing with the project scope and general results, and the final five reporting on specific tasks as follows:

Section 2 is the detailed report of the interface leakage investigations conducted. Twenty-four experiments were conducted on commercially available gaskets, on gasket materials and on novel designs.

Section 3 covers the design, fabrication, assembly, and testing program for a four inch high temperature flanged connector designed for operation at 500°F and an internal pressure of 500 psi.

Section 4 explains a similar program for the design, fabrication, and testing of a twelve inch flanged connector for cryogenic service (-320°F). The two flanges were of 347 stainless steel and 2024 aluminum. Strain gage testing of this connector verified the correctness of the analytical procedure of flange design developed for this purpose.

Section 5 details the "proof by testing" program of a tube connector. The connector was designed for a one inch tube and is typical of connectors for tubing of one inch and smaller. The connector was designed for service at 3000 psi fluid pressure over the temperature range of -320°F to +500°F and with a transverse moment of 450 inch pounds.

Section 6 describes the experimental leakage tests conducted on MC fittings. Several one half inch, three quarter inch, and one inch stainless steel and aluminum MC fittings were leak tested. The effects of the flaring process, surface finish, external torque, internal pressure and fitting material were studied. The repeatability of leakage results, torque relaxation, use of crush washers, plating of fittings, and antifriction bearing surfaces for nuts were also considered. The tests were conducted at room temperature at a maximum internal pressure of 3000 psi.

1.4 "Proof-of-Principle" Testing Results

Presented below in tabular form are the experimental leakage results of tests accomplished on the three separable connectors designed and manufactured.

1.4.1 Four Inch High Temperature Connector

Gasket Type	Temperature (^{o}F)	Internal Pressure (psig)	External Applied Moment (in - lb)	Leakage (atm cc/sec)
Copper O-Ring	70	500	0	$< 1 \times 10^{-8}$
"	70	500	5000	$< 1 \times 10^{-8}$
"	500	500	0	$< 1 \times 10^{-8}$
"	500	500	5000	$< 1 \times 10^{-8}$
Flexitallic	70	100	0	5×10^{-3}
"	70	500	0	1.8×10^{-1}

1.4.2 Twelve Inch Cryogenic Connector

Gasket Type	Temperature (^{o}F)	Internal Pressure (psig)	External Applied Moment (in - lb)	Leakage (atm cc/sec)
Allpax 500	79	200	0	10^{-8}
"	79	200	48000	10^{-8}
"	-321	200	0	10^{-8}
"	-321	200	48000	10^{-2}
Lox grade Kel-F	79	200	0	10^{-6}
"	79	200	48000	10^{-6}
"	-321	200	48000	$> 10^{-2}$
Annealed Copper	86	200	0	10^{-8}
Shear O-Ring	86	200	48000	10^{-8}
"	-321	200	48000	10^{-6}

1.4.3 One Inch Threaded Connector
(Welded Knife Edge, Copper Gasket Design)

Temperature (^{o}F)	Pressure (psig)	Externally Applied Moment (in - lb)	Leakage atm cc/sec	Notes
70	1500	450	$< 9 \times 10^{-9}$	
500	1500	450	$< 2 \times 10^{-6}$	A
500	1500	500	8×10^{-5}	A
-300	1500	450	$< 6 \times 10^{-6}$	
70	1500	450	$< 1 \times 10^{-5}$	B
70	1500	450	$< 3 \times 10^{-6}$	C
70	1500	450	$< 9 \times 10^{-7}$	C
70	1500	450	3×10^{-4}	C
70	1500	450	$> 1 \times 10^{-7}$	C
70	1500	450	$< 3 \times 10^{-6}$	C
70	1500	450	$> 8 \times 10^{-3}$	C

A = Same copper gasket, same assembly

B = Time test for 72 hours

C = Same gasket in all tests, successive reassemblies

1.5 Plans for Third Contract Period

During the third contract period (January 1964 through December 1964), the following tasks will be undertaken.

Task A - Study of Interface Sealing Action

Task A-1 - Perform experimental work to learn more about the action of sealing and the assumptions that one may realistically make in setting up a mathematical model for predicting the leakage probability function. It is appreciated that to accurately include in the analysis all phenomena which do or could take place on both the microscopic as well as macroscopic scale would be impractical. Any analysis will, therefore, be an approximation and the purpose of this phase is to determine which phenomena must be accounted for and what assumptions may be made.

Task A-2 - A mathematical model will be developed consistent with results obtained from experiments outlined in paragraph A above from which one could estimate the probability of leakage exceeding a stated value with a given set of input parameters. The input parameters will include detailed dimensions, materials used, and their physical properties, surface finish characteristics, pressure on either side of the seal, etc. The parameters to be used in the model will consist solely of those that can be given as, or are determined by, engineering specifications.

Task A-3 - Experimental verification of the analytic work of paragraph A-2 will be conducted.

Task A-4 - A compilation will be made of parameters, which are determined by engineering specifications but are not given by them directly, needed to estimate leakage rate probability. For example, a machined surface may be specified as cylindrically ground with an 8 microinch RMS finish. This defines the surface but does not directly give information on the directional characteristics of the grinding, nor does it directly give information on the profile shape. As a second example, if a metal gasket material is specified by ASME or other standard designation we have indirectly, but not directly, specified its yield strength, work hardening coefficient, etc. A compilation of the numerical values of the parameters which are needed but specified only indirectly would be most useful to a designer.

Task B - Elastic seal. Most sealing to very low leakage levels is dependent on plastic flow of one of the sealing members and essentially all of the effort to date on this contract, NASA 8-4012, has been based on investigating seals where stresses beyond the yield point develop locally in the seal area. There is some evidence that suggests that with properly prepared surfaces elastic deflection alone is sufficient. Such a seal would have significant appeal where a connector must be opened and remade a number of times without deteriorating in performance.

Task B-1 - An investigation will be made into techniques for economically developing finishes which would be free of "channels" that cannot be sealed by elastic deformation. Presumably then a seal could be made with just elastic deformation and no permanent plastic flow. Representative samples will then be made and tested to establish attainable leak rates and their dependents on connector seal forces and fluid pressure.

Task B-2 - Assuming paragraph B above produces seals which are sufficiently low leak rate, basic designs of elastic seal connectors would be presented and rules for designing such connectors would also be presented.

2. SEAL INTERFACE EXPERIMENTAL STUDIES

by

F.O. Rathbun, Jr., and T.P. Goodman

2.0 Introduction

During the first phase of NASA Contract 8-1042, consideration was given to the problem of leakage through passages at the interface of a gasket-sealing system. Analytical and experimental studies were made involving leakage rates, material strength properties, sealing stresses, and surface finishes. Many experiments were performed involving a large number of gasket materials and sealing surfaces. The results of those investigations have been reported in Vol. III of the final report for the first contract period entitled "Sealing Action at the Seal Interface", edited by F. O. Rathbun, Jr., N63-1859, NASA-CR-500559.

The interface leakage investigations accomplished during the first contract period had as their goal the promotion of an understanding of the fundamentals involved in leakage flow. The relationship between the leakage rate existing in a sealing system and those measurable parameters describing the system was sought. So that the problem could be approached fundamentally, the scope of the investigations was limited to the study of systems employing flat annular gaskets. It was hypothesized that the parameters affecting the leakage rate were the strength properties of the structural and gasket materials, (namely yield strength, Y, and the strain hardening coefficient, n), the stress applied to the gasket, (σ), the pressure differential acting across the seal ($\triangle p$), and the surface finishes existing initially on the mating parts, (S.F.). An analytical relationship, validated by experimental evidence, such as

$$L = f(Y,\ n,\ \sigma,\ \triangle p,\ S.F.) \qquad (1)$$

would represent a successful completion to the investigation.

During the first contract period, empirical results were gained which related leakage to the material properties, the internal pressure, the sealing stresses, and the surface finishes, for those systems investigated. An analysis was accomplished which agreed qualitatively very well with some experimental results. However, while the results answered many questions about the sealing phenomenon, many questions were left unanswered and many new questions were posed.

The work reported herein, which is an extension of the first contract period effort, has been a continuation of experiments conceived to yield more information about the fundamentals of the interface problem. In particular, answers to the following questions were sought:

a) What is the required normal stress level for attainment of a low leakage rate level in systems employing no gaskets? What are the characteristics of such a system with regard to leakage rates versus normal stress for various sealing surfaces?

b) When a certain minimum stress level has been established for a given metal-to-metal seal (utilizing a given surface finish), how are the parameters changed when the system is re-used? Can a metal-to-metal seal be successfully re-used under the same design parameters?

c) Can the cold flow found in plastic gasket systems be reduced to the point where it no longer becomes a serious problem in a seal design?

d) Can basic geometries other than flat annular gaskets be used to reduce the sealing force required? Does the shear deformation phenomenon suggested in the final report for the first contract period work effectively when employed in a knife-edge or shear O-ring design?

Thus, the scope of experimental effort was enlarged over that of the previous work to include time dependence tests, tests involving direct contact of sealing surfaces, and tests with gaskets other than flat sealing surfaces and annular flat gaskets.

2.1 Conclusions

While the details of each experiment conducted are reported in Section 2., the major conclusions of significance are listed below:

1. The cold flow rate of flat Teflon gaskets can be reduced considerably by decreasing the gasket thickness so that it is of the same order of magnitude as the sealing surface asperities. In the same test, the gasket width to thickness ratio was, of course, increased. It was shown in three tests (thickness reduced in each successive test) that the cold flow rate could be reduced to a negligible rate.

2. Minimum sealing stress levels can be established for systems using no gaskets (metal-to-metal); but these systems do not necessarily respond in the same manner when reused.

3. The knife-edge sealing surface geometry, when utilized with a soft metal gasket, will seal at extremely low loads. A force of only 350 pounds per inch of periphery was required to seal a system containing an internal pressure of over 1100 psi.

4. A new gasket-sealing surface geometry, that of a solid soft metal O-ring compressed between two sealing surfaces having semi-circular grooves, shows promise as a design that will seal at low sealing loads. Loads as low as 600 pounds per inch of periphery have retained internal pressures up to 1100 psi.

5. The theoretical statistical analysis describing the leakage flow through an annular seal as a function of stress is reasonably accurate for the lower stress levels. While the theoretical curve of leakage vs. normally applied stress resembles in shape that found experimentally, the theoretical stress level at which leakage begins to decrease rapidly is much larger than that found in practice. Hence, the theoretical prediction is conservative.

6. In general, all sealing systems tested appear to have a definite laminar flow characteristic under high internal pressure. In nearly all cases, the leakage path apparently opens up during the increase in internal pressure and this phase of the experiment does not represent the behavior of a leak of constant size. Molecular flow characteristics are present under low internal pressure in many cases. While it is not possible to state in all cases the leakage rate at which the flow becomes laminar, it appears that the transition between molecular and viscous flow occurs around 10^{-6} atm cc/sec.

2.2 Experimental Procedure

During the first contract period the experimental procedure used in varying internal pressure and stress levels was as shown in Figure 2.1. Starting at one atmosphere pressure differential, the normal stress was increased until the leak rate fell off to approximately 10^{-8} atm cc/sec. Then the internal pressure was increased to an arbitrary peak of 1100 psi. At this time, the pressure differential was reduced to approximately 500 psi, and the stress was reduced incrementally until a large leak rate was produced.

FIGURE 2.1

Former Test Procedure

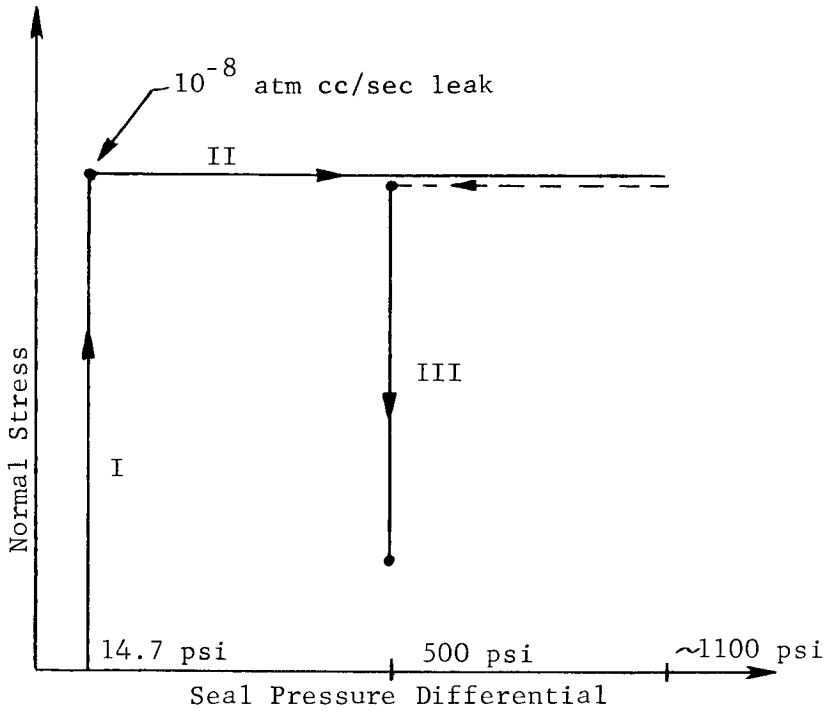

Wherever relationships among leakage rate, stress level, and internal pressure were sought during the second contract period, the test procedure shown in Figure 2.2 was used. In the modified procedure, four phases were used rather than three. At the completion of phase II, when the seal had been subjected to a high internal pressure, an increase in leakage above the rate existing at a one-atmosphere pressure differential was generally noted. Rather than the normal stress being reduced at this time (as was done previously), the normal stress was increased (phase III, Figure 2.2) until the leakage rate again was diminished to near-zero. The sensitivity to the removal of normal stress was then observed in phase IV. It has also been found possible, without any danger, to conduct the latter phase at higher internal pressures than were attempted previously. It must be noted that, with the new procedure, any post-experiment observation of the mated surfaces shows the degree of mating due to the stress level at the end of phase III. All tests were accomplished at room temperature.

FIGURE 2.2

New Test Procedure

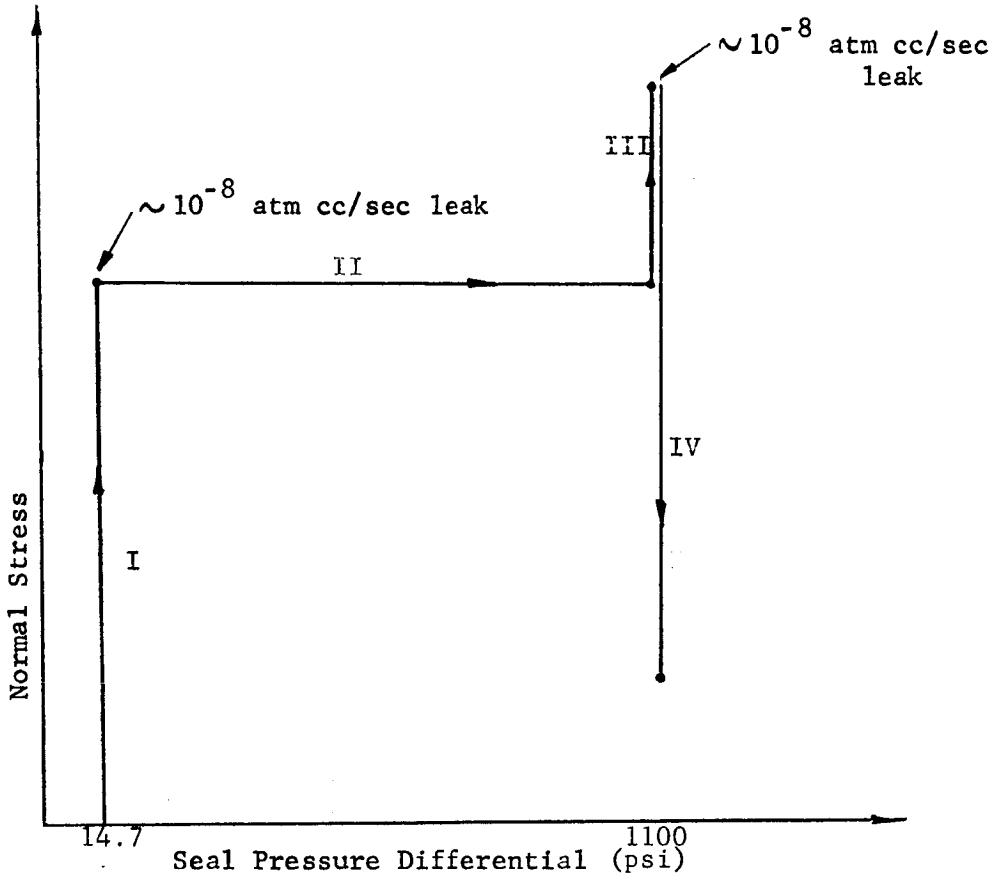

2.3 Scope of Experiments

The twenty-four separate experiments conducted are listed in Table 2.1. Shown are the sealing surface material used, the gasket material, the gasket dimensions, and the sealing surface finishes employed.

TABLE 2.1

LIST OF EXPERIMENTS CONDUCTED

Test	Sealing Surface Material	Gasket Material	Seal Width	Gasket Thickness	Sealing Surface Finish
1	aluminum	* Teflon TFE	0.125"	0.060"	Circumferentially machined, no lead, 50 micro-in. CLA
2	aluminum	* Teflon TFE		0.010"	"
3	aluminum	* Teflon TFE		0.005"	"
4	aluminum	* Indium		0.060"	"
5	stainless steel	none		n/a	Lapped, 6 micro-in. CLA
6	aluminum	none		n/a	Diamond burnished, 4 micro-in, CLA
7	stainless steel	none		n/a	Radially ground, 40 micro-in, CLA
8	stainless steel	none		n/a	Same specimens as in Test 7 reused.
9	aluminum	none		n/a	Circumferentially machined, no lead, 75 micro-in, CLA
10	aluminum	none		n/a	Same specimens as Test 9 reused.
11	aluminum	none		n/a	Same specimens as Test 10 reused.
12	aluminum	none		n/a	Same specimens as Test 11 reused.

*Time Test n/a - not applicable

TABLE 2.1 (Cont.)

LIST OF EXPERIMENTS CONDUCTED

Test	Sealing Surface Material	Gasket Material	Seal Width	Gasket Thickness	Sealing Surface Finish
13	stainless steel	aluminum	0.050"	0.050"	Knife-edge, 106° included angle.
14	stainless steel	aluminum	0.050"	0.050"	Same specimens as Test 13 reused.
15	stainless steel	combination spiral wound asbestos filler (Flexitallic)	0.19"	0.1305"	Circumferentially machined surface, 32 micro-in. CLA
16	stainless steel	asbestos, impregnated with Flouro-lube (Alpax)	.125"	0.070"	Same specimens as Test 15 reused.
17	stainless steel	Anaconda 372 copper	O-Ring D = .94 d = .062	n/a	Recessed semi-circular groove D = .94 d = .04
18	"	"	"	n/a	"
19	"	"	"	n/a	"
20	aluminum	Fluorogold	0.375"	0.060"	32 rms circumferential
21	aluminum	KEL-F	0.375"	0.064"	32 rms circumferential
22	aluminum	CG-12	0.375"	0.064"	32 rms circumferential
23	aluminum	none	0.125"	n/a	one-4 rms diamond burnished
24	aluminum	none	0.125"	n/a	Test 8 samples reused. n/a - not applicable

In brief, experiments 1 through 4 were designed to investigate the cold flow phenomenon and the sensitivity of the material flow to gasket thickness.

Experiments 5 through 12 employed systems with no gaskets, but rather the sealing surfaces mated together directly. Included in this series were several systems re-used for investigation of the reusability of the system.

Experiments 13 and 14 employed knife edge sealing surface geometries along with soft rectangular metal gaskets. Tests 15, 16, 20-22 allowed investigation of commercial gasket materials which were to be used in the testing of fabricated separable connectors (Sections 3 and 4).

In experiments 17 through 19, the shear O-ring concept was examined. Experiment 23, that of a radially ground surface finish mated with a diamond burnished finish, was conducted to provide experimental data with which to compare a previously accomplished analytical investigation (Ref. 1).

The final experiment, number 24, was done to investigate phase II of the experiment in detail, i.e., the leakage rate-pressure relationship for a given leak path.

2.4 Experimental Results

2.4.1 Gasket Cold Flow Tests (Experiments 1-4).

It had been shown in tests conducted during the first contract period that flat annular gaskets constructed from some plastics and some soft metals will creep under normal stresses at room temperature. This phenomenon has been given the name "cold flow" as opposed to the "creep" description. Such a phenomenon in a connector system causes severe problems of design. When the gasket flows, the sealing stress is reduced and the connector may leak. Hence, when a connector is constructed using gasket materials which "cold flow", the presence of this phenomenon must be accounted for in the design.

In order to determine how serious this problem is, four separate experiments have been conducted. Of the metal gaskets previously used, indium was again tested, with time as a variable in the leakage test. From the plastics previously tested, Teflon TFE (the plastic which exhibited the worst "cold flow" tendency) was retested with time as a variable under three different gasket geometries.

The procedure used for these experiments was to raise the normal sealing stress to the point where only permeation flow through the gasket existed (in the case of plastics) or when zero leakage was attained (in the case of indium). The internal pressure at this time was 500 psi. Immediately upon attaining the final leak rate, the normal stress was kept constant and the decrease in thickness of the gasket was recorded at 15-minute intervals for several hours.

2.4.1.1 Teflon TFE Tests (Experiments 1-3).

The test described above was conducted with Teflon TFE as the gasket material. The sealing surfaces used were 50 microinch rms machined surfaces (concentric circles, no spiral). The resultant rate of change of gasket thickness during the time which the normal stress was kept constant was extremely high during the first two hours. After that time, however, the rate was constant and equal to 0.23×10^{-3} in/hr. This is equivalent to a 12.6×10^{-3} in/in/hr strain rate.

In order to discern the important parameters which affect the cold-flow rate in a flat annular gasket, two more tests were conducted with all parameters being kept the same except gasket height. Where the first gasket was 0.06 inches thick, the second gasket was 0.01 inches thick initially and the third gasket was 0.005 inches thick initially. Hence, the ratio of gasket width to gasket thickness increased progressively and the rates of gasket thickness to sealing surface asperity height decreased. The results of the second test were very similar to the results of the first test. For the first three hours the rate of change of gasket thickness was extremely high. For the final three hours of the test the ratio appeared constant and of a magnitude of 0.332×10^{-4} in/hr. This is equivalent to a strain rate of 0.322×10^{-3} in/in/hr. Hence, the strain rate in the second case was approximately one-fourth the strain rate experienced in the first test. The results of the third test, where the very thin gasket was used, showed that the cold flow can be almost completely curtailed. During the first hour of the test a measurable strain rate was evidenced. Within the limits of the measuring techniques

available, the rate can be assured to be less than 10^{-6} in/hr. In all three of the tests the amount of total deformation of the gaskets was very small; and the total strain in the gaskets decreased with the initial gasket thickness.

2.4.1.2 Indium Test (Experiment 4).

Once the near zero-leakage level (10^{-8} atm cc/sec) had been attained in this test, no change in leakage was experienced throughout the time-variable portion. During the six hours during which the time test was conducted, the rate of change of thickness of the gasket reduced gradually but never became negligible. During the first 3 hours the rate of thickness change was quite high; between 3 and 6 hours the rate diminished. The initial thickness of the gasket was 0.06 inch with a load-supporting area of 0.431 in^2. The final thickness was 0.0133 inch with a final load-supporting area of 1.78 in^2.

It cannot be concluded from this test whether the cold flow could have been reduced to a negligible rate. However, at the termination of the experiment the ratio of gasket thickness to sealing-surface asperity height was still very high.

2.4.2 Metal-to-Metal Tests (Experiments 5-12).

In all earlier tests conducted involving flat annular gaskets between two flat sealing surfaces, there was a tendency for large shearing stresses to build up at the interface. Because of this, the mode of material flow in the gasket was similar to that described in the plane strain problem; (Ref. 1) shearing deformations along the interfaces were promoted, and increased sealing due to this deformation was effected. These phenomena were caused by the difference in yield strengths between the sealing surface materials and the gasket materials. In many cases the sealing surfaces appeared as infinitely stiff bodies when compared to the gasket material flow.

The metal-to-metal tests were conducted on raised flat surfaces as shown in Fig. 2.3. Shoulders were cut into the sealing surfaces, leaving an annular rise of 0.030 inch in height (on both the head and the body). The inside diameter of this rise was 0.9375 inch and the outside diameter was 1.125 inches. The diameters are the same as those used for gaskets tested in other parts of the investigations. Various surface finishes were machined, lapped, burnished, or ground onto the resultant flat tops of the rises. Hence, geometrically, the tests involving metal-to-metal systems are very similar to those using gaskets.

FIGURE 2.3

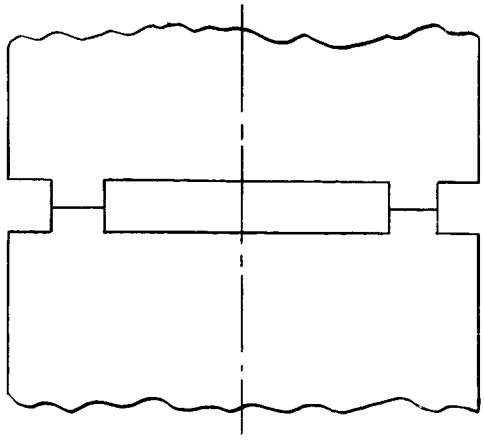

Metal-to-Metal Test Geometry

In the metal-to-metal cases, however, wherever a tendency for metal to deform radially existed on the upper sealing surface, the same tendency existed on the lower sealing surface due to the symmetry and the equal strength. Hence, the mode of flow did not involve high shear stresses nor shear deformations at the interface. Because of this, one would not expect the shear deformation nor any large degree of mating at the edges of the surfaces as was noted in tests using soft metal gaskets. The experimental results were in agreement with these expectations.

2.4.2.1 Lapped Surface Tests (Experiment 5).

The surfaces to be mated were hand lapped using normal shop procedure. This resulted in two very smooth surfaces (approximately 8 micro-inches rms), with isolated scratch marks randomly oriented. The lapping operation, however, caused a curvature at the edges of the surfaces to be mated. Hence, when the pieces initially were placed together they would first mate at the center and then gradually draw together toward the edges.

Post experiment inspection of the surfaces showed that the mating action between the original smooth faces caused large randomly distributed hills and valleys to be formed on each. These hills and valleys were of the order of 100 to 150 micro-inches in height and as wide as 0.3 inch. In order to seal this system to 10^{-8} atm cc/sec helium flow at an internal pressure of 1120 psi, it was necessary to impose a normal stress of 2.86 times the yield strength. As this stress was slowly removed, the seal proved to be moderately sensitive to relaxation of normal stress. At a normal stress of 1.69 times the yield strength, the leakage rate increased to approximately 10^{-5} atm cc/sec.

While the lapped surface is a very smooth surface, the individual randomly oriented scratches in the surface negate the usefulness of the smoothness. While 90-95% of the surface can be mated because of the smoothness, it is extremely difficult to fill the few random cracks which cause high leakage rates.

2.4.2.2 Diamond Burnished Surface (Experiment 6).

The surfaces to be mated were subjected to the diamond burnishing process. The edges of the sealing surfaces curved over to give a very small flat portion to the actual surfaces to be mated. The roughness in the circumferential direction was less than 1 microinch CLA. The only scratches evident in the surface were tangential and extremely small. A post-experiment inspection of the surfaces showed that they changed very little during the mating process. The scratches which were evident prior to the test were present after the test. The normal stress to cause sealing in this case, however, was much lower than in the case of the lapped surfaces. A stress of 0.84 times the yield strength was needed to seal the joint at 1130 psi (leakage 10^{-8} atm cc/sec). This system was quite insensitive to the removal of load; at a stress level of 0.221 times the yield strength, the leakage rate has risen to approximately 10^{-5} atm cc/sec. The significant difference, obviously, between the lapped surface seal and the diamond burnished surface seal is the difference in direction of the existing scratches. While a diamond burnished series was not retested, the relatively low sealing stress needed and the nearly complete maintenance of the original surface shows that it would have a rather high factor of reusability. The very different surface formation of the lapped joint after test shows that the reusability in that case would be poor.

2.4.2.3 Radially Ground Surfaces (Experiments 7, 8).

In order that an absolute maximum value of sealing stress be established for a metal-to-metal junction, without reference to a prescribed surface finish, a set of sealing surfaces were radially ground. While it is not likely that a sealing surfaces would be intentionally designed with asperities running in this direction, this sealing surface finish was deemed to represent the worst possible condition. The roughness in the tangential direction which is indicative of the asperities running in the potential leakage flow direction was approximately 34 microinches CLA. The surfaces were brought together in a leak test with the results shown in Figure 2.4. It will be noted that the leakage rate dropped radically at a normal stress approximately equal to twice the yield stress of the stainless steel. At a stress level of 2.3 times the yield strength, the leakage rate was less than 10^{-8} atm cc/sec with an internal pressure of 14.7 psi. As the internal pressure was increased to 1130 psi, the leakage rate increased to 6×10^{-4} atm cc/sec. However, by increasing the normal stress to 2.45 times the yield strength, the leakage rate was again reduced to approximately 10^{-8} atm cc/sec. Hence, an increment of stress equal to 0.15 times yield strength of the material was sufficient to cause sealing. This agrees well with the results published in Volume 3 of the final report for the first contract period (P31-5) which stated that this increment would be less than .25 times yield strength.

In order to check the reusability of such a metal-to-metal seal, the same surfaces were reassembled in a joint and leak tested once more. To insure that the pieces were mated in a different orientation, the top sealing surface was rotated 180° from its previous position. For the second test, the sealing surfaces did not resemble at all those used initially. In the first test the surface finish was made up of sharp peaks and valleys with a

FIGURE 2.4 (EXPERIMENT 7)
LEAKAGE TEST RESULTS -
RADIALLY GROUND SEALING
SURFACES, INITIAL USE

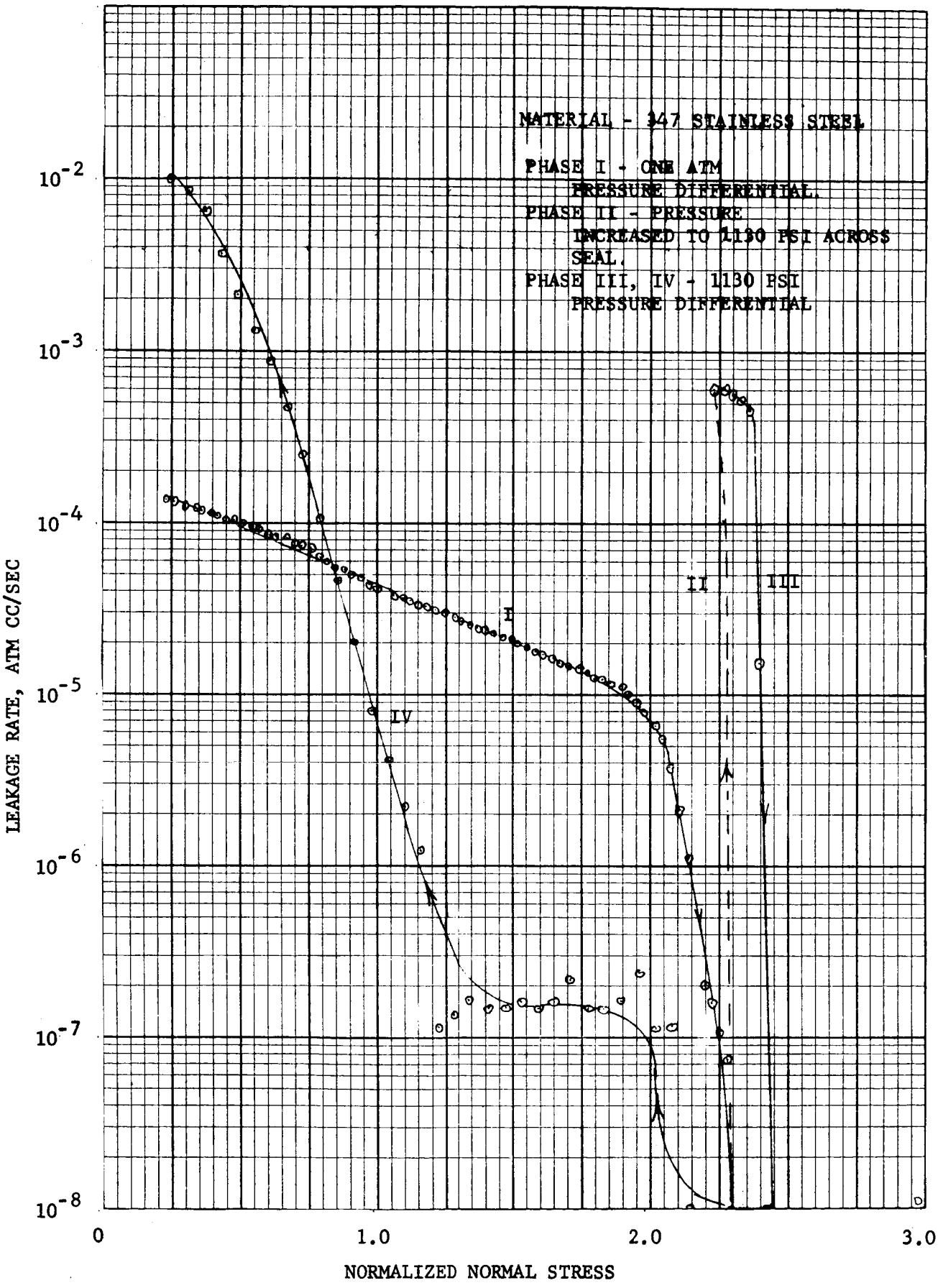

FIGURE 2.5 (EXPERIMENT 8)
LEAKAGE TEST RESULTS -
RADIALLY GROUND SEALING
SURFACES REUSED

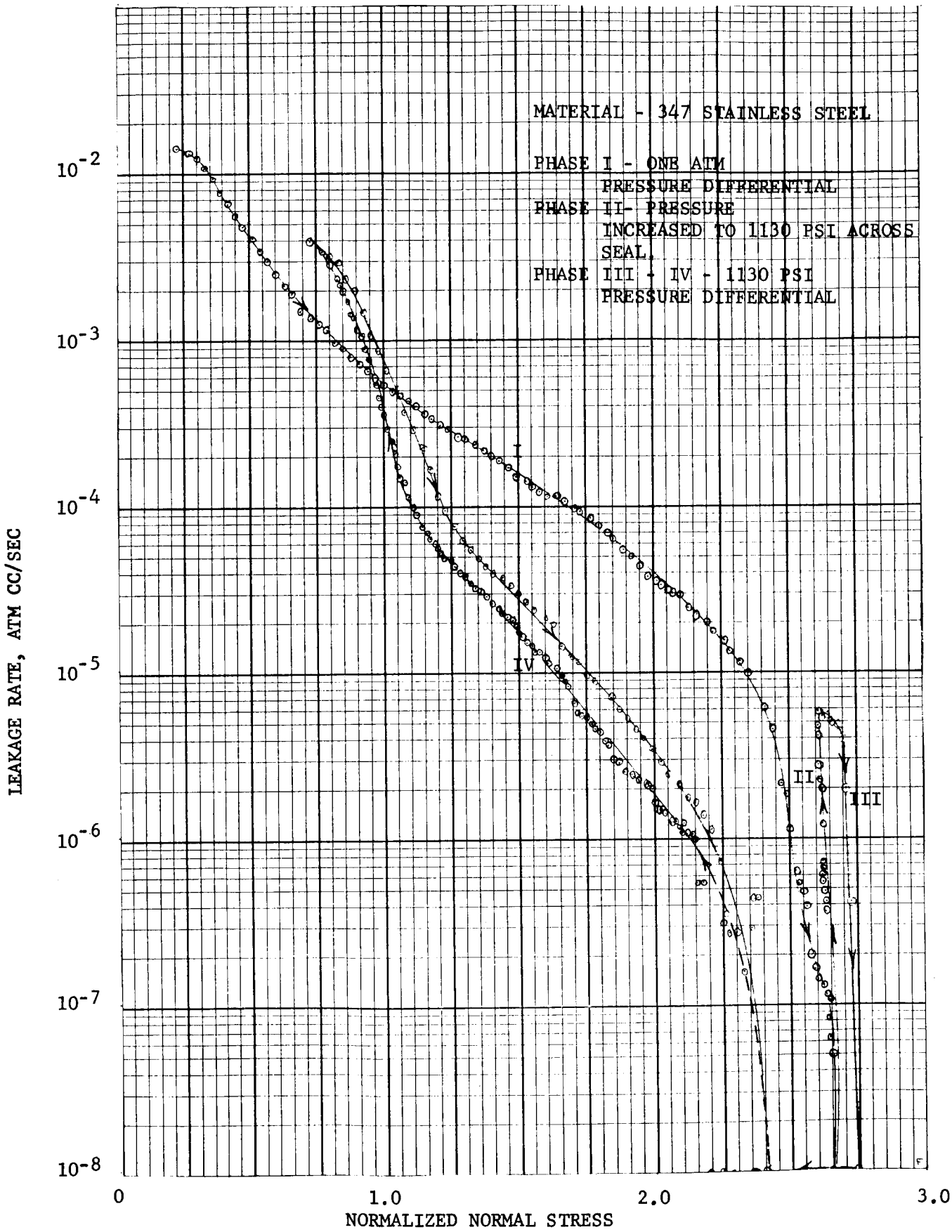

rather even distribution due to the grinding process; the surfaces after the first test showed higher peaks and deeper valleys and a lower frequency. This is indicative of gross yielding on the surface across areas as large as 0.02 inch on a side. Thus, for the second test, the original surface finish has little bearing on the results. The results of the second test shown in Figure 2.5 showed that sealing with a one atmosphere pressure differential occurred at 2.65 times yield strength; at an internal pressure of 1120 psi the sealing stress required was 2.75 times yield strength. The referenced yield strength is that which is attained in a normal tensile test.

In the first test the system showed a very low sensitivity to removal of load, the leakage being less than 10^{-6} atm cc/sec at a stress level of 1.15 times yield strength. On the second test the sensitivity to removal of load was much greater. The leakage had risen to 10^{-6} atm cc/sec at a stress level of 2.2 times yield strength. As a check on the reproducibility of the leakage-rate-vs-stress-level results for a given amount of surface deformation, the stress level was again raised to its peak value in the test shown in Figure 2.5. It can be noted that the leakage varies with the stress level in nearly the same manner during both the increasing and the decreasing of stress level.

From these tests it can be seen that local surface plastic deformation between individual asperities causes mating that is somewhat insensitive to removal of load. As the distance between asperities increases and the surface tends to be wavy rather than rough, the sensitivity to removal of load increases. As the surface becomes rather flat with a low relief roughness pattern, the mating becomes more difficult to accomplish, and is more sensitive to load removal. A conclusion which can be drawn from these tests is that <u>if valleys on the surface must be filled in order to promote sealing, then that same surface must have peaks from which this material can flow</u>.

2.4.2.4 Circumferentially Machined Surface Finish (Experiments 9-12).

If a seal were designed to take advantage of a particular surface roughness pattern, then that surface roughness pattern must have asperities running circumferentially with a high guarantee that there are no scratches or grooves in a radial (potential leakage flow) direction. In order to evaluate such a surface, the two sealing surfaces were machined circumferentially with no lead permitted. A tool with 115^{o} included angle was used; a pitch of 0.001 inch was employed. The resultant surface finish was a series of concentric wedges spaced 0.001 inch apart. Both surfaces were indentically produced. This combination of surfaces was tested four times in succession to check the reusability of such a system. The two pieces were brought together normally in each test; however, the locating device used did not insure that they were pressed absolutely concentrically. (nor would any seal in the field be assured of this.) During the first test the system sealed to a leakage rate of less than 10^{-8} atm cc/sec at a stress level of 0.7 times yield strength across a 1 atm pressure differential (Figure 2.6). When the pressure was increased to 1120 psi the seal failed and the leakage rate soared to 2×10^{-3} atm cc/sec. In order to acquire a zero leakage at 1120 psi, the final stress level necessary was 1.3 times yield strength. The seal proved quite insensitive to the removal of load, and the leakage rate was less than 10^{-6} atm cc/sec at a stress level of 0.4 times yield strength. Post experiment investigation of

FIGURE 2 - EXPERIMENT 9

LEAKAGE TEST RESULTS -
CIRCUMFERENTIALLY MACHINED
SEALING SURFACES - INITIAL USE

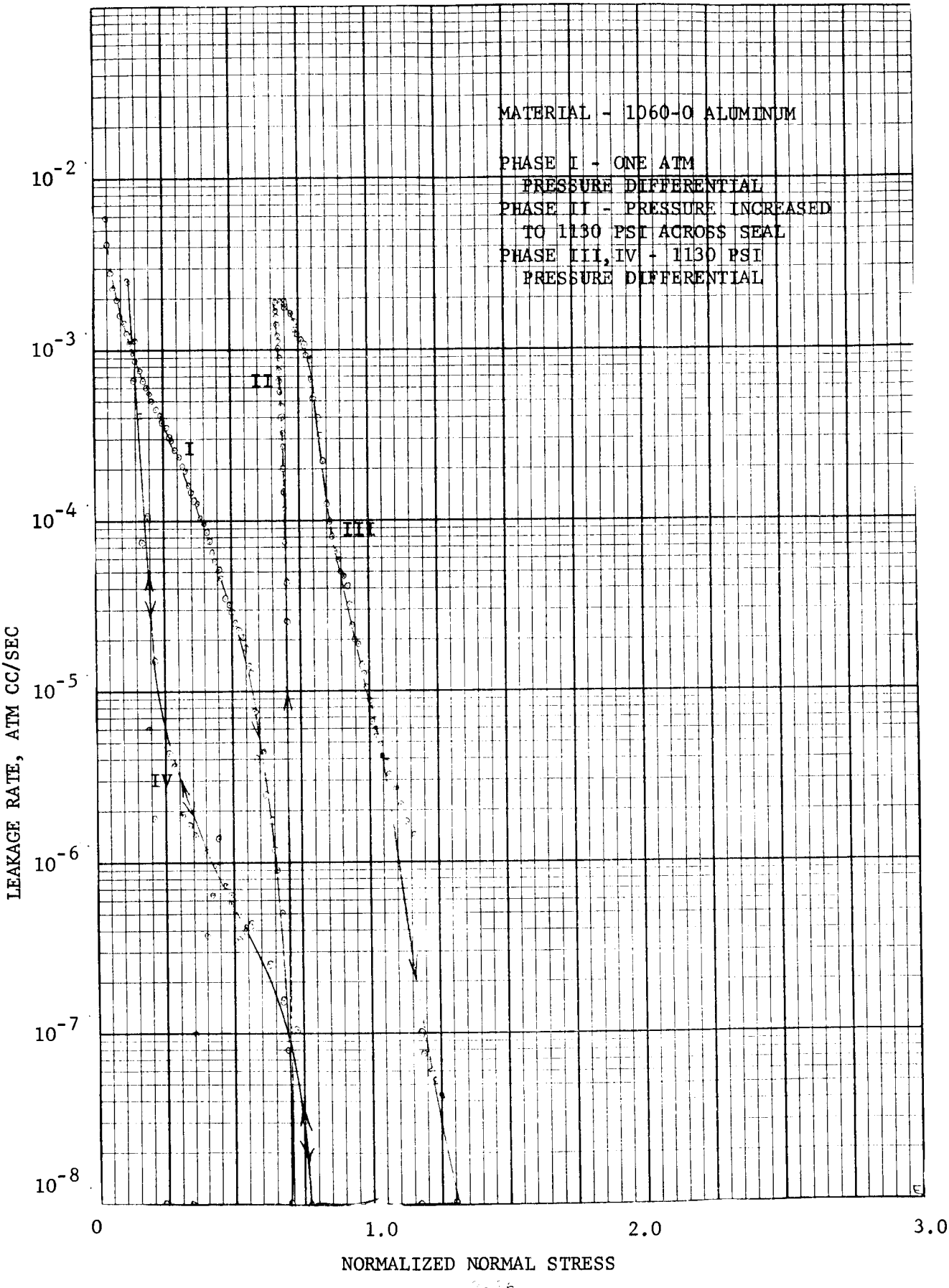

the surfaces showed very little damage evident. However, the results of the second, third, and fourth tests showed a much higher sealing stress necessary (above 2 times yield strength in each case). After each test the damage to the surfaces was not evident visually.

The conclusion from this series of tests is that the amount of damage locally on such a surface that is needed to change the sealing characteristics is very small. Also, the same sealing stress which can be used the first time the joint is tightened cannot be used thereafter, and a new criterion for sealing stress must be applied. It must be noted that in each test the two surfaces were brought together in a different orientation, i.e., the upper surface was rotated 180° after each test.

2.4.3 Knife-Edge Tests (Experiments 13, 14).

One of the important conclusions drawn from the experimental work accomplished during the first contract period was that the best mating between two surfaces occurred when the two surfaces had undergone shear deformation at the interface. (Ref.1) In order to utilize this principle in a gasket design, a soft gasket with a square cross-section was employed between two knife edges. The knife edges were quite stiff compared to the gasket material (347 SS knife edges, 1060-0 aluminum gasket). Two tests were accomplished. In the first test the load was allowed to be

FIGURE 2.7

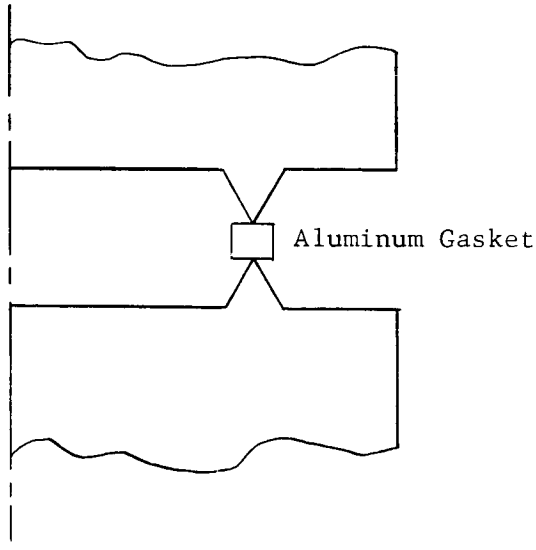

Knife-Edge Design

FIGURE 2.8 (EXPERIMENT 13)

LEAKAGE TEST RESULTS -
STAINLESS STEEL KNIFE EDGES,
SOFT ALUMINUM GASKET

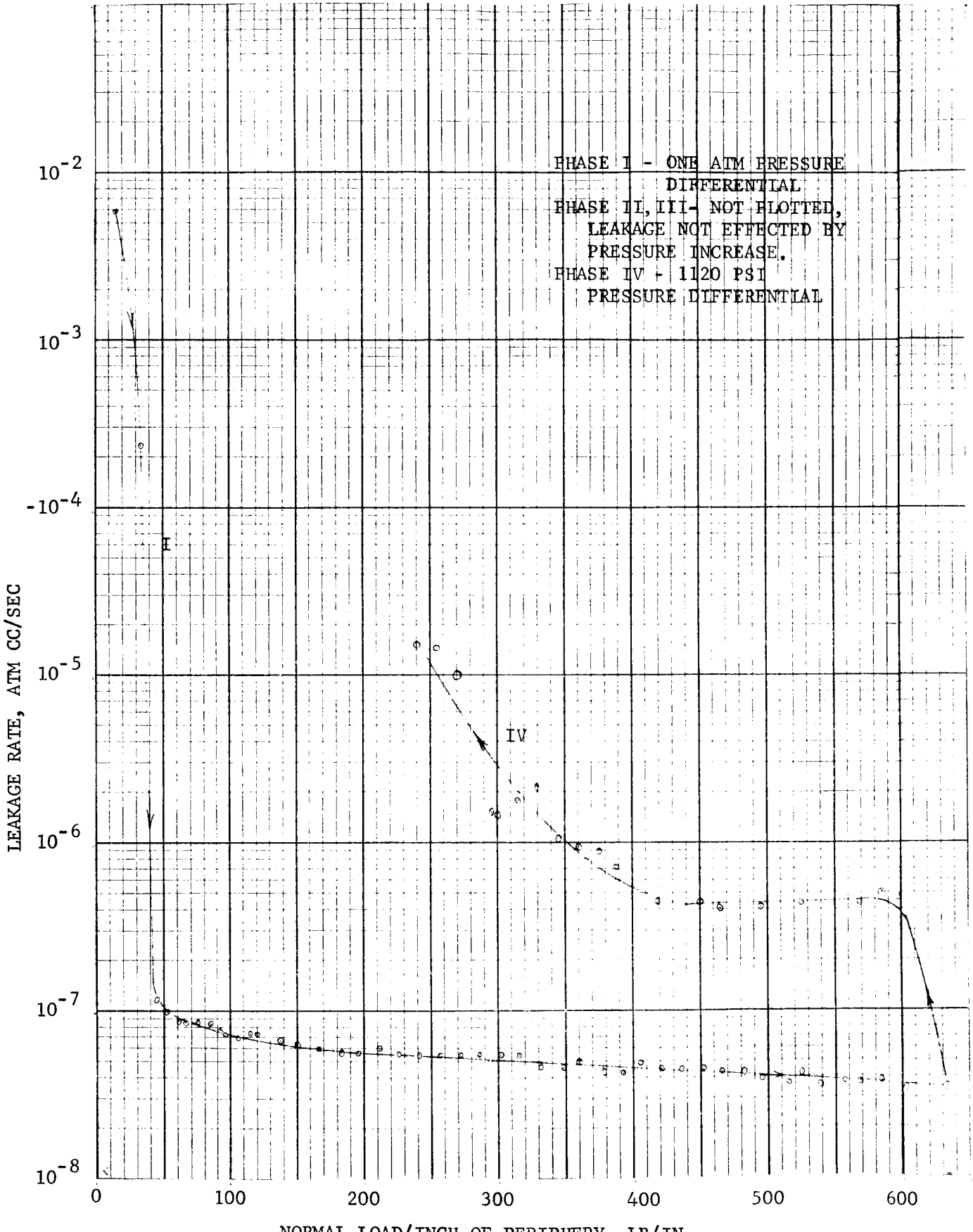

increased almost to the point where the gasket was cut in half. As opposed to earlier tests where the leakage rate decreased at some high value of stress, the results of this test showed that the leakage rate dropped to a very low value at an extremely low stress level, (Figure 2.8). Further increase in stress did not appreciably reduce the leakage rate. The second test was allowed to continue only to the point where the leakage rate initially dropped to approximately 10^{-8} atm cc/sec. The results of this test showed that in order to seal the system at an internal pressure of 1120 psi, a load of only 258 lb/linear inch of periphery was required. During the first test the load was decreased to check the sensitivity of load removal; the system proved extremely insensitive to load removal. During the second test the sealing load was so small compared to the internal pressure that no reduction was deemed advisable. Post-experiment inspection of the knife edges after each test showed that very little damage was done.

2.4.4 Tests of Flat Commercial Gaskets (Experiments 15, 16, 23-25).

To assist in connector design work that was accomplished under this contract, tests were made on five types of commercial gaskets. Each was a flat gasket compressed between two flat surfaces. The flat sealing surfaces were finished with a normal circumferential machining operation with approximately a 32 microinch finish. The gaskets employed were a combination spiral wound gasket, a Fluorolube impregnated asbestos gasket, a Fluorogold gasket, a KEL-F, and a CG-12 gasket.

2.4.4.1 Metal-Asbestos Spiral Would Gasket (Experiment 15).

The spiral wound gasket used was a gasket with an initial thickness of 0.13 inch, an inside diameter of .997 inch and an outside diameter of 1.382 inches. Only with a load exceeding 3000 pounds per inch of periphery was it possible to reduce the flow rate below 10^{-6} atm cc/sec. The gasket, compressed to a final thickness of 0.099 inch, proved to be moderately insensitive to the removal of load. A second test of this gasket showed that it does not have much flexibility. Upon removal of load it does not appreciably regain thickness even when the maximum load was less than the recommended load.

2.4.4.2 Fluorolube Impregnated Asbestos Gasket (Experiment 16).

A leakage test was accomplished on a Fluorolube-impregnated gasket of an inside diameter of 0.94 inch, an outside diameter of 1.18 inches, and thickness of 0.07 inch; it was impossible to attain a leakage rate less than 10^{-5} atm cc/sec even with a normally applied stress of 4310 psi for this gasket. An internal pressure of 1120 psi was used. It was noted after the test that a great deal of Fluorolube in the gasket had flowed from the gasket and had left a sticky liquid on the sealing surfaces. This liquid flowed in both directions inward and outward radially to a distance of about a gasket width.

2.4.4.3 Fluorogold Gasket (Experiment 20).

The fluorogold gasket was of a typical thickness, approximately 0.06 inch, but was much wider than previous gaskets, having an inside diameter of 0.75 inch and an outside diameter of 1.5 inch. The gasket was selected of these dimensions so that its width to thickness ratio would be the same as those to be used on the 12 inch flange tests (in that the purpose of the test was to gain data for later flange tests).

It was possible to lower the leakage rate in the fluorogold sealing system to 5.9×10^{-7} atm cc/sec with a normal stress of 6700 psi with an internal pressure of one atmosphere. When the internal pressure was increased to 1070 psi, the leakage rate immediately increased to 1.2×10^{-5} atm cc/sec. As the normal stress was further increased, it was essentially impossible to reduce the leakage further. At an ultimate normal stress of 9800 psi, the leakage rate remained 0.9×10^{-5} atm cc/sec. This gasket, did, however, prove to be very insensitive to the removal of load. As the stress was decreased, a leakage rate of 2×10^{-5} atm cc/sec was maintained down to a stress level of 3900 psi. Below that level the leakage rate increased rapidly.

2.4.4.4 Kel-F Gasket (Experiment 21).

It was possible to reduce the leakage in the Kel-F gasket system to 3×10^{-7} atm cc/sec with a stress level of only 2900 psi at internal pressure of one atmosphere. Comparing this with previous tests performed on Kel-F, the leakage rate approaches the diffusion rate. As the internal pressure was increased during this test to 1120 psi, the leakage rate rose to 1×10^{-5} atm cc/sec. However, as the stress was increased further, it was not possible to reduce the leak substantially, even at a stress level of 6800 psi. The leakage rate remained 4×10^{-6} atm cc/sec. Hence, it was impossible to produce as low a leakage as was found with one atmosphere internal pressure with an eighty atmosphere internal pressure, even when the stress level was allowed to increase by a factor of two. This is probably due to diffusion leakage through the gasket which is insensitive to stress level. As the stress was removed the leakage rate remained constant down to 3000 psi and then rose abruptly.

2.4.4.5 CG-12 Gasket Test (Experiment 22).

A CG-12 gasket of the dimensions specified in the above section was purchased from a registered vendor. This gasket cannot be cut from a flat stock material since it is an edged gasket having properties along the inside and outside diameters different from the bulk material.

It was possible to reduce the leakage to a rate of 1.5×10^{-6} atm cc/sec at a stress level of 3800 psi with a one atmosphere internal pressure. When the pressure was increased to 960 psi the leakage rate rose to 2×10^{-5} atm cc/sec.

When the stress level was gradually increased in an attempt to further reduce the leakage, it was found that reduction was impossible. The leakage rate increased slightly to 6×10^{-5} atm cc/sec at a stress level of 6500 psi. The reasons for this increase in leakage with increasing stress are not fully understood; however, since the gasket is not a homogeneous material throughout,

but a composite gasket, it is suspected that the increased stress effected either the bonding between the two gasket materials or detracted from the sealing properties of the edge materials.

The CG-12 gasket material proved quite insensitive to load removal, maintaining a 1×10^{-4} atm cc/sec leakage rate down to a 2400 psi stress level. Below that stress level, the leakage rate rose abruptly.

2.4.5 Shear O-Ring Design (Experiments 17-19).

The knife-edge design described in section 2.4.3 used the shear deformation concept for attaining a satisfactory mating between sealing surfaces. Another design which incorporates shear deformation of the gasket is that shown in Figure 2.9. A soft solid metal O-ring is compressed

FIGURE 2.9

O-Ring Shear Design

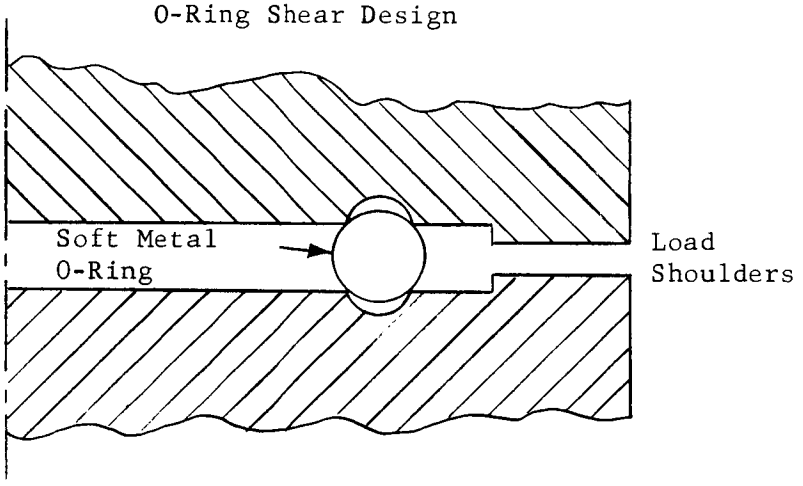

between two flat sealing surfaces, each having a semi-circular shaped groove to receive the O-ring. The annular groove, which has the same annular diameter as the O-ring, has a groove radius less than that of the O-ring. Hence, the compression will require that the tips of the grooves cut into the O-ring, deforming it as shown in Figure 2.10.

FIGURE 2.10

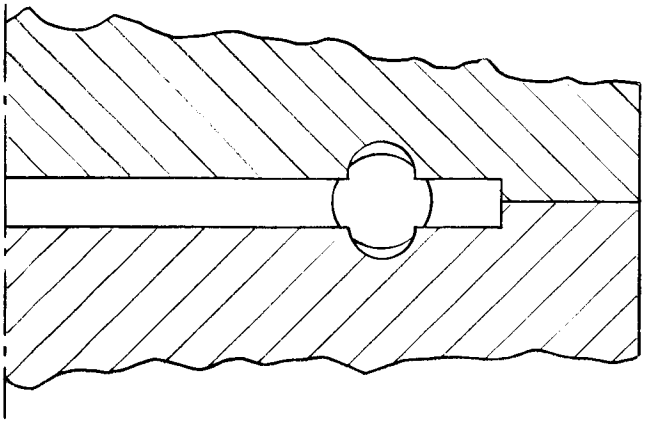

Gasket Deformation

Most of the resultant area of contact between the gasket and the sealing surfaces should be the result of shear deformation. The presence of the shoulders provides definite limitations to the amount of deformation which can be put into the gasket and, in a connector design, could disassociate the sealing path from the loading path, and thus producing parallel paths for the sealing load and a structural compressive load. It is to be noted that the load per peripheral inch is a more meaningful parameter than stress in this configuration since the area of contact and direction of stress is not known.

Three such tests were accomplished, each with an annealed copper O-ring. In the first test, the O-ring proved to be slightly eccentrically located. The sealing phenomenon did not occur until a normal load of 800 pounds per inch of circumference was applied (across one atmosphere pressure differential). However, this load was sufficient to keep the leak less than 10^{-8} atm cc/sec even at 1120 psi across the seal. The second and third tests proved more encouraging. While the first test gasket did not deform under the 800 pounds per inch to the shape shown in Figure 2.10, the later tests involved much higher loads such that the shoulder nearly seated. In the second test, a 10^{-8} atm cc/sec leak (across one atmosphere pressure differential) was attained at a load of 300 lb/in. The load was increased to 2400 lb/in to provide the gross deformation required. As a result, the increase in internal pressure to 1130 psi did not cause any increase in leakage. As the load was removed (with 1130 psi across the seal) the seal was maintained until the load dropped to 1000 lb/in. The third test, accomplished with a gasket annealed for the second time, was even more promising. The results are shown in Figure 2.11. The behavior was similar to that of the second test, but it was even less sensitive to removal of load. In both tests, the load-deflection curve showed an increasing stiffness under increasing load.

It can be concluded from these tests, that:

a) the design employs shear deformation to good advantage

b) the system is quite insensitive to removal of load,

It can also be seen that the gasket, (when deformed) provided some radial restraint to relative motion, which is a positive attribute to a design, and also that the sealing surface shearing edges are inherently protected due to the low relief designs, as compared with knife edges which are high relief edges.

Comparing the knife edge to the shear O-ring, the knife edge allows a slightly lower required stress level to seal. The O-ring has inherently protected edges, as opposed to the knife edge. The O-ring is more dependent on proper location than the knife edge. Both are quite insensitive to load removal.

2.4.6 Metal-to-Metal Sealing System Tests (Experiments 23,24).

Two other metal-to-metal tests were accomplished; both the head and body of the test apparatus were machined to leave 0.030" annular rises. The inside diameter of these annular rises was 0.9375" and the outside diameters were 1.1875".

2.4.6.1 Radially Ground and Diamond Burnished Surfaces (Experiment 23).

In an attempt to understand leak rates and be able to predict them, an analysis, given in Section 33 of the final report for the first contract period, was prepared predicting leakage as a function of the sealing load and the surface roughness profile normal to the direction of leakage flow. To check the analysis, experiments were designed to give a purer relationship to the mathematical model than is normally found in practical seal systems. These utilized either radially ground surfaces or diamond burnished surfaces and gave better correlation of experiment and analysis than did more usual machining methods where the direction of surface roughness is primarily at right angles to the direction assumed by the simplified analysis. It would be desirable to eventually perform a more sophisticated analysis wherein the surface finish is described not by one RMS finish number, but by its total characteristics including orientation in the seal. But before attempting a more complex analysis, it was deemed desirable to check the simpler mathematical model experimentally.

In previous tests with two radially ground surfaces it was noted that the lay of the grinding marks were not parallel and the presumed test conditions were not actually satisfied. To avoid this problem a test was devised utilizing a radially ground surface mated with a diamond burnished surface. The results of this test and a comparison with the analytic predictions are discussed in Section 2.5.

2.4.6.2 Radially Ground and Diamond Burnished Surfaces Reused (Experiment 24).

The same specimens in the Section 2.4.6.1 were again used in a leakage test for the purpose of gaining an insight into the type leakage flow evidenced during Phase II of the experiment. During this experiment no effort was made in recording data during the other phases. However, the increments of internal pressure at which leakage rates were recorded were extremely small, thus allowing a better curve of leakage flow vs. internal pressure to be made than was previously possible. The results of this experiment are discussed in Section 2.6.

FIGURE 2 11 (EXPERIMENT 17)
LEAKAGE TEST RESULTS -
SOFT COPPER O-RING WITH
SEMI-CIRCULAR GROOVES IN SEALING SURFACES

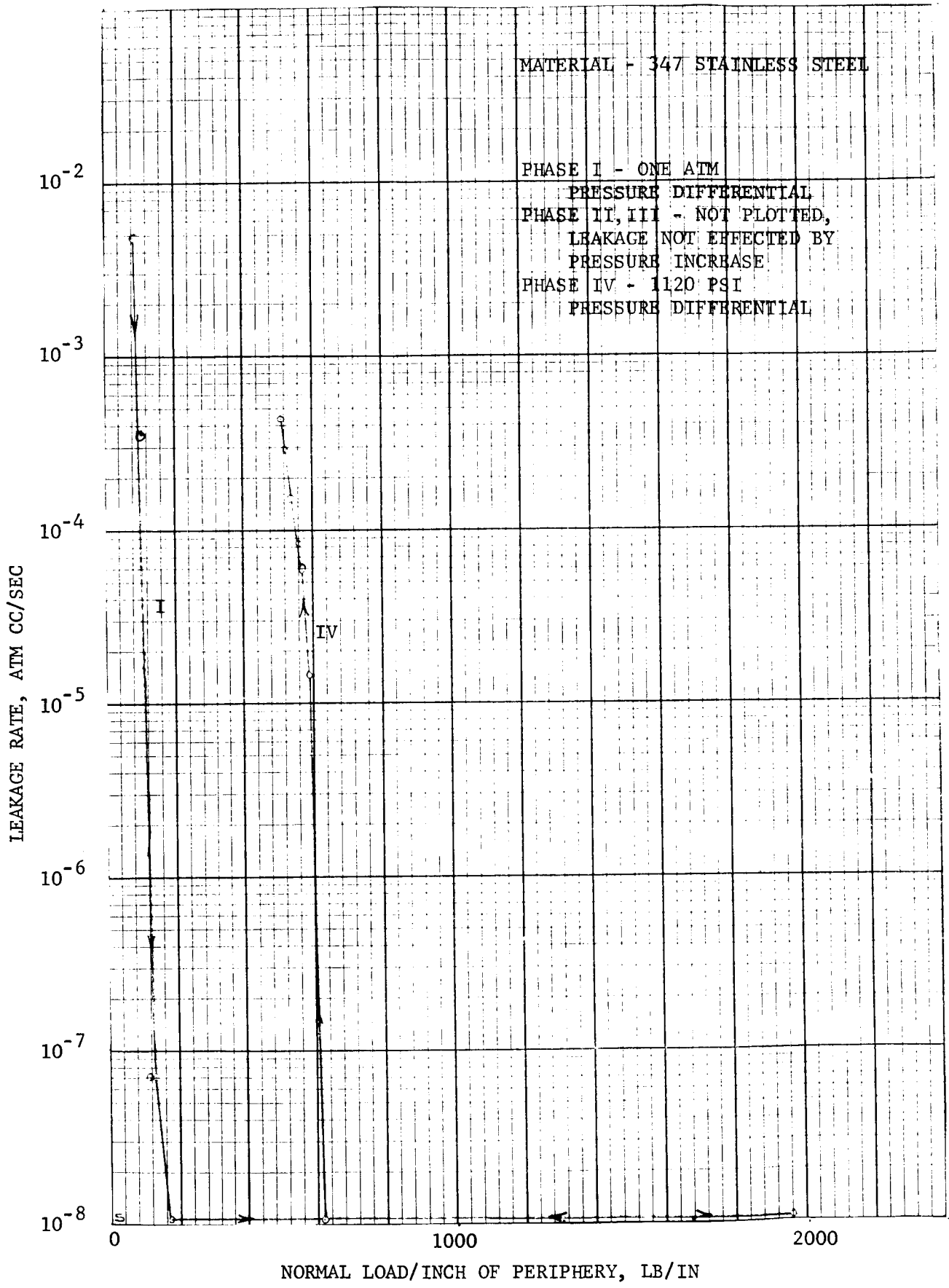

2.5 Comparison of Experimental Results with Theoretical Analysis

2.5.1 Summary and Background

To provide a direct comparison between calculated and measured leakage flow as a function of sealing pressure, a leakage test was run with a radially ground aluminum sealing surface mating with a diamond burnished aluminum sealing surface. The results of the test are compared graphically with calculated results in Fig. 2.12. This comparison indicates that the calculations assuming no strain hardening, give a conservative estimate of the leakage to be expected at a given sealing stress level.

Our investigation of the sealing action at the seal interface, reported in Volume 3 of Ref. 1, was both analytical and experimental. Because of the many assumptions on which the analysis had to be based, greater reliance was placed on the experimental results. However, the analytical investigation provided additional insight into the mechanism by which the sealing action takes place.

It is of interest, of course, to compare the analytical and experimental results. The experimental results reported in Section 36 of Ref. 1 did not provide a direct comparison, because the metallic gasket surfaces were all circumferentially machined. Their surface roughness profiles in the direction of flow were known from profilometer traces and from interference photomicrographs, but their surface roughness profiles across the direction of flow (along the crests of the circumferential peaks) were unknown. The analysis of Section 33 of Ref. 1 was for seal interfaces whose surface roughness profiles across the direction of flow were known statistically, but whose surface roughness profiles in the direction of flow were only slowly varying (see page 33-5 of Ref. 1). As indicated in Section 36 of Ref. 1 and in Section 11.2 of Quarterly Report No. 2, that analysis could be extended to wavy (e.g., circumferentially machined) surfaces, but it is still desirable to have an experimental result that could be directly compared with the basic analysis of Section 33 of Ref. 1.

An indirect comparison between the analytical and experimental results was made in Section 37.1.8 of Ref. 1. There it was pointed out that the shapes of most of the experimental leakage curves, Figs. 36.6 through 36.9, are in general agreement with the calculated curve of Fig. 33.9 for <u>zero strain hardening</u>. However, the experimental curves show that the stress required for complete sealing is less than the three times the yield stress predicted by the calculations. This suggests that the mutual interaction of asperities, which is beneficial for sealing, more than offsets the adverse effect of strain hardening.

Another point of comparison between calculated and experimental curves is the inflection point of each curve, which occurs when the stress is about half of the final stress needed for complete sealing. The ordinate of the inflection point may be stated in terms of either flow or effective passage height. In Section 37.1.8 of Ref. 1, the ordinate of the inflection point

was stated given in terms of the effective passage height, and it turned out that for circumferentially machined surfaces mating with other circumferentially machined surfaces, the rms surface roughness across the direction of flow, as calculated from the inflection points of the curves of flow vs. stress, is between 3% and 10% of the measured rms surface roughness in the direction of flow. This result is plausible, but it would be preferable to have a direct comparison with surface finishes measured in the same direction.

A check was made of the radial ground vs. radial ground metal-to-metal leakage described in Section 2.4.2.3. For this test, the experimentally measured flow was far below the calculated flow for the measured rms surface roughness of the two mating surfaces. However, photomicrographs taken after the tests showed that the radial grooves in the two surfaces, instead of being parallel, intersected at an angle of approximately 30^{o}. Thus, the mating action was similar to that of a radially ground surface mating with a circumferentially machined surface. As pointed out on page 37-17 of Ref. 1, that case also produced localized mating action which gave far better sealing than the calculations predicted.

To provide a more direct comparison with calculated results, it was decided to run a test with one mating surface radially ground and the other mating surface as nearly flat as practicable, namely diamond burnished. This test is described in Section 2.4.7.

2.5.2 Equivalent Passage Height for Molecular Diffusion Flow

The calculations of equivalent passage height in Section 33 of Ref. 1 and the comparisons between measured and calculated passage height given in Section 37.1.8 of Ref. 1 were for laminar flow through the leakage path. The assumption of laminar flow is probably correct at the beginning of the sealing process, when low sealing stresses are applied; however, as the equivalent passage height becomes smaller, the laminar flow changes to molecular diffusion flow, as shown by the calculations of Section 22 of Ref. 1. For any given passage height, the flow rate calculated by assuming pure molecular diffusion is greater than the flow rate calculated by assuming pure laminar flow. For most of the range of equivalent passage heights that is of interest for the sealing phenomenon, the flow is in a transition between laminar and molecular flow. It would be difficult to calculate the actual flow in this range, since it would be necessary to sum up the flows through the different sizes of passages that are averaged to give the equivalent passage height. However, it is relatively simple to calculate the flow for two cases that bracket all possible flows: the case of pure viscous flow, treated in Section 33 of Ref. 1; and the case of pure molecular diffusion flow, treated in the next paragraph.

Whereas the effective passage height for laminar flow, h_e, is found by taking the cube root of the weighted average of the cubes of all the different possible passage heights between the two interfaces, the equivalent passage height for molecular diffusion flow, h_d, is found by taking the square root of the weighted average of the squares of all the passage heights. This difference arises because the flow rate in viscous flow is proportional to the cube of the passage height, while the flow rate in molecular diffusion flow is proportional to the square of the passage height, as shown in Section

22 of Ref. 1. Thus, corresponding to Equation (3) on page 33-8 of Ref. 1, we may write the following equation for h_d:

$$h_d^2 = \int_o^\infty h^2 \, p(h) \, dh$$

$$= 1/2 \, (s^2 + h_r^2) \left[1 + \text{erf} \, (s/\sqrt{2} \, h_r)\right]$$

$$+ (sh_r/\sqrt{2\pi}) \, \exp \, (-s^2/2h_r^2)$$

Equations (1) and (2) on the same page hold for both viscous flow and molecular diffusion flow.

Corresponding to Fig. 33.9 of Ref. 1, which applies for viscous flow, the curves of Fig. 2.13 have been plotted for molecular diffusion flow. It will be noted that the shapes of the two sets of curves are quite similar, although the ordinates differ in the middle range of stresses.

2.5.3 Comparison Between Calculated and Experimental Results

To provide experimental leakage-flow-vs.-stress data matching as nearly as possible the conditions for which the calculations of Section 33 of Ref. 1 were made, Test 24 was performed. In this test, two aluminum sealing surfaces were used without a gasket. One surface was radially ground, with an rms surface finish of approximately 45 microinches, measured across the direction of flow. The other surface was diamond burnished, with an rms surface finish in the direction of flow of approximately 5 microinches, and an rms surface finish across the direction of flow that was even smoother. Thus the rms surface finish of the two surfaces in combination was approximately h_r = 45 microinches, although the slight waviness of the diamond-burnished surface in the direction of flow is expected to act to reduce the actual flow as compared to the predicted value (see Section 33.6 of Ref. 1).

The test setup was as shown in Fig. 35.4 of Ref. 1, with helium at atmospheric pressure inside the joint and a vacuum outside. The measured flow is plotted as a function of sealing stress in Fig. 2.12.

For comparison, the flow rates calculated for pure laminar flow and for pure molecular diffusion flow, using the dimensions of the rest fixture and h_r = 45 microinches, are also shown in Fig. 2.12. The curve for pure laminar flow is obtained from the curve of Fig. 33.9 of Ref. 1 with zero strain hardening, and the curve for pure molecular diffusion flow is obtained from the curve of Fig. 2.13, with zero strain hardening. It will be observed that while the ordinates of the two calculated curves differ by a factor of 2 to 1 in their mid-range, the two curves are close together at both ends. The actual

flow is probably closer to laminar flow at the left side of the graph, and closer to molecular diffusion flow at the right side of the graph.

Comparing the calculated and measured results, two discrepancies are evident:

1. The calculations predict that complete sealing should take place when the sealing stress is three times the yield point, whereas the experiment shows that complete sealing takes place when the sealing stress is just over twice the yield point. As noted on page 37-16 of Ref. 1, this discrepancy may be due to the mutual interaction of asperities and the non-uniformity of sealing over the seal surface. An additional factor of the gross elastic and plastic deformation of the supporting structures of the two sealing surfaces was not included in the calculations. Experimental stress-strain curves obtained during the leakage test show total deformations several times those attributable to plastic deformations of the asperities; this confirms that gross deformations are taking place.

2. At sealing stresses just below the yield point, the measured flow rate is only about half the flow rate calculated for laminar flow, and only about one-third of the flow rate calculated for molecular diffusion flow. This discrepancy may be due to the waviness of the diamond-burnished surface, which was not included in the calculations, as well as due to elastic and plastic deformations of the supporting structures.

   The achievement of complete sealing at twice the yield stress is consistent with the results of a previous investigation (Ref. 2) in which an annealed copper specimen with wedge-shaped asperities of 500 microinches rms surface roughness was pressed against another annealed copper specimen with a ground non-directional 8-microinch surface roughness. In that investigation, the degree of mating was determined by observing the percentage area of contact at the end of compression, and it turned out that 100% of the area was in contact when the normal stress was approximately twice the yield point.

The comparison between calculated and experimental results presented in Fig. 2.12 indicates that the calculations give a conservative prediction of the leakage to be expected. A less conservative and more accurate prediction could presumably be obtained by introducing more refinements into the assumptions on which the calculations are based. The two dimensional characteristics of the asperity distribution and the possibility of a leakage flow in other than a purely radial direction would be the next likely refinements to make.

FIGURE 2.12
COMPARISON BETWEEN CALCULATED AND
MEASURED LEAKAGE RATES FOR TEST 8

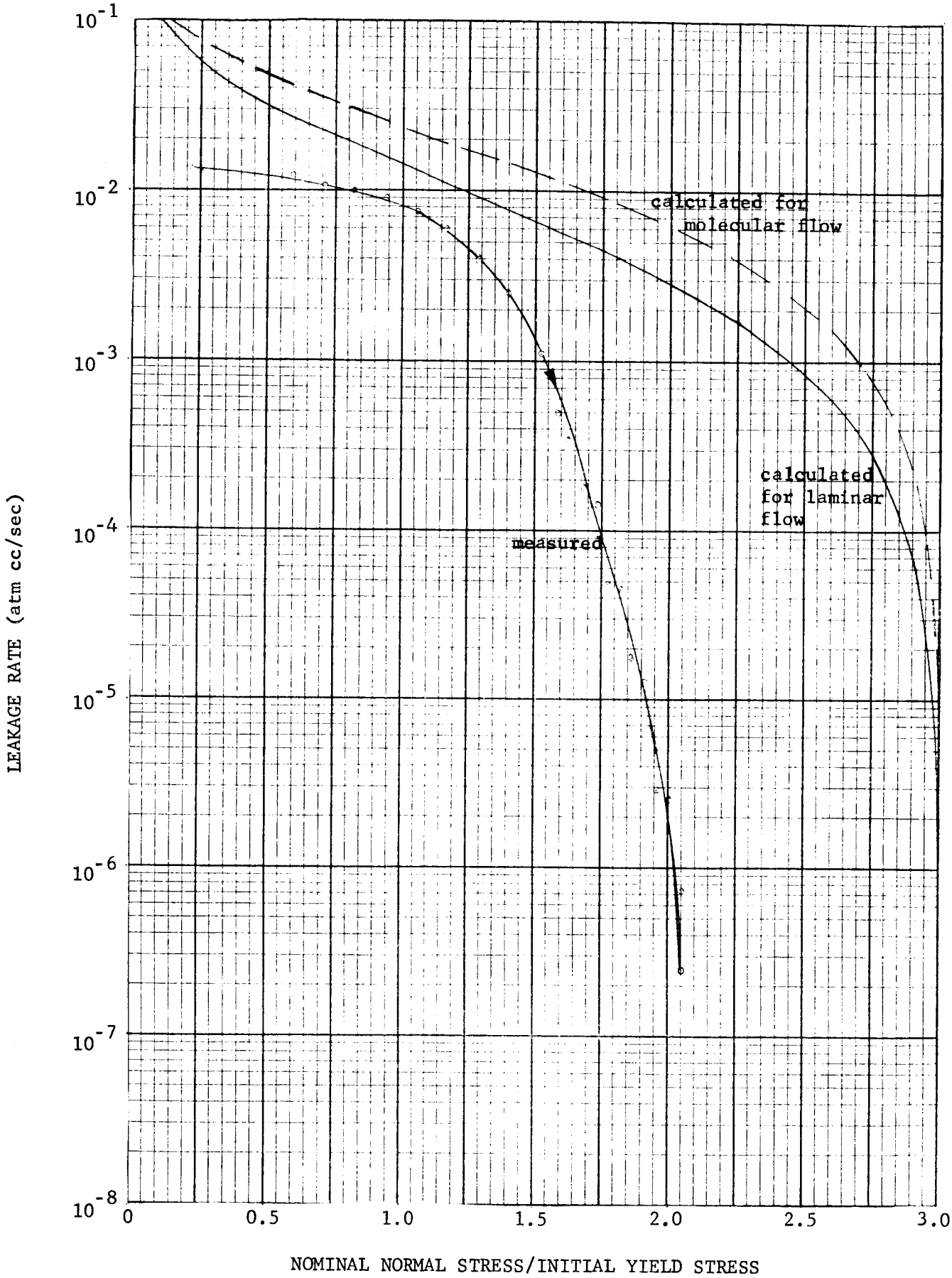

FIGURE 2.13

CALCULATED EFFECT OF SEALING PRESSURE ON EQUIVALENT PASSAGE HEIGHT FOR MOLECULAR DIFFUSION FLOW

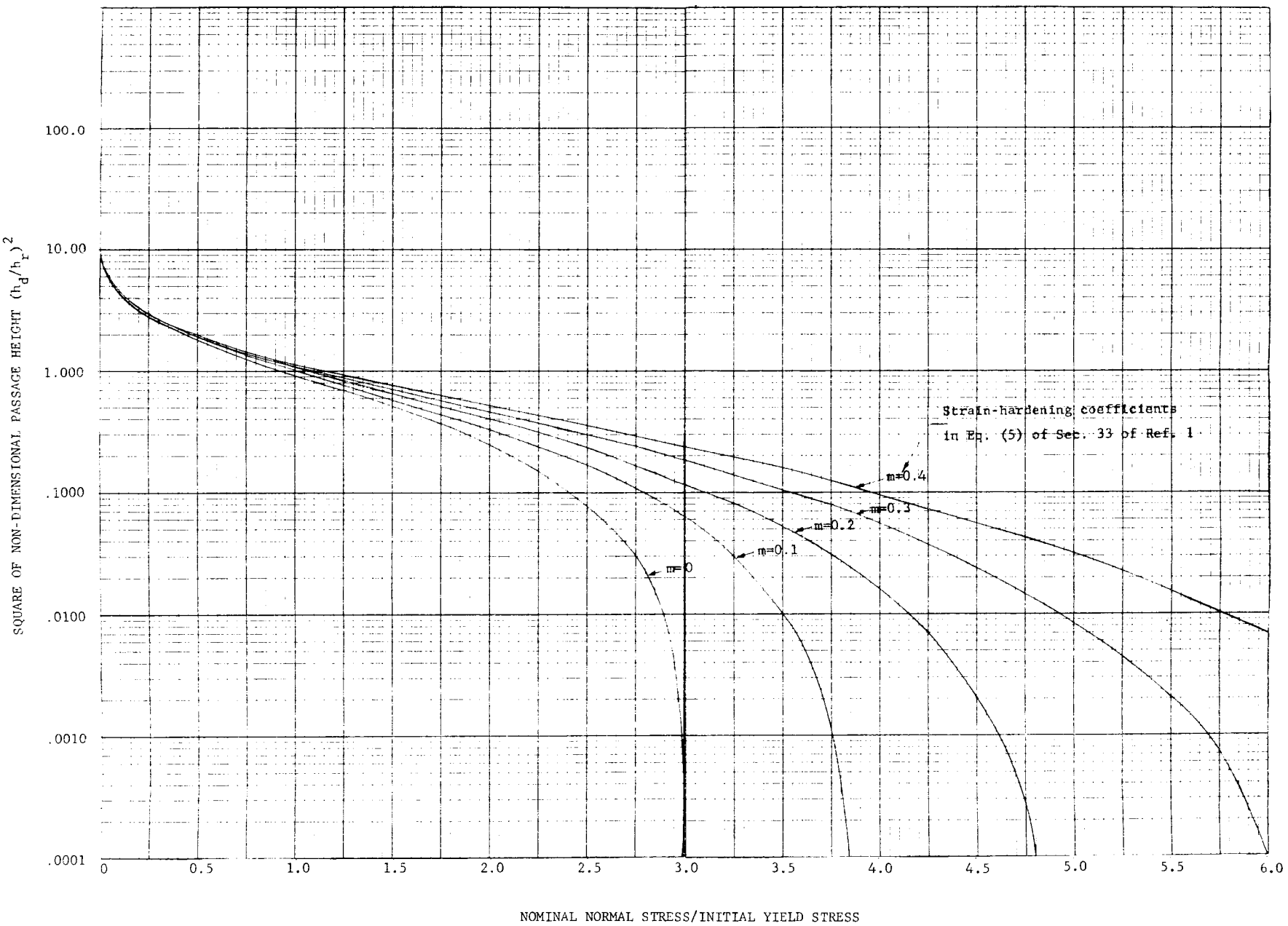

2.6 Evaluation of Measured Leaks as a Function of Internal Pressure

It is well known that flow through small capillaries can be either molecular flow, transitional flow (between molecular and viscous flow), viscous flow (either laminar or turbulent), or choked flow. Leakage flow existing across an annular gasket-sealing surface interface conceivably could be any of these flow modes; such flow is probably a combination of some or all of these modes since many flow paths of varying sizes can exist. Also, a flow path may be sized such that two or more of these flow modes exist in series across the seal.

One improvement in the level of information known about leakage flow through gaskets would be to appraise the total flow in terms of its flow mode, either laminar, choked, or molecular. If leakage flow is measured as a function of internal pressure, it is known that if a flow is purely laminar then the rate of flow will be proportional to the square of the internal pressure (when the absolute external pressure is essentially zero). If the flow is either molecular, choked, or turbulent, then the rate of flow will be proportional to the first power. It may be concluded that for a system that may have many modes of leakage flow, flow would be proportional to the internal pressure to some power between 1 and 2.

However, when flow rate vs. internal pressure data for previous tests is plotted on log-log paper a true straight line does not result in many cases (Figure 2.14).

FIGURE 2.14
Typical Flow - Internal Pressure Traces (Phase II)

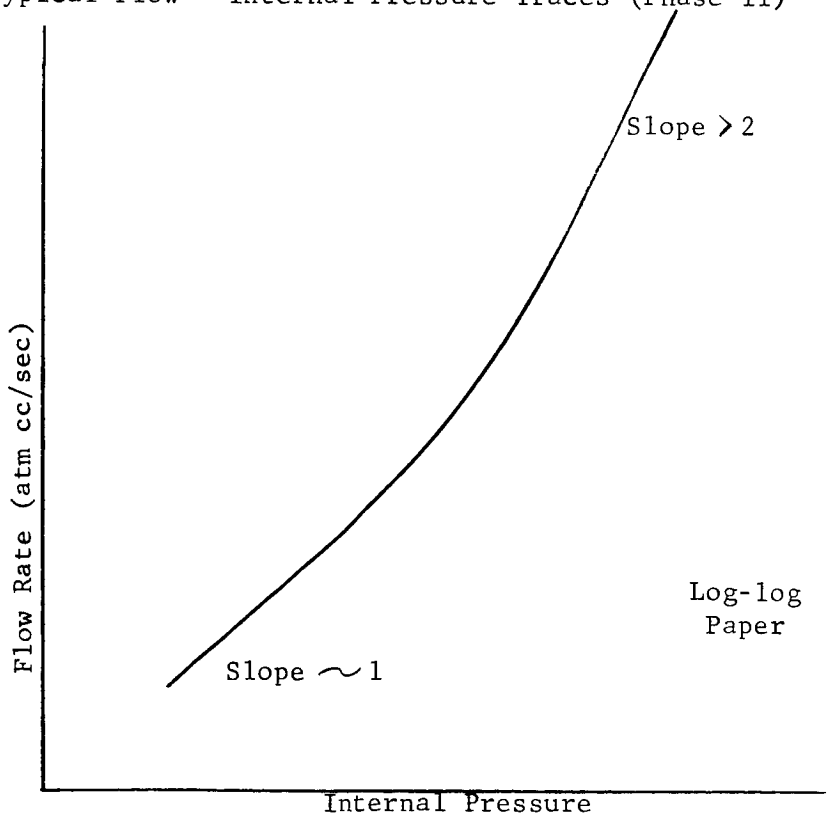

This could be expected due to a change in mode of flow with internal pressure and flow rate. However, where a straight line is evidenced, the slope of this line exceeds two in several cases.

Since a slope greater than two is not theoretically possible with fixed passage geometry, it is obvious that something happens to the passage size during the increase in pressure. In experimental tests conducted previously, too few bits of data were taken to discern whether the leakage rate vs. internal pressure curves were smooth or not. In some cases it appeared that the curve would be smooth for a small range of pressure, then would exhibit a jump in flow rate followed by another smooth curve.

In order to study this experimental phase in more detail, test number 27 (described in Section 2.4.7) was accomplished. The results of this test are shown schematically in Fig. 2.15. It will be noticed that as the internal pressure is initially increased (1-2) from one atmosphere the slope of the curve is approximately one, denoting molecular flow. At a certain level of internal pressure, a break in the curve is noticed (2-3) and the flow increases drastically. The remainder of the curve extends with a

FIGURE 2.15

Flow-Internal Pressure Trace, Experiment 8

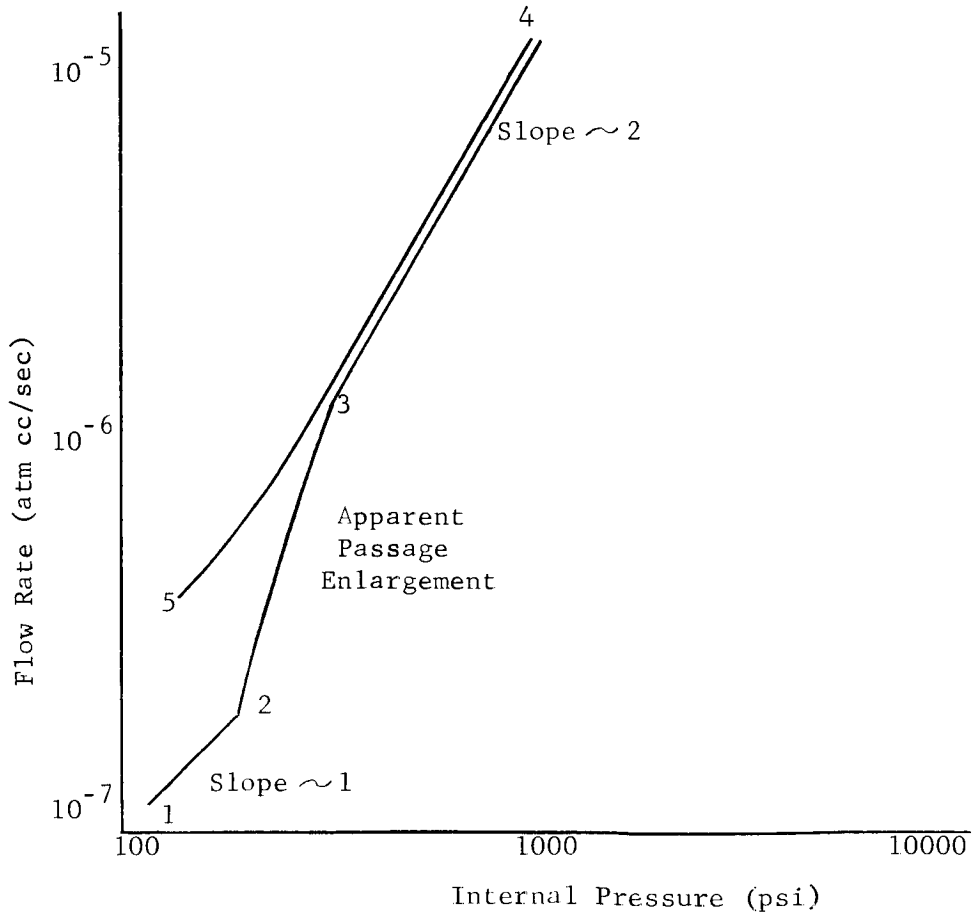

slope of two, (3-4) denoting laminar flow. At no point on either curve is the slope greater than two, as must be expected. However, the jump in the curve does show that the actual leakage path suddenly increased in size. In order to insure that this explanation is adequate in describing this phenomenon, the internal pressure was decreased in increments down to one atmosphere. The plot of this data is shown from points 4 to 5 in the figure. It will be noticed that this line is continuous and of approximately a slope of 2. The continuity of this line shows that the final leak size maintained itself and does not close up.

One conclusion from this test is that a leak opening up in size during an increase in internal pressure is quite possible even in systems which are adjudged to be extremely clean. Several possibilities for this present themselves, dirt particles present on the sealing surfaces at assembly, or even generated by the act of assembly, microscopic particles in the helium system, which initially become barriers to leakage flow and are later blown out, or moisture existing in the system or adsorbed on the sealing surfaces. In all experiments, a one micron filter was used in the helium system to insure that dirt did not plug leaks. However, no attempt was made to insure a dry system. In any case, the present system is believed to be a great deal cleaner than any field use of connectors. Hence, the phenomenon of increasing leakage path size can be expected in field use. The question then arises whether data for leakage rates obtained at a lower than operational pressure can be used in extrapolation to find the leakage rate at a higher pressure. Also, the question arises as to whether the very low leak rate tests are perhaps optimistic, and finally whether such a system would be stable or lose its adsorbed gases and "open up" a leak path.

Another conclusion based on this and previous experiments is that the transition between molecular and laminar flows may be related approximately to a certain flow rate. While this flow rate is obviously a function of internal pressure and the number and size of the individual leaks making up the whole, it appears that, for seal systems of the types tested, laminar flow commences at approximately 10^{-6} atm cc/sec.

2.7 References

1. T. P. Goodman, et al., Design Criteria for Zero-Leakage Connectors for Launch Vehicles, NASA Contract NAS 8-4012, Final Report for First Contract Period, General Electric Company, Schenectady, New York, 1963.

2. G. W. Cunningham and J. W. Spretnak, "A Study of the Effect of Applied Pressure on Surface Contact Area", International Journal of Mechanical Science, Vol. 4, 1962, pp. 231-240.

3. DESIGN AND TESTING OF A FOUR INCH FLANGED CONNECTOR

by

P. N. LeFort

3.0 Summary

This section describes the design and testing of a 4-inch separable connector that is to meet the following design conditions.

A. Pressure
   Operating pressure = 500 psi
   Proof pressure = 750 psi

B. Temperature
   Low temperature = Room temperature
   High temperature = 500°F

C. External Load
   5,000 lb-in transverse moment at operating pressure

The starting point in the design for the four inch connector was a design used on an existing launch vehicle which is reproduced in Figure 3.11. An analysis of this drawing indicated a stress condition that would cause yielding at both places that the pipes joined the flanges under a loading that was determined sufficient to produce sealing. A modification was made to the design by introducing contact outside the bolt circle which, by calculation, was an adequate design. Tests were subsequently conducted with this design using a spiral-wound metal gasket with an asbestos filler and metallic o-rings.

3.1 Sealing Requirements

The spiral-wound gasket shown in the sketch was tested in the ATL leak

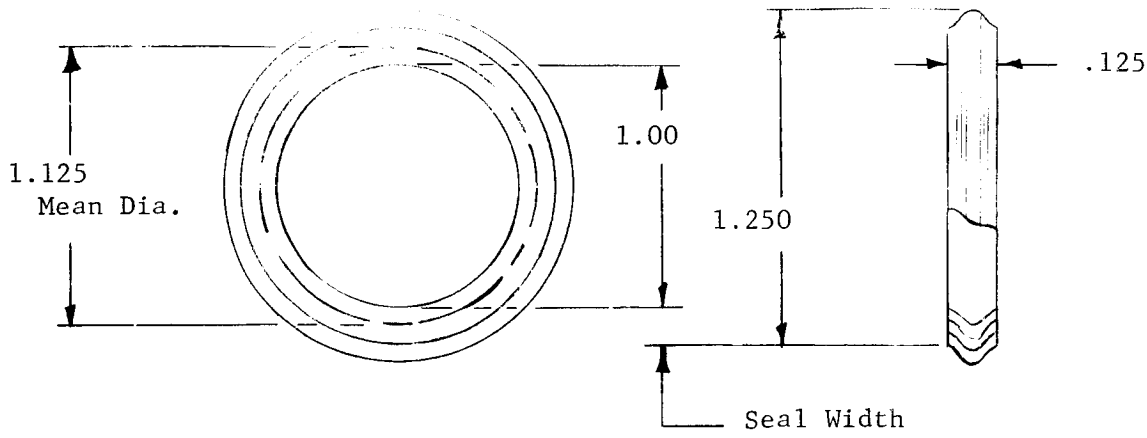

facility. For this gasket at the manufacturer's recommended deflection of 25 mils, which required a gasket load of 7,250 pounds, the leakage was 1.2×10^{-6} atm - cc/sec. of helium at an internal pressure of one atmosphere and a pressure difference of one atm. At 500 psi internal pressure, with the same gasket load, the leakage increased to 1×10^{-4} atm - cc/sec. Deflection measurements showed that after removal of the load the gasket did not return to its original thickness. After a deflection of 19 mils a second gasket returned only one mil when the load was decreased to one half the original value. These tests indicated that this type of seal was not suitable for "zero leakage" application in the 4" connector where the increase in gasket diameter would increase the leakage at 500 psi to 4×10^{-4} atm - cc/sec. The inability of the gasket to follow an axial separation of the flanges at the seal, as demonstrated in the second deflection test, and the buckling of the gasket under high compressive forces (buckling was evident upon inspection of a test gasket that had been deflected 37 mils) leads to the conclusion that this type of gasket will perform at its best under variable bolting force only when it is used with a groove to limit the deflection and when there is no relative axial motion between the flanges at the seal.

Using the ASME Code, Reference 1, as a guide the gasket load to assure a tight joint is

$$H_p = 2b\pi Gmp$$

where b is the effective seal width, in this case $\left(\frac{\text{seal width}}{2}\right)$
G is the mean diameter of the sealing surface
m is the gasket factor, a constant for flexitallic seals.

If we take the test gasket as gasket 1 and the proposed gasket, Figure 3.11, as gasket 2

$$H_p\Big|_2 = H_p\Big|_1 \left(\frac{b_2 G_2}{b_1 G_1}\right) = 5.875\ H_p\Big|_1$$

Or in our case where $H_p\Big|_1 = 7,250$ pounds, $H_p\Big|_2 = 42,500$ pounds.

That is, a gasket load near 42,000 pounds is required to seat the gasket in the 100 mil groove. At a later date tests showed that this number could be high by as much as 150% (see Section 3.7.3). However for lack of further information at the time of analysis, this gasket load was used for the calculations on the original design.

3.2 Results of Analysis for SK20-1061

Appendix I (Section 3.9) contains the development of the general formulae and the calculations for the results presented for the initial design. The stress levels for sections ② and ④, of the sketch below, were found to indicate gross yielding for the initial design.

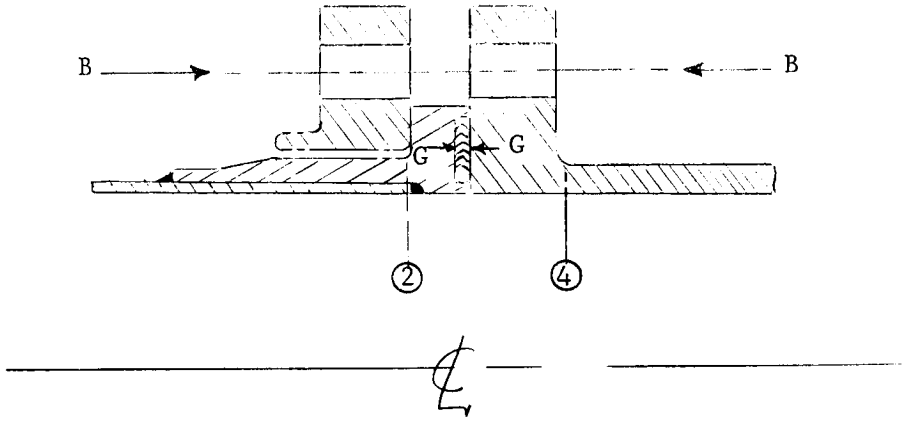

$$B\Big|_{\text{assem.}} = 2{,}200 \text{ lb/in}$$

$$G_T\Big|_{\substack{500^\circ \\ 500 \text{ psi}}} = 42{,}000 \text{ lb}$$

$$G\Big|_{\substack{500^\circ \\ 500 \text{ psi}}} = 3{,}160 \text{ lb/in}$$

$$\sigma_2\Big|_{\substack{500^\circ \\ 500 \text{ psi}}} \approx 119{,}000 \text{ psi}$$

$$\sigma_4\Big|_{\substack{500^\circ \\ 500 \text{ psi}}} \approx 150{,}000 \text{ psi}$$

3.3 Redesign of SK20-1061

A common method used to prevent excessive rolling of flanges, and the method used here, is to provide flange contact outside of the bolt circle. An undesirable feature of this design is that part of the bolting force must be diverted from the sealing area so that the total bolt load will become substantially higher. As the rough calculation in Section 3.10.3 shows it was necessary to increase both the bolt size and the outer diameter of the flange.

A set of formulae were developed and calculated values for various loading conditions were determined using the same method as the analysis of the original design. The results of this analysis are tabulated in the latter part of Appendix II (Section 3.10).

3.4 Metallic Shear O-Ring

Since preliminary tests of spiral-wound, asbestos filled, gaskets indicated leakage levels above $1x10^{-4}$ atm - cc/sec. could be expected the test connector was modified so that testing of metallic shear o-rings could also be carried out. The metallic o-ring concept had been tested on the ATL facility with excellent results and demonstrated that the design employs shear deformation to good advantage, provides some radial restraint to relative motion, and is quite insensitive to removal of load. No attempt was made to analyze the supporting structure for this gasket since both the bolt and gasket loads required to seal with the o-ring were less than the values assumed in the design of the flange.

3.5 Test Equipment

The test was designed to permit

a) pressurization of the connector
b) heating of the connector
c) application of a transverse moment to the connector
d) collection and measurement of the leakage through the test gasket, and
e) measurement of strains imposed on the connector.

The system used was similar to that shown in Figure 5.9 of Section 5.4 which shows the test set-up for the tube connector tests.

Pressurization is by means of the bottled gas supply fitted with a pressure regulator.

During part of the testing the connector was heated to 500°F by means of resistance heaters mounted inside the connector, Figure 3.1, on both ends of the test fixture, and around the outside of the vacuum chamber, drawing number 544E537. The heaters are not visible in the above mentioned Figure 5.5 because of the insulation but the control variacs can be seen below the test bench.

Some testing was done with a transverse moment applied to the connector by means of the moment rods, Figure 5.9 and drawing number 544E537. One end of the rod pushes (or pulls) on the slotted end plate of the connector as the nuts on the other end are adjusted against the loading bracket.

The leak detector of Figure 5.9 is a vacuum system and a mass spectrometer used in conjunction with a micro-ammeter. This method of leak measurement requires that the detector maintain a vacuum between the source of leakage and the spectrometer which is the reason for the vacuum chamber, drawing number 544E537, and its gasket, drawing number 115A4731-1. Helium is the most readily detectable gas for this system and was used as the contained gas throughout the testing.

Strain gages and thermocouples were mounted on the connector, Figure 3.3 through 3.6, to record the reaction of the structure during the tests and monitor the temperature of the connector. In addition four of the 16 bolts used on the connector were instrumented with straingages (Figure 3.1) to monitor bolt load. These bolts had tinned leads and did not function as strain indicators during high temperature testing because the electrical connections could not be maintained.

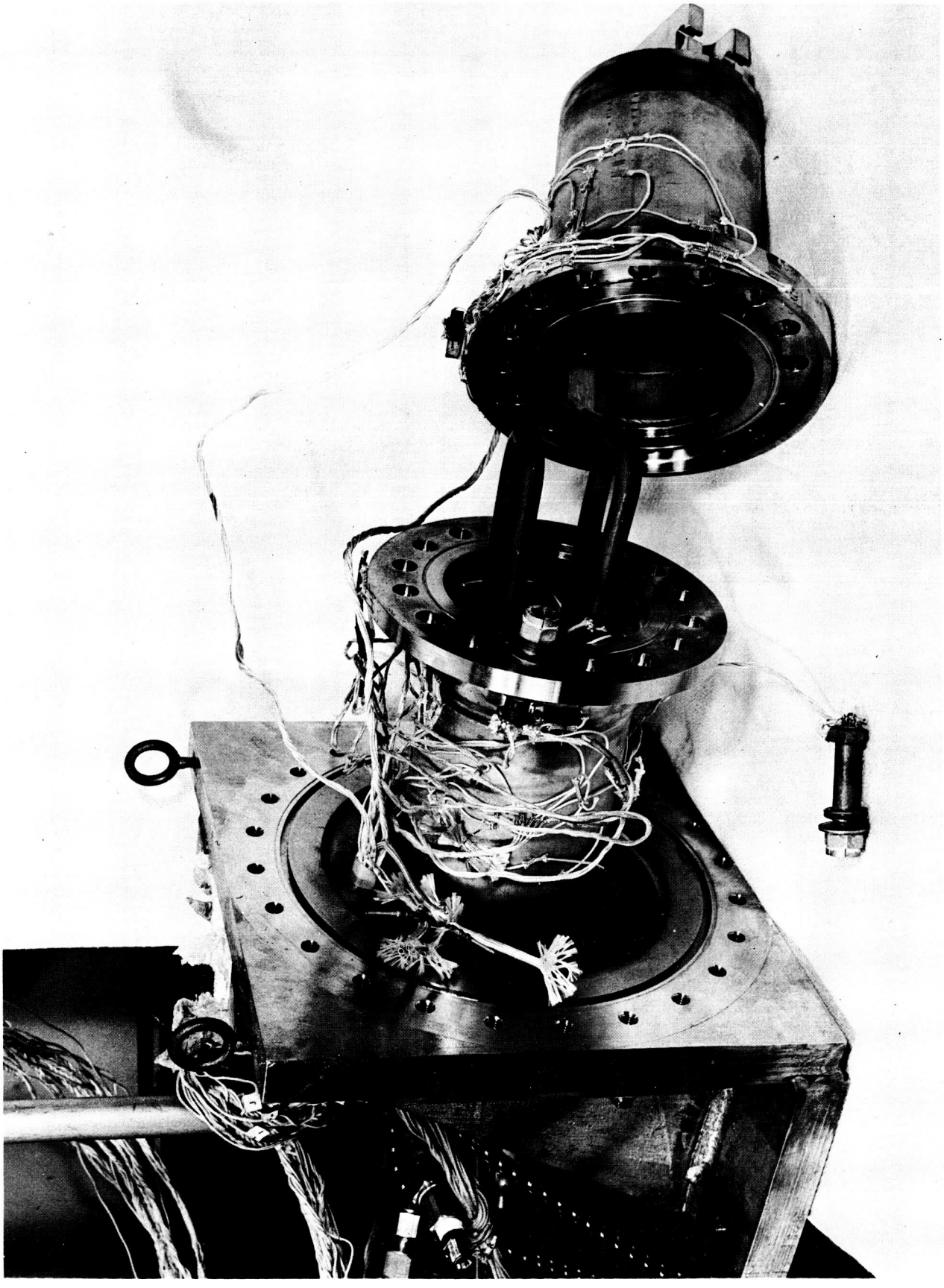

FIGURE 3.1

FOUR INCH HIGH TEMPERATURE FLANGE CONNECTOR

FIGURE 3.2

FOUR INCH HIGH TEMPERATURE FLANGE CONNECTOR

FOLDOUT FRAME 1

FOLDOUT FRAME 2

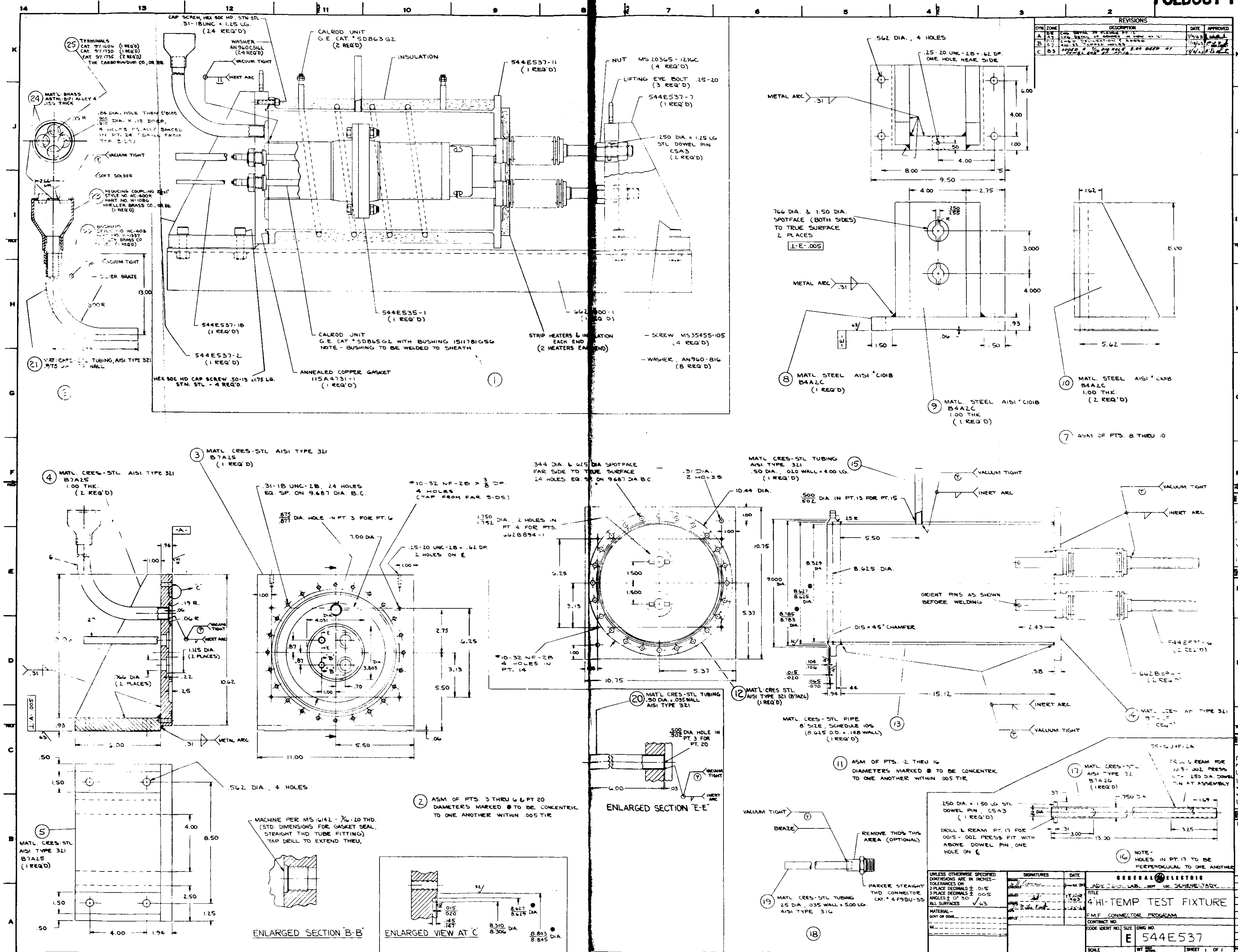

ORIGINAL PAGE IS OF POOR QUALITY

ORIGINAL PAGE IS OF POOR QUALITY

SIZE	115A4731	SHEET	REV
A			A

REVISIONS			
SYM	DESCRIPTION	DATE	APPROVED
A	CHG. INSIDE DIA., CHG. THICKNESS OF COPPER, ADDED PT. 2	7/9/63	J. Wallach

NOTES -

DIAMETERS TO BE CONCENTRIC TO ONE ANOTHER WITHIN .010 TIR.

GASKET TO BE FLAT WITHIN .06 MAX. WHEN RECEIVED (INSPECTION NOTE)

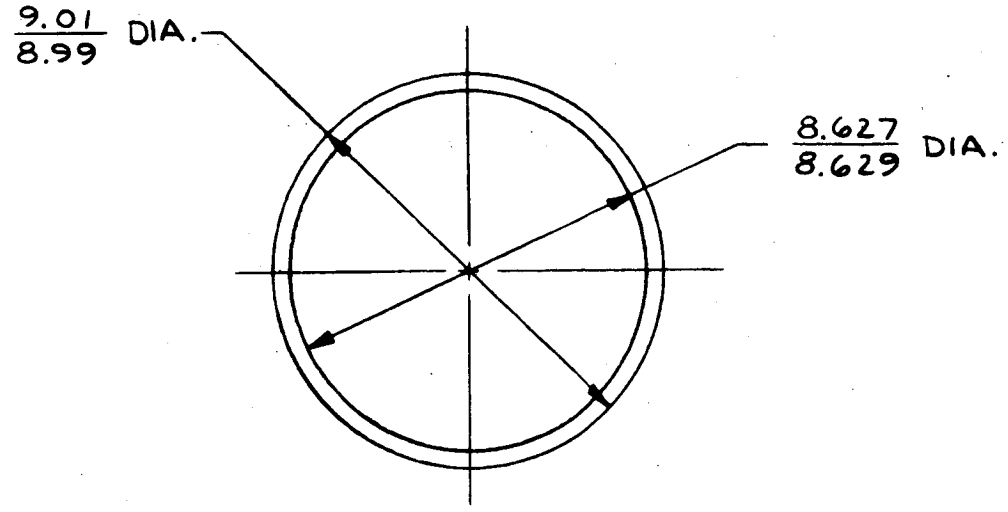

(1) MATL. CERTIFIED OFHC COPPER (OXYGEN FREE) ANACONDA ALLOY #121, ASTM SPEC. B152 TEMPER SOFT, ROCKWELL HARDNESS #F45 .065 ±.003 THICK

(2) MATL. ANNEALED ALUM. AA 1100-0 (25-0) .063 ±.003 THK.

PURCHASE PART DWG.

UNLESS OTHERWISE SPECIFIED DIMENSIONS ARE IN INCHES. TOLERANCES ON: FRACTIONS ± DECIMALS ± ANGLES ±	SIGNATURES	DATE
ALL SURFACES ✓	DRAWN H. D. Rehmer	June 24 1963
MATL GOVT OR COML	CHECKED	
	ISSUED [illegible]	24 June '63
GE	ENGR P. J. Lafond	6-24-63
NEXT ASM 544E537	MFG	
PRINTS TO	MATLS	

GENERAL ELECTRIC
ATL DEPT. LOC SCHENECTADY

TITLE GASKET
FMF CONNECTOR PROGRAM

CONTRACT NO.

CODE IDENT NO.	SIZE	DWG NO.
	A	115A4731

SCALE NONE | WT CALC ACTUAL | SHEET

FN-901-F (5-63) PRINTED IN U.S.A.

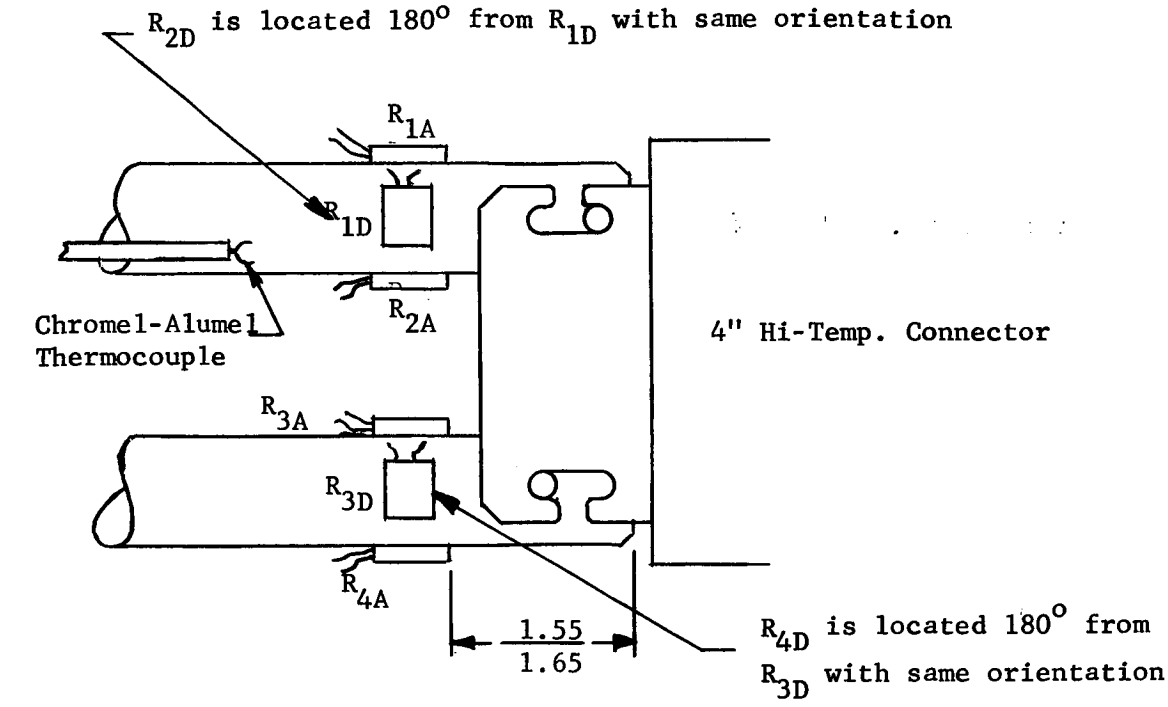

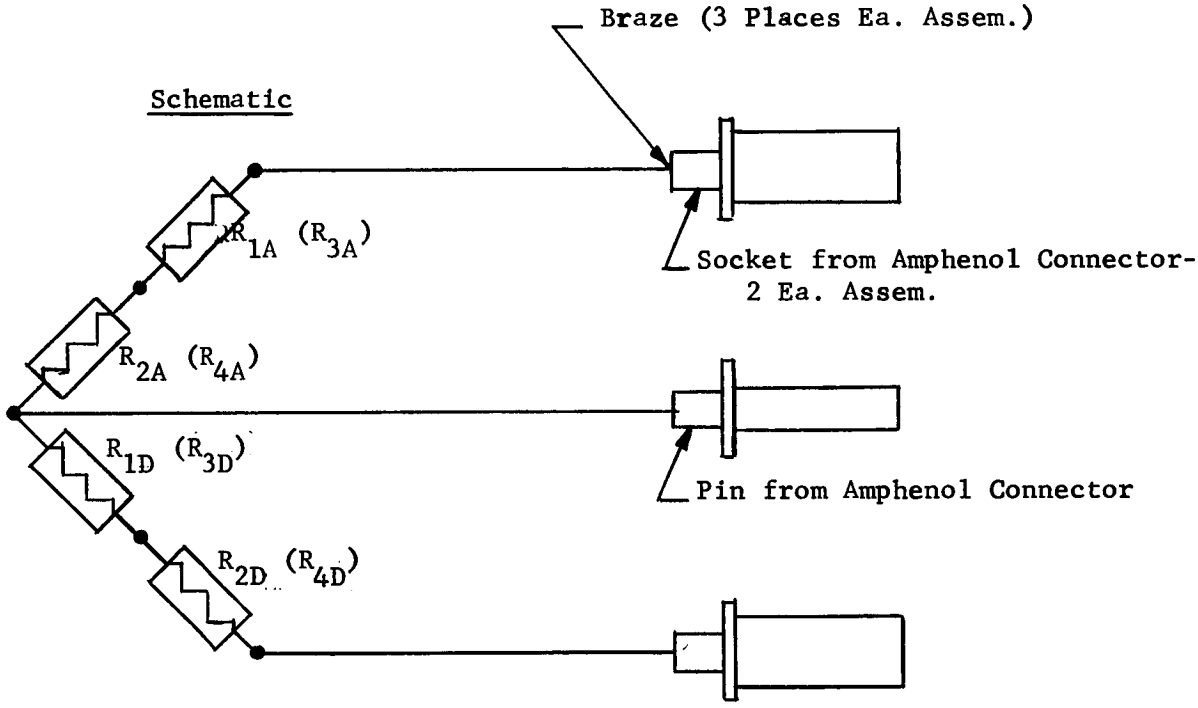

Notes:
1. Use Budd Metalfilm #C9-620.
2. Connections made by spot-welding.
3. Leads to be of the same length (@ 3') and to be wound together after insulating with glass sleeving.

Figure 3.3

MOMENT ROD STRAIN GAGE INSTALLATION

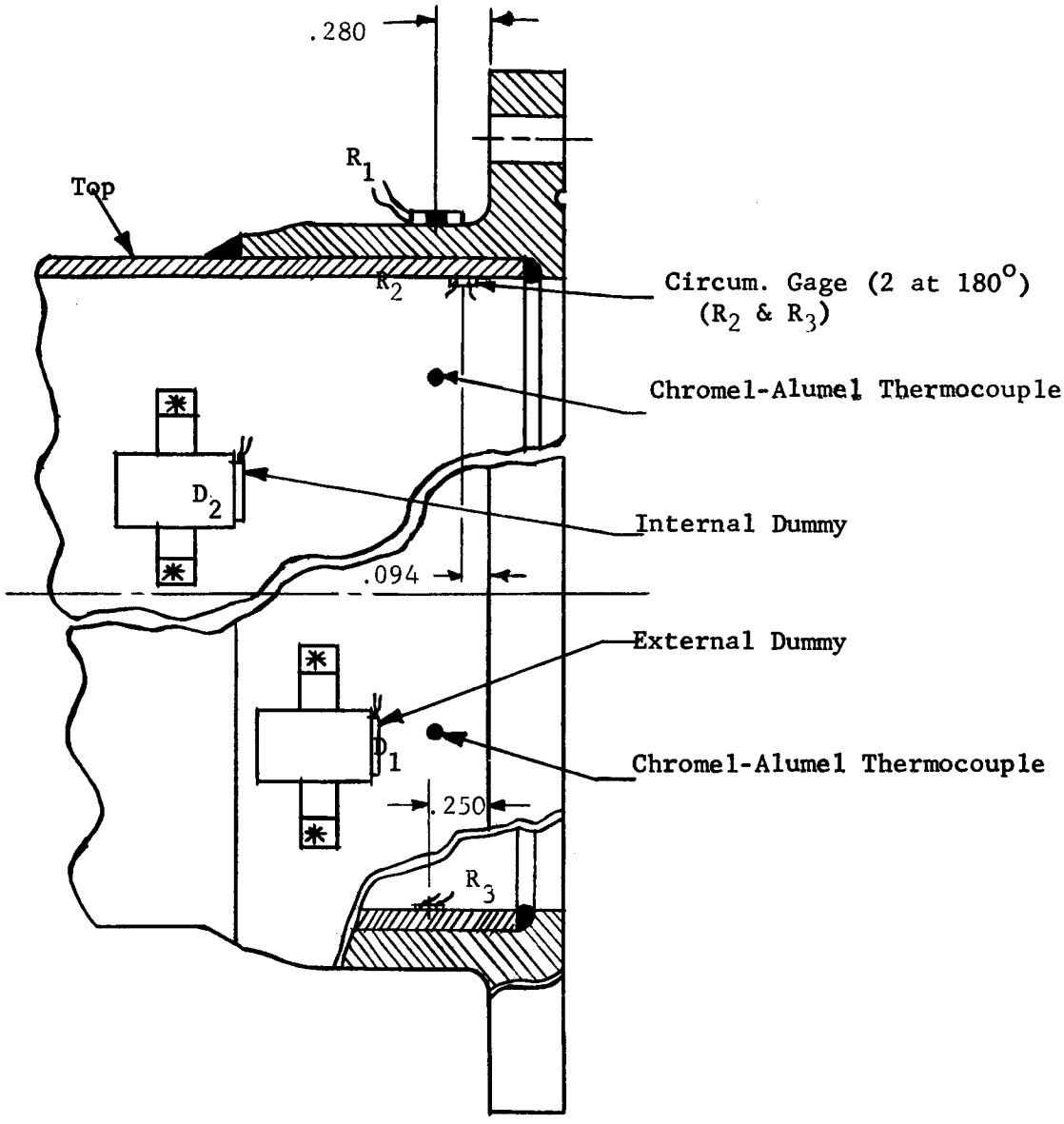

Schematic

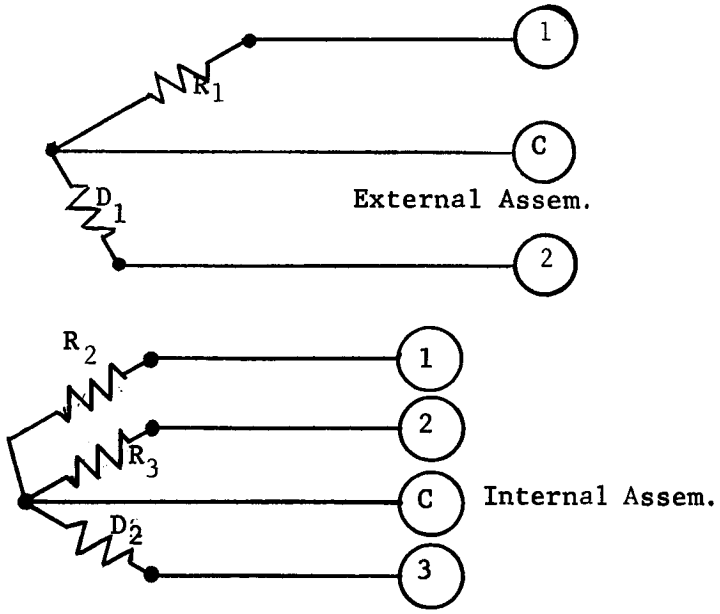

Notes:

1. Use Budd C 9-620 Gages.
2. Connections made by spot welding.
3. Leads in the same assem. have the same length (10'), are insulated for 4', and wrapped together for 4'.

Figure 3.4

FULL FLANGE STRAIN GAGE INSTALLATION

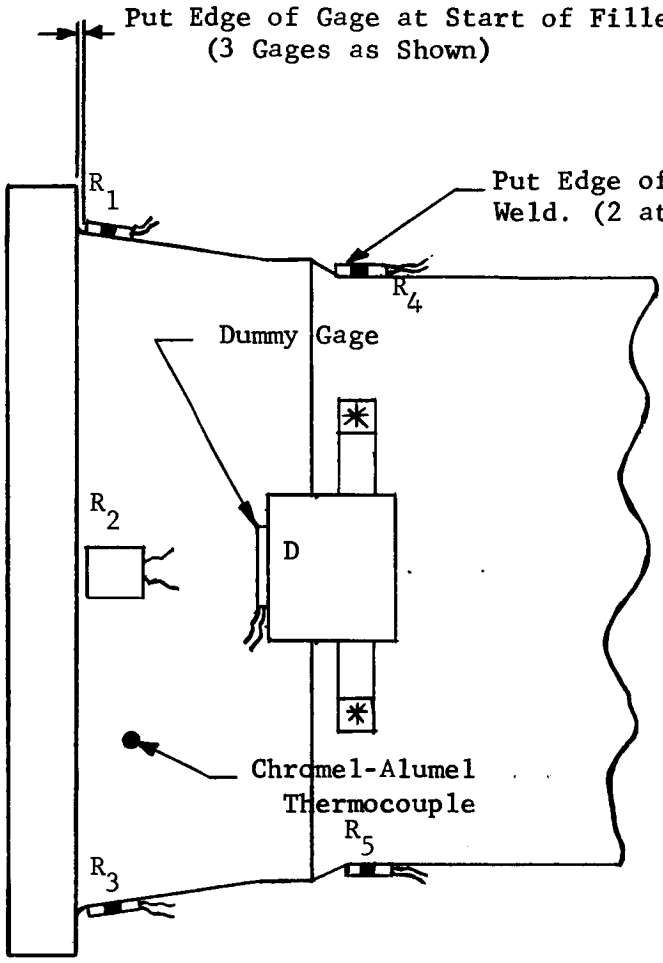

Notes:

1. Use Budd C 9-610 Gages.
2. Connections made by spot welding.
3. Leads to have the same length (10') and to be insulated for 4' and wrapped together for 4'.

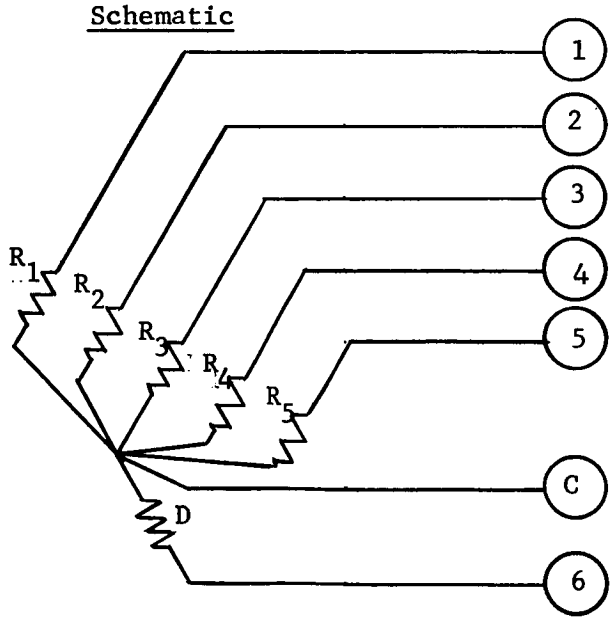

Figure 3.5

FERRULE STRAIN GAGE INSTALLATION

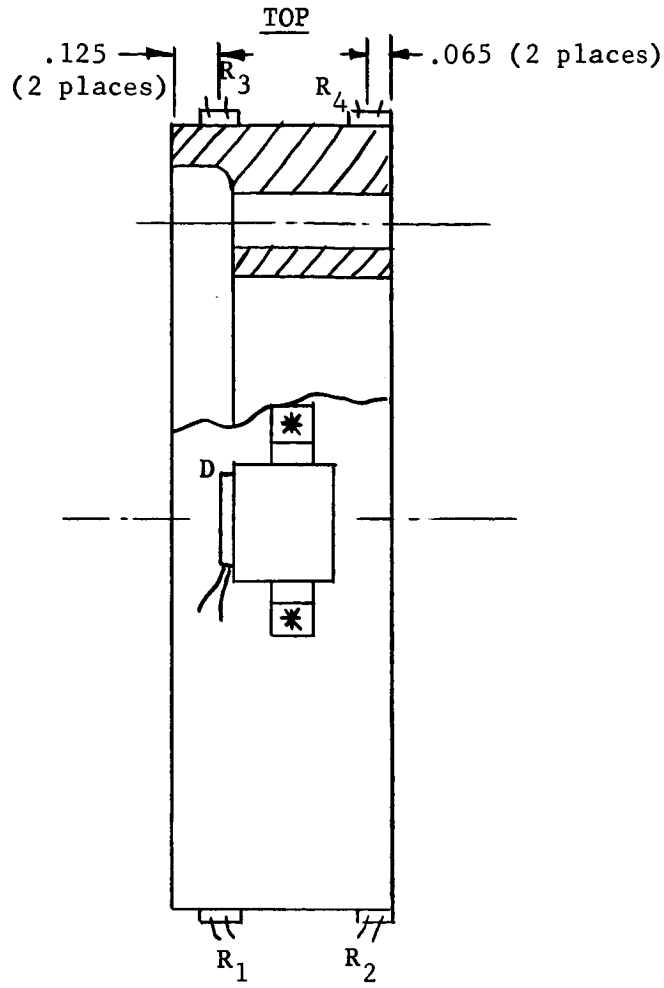

Schematic

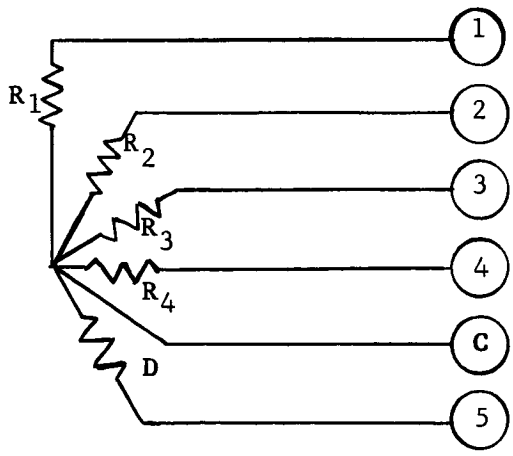

NOTES:

1. Use Budd C9-610 Gages.
2. Connections made by spot welding.
3. Leads to have the same length (10') and to be insulated for 4' and wrapped together for 4'.

FIGURE 3.6

FLOATING RING STRAIN GAGE INSTALLATION

3.6 Test Procedure

3.6.1 Purpose

Determine the sealing capabilities of solid metal "O" ring gaskets and spiral-wound metal gaskets with asbestos filler in 4" diameter hot GOX line flanges, and obtain strain readings to check the analysis of the connector.

3.6.2 Hardware

a. 544E537, "4" Hi-Temp. Test Fixture"

b. 544E535, "4" Hi-Temp. Test Flange," solid wire ring gasket type

c. 544E538, "4" Hi-Temp. Test Flange," spiral-wound gasket type

3.6.3 Equipment

a. (1) H_e supply with gauge, capability in excess of 500 psi

b. (1) 240V, 20 amp. Variac for external calrods

c. (2) 120V, 4 amp. Variacs for strip heaters

d. (1) 240V, 8 amp. Variac for internal calrod

e. (1) thermocouple vacuum gauge

f. (1) vacuum roughing pump

g. (1) G. E. mass spectrometer

h. (1) Keithley amplifier, Model 410

i. (1) set of calibrated leaks

j. (1) 20-point, switch box, for strain gages

k. (1) 6-point switch box, for strain gages

l. (1) switch box for thermocouples

m. (2) SR-4 strain indicators

n. (1) portable potentiometer

3.6.4 Inspection

a. Assure that all torque wrenches, pressure gages and thermocouples have been recently calibrated.

b. The following inspection is required prior to and after testing:

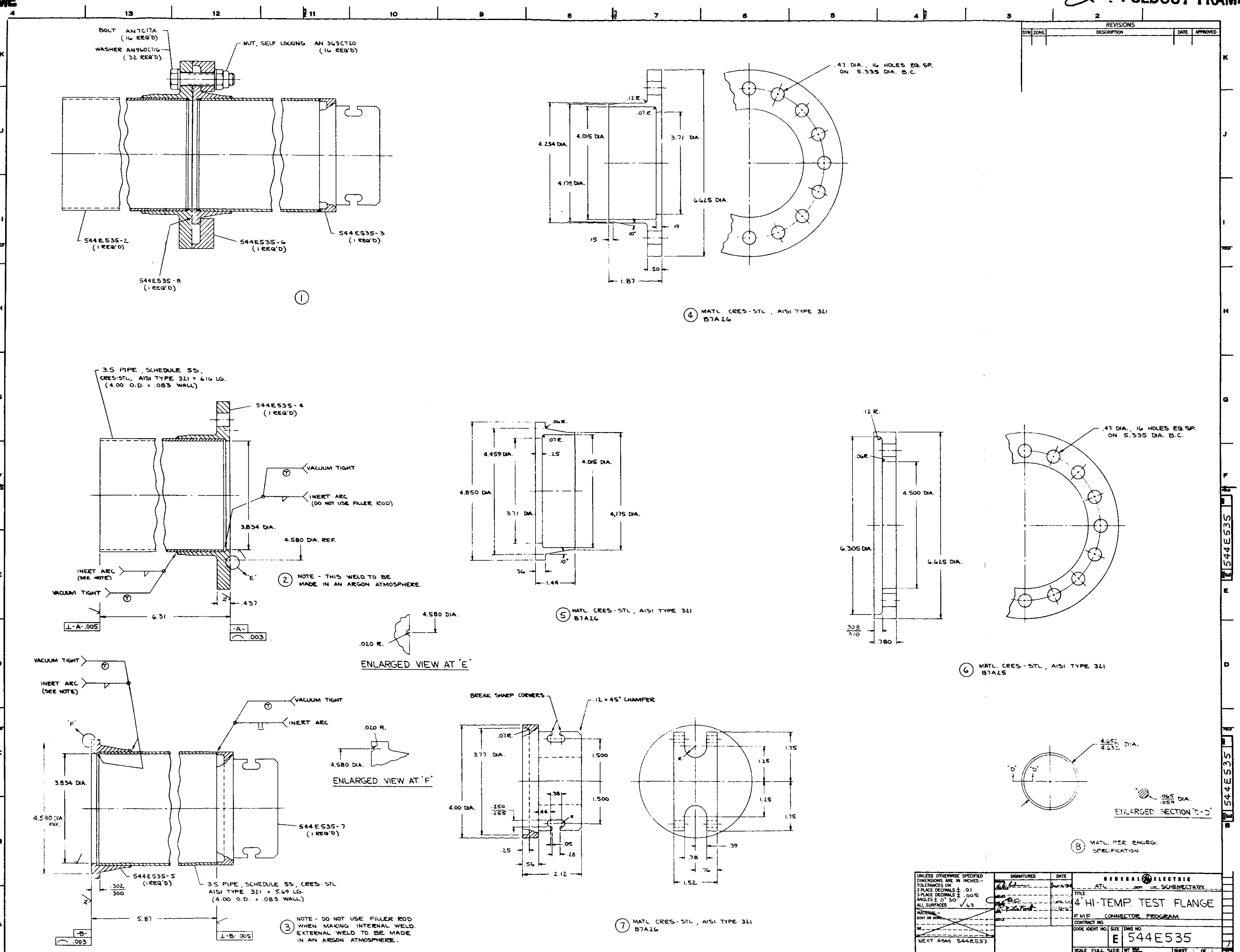

ORIGINAL PAGE IS OF POOR QUALITY

FOLDOUT FRAME

FOLDOUT FRAME 2

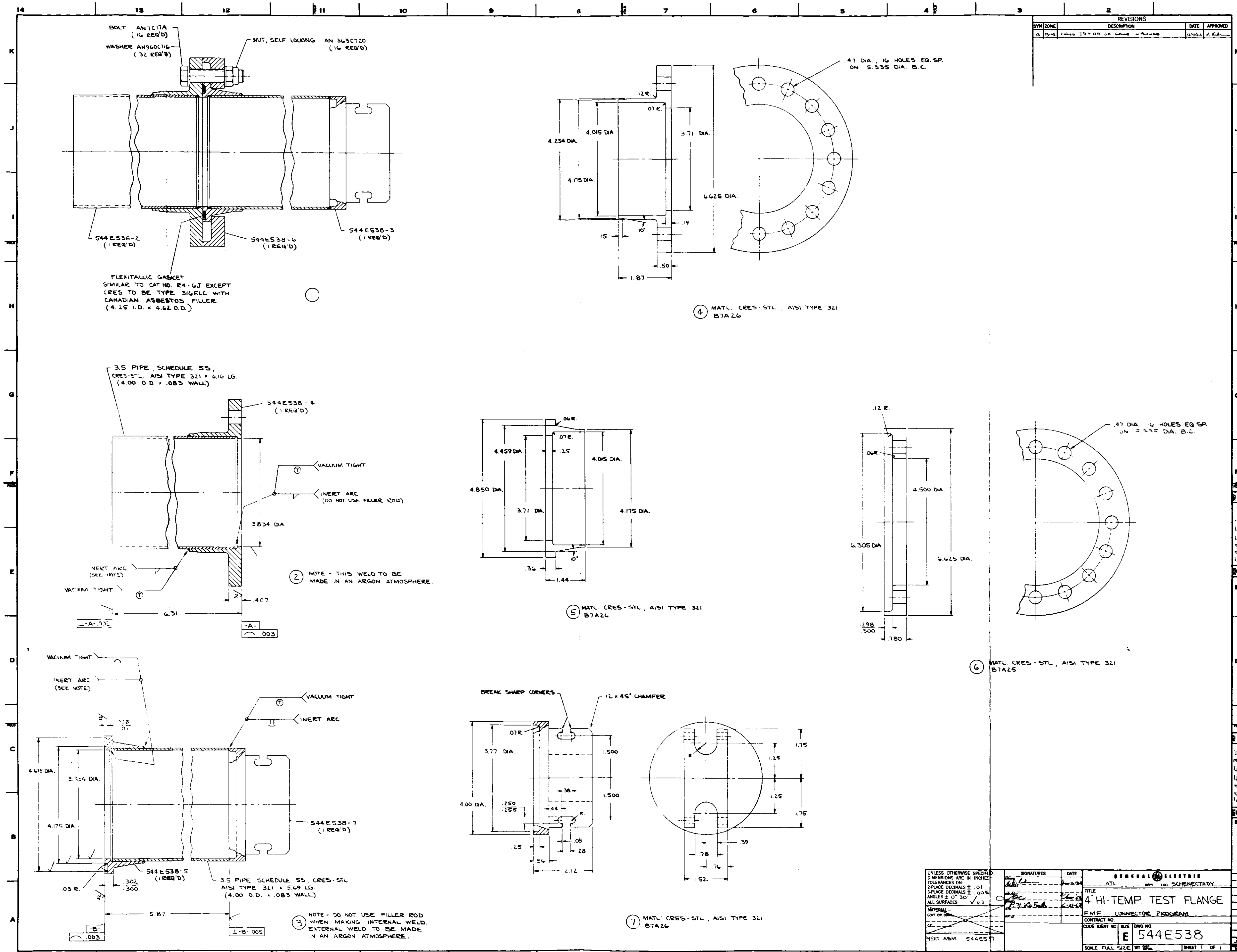

ORIGINAL PAGE IS OF POOR QUALITY

ORIGINAL PAGE IS OF POOR QUALITY

1. Check thickness and flatness of gasket at 6 equally spaced points and record.
2. Visually inspect flange surfaces and gasket for evidence of damage, irregularities or radial scratches.
3. Check strain indicator batteries.

3.6.5 Assembly

a. Install gasket to be tested with the connector in a vertical plane. Care should be taken not to damage the flange surfaces or gasket.

b. Put the flanges together with locating marks alligned and position the ring, 544E535-6 (544E538-6) so that the locating marks are aligned. Take care that the gages on the taper hub are not damaged.

c. Spray moly-kote on connector bolts, nuts, and washers as directed on the dispenser.

d. Put the bolts in their holes and thread the nuts on by hand. Be sure that the strain gage bolts (#1, 5, 9, 13) are in the correct bolt holes as shown on Sketch #1.

e. Following the torque sequence of Sketch#1 snug all bolts using cross torque to 60 (90) in-# record strains.*

f. Using cross torque method, increase bolt torque to 110 (150), 160 (210), 210 (270) in-lbs. Strain indicating bolt reading of 1005 (1390) μ in/in is to take precedence over 210 (270) in-# torque reading. Record date of assembly.

g. Twenty-four hours after assembly check bolt strain for bolt relaxation due to gasket set. Retorque to strains recorded previously at 210 (270) in-lb if necessary. Record torque wrench readings. Repeat this step in 24 hr intervals until no bolt relaxation occurs. Record number of retorqueings needed.

h. Install the vacuum enclosure together with its gasket, assembling the push-rods to the end cap, and connecting the leads from the push-rods.

i. Connect the leak detection equipment and evacuate the vacuum chamber.

k. Leak check the vacuum enclosure at the shear gasket, the stand pipe, and all welds.

3.6.6 Tests

I. Room Temperature Test (without moment)

a. Evacuate the vacuum chamber

---

* When two values are given the first is for the solid o-ring test and the second, in parentheses, is for the spiral-wound gasket test.

Bolt Numbering and Torque Sequence Looking
At Nuts From Push-Rod End of Assembly

⊕ Strain gage Bolts

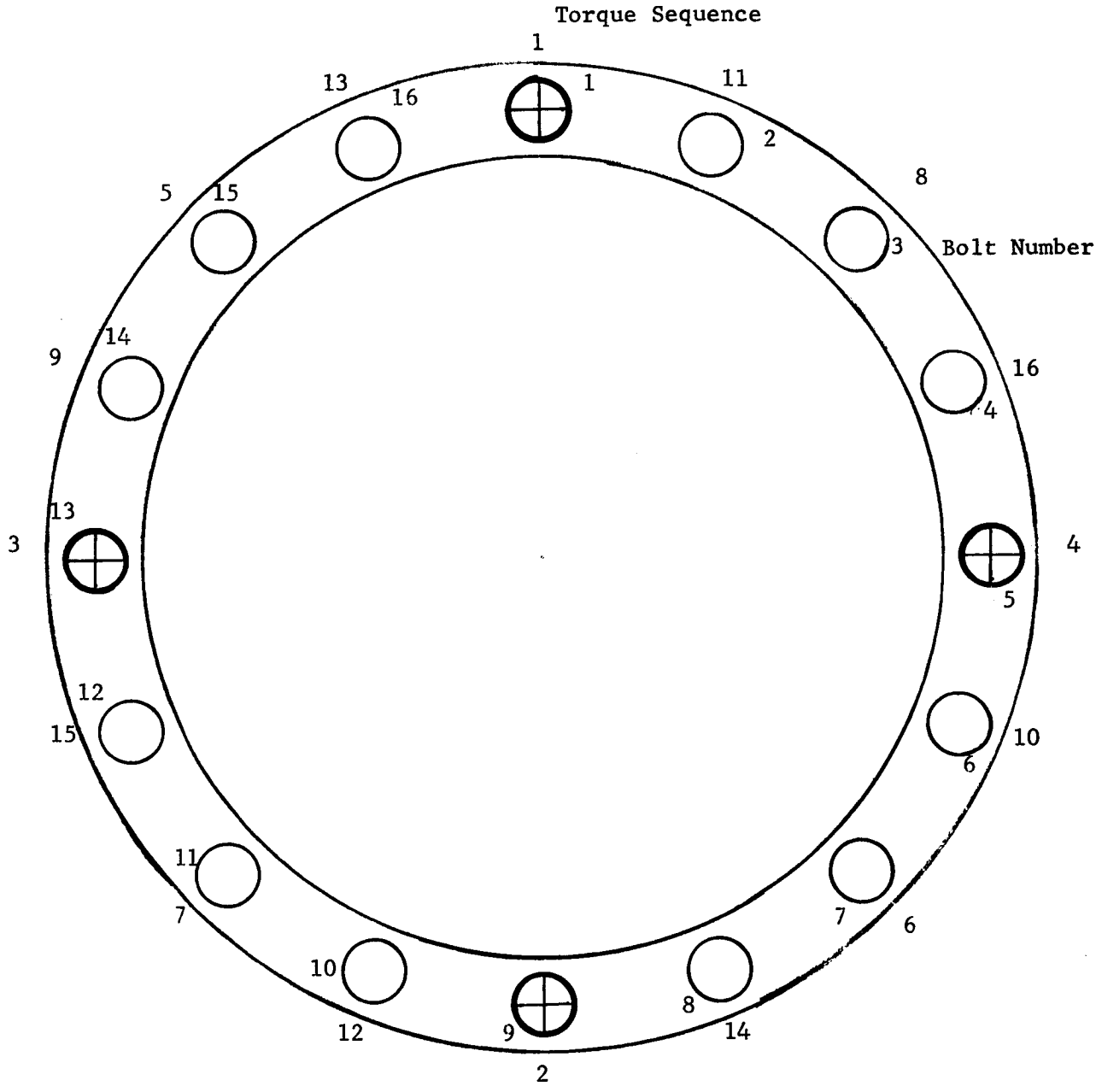

LEAK PROOF CONNECTOR-4INCH, SKETCH # 1

b. Record strains

c. Pressurize to 200 psig at a max. rate of 100 psi/min. Record leakage and strains.

d. Increase pressure in steps of 100 psi up to 500 psig, recording leakages and strains at each step.

e. Vent pressure chamber at a max. rate of 100 psi/min and record residual strains.

II. Room Temperature Test (with moment)

a. Apply moly-kote lubricant to the rod threads, nuts, and contact area of the angle plate and tighten the appropriate nuts until a compressive strain of 311 μ in is recorded for the top rod and a tensile strain of 291 μ in/in is recorded for the bottom rod. This applies a moment of 5,000 in-# on the connector.

b. Record strains.

c. Loosen nuts on rods and pressurize to 200 psig at a max rate of 100 psi/min. Apply the moment as in step a) above.

d. Record leakage and strains.

e. Repeat steps c) and d) above for internal pressure of 300, 400, and 500 psig.

f. Remove moment load by loosening the nuts and record leakage and strains.

g. Vent pressure chamber and record residual strains.

III. High Temperature Test (without moment)

a. Vent pressure chamber to atmosphere.

b. Heat assembly to 500^{o}F and allow temperature to stabilize.

c. Repeat test I.

IV. High Temperature Test (with moment)

a. Repeat test II.

V. Transient Temperature Test

a. Vent vacuum and pressure chambers to atmosphere and cool assembly to room temperature.

b. Evacuate the vacuum chamber.

c. Record strains.

d. Pressurize to 500 psig at a max. rate of 100 psi/min. Record leakage and strains.

e. Heat assembly to 500°F at a max. rate of 50°F/min, recording temperature and leakage rate together with readings of highly strained gages continuously until temperature stabilizes at 500°F.

f. Evacuate pressure chamber and record residual strains.

g. Vent vacuum and pressure chambers to atmosphere and cool assembly.

h. Evacuate vacuum chamber and record residual strains.

3.6.7 Disassembly

a. Be sure that vacuum and pressure chambers are vented to atmosphere. Remove angle bracket holding rods.

b. Remove outer shell taking care to disconnect strain gage and thermocouple leads that come from the rods.

c. Disassemble connector taking care with all leads.

d. Perform inspection as outlined in Section 3.6.4 above.

3.7 Tests

3.7.1 Aluminum Shear O-ring

A shear O-ring made of 99 percent pure aluminum, alloy #1100-0, was used in a preliminary test to find any deficiencies in the test procedure, point up trouble spots, and cycle the strain gages. Some trouble was experienced in locating the gasket as the gasket diameter (as opposed to the wire diameter) was too large for the groove. The connection was tested at room temperature and internal pressures of 200, 300, 400, and 500 psig, and also at 125 psig internal pressure with a transverse moment of 2,250 in/lb. The temperature was increased to 520°F and tests conducted at 200 and 500 psig internal pressure. There was no measurable leakage until the condition of 520°F and 500 psig when a level of 5×10^{-3} atm cc/sec was reached before the test was terminated. Inspection of the gasket after disassembly showed that it had not been properly centered, had too large a gasket diameter (not wire diameter) for the groove, and contained an irregularity at the joint showing a deficiency of deformed material. Unfortunately the test schedule did not allow further tests to be performed on a modified aluminum O-ring.

3.7.2 Copper Shear O-ring

A shear O-ring of annealed, soft, oxygen free copper was tested after it had been modified to correct the trouble experienced with the aluminum O-ring. The modification consisted of

a. opening the joint
b. fitting the gasket to the groove and removing the excess material
c. butt brazing with an 80 Cu-15Ag-5P alloy in the shape of a disk fitted between the two ends.

The testing was carried out according to the procedure of Section 3.6 with no measurable leakage during tests at constant temperature. During the transient temperature tests; i.e., while the internal pressure is held constant at 500 psi the temperature is raised from room temperature to 500°F, there was measurable leakage as reported in Section 3.8.

3.7.3 Spiral-wound Metal Gasket

After the test flange was machined to conform to drawing number 544E538 tests of the metallic, spiral-wound, asbestos filled gasket were conducted without moment at room temperature with internal pressures of 1 atm., 100, 200, 300, 400, and 500 psig. At this point, because of the high leakage levels attained, plans for further leak testing were abandoned.

Because of the large discrepancy between calculated stresses for this design and the strain gage results obtained, which were considerably lower than expected, a load deflection test of this gasket was performed and showed the minimum gasket load, G_T = 34,800 pounds, that had been assumed necessary to seat the gasket in the groove was high by 160 percent.

3.8 Test Results

3.8.1 Aluminum O-ring

As previously noted trouble was experienced in locating the O-ring due to a mismatch between the ring and groove, which may account for the leakage at maximum temperature and pressure. While the maximum leak recorded was only 5×10^{-3} atm - cc/sec., the leak appeared to be opening quite rapidly and testing was stopped lest the vacuum in the detector be lost and the spectrometer shut down for repairs. Table 3.1 is a condensation of the test data. Before testing, the O-ring had a measured diameter of .0624" with a reading of .058" at the joint. After testing the average thickness, t, was .0583 and the average height of the web, h, was .0172"

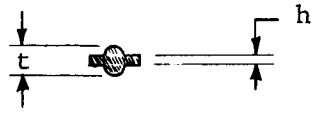

O-ring (After testing)

Visual inspection of the full flange, 544E535-2, indicated that yielding had occurred in the flange hub area. Measurement showed the flange had rotated as shown in Figure 3.7. Looking at Table 3.1, it appears the greater part of this yielding took place during bolt-up and could have been avoided if the lip on the floating ring had been 5 or 10 mils longer so that contact outside the bolt circle, which would resist this rotation, could have been made sooner.

3.8.2 Copper O-ring

A more thorough series of tests were made with the copper O-ring after it had been sized to the groove, as outlined in Section 3.7.2, to avoid a repetition of the trouble experienced with the aluminum O-ring. Table 3.2 presents some data for the steady state tests, which showed no measurable leakage, while Figure 3.8 plots temperature versus time and leakage versus temperature for the transient test in which the connector was pressurized to 500 psig at room temperature and, while this pressure was maintained, the connector was heated to 500°F in a time interval of 23 minutes. The rate of heating was the maximum possible with this test set-up. Although the O-ring leaked during this rapid temperature rise, (maximum rate was 40°F/min, which occurred from room temperature to 220°F) the leak did not exceed 6.1×10^{-8} atm -cc/sec and this was only a temporary peak and was greatly reduced as the temperature distribution became more uniform throughout the joint.

Before testing, the O-ring had a measured diameter of .0621" while after testing the average thickness, t, was .0635" with the average height of the inner web, h_i, .0235" and the average height of the outer web, h_o, .0227".

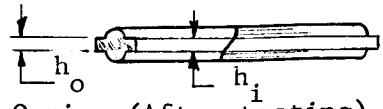

O-ring (After testing)

Table 3.1: Aluminum O-ring Test Data (Partial) [a]

Test Number	1	2	3	4	5	6	7	8	9	10	11
Temperature (^{o}F)	← 70 →							← 520 ± 15 →		70	70
Internal Pressure (psig)	0	0	0	200	500	125	0	0	500	0	0
Transverse Moment [b] (in-lb)	← 0 →					2250	← 0 →				
Bolt Load, Avg (lb)	0	850	2800	2350	2275	〃	2250	〃	〃	〃	0 [d]
Leakage (atm-cc/sec)	← less than 10^{-9} atm - cc/sec →								$>5 \times 10^{-3}$	0	0
Recorded Strains [c] ~ Microinches/inch											
Integral Flange											
External Fillet, Axial			1045	1085	1140	1135	1025	840	1035	550	240
Internal, Top, Circum.			410	505	650	540	480	245	460	210	145
Internal, Bottom, Circum.			580	1220	1550	1305	1220	1175	1530	1080	840
Ferrule											
Fillet, Avg, Axial			230	305	380	〃	250	-100	65	-235	-85
Weld, Avg, Axial	-X	0	-20	70	170	〃	25	-75	140	-180	-150
Floating Ring											
Inner, Avg, Circum.			-650	-605	-590	〃	-570	-435	-395	-280	-140
Outer, Avg, Circum.			420	435	400	〃	440	175	205	220	125

NOTES:

(a) Additional data points were 300 and 400 psig at room temperature, 200 psig at 520°, and additional "0" pressure readings to check gages.

(b) Moment was as shown

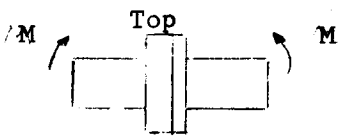

(c) An unknown value x, the strain at 850 pounds bolt load, must be added to all strains to correct strains to zero values for the unloaded case.

(d) All bolts were removed but connector was stuck fast by the O-ring. The connector had to be pried apart later.

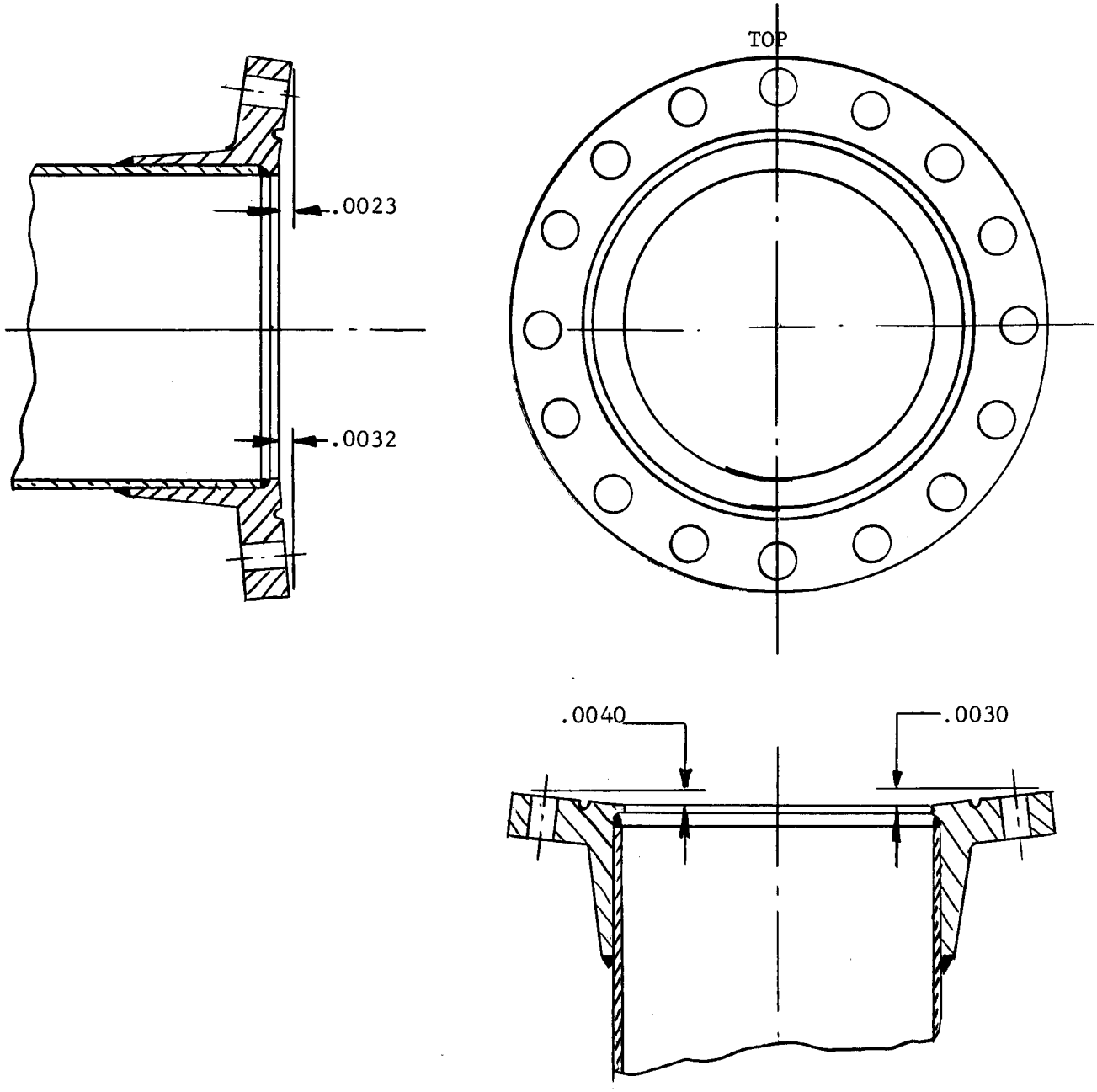

FIGURE 3.7

PERMANENT SET OF FLANGE, 544E535-2, AFTER ALUMINUM O-RING TEST

Table 3.2: Copper O-ring Test Data (Partial) [a]

Test Number	1	2	3	4	5	6	7	8	9	10
Temperature (°F)	←		70	→	←		495 ± 15	→	70	70
Internal Pressure (psig)	0	0	500	500	0	500	500	0	0	0
Transverse Moment [b] (in-lb)	←	0	→	5000	0	0	4800	0	0	0
Bolt Load, Avg (lb)	0	3000	2925	〃	〃	〃	〃	〃	1500	0
Leakage (atm - cc/sec)	〃	〃	← Leak < 1×10^{-8} →		〃	← Leak < 1×10^{-8} →		〃	〃	〃
Recorded Strains ~ Microinches/inch										
Integral Flange										
External Fillet, Axial	↑	805	905	750	785	960	820	785	610	45
Internal Top, Circum.		380	615	585	380	545	515	305	315	70
Internal Bottom, Circum.		325	650	655	425	815	800	435	355	135
Ferrule										
Fillet, Avg, Axial	0	265	375	〃	-20	100	〃	-60	205	-110
Weld, Avg, Axial		70	210	〃	40	250	〃	50	60	10
Floating Ring										
Inner, Avg, Circum.		-685	-680	〃	-550	-540	〃	-540	-710	-135
Outer, Avg, Circum.	↓	400	365	〃	270	230	〃	305	350	140

NOTES: (a) Additional data points were 200, 300, and 400 psig, with and without moment, at 70° and 500°; together with the transient test.

(b) Moment was as shown

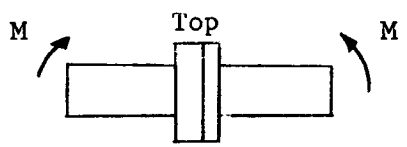

FIGURE 3.8

TRANSIENT TEST OF COPPER O-RING

Notes:

1. Internal Pressure of 500 psig.
2. No external moment.
3. Temperature measured on outer surface of integral flange hub (Fig. 3.4 shows thermocouple location).

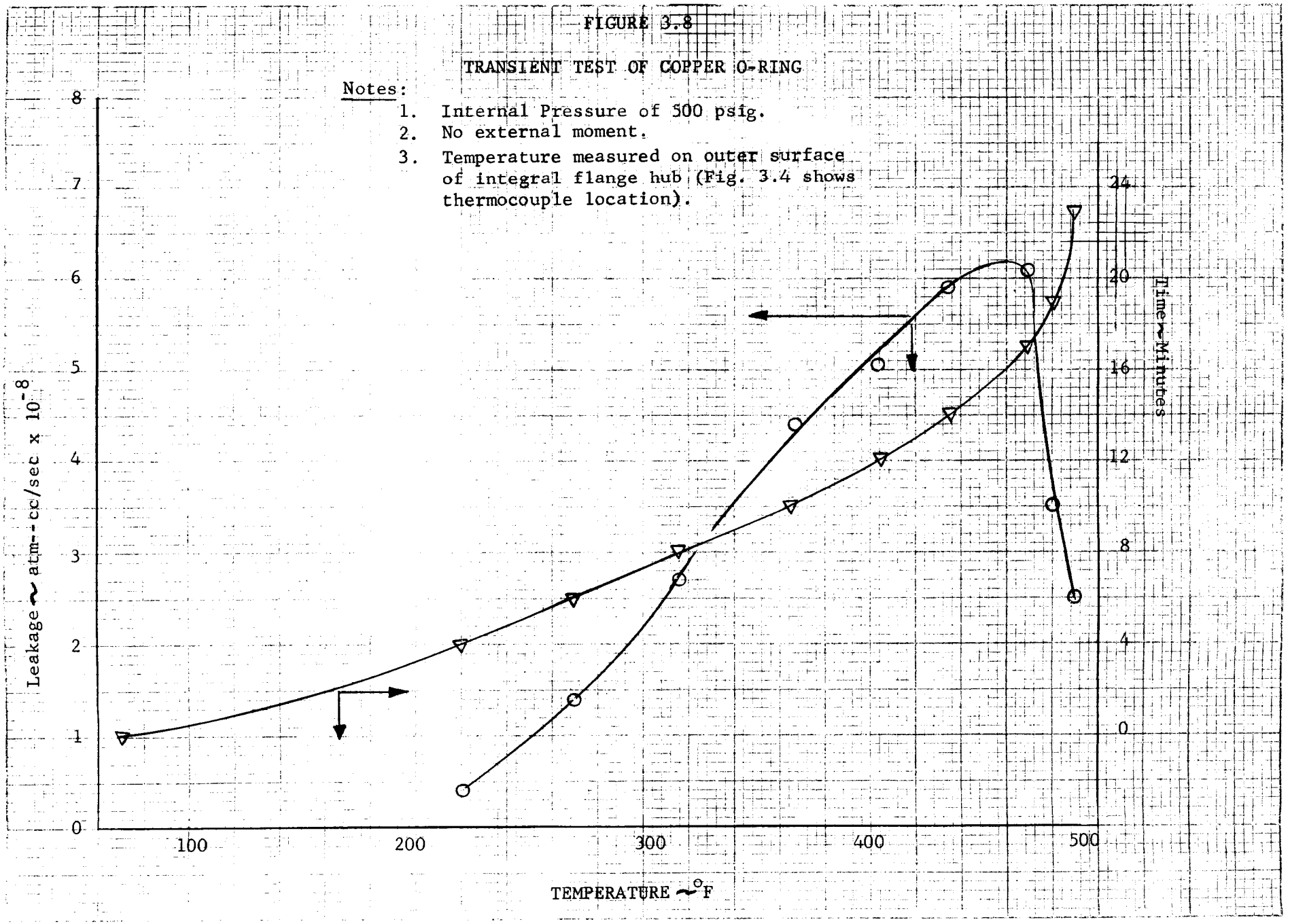

3.8.3 Spiral-wound Metal Gasket

After the connector had been machined to drawing number 544E538, the spiral-wound gasket was installed dry and tested at room temperature without the application of the moment. The leak that developed under these conditions was so large, 10^{-1} atm - cc/sec, that no further tests were made. Since the gasket had bottomed during assembly no advantage could be taken of the increased bolt load at elevated temperature and the leak could not be expected to reduce in size. The test data is presented in Table 3.3 and Figure 3.9.

A deflection test was preformed on a second dry gasket to determine the load required to seat the gasket in a .100" groove. The results are shown in Figure 3.10 together with results of a check on the smaller test gasket referred to in Section 3.1

Table 3.3: Spiral-Wound Gasket Test Data

Test Number	1	2	3	4	5	6	7
Temperature (^{o}F)	←			70			→
Internal Pressure (psig)	0	0	100	200	300	400	500
Bolt Load, Avg., (lb)	0	4000	〃	〃	4025	〃	4050
Leakage (atm - cc/sec)	0	5.8×10^{-6}	5×10^{-3}	3.2×10^{-2}	9.0×10^{-2}	1.6×10^{-1}	1.8×10^{-1}
		Recorded Strains ~ Microinches/inch					
Integral Flange							
External Fillet, Axial	↑	-75	-60	-40	0	20	50
Internal, Top, Circum.		0	25	65	120	175	230
Internal, Bottom, Circum.		45	100	160	235	310	385
	0						
Ferrule							
Fillet, Avg., Axial		50	80	110	145	190	230
Weld, Avg., Axial	↓	-40	-20	5	40	75	110
Floating Ring →	All gages inoperative after re-machining.						

FIGURE 3.9

LEAKAGE VS. PRESSURE, FLEXITALLIC TEST

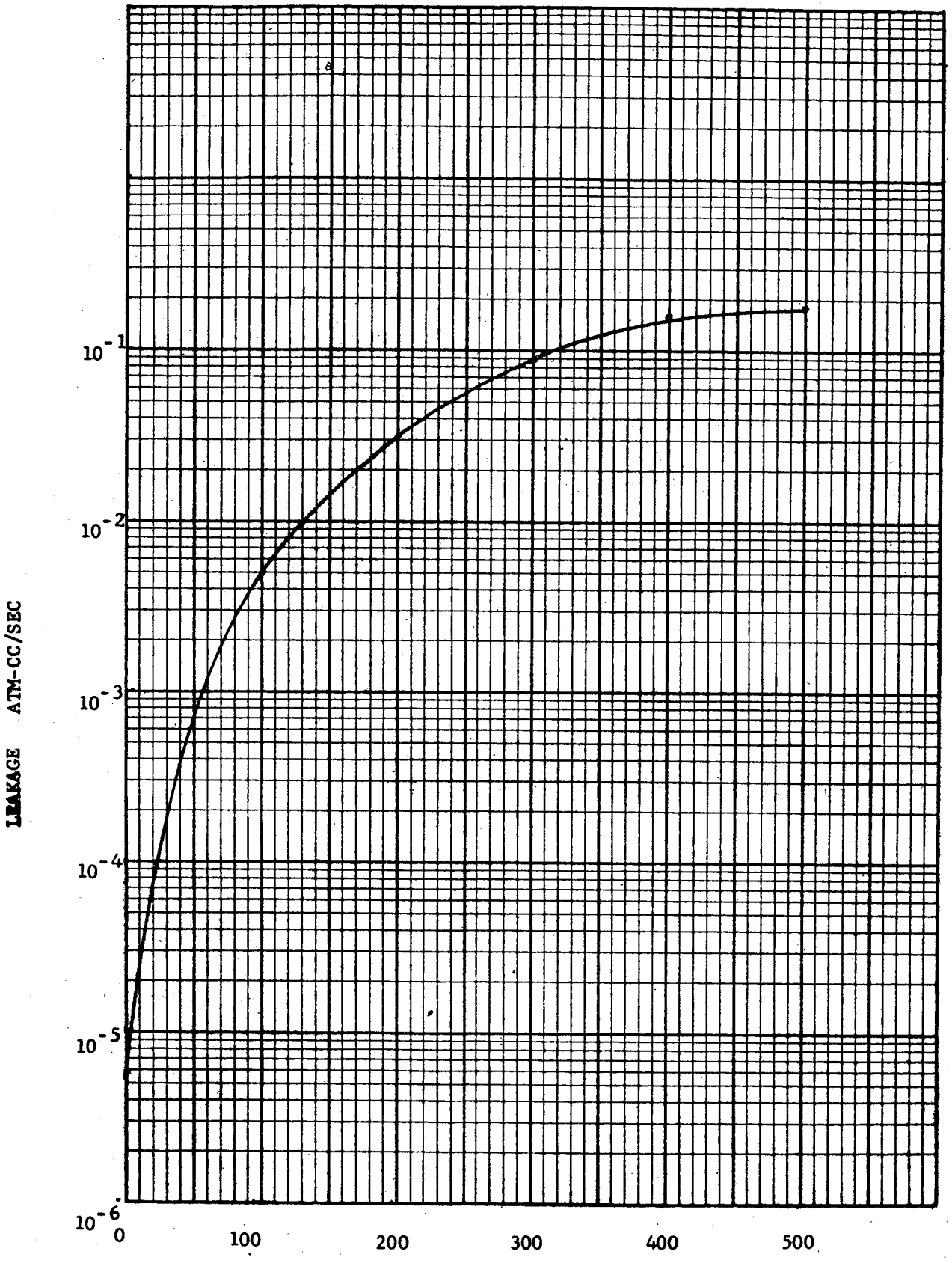

FIGURE 3.10

SPIRAL-WOUND GASKET DEFLECTION TESTS

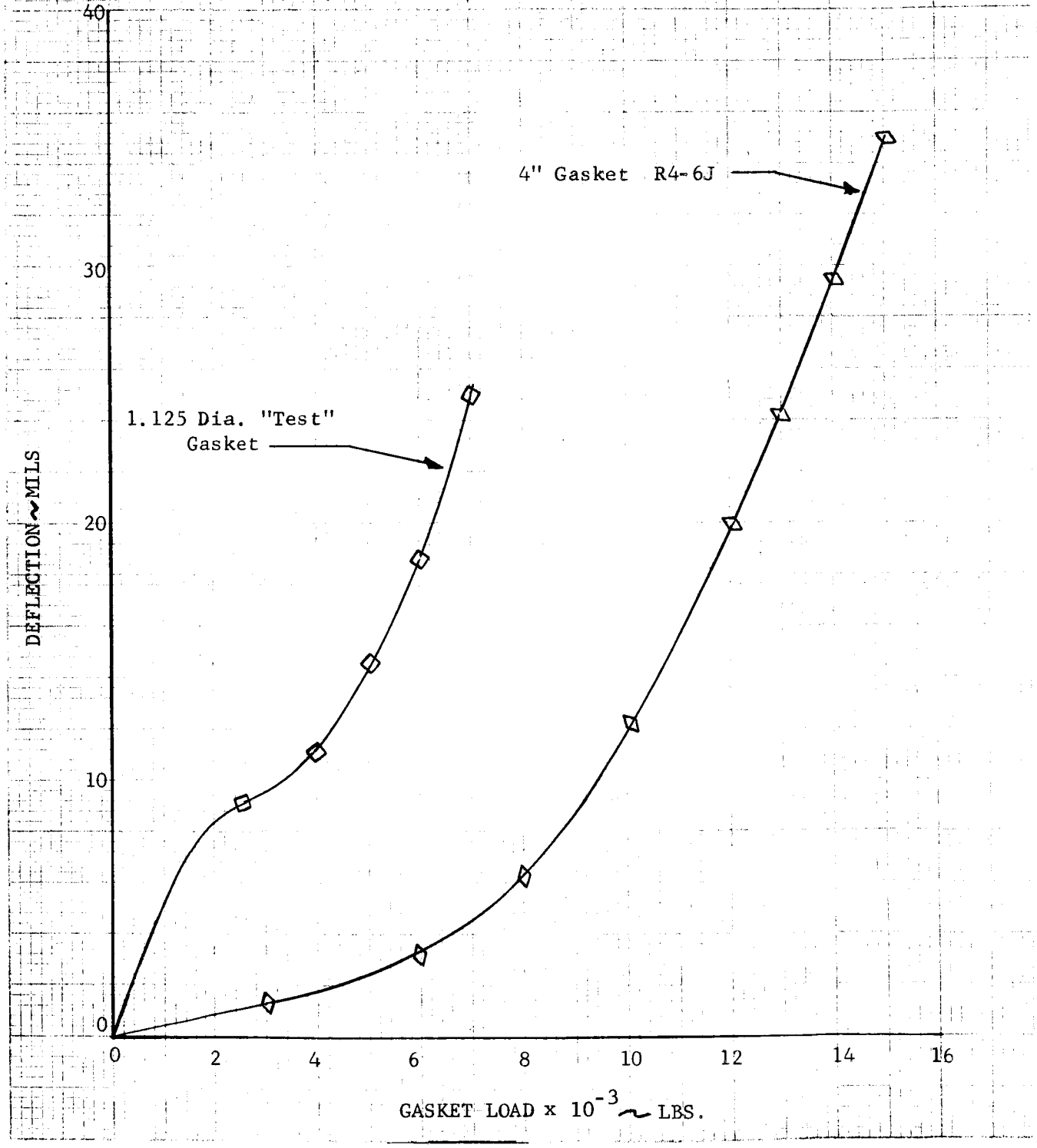

3.9 APPENDIX I (ANALYSIS OF SK20-1061)

3.9.1 Symbols and Nomenclature

a	mean pipe radius - inches
$\bar{a}$	radius to center of gravity of section - inches
c	inner pipe radius - inches
h	pipe wall thickness - inches
ℓ_f	axial length of flange - inches
ℓ_i	axial distance from C.G. of flange to location of Y_i, inches
ℓ_p	axial distance from C.G. of flange to center of pressure load p
r_i, r_k	radial distance to Y_i or X_k - inches
A_f	cross-sectional area of flange - in^2
Ixx	moment of inertia of flange about x-x axis - in^4
M_T	bending moment on flange cross-section - in-lb
X_k	generalized force in the axial direction - lb/in of circum.
Y_i	generalized force in the radial direction - lb/in of circum.
β	$\sqrt[4]{3(1-\nu^2)/\ a^2\ h^2}$
γ	correction factor for thick-walled pipes; $\gamma = \sqrt{1 + .59\ h/a}$
θ	rotation - radians

3.9.2 General Formulae

We consider the connector to have a spiral-wound metal gasket with an asbestos filler as specified in Figure 3.11. The flange performance is studied to determine the relationship between the bolt load, the gasket load and the stress in critical areas.

The treatment can be considered as (1) the determination of the deformation of the flanges, treated as rings free of cross-sectional distortion, (2) the determination of the deformation of the pipe, and (3) the interaction between the pipe and flange.

In Section 42. of Reference 2 we have the following formulae:

The rotation of the flange will be

$$\theta = M_T\ \bar{a}\ /\ EI_{xx}$$

and the stress due to rotation

$$\sigma = M_T\ y\ /\ I_{xx}$$

where

$$M_T = \sum_{1}^{k=K} X_k\ r_k^{\ 2} + \sum_{1}^{i=I} Y_i \ell_i r_i + M\ a + (\ell_f\ p)\ \ell_p c$$

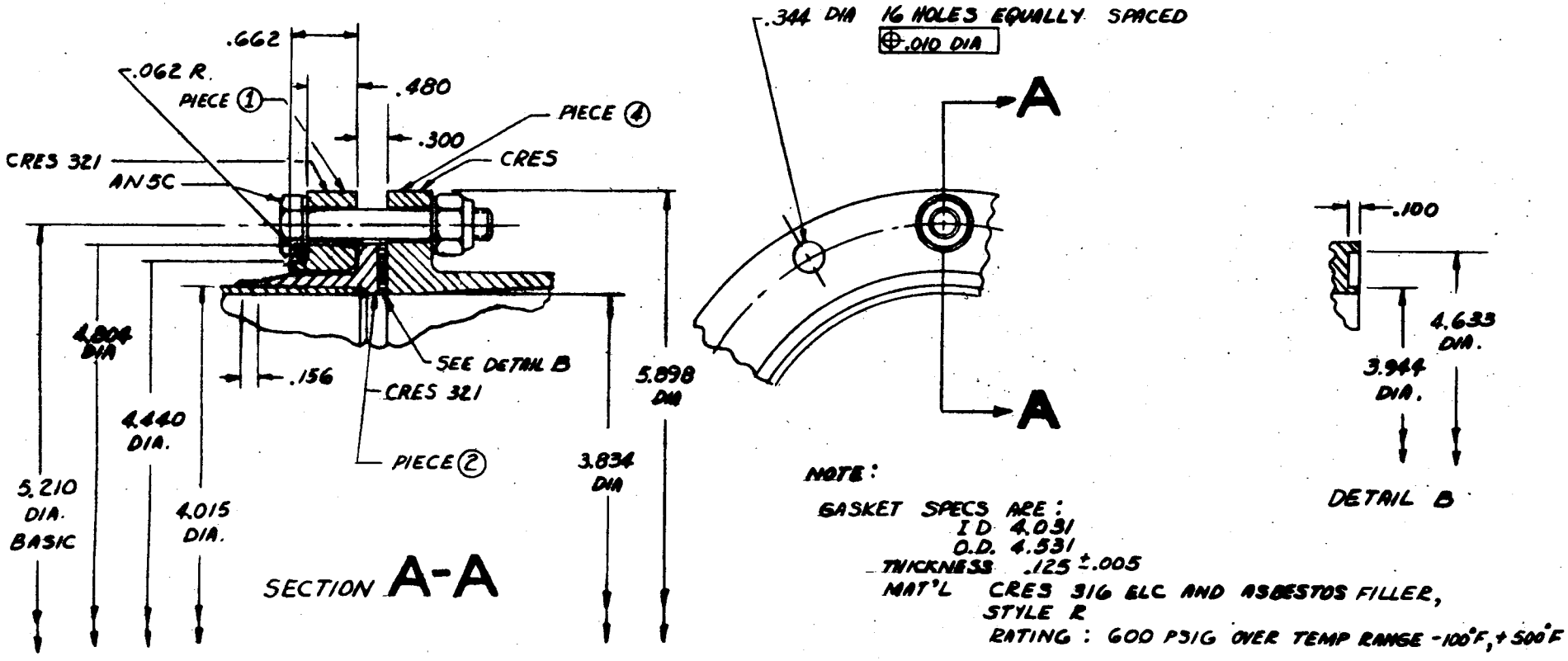

FIGURE 3.11

REPRODUCTION OF SK 20-1061

The deflection and slope of the wall at the end of a long pipe due to pressure and an axisymmetric moment, shear, and tension at the mid-thickness is

$$U_p = (2\,a^2\,\beta^2/Eh)M - \gamma\,(2\,a^2\beta/Eh)Q + (a/Eh)(pa-\nu F)$$

$$\theta_p = -\gamma\,(4\,a^2\,\beta^3/Eh)M + (2\,a^2\,\beta^2/Eh)Q$$

The radial deflection of the flange at its center of gravity is,

$$U_{C.G.} = (\bar{a}\,c\,p\,\ell_f/EA_f) + (\bar{a}/EA_f)\sum_{1}^{i=I} Y_i \quad r_i$$

while the radial deflection at a point axially distant ℓ inches from the center of gravity is

$$U_\ell = U_{C.G.} + \theta\,\ell$$

3.9.3 Floating Ring

Piece ①, of Figure 3.11, has the following properties (neglecting the removal of material at the bolt circle)

$A_f = .404\ in^2$

$I_{xx} = .00905\ in^4$

$\bar{a} = 2.530\ in$

$\ell = .252\ in$

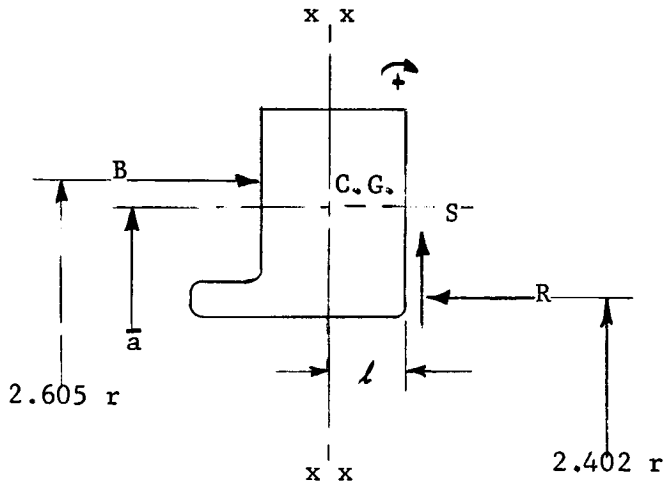

and is under the force system shown if we assume the bolt load to be a line load on the bolt circle and that pc. ① rotates more than piece ② . At a later time we will determine if the direction of the friction force S has been properly assumed.

$$M_T = (2.605)^2 B - (2.402)^2 R - (2.402)(.252)S$$

Using a Young's Modulus of 30×10^6 psi

$$\theta_1 \times 10^6 = \left[2.530/(30)(.00905)\right] M_T \quad \text{or}$$

$$\theta_1 \times 10^6 = 63.4B - 53.9R - 5.64S \tag{1}$$

$$U_1 \times 10^6 = (2.402)(2.530)S/(30)(.404)$$

$$U_1 \times 10^6 = .502S \tag{2}$$

3.9.4 Ferrule*

Piece ② of figure 3.11 has the following properties.

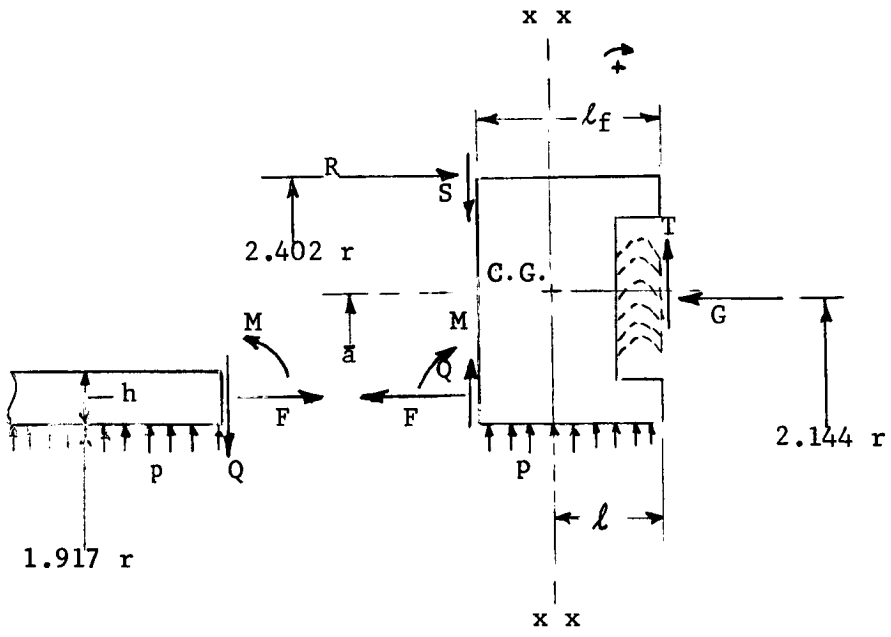

$A_f = .111 \text{ in}^2$

$I_{xx} = .00061 \text{ in}^4$

$\bar{a} = 2.163$ in

$\ell = .181$ in

$\ell_f = .300$ in

$h = .200$ in

*Note: In all following calculations we have assumed the junctures of pipe to flange to act as a solid section.

For the loading we have assumed the friction force, T, to be acting at ℓ from the C.G. and have assumed G to be the total normal force present on the sealing face.

For this loading condition

$$M_T = (2.402)^2R-(2.144)^2G-(2.017)^2F-(2.144)(.181)T-(2.402)(.300-.181)S + (2.017)(.300-.181)Q + 2.017M - (1.917)(.3)(.181-.300/2)p$$

and

$$\theta_2 \times 10^6 = 682R - 545G - 480F - 45.9T - 33.8S + 28.4Q + 238M - 2.11p$$

$$U_2 \times 10^6 = \frac{2.163}{(30)(.111)} \left[(1.917)(.3)p + 2.144T+2.017Q - 2.402S\right]$$

$$U_2 \times 10^6 = .374p + 1.395T + 1.31Q - 1.56S$$

We consider the pipe to be long enough to use the formulae cited in 3.9.2.

$$\beta = \sqrt[4]{\frac{3(1-.3)^2}{(2.017)^2(.2)^2}} = 2.02$$

$$\gamma = \sqrt{1 + .59(.2)/2.017} = 1.03$$

and

$$U_p \times 10^6 = \frac{1}{(30)(.2)} \left[2(2.017)^2(2.02)^2M-(1.03)(2)(2.017)^2(2.02)Q + (2.017)(2.017p - .3F)\right]$$

$$U_p \times 10^6 = 5.53M - 2.82Q + .644p - .101F \qquad (3)$$

with

$$\theta_p \times 10^6 = \frac{(2.017)^2(2.02)^2}{(30)(.200)} \left[-(1.03)(4)(2.02)M + 2Q\right]$$

$$\theta_p \times 10^6 = -23.1M + 5.55Q \qquad (4)$$

At the juncture of pipe and flange their respective rotations and deflections must be equal.

$$U_p = U_2 + (.300-.181)\theta_2$$

$$\theta_p = \theta_2$$

With these two equations we solve for unknowns M and Q in terms of the other forces.

$$M = 1.803G - 2.266R + 1.591F + .1742T + .0873S + .00272p \quad (5)$$

$$Q = 3.12G - 3.92R + 2.74F + .0103T + .478S + .0612p \quad (6)$$

Substituting these values in the expressions for θ_2 and U_2 we get

$$\theta_2 \times 10^6 = 30.6R - 24.34G - 21.54F - 4.072T + .630S + .276p \quad (7)$$

$$U_2 \times 10^6 = 4.09G - 5.14R + 3.59F + 1.406T - .935S + .455p \quad (8)$$

3.9.5 Full Flange

Piece ④ of figure 3.11 has the following properties and the force system shown.

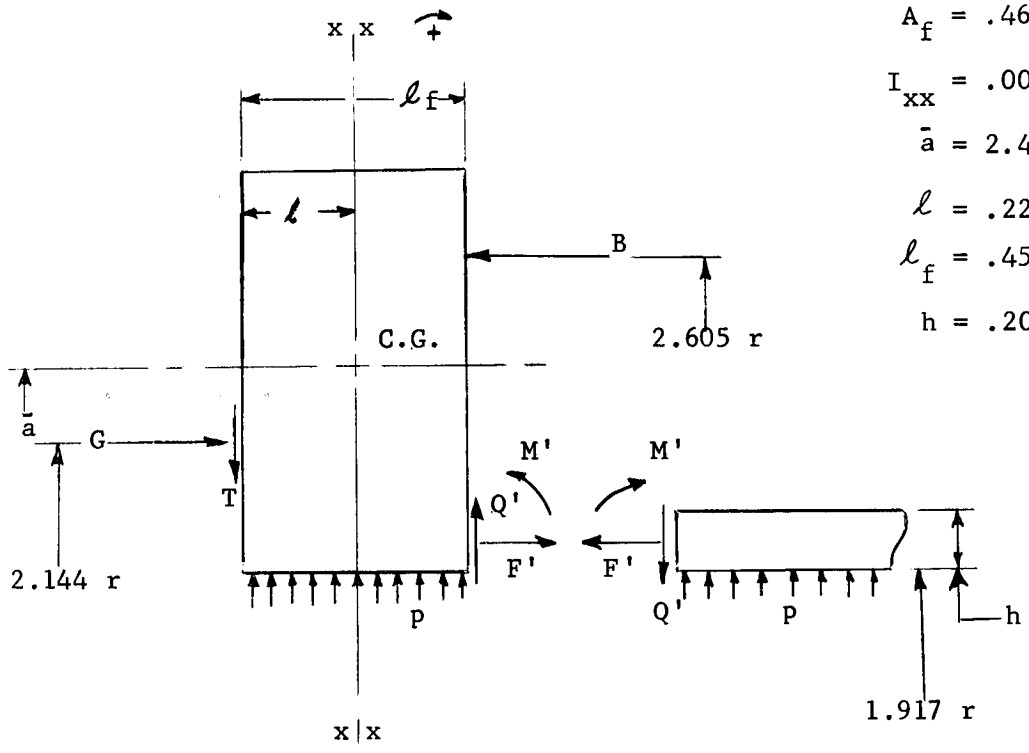

$A_f = .465$

$I_{xx} = .00785$

$\bar{a} = 2.433$

$\ell = .225$

$\ell_f = .450$

$h = .200$

$$M_T = (2.144)^2G+(2.017)^2F' - (2.605)^2B-2.144(.225)T-(2.017)(.450-.225)Q'$$
$$- 2.017M'+(1.917)(.45)(.225-.45/2)p \rightarrow 0$$

$$\theta_4 \times 10^6 = 47.7G + 42.1F' - 70.4B - 20.9M' - 5.01T - 4.71Q'$$

$$U_4 \times 10^6 = \frac{(2.433)}{(30)(.465)} \left[(1.917)(.450)p + 2.017Q' - 2.144T\right]$$

$$U_4 \times 10^6 = .1509p + .352Q' - .3745T$$

For the pipe we obtain the negative of equations (3) and (4) in M', Q', and F'

Similarly at the juncture of pipe and flange

$$U_p = U_4-(.450-.225)\theta_4$$

$$\theta_p = \theta_4$$

We solve for M' and Q' in terms of the other forces.

$$M' = 1.138G - 1.68B + 1.002F' - .1179T + .00218p \quad (9)$$

$$Q' = 2.77G - 4.07B + 2.41F' - .201T + .1171p \quad (10)$$

And the final expressions for θ_4 and U_4 are

$$\theta_4 \times 10^6 = 10.9G - 16.1B + 9.8F' - 1.57T - .598p \quad (11)$$

$$U_4 \times 10^6 = .976G - 1.437B + .85F' - .4454T + .1922p \quad (12)$$

3.9.6 Method of Solution

For the assembly of the connector

$$p = F = F' = 0$$

and from axial equilibrium of pc. ①

$$R = 1.084B$$

from axial equilibrium of pc. ④

$$G = 1.215B$$

We must have two further equations to solve for the frictional forces S and T. The coefficient of static friction for steel on steel was chosen as

.1 and that for the asbestos-steel combination on steel as .2 so that

$$-.1R \leq S \leq .1R \quad \text{and} \quad -.2G \leq T \leq .2G$$

In addition $-.1R < S < .1R$ only if there is no slip at the point of contact between pcs. ① and ② or conversely if we assume no slip at the point of contact such that

$$U_1 - .252\theta_1 = U_2 + .119\theta_2$$

It follows that in the solution if $S \gtrless \left| \pm .1R \right|$ we have made an improper assumption and slip will occur. The value of S is therefore taken to be its maximum value, $\pm .1R$, and the calculation repeated.

The same type of discussion applies to the equations defining the value of T,

$$U_2 - .181\theta_2 = U_4 + .225\theta_4$$

or

$$T = \pm .2G$$

For this case it was found that the conditions

$$S = +.1R; \quad U_2 - .181\theta_2 = U_4 + .225\theta_4$$

resulted in displacements and rotations ($\theta_1 > \theta_2$) that were compatible with the assumptions.

For the condition of 500 psi internal pressure and an ambient temperature of $500^{\circ}F$

$$F = F' = \frac{\pi c^2}{2\pi a} p$$

and from axial equilibrium

$$R = 1.084B$$

$$G = 1.215B - .94F'$$

But even though we assume the bolt to be of the same material as the connector and thereby neglect the effect of ΔT, which would cause increased rotations, there is a change in bolt load due to the change of Young's Modulus for the bolt with temperature.

At assembly the strain in the bolt is

$$e = \frac{2\pi\ (2.605)\ B_o}{16\ A_b\ E} \quad ; \text{ where } B_o = B \text{ of the assembly calculation.}$$

For a 5/16 bolt the shank area is .0767 in^2 and for 321 CRES Young's Modulus is 28.5 x 10^6 psi so that the stretch of the bolt over its grip length is

$$U = \frac{2\pi\ (2.605)(1.23)}{(16)(.0767)(28.5)} \times 10^{-6}\ B_o$$

At 500°F Young's Modulus decreases to 26 x 10^6 psi so that for a load of B

$$U_T = \frac{2\pi\ (2.605)(1.23)}{(16)(.0767)(26)} \times 10^{-6}\ B$$

and the change in bolt length between room temperature and 500°F is

$$\delta_B = \frac{2\pi\ (2.605)(1.23)}{(16)(.0767)} \left[\frac{B}{26} - \frac{B_o}{28.5} \right] \times 10^{-6}$$

or

$$\delta_B = .631 \times 10^{-6}\ (B - .912\ B_o) \qquad (13)$$

Corresponding to this change in bolt stretch is a change in flange rotations such that

$$\delta_B = (2.605\text{-}2.402)(\theta_{1_{initial}} - \theta_1) + (2.605\text{-}2.402)(\theta_4 - \theta_{4_{initial}}) \qquad (14)$$

where $\theta_{1_{initial}}$ and $\theta_{4_{initial}}$ are the θ_1 and θ_4 of the assembly calculation.

Equations (13) and (14) combine to give

$$B = .912\ B_o + .322 \left[\theta_{1_{initial}} - \theta_{4_{initial}} + \theta_4 - \theta_1 \right] \times 10^6 \qquad (15)$$

Again assumptions are made concerning the values of the frictional forces S and T until compatible results are obtained.

For this case it was found that the conditions

$$S = +.1R; \quad U_2 - .181\ \theta_2 = U_4 + .225\theta_4$$

resulted in displacement and rotations that were compatible with the assumptions.

3.9.7 Stresses

Hoop stress in a flange due to radial deflection and rotation is given by

$$\sigma_H = \frac{E}{\bar{a}} \left[\theta \ \ell + U \right] \quad \text{where } \ell = \text{axial distance from C.G.} \tag{16}$$

For a pipe under moment M the meridional bending stress is given by

$$\sigma = 6M/h^2$$

Adding to this the effect of axial tension F (lbs./in)

$$\sigma_p = 6M/h^2 + F/h \tag{17}$$

The results of these calculations are given in Table 3.4 for an assumed initial B of 1500 lb/in.

Table 3.4: Calculations* for SK20-1061

	p=0; T=70°F	p=500 psi; T=500°F
Bolt Load (lb/in)	1500	1420
Gasket Load (lb/in)	1820	1300
$U_1 \times 10^6$ (in.)	81.6	77.4
$U_2 \times 10^6$ "	-716	-574
$U_4 \times 10^6$ "	-489	-390
$\theta_1 \times 10^6$ (radians)	6600	6250
$\theta_2 \times 10^6$ "	4560	5115
$\theta_4 \times 10^6$ "	-4685	4910
M (in-lb/in)	-338	-375
M' (in-lb/in)	-475	-477
θ_{H_1}, Max. hoop stress, pc. ①	30,680	27,150
θ_{H_2}, Max. hoop stress, pc. ②	-20,310	-18,000
θ_{H_4}, Max. hoop stress, pc. ④	-18,050	-16,000
θ_{P_2}, pipe stress	50,700	58,300
θ_{P_4}, pipe stress	71,250	73,900

*Coefficient of static friction, steel on steel, taken as .1
" " " " steel-asbestos on steel, taken as .2

3.10 Appendix II (Redesign of SK20-1061)

3.10.1 Symbols and Nomenclature

Symbols will be used in accordance with section 3.10.1.

3.10.2 General Formulae

The general formulae set forth in section 3.10.1 will be utilized.

3.10.3 Modification of Connector

The first step taken was to change the gasket to a standard size while reducing the gasket load requirement by using a narrower sealing width. The gasket load for the new configuration was estimated to be 34,800 lb. from the test of section 3.1 and manufacturer's data. The gasket O.D. was larger than the original gasket so that in turn the groove outer diameter was increased and the maximum dimension of the ferrule increased by the same amount.

While the anticipated support outside the bolt circle was expected to reduce the stress in the pipe at the base of the full flange it was not expected to appreciably affect the rolling of the ferrule. For this reason the ferrule hub was modified to a taper hub.

The minor diameter of pc. ① must be increased to clear the added hub on pc. ② and the configuration of pc. ① is

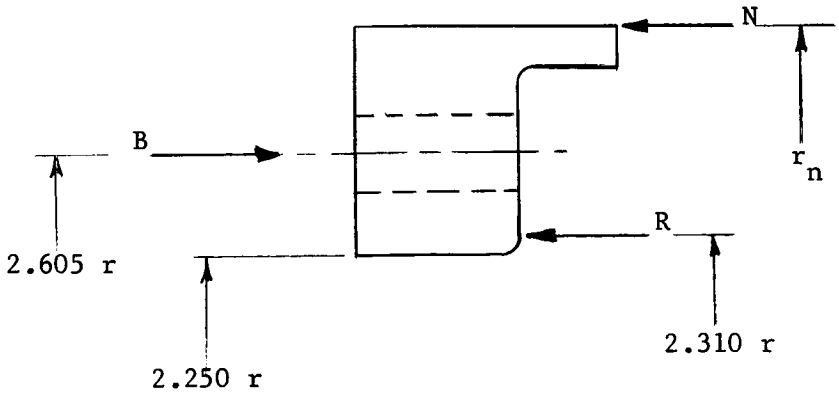

if we assume pc. ② rolls positively with respect to pc. ① and pcs. ① and ④ have line contact at the O.D.

$$\Sigma F = 0 = 2\pi \left[2.605B - 2.310R - r_n N \right] \quad (1)$$

Since the rolling in this type of design will be small; neglecting friction we assume

$$\Sigma M = 0 = (2.605)^2 B - (2.310)^2 R - r_n^2 N \quad (2)$$

and from equations (1) and (2)

$$r_n = \frac{(2.605)^2 B - (2.310)^2 R}{(2.605)B - (2.310)R} \quad (3)$$

For pc. ②

$$\Sigma F = 0 = 2.310R - 2.188G - \frac{(1.917)^2}{2} p$$

The minimum value of G that must be maintained is

$$G = 34{,}800/\pi\ (4.375) = 2{,}530$$

and for an internal pressure p = 500 psi

$$R = 2790$$

The allowable bolt load B_o at 500 psi and room temperature is

$$B_o = (Y.S.)(.9)(A_r) - E\ (\alpha_f - \alpha_b)\ \Delta T\ A_b \quad (4)$$

where

A_r = root area of bolt

α_f = coefficient of thermal expansion of flange (321CRES)

α_b = " " " " of bolt (16 C_r-2 N_i)

A_b = shank area of bolt

$B_o = (80{,}000)(.9)(.058) - (26.5)(9.3-6.5)(430)(.0767)$

$B_o = 4{,}175 - 2{,}440 = 1{,}735$ which is not sufficient to satisfy Eq. (1) for positive N and r_n.

Substituting a 7/16" bolt equations (3) and (4) become

$$r_n = \frac{(2.667)^2 B - (2.310)^2 R}{2.667B - 2.310R}$$

and $B_o = 8,570 - 4,790 = 3,780$

$$B = \frac{3780(16)}{2\pi\ (2.667)} = 3,610$$

which results in $r_n = 3.38$. Admittedly the above calculations are highly speculative but they led to a value of 3.312 being chosen as the flange O.D. and the following analysis is made of the connector shown in dwg. no. 544E538.

3.10.4 Floating Flange

Piece ⑥, of Dwg. 544E538, has the following properties (neglecting the removal of material at the bolt circle).

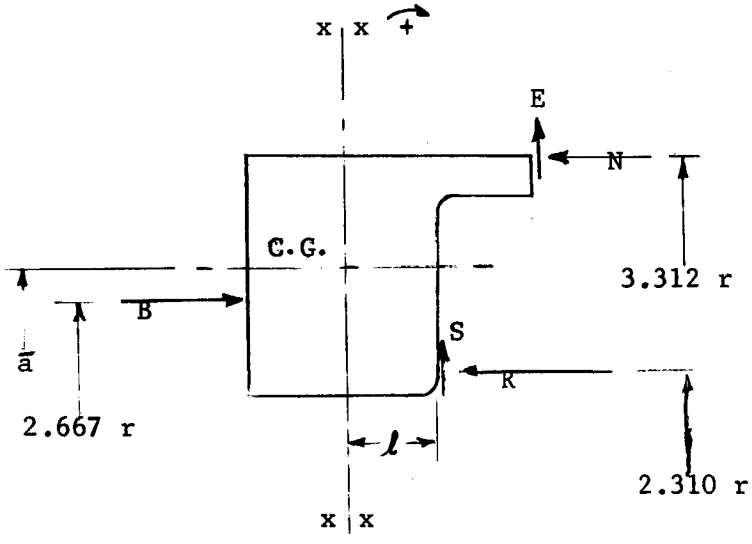

$A_f = .5575$

$I_{xx} = .01682$

$\bar{a} = 2.820$

$\ell = .206$

and is under the force system shown if we assume pc. ⑥ rolls positively with respect to pc. ④ and negatively with respect to pc. ⑤. At a later time we will determine if the direction of the friction forces, S and E, has been properly assumed.

$$M_T = (2.668)^2B - (3.312)^2N - (2.310)^2R - (2.310)(2.06)S - (3.312)(.506)E$$

Using a Young's Modulus of 26×10^6 psi for 321 CRES (at 500°F)

$$\theta_6 \times 10^6 = (2.820)M_T/(26)(.01682) \quad \text{or}$$

$$\theta_6 \times 10^6 = 45.9B - 70.6N - 34.4R - 3.068S - 1.080E \tag{5}$$

$$U_6 \times 10^6 = \frac{2.820}{(26)(.5575)}\left[2.310S + 3.312E\right] \quad \text{or}$$

$$U_6 \times 10^6 = .450S + .645E \tag{7}$$

3.10.4 Full Flange*

Piece ④ of 544E538 has the following properties and the force system shown.

$A_f = .568$

$I_{xx} = .00783$

$\bar{a} = 2.614$

$\ell = .2035$

$\ell_f = .407$

$h = .200$

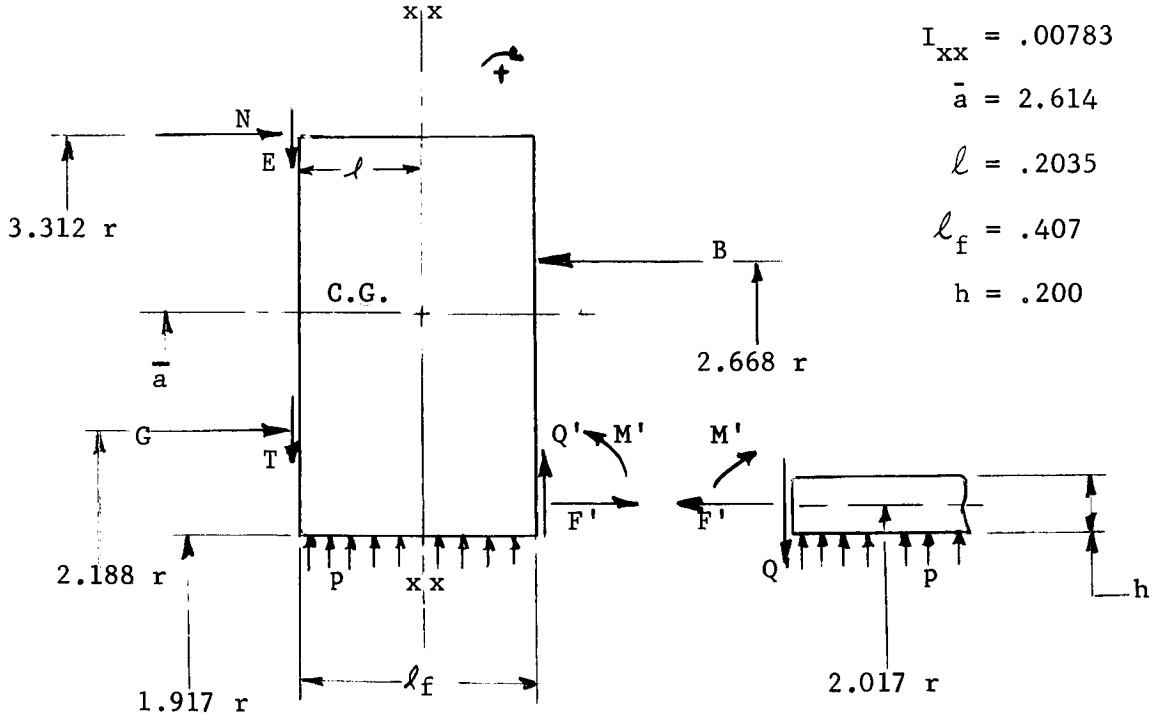

*Note: In all following calculations we have assumed the juncture of pipe to flange to act as a solid section.

whereupon

$$M_T = (2.188)^2G + (2.017)^2 F' + (3.312)^2N - (2.668)^2B - (3.312)(.203)E$$
$$- (2.188)(.203)T - (2.017)(.203)Q' - 2.017M'$$

from which we obtain an expression for θ_4.

$$U_4 = \frac{2.614}{(26)(.568)} \left[(.407)(1.917)p + 2.017Q' - 2.188T - 3.312E\right]$$

For the pipe we obtain the equations used in section 3.9.5 except they are multiplied by (30)/(26) to correct the value of Young's Modulus used previously. At the juncture of pipe and flange

$$U_p = U_4 - (.407-.203)\theta_4$$
$$\theta_p = \theta_4$$

and we solve for M' and Q' in terms of the other forces.

$$M' = 1.235G + 2.827N - 1.839B - .1127T - .1708E + 1.048F' + .00285p \quad (8)$$

$$Q' = 2.97G + 6.79N - 4.415B - .1919T - .2910E + 2.495F' + .1301p \quad (9)$$

and the final expressions for θ_4 and U_4 are

$$\theta_4 \times 10^6 = 13.85G + 31.75N - 20.64B - 1.772T - 2.683E + 11.93F' - .7567p \quad (10)$$

$$U_4 \times 10^6 = 1.06G + 2.424N - 1.575B - .4557T - .690E + .8901F' + .1844p \quad (11)$$

3.10.5 Ferrule*

Piece ⑤ of 544E538 has the following properties

$A_f = .1274$

$I_{xx} = .000823$

$\bar{a} = 2.163$

$\ell = .170$

$\ell_f = .300$

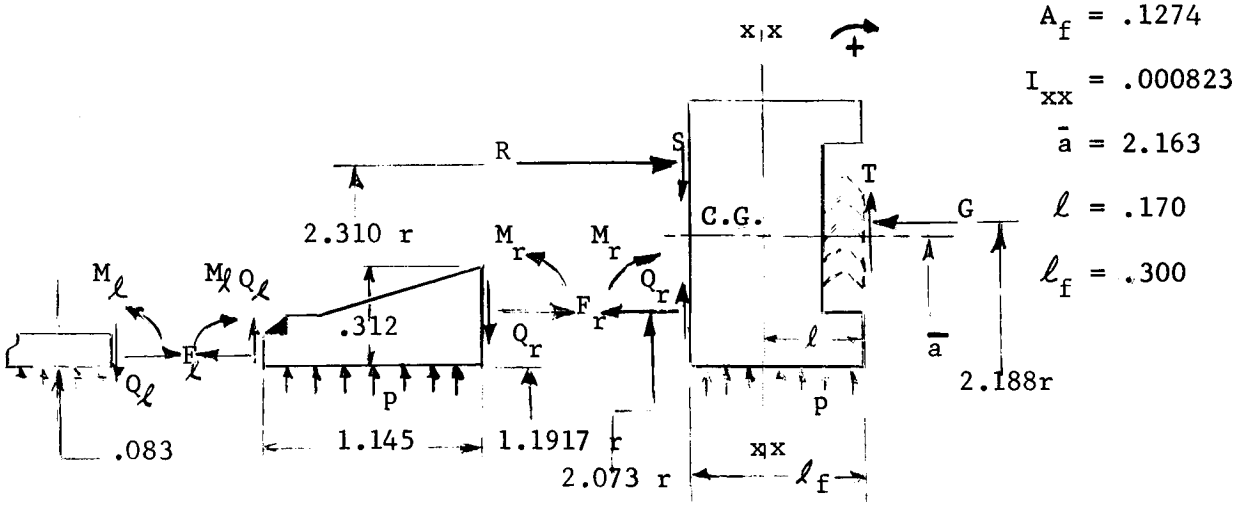

*Note: In all following calculations we have assumed the juncture of pipe to flange to act as a solid section.

C-2

For the loading we have assumed the friction force, T, to be acting at ℓ from the C.G. and have assumed the total normal force on the sealing face to be located at G.

The formulae of 3.9.2 provide the deflection and rotation of the pipe section caused by M_ℓ , Q_ℓ , F_ℓ , and p

$$E\theta_p = 941\ Q_\ell - 6{,}140\ M_\ell \tag{12}$$

$$E\ U_p = 941\ M_\ell - 298.6\ Q_\ell - 7.08\ F_\ell + 45.25p \tag{13}$$

For the flange section

$$E\ \theta_5 = 14{,}020R - 12{,}580G - 977.5T - 789.5S - 30.23p + 5{,}450\ M_r + 708\ Q_r - 10{,}670\ F_\ell$$

$$E\ U_5 = 37.15T - 39.2S + 35.2\ Q_r + 9.76p$$

A computer program for shells of revolution (No. L-24700) was used to obtain influence coefficients (C_i) for the taper hub. For example the rotation at the right end of the taper hub is expressed as

$$\theta_r = C_1\ M_\ell + C_2\ Q_\ell + C_3\ M_r + C_4\ Q_r + C_5\ F_\ell + C_6\ p$$

The problem then became one of matching deflections and rotations of the pipe, hub, flange system with the resulting expressions

$$Q_r = -3.055R + 2.75G - .062T + .462S + 2.252F_\ell + .0038p \tag{14}$$

$$M_r = -2.087R + 1.872G + .1729T + .0884S + 1.595F_\ell + .00788p \tag{15}$$

$$Q_\ell = -.142R + .129G + .03405T - .01745S + .0642F_\ell + .0223p \tag{16}$$

$$M_\ell = .0005R - .0005G + .00280T - .003025S - .00705F_\ell - .00149p \tag{17}$$

$$\theta_5 \times 10^6 = 18.38R - 16.59G - 3.05T + .731S - 14.66F_\ell + .591p \tag{18}$$

$$U_5 \times 10^6 = -4.135R + 3.723G + 1.346T - .882S + 3.048\ F_\ell + .3805p \tag{19}$$

3.10.6 Method of Solution

From axial equilibrium of pc. ⑥ and pc. ⑤

$$0 = 3.312N + 2.310R - 2.668B$$

$$0 = 2.310R - 2.188G - 1.958\ F$$

and

$$F_\ell = \frac{(1.917)^2}{(2)(1.958)} p = .939p$$

so that

$$R = .947G + .795p \tag{20}$$

$$N = .806B - .661G - .554p \tag{21}$$

As described in section 3.9.6 we have three additional equations we can write to define the values of S, T, and E.

$$U_1 - .206\theta_1 = U_2 + .130\theta_2 \text{ with } -.1R < S < .1R \quad \text{or } S = \pm .1R$$

$$U_1 - .506\theta_1 = U_4 + .2035\theta_4 \text{ with } -.1N < E < .1N \quad \text{or } E = \pm .1N$$

$$U_2 - .170\theta_2 = U_4 + .2035\theta_4 \text{ with } -.2G < T < .2G \quad \text{or } T = \pm .2G$$

Because of the addition of the force N to the system there must be an additional equation. This results from a consideration of compatible rotations of the members.

If the body shown rotates through a small angle θ the point I moves to the right a distance d (1-cosθ) and the point P moves a distance of $\ell\sin\theta$ to the left with respect to I so that the total motion of P is

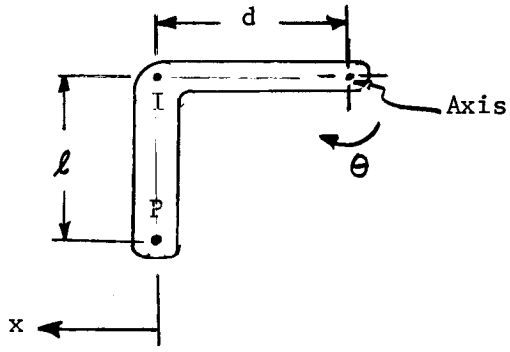

$$X = \ell\sin\theta - d\ (1-\cos\theta)$$

For small θ; $x = \ell\theta$

Now considering the sketch below if contact is to be maintained at the points designated then

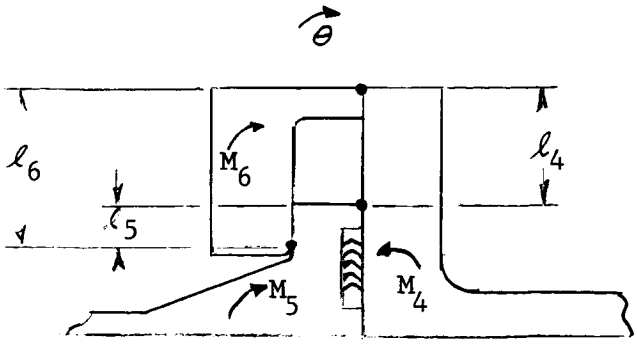

$$\ell_6\,\theta_6 = \ell_5\,\theta_5 + \ell_4\,\theta_4$$

and our desired equation is

$$1.002\theta_6 = .1150_5 + .887\theta_4 \tag{22}$$

This system of equations can be solved in terms of B for p=0 and room temperature under condition that

$$-.1R < S < .1r; \quad -.2G < T < .2G; \quad E = -.1N$$

We designate the load per inch at the bolt circle under this no load condition as B_o. Under an internal pressure p there will be some change in the rotations of the flanges which will combine with a change in bolt load per inch to B such that a static equilibrium is maintained. If there is a change in θ_6 of $\Delta\theta_6$ and a change in θ_4 of $\Delta\theta_4$ there will be a corresponding change in the strain in the bolt of

$$\Delta e = \frac{(3.312-2.668)(\Delta\theta_6-\Delta\theta_4)}{\ell_b}$$

where ℓ_b is the grip length of the bolt.

This change in strain corresponds to a change in bolt stress and bolt load per inch of

$$\Delta B = \frac{(N_b)(A_b)E\ \Delta\ e}{2\pi\ (2.668)}$$

where N_b = number of bolts

A_b = shank area of bolt

and the resultant bolt load is

$$B = B_o + \frac{(16)(.150)(26)(.644)(\Delta\theta_6-\Delta\theta_4)x10^6}{2\pi\ (2.668)(1.230)}$$

or

$$B = B_o + 1.95\ (\Delta\theta_6 - \Delta\theta_4)\ x\ 10^6 \qquad (23)$$

This system of equations can now be solved under the condition that the minimum gasket load, 2530 lb/inch must be maintained (in our calculations the gasket load maintained was 2575 lb/inch) and numerical substitution can be made in the first case of p=0. The conditions that satisfied the pressurized case were again

$$-.1R < S < .1R; \quad -.2G < T < .2G; \quad E = -.1N$$

For the calculations at 500 psi and 500°F the general equations were revised so that the forces acting on the sealing face were as shown in the sketch.

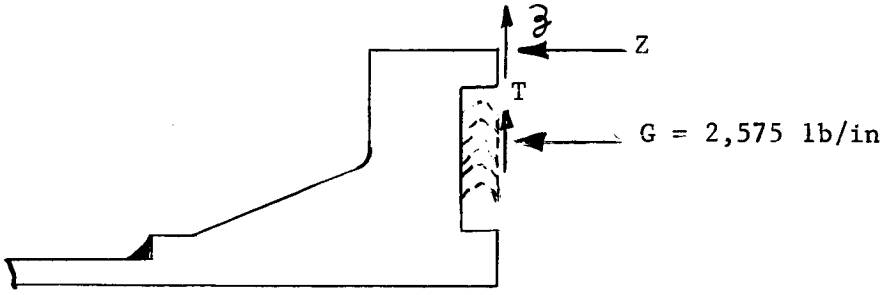

In addition equation (23) was revised to include temperature effects.

The change in length of the bolt from the unloaded condition at room temperature to the loaded condition at high temperature is given by

$$\delta_b = \frac{2\pi\, r_b\, \ell_b}{A_b\, N_b\, E_{500^o}} \left[B - B_o \left(\frac{E_{500^o}}{E_{70^o}} \right) \right] + \alpha_b\, \ell_b\, \Delta T$$

This may also be written in terms of the thermal expansion and rotation of the flanges;

$$\delta_b = .644\, (\Delta\theta_6 - \Delta\theta_4) + \alpha_f\, \ell_f\, \Delta T$$

For $\alpha_f = 9.3 \times 10^{-6}$ in/in-°F (321 CRES)

$\alpha_b = 6.5 \times 10^{-6}$ in/in-°F $(16\, C_r - 2\, N_i)$

$$B = 8{,}275 + 1.95\, (\Delta\theta_6 - \Delta\theta_4) \times 10^6 \qquad (24)$$

Equation (24) replaces (23) in the set of equations and solution is achieved by proper assumptions of S, T, $\mathcal{Z}$, and E. The solution was obtained assuming

$$-.1R < S < .1R; \quad -.2G < T < .2G; \quad E = .1N; \quad -.1Z < \mathcal{Z} < .1Z$$

3.10.7 Stresses

Stresses were evaluated by equations (16) and (17) of section 3.9.7;

$\sigma_H = \frac{E}{a} \left[\theta \ell + U\right]$ and

$\sigma_p = 6M/h^2 + F/h$

The results of these calculations are given in Table 3.5 for an initial B of 3,800 lb/in which will maintain a minimum gasket load, G, of 2575 lb/in.

Table 3.5: Calculations* for E-544E538

	p = 0 T = 70°F	p = 500 psi T = 70°F	p = 500 psi T = 500°F
Bolt Load (lb/in)	3,800	4,010	7,045
Gasket Load (lb/in)	2,838	2,575	2,575
$U_6 \times 10^6$ (in.)	-157	-149	12
$U_5 \times 10^6$ "	-131	-76	27
$U_4 \times 10^6$ "	-104	-46	34
$\theta_6 \times 10^6$ (radians)	-1,070	-1,585	-518
$\theta_5 \times 10^6$ "	1,580	1,936	687
$\theta_4 \times 10^6$ "	-1,450	-2,040	-627
M_ℓ (in-lb/in)	##	-2.88	-3.85
M_r (in-lb/in)	-278	-300	-125
M' (in-lb/in)	-220	-156.3	-42
$\theta_{P_{5\ell}}$, pipe stress, psi	##	8,200	9,100
$\theta_{P_{5r}}$, pipe stress, psi	17,100	20,000	9,200
θ_{P_4}, pipe stress, psi	33,000	25,700	8,600

* Coefficient of static friction, steel on steel, taken as .1
" " " " , steel-asbestos on steel, taken as .2

3.11 References

1. Unfired Pressure Vessels, A.S.M.E. Boiler and Pressure Vessel Code,Section VIII, 1959 Edition

2. Design Criteria for Zero-Leakage Connectors for Launch Vehicles, Vol. 4, NASA Contract NAS 8-4012, Final Report for First Contract Period, General Electric Co., Schenectady, New York, 1963.

3. George C. Marshall Space Flight Center drawing numbers SK20-1061 and A-10438409.

4. THE DESIGN, FABRICATION, INSTRUMENTATION AND TESTING OF THE TWELVE INCH CRYOGENIC FLANGE CONNECTOR

by
B.T. Fang and A.J. Martenson

4.0 Summary

In this section the design, fabrication, instrumentation and testing of the 12 in. cryogenic flange connector is described. Test results are compared with theoretical predictions. Any significant experience encountered during the process is also noted.

4.1 Introduction

For certain space applications, pipes as large as twelve inches in diameter are used to carry cryogenic fluids. The design of adequate connectors for this piping presents some problems because of the large diameter and low temperature environment. A twelve inch flanged connector was designed according to the principles established in NASA Contract NAS 8-4012. This connector was built and tested under simulated operating conditions in order to establish the usefulness and validty of the theoretical analysis. Good agreement was obtained. In the following sections, the process of design, fabrication and instrumentation of the connector are discussed; comparisons are made between the test result and theoretical predictions.

4.2 Design

The connector is designed in accordance with the following specified design conditions:

1. Tubes to be connected:
   Inside diameter = 12 in.
   One tube made of 2024T4 aluminum alloy, 0.323 in. thick
   One tube made of 347 stainless steel, 0.062 in. thick

2. Pressure:
   Operating pressure = 200 psi
   Proof pressure = 300 psi

3. Temperature:
   Liquid nitrogen temperature (normal boiling point - 321^{o}F)

4. External load:
   48,000 lb-in moment at operating pressure

Operating pressures above 200 psi may occur for some applications of large cryogenic connectors. However, it was felt that a test flange designed for 200 psi would be adequate for checking the validity of the theoretical analysis.

The design considers the use of an asbestos gasket which is impregnated with a highly viscous and LOX insensitive lubricant. Its thickness is 1/16 inch. The initial load in the flange bolts must produce a gasket stress of 3360 psi. According to tests run at ATL, this initial gasket stress is needed to produce a good seal. Once the seal has been established, it can be maintained with lower gasket stresses. The gasket factor for the impregnated asbestos gasket can be taken as 2.75 in accordance with the ASME code. Our design criteria then became:

1. The initial bolt load should compress the gasket to a seating stress of 3360 psi.

2. A minimum gasket stress of 2.75 times the internal fluid pressure shall be maintained under all loading and temperature conditions.

3. No over-stressing and over-straining of structural components should occur under the above conditions.

4. Minimum weight should be attained.

Detailed design procedure is given in Appendix I (section 4.9), in which basic design principles are emphasized so that the procedures outlined have wide applicability.

The connector actually fabricated and tested corresponds to the drawings in Appendix V (section 4.13). This was made somewhat more conservative than the optimum design connector given in Appendix I. The compromise was made

because of expediencies in testing and because we wanted to insure no catastrophic failure would destroy the planned test.

4.3 Test Fixture

The drawings for the test fixture are given in Appendix V (section 4.13). A schematic diagram for the test set-up is shown in Figure 4.1.

The dewar is made of stainless steel sheet and polystyrene foam insulation. Outside of the test connector is a vacuum enclosure. Any gas that leaks out of the test connector is collected in the vacuum chamber and pumped to the mass spectrometer leak detector. Because of the necessity of assembling the test connector and because of the poor weldability of the 2024T4 aluminum flange, the vacuum enclosure is composed of several separate pieces. Bolted connections with indium wire gaskets are used to secure these pieces together. These connections proved to be vacuum tight at room temperature but leaked at liquid nitrogen temperature. The trouble was traced to the uneven gasket compression and was remedied by doubling the number of bolts and adding a thick flange ring. Notice in the drawing that there are two large size bolts going through the aluminum flange. Tightening the bolt on the left tends to push the flanges apart while tightening the bolt on the right tends to pull the flanges together. This simulates a moment loading on the connector. The magnitude of the moment loading was measured with strain gages mounted on these bolts. It was anticipated that tightening the bolts might become a problem at liquid nitrogen temperature because of differential thermal expansion, and maximum tolerances at the threads were called for. Unfortunately, it was found later that tightening of bolts was still not possible at liquid nitrogen temperature. It was necessary to tighten the bolts at room temperature before dipping the fixture into the liquid nitrogen bath. This, of course, changed the magnitude of the moment load somewhat, but strain gage readings indicated that the change was small. Another unfortunate happening was that galling of the stainless steel threads made the bolt on the right inoperative for the initial tests. As result, the effect of the external moment had to be simulated with an equivalent tensile load in the flange produced by the left-hand side bolt alone.

4.4 Instrumentation

The instrumentation is also shown in Figure 4.1. The leakage rate was measured by a mass spectrometer leak detector. Depending on the "cleaniness" of the system, leakage rates down to 10^{-9} atm cc/sec could be measured. For our system, the maximum sensitivity was 10^{-8}. However, a 10^{-9} leak could still be detected even though its exact value could be in error by a few hundred percent. A calibrated pressure gage was used to measure the helium pressure in the test connector. The temperature was monitored by a copper-constantan thermocouple soldered to the less conductive stainless steel flange. Eight out of the twenty-four 2024T4 aluminum bolts used to tighten the connectors were instrumented with iso-elastic strain gages by the Strainsert Company in Bryn Mawr, Pa. These instrumented bolts were evenly spaced around the flange circumference and gave a good indication of the total bolt load from initial tightening to the operating conditions. In addition to the instrumented bolts, strain gages were attached to critical areas on the flanges to measure the rotations of the flanges and the stresses in the flanges. Three sets of gages were located at 120^{o} apart circumferentially. It was hoped that by taking the averages of these readings we would be able to reduce any non-axisymmetrical loading effect because of uneven bolt loading. The exact locations of all the gages are given in Appendix VI (section 4.14). It was decided that it would be

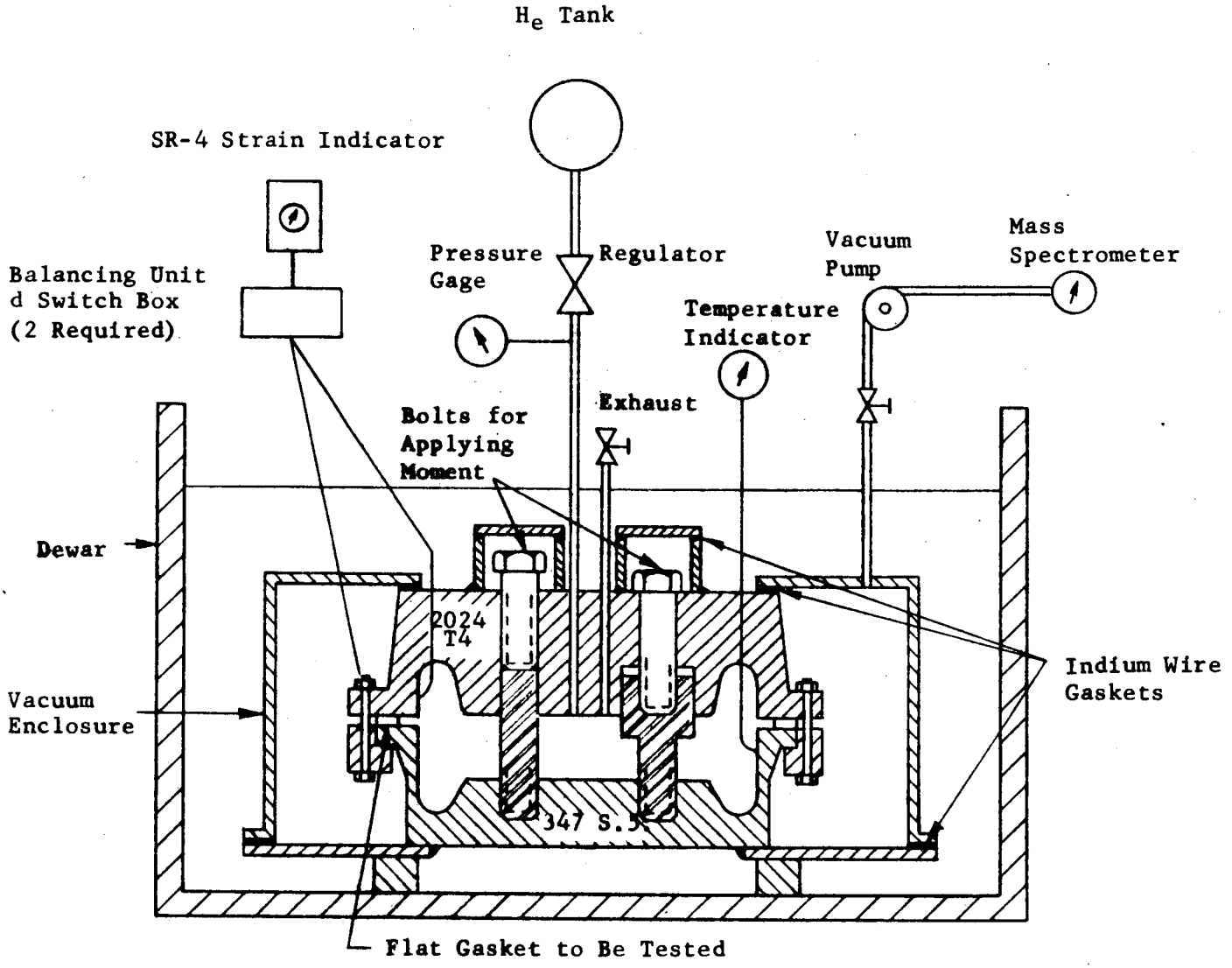

Figure 4.1 Schematic of Test Setup

desirable to obtain some strain reading at cryogenic temperature even though most of the strain readings we need can be obtained at room temperature. Therefore, Nichrome-V foil gages were used (with the exception of the eight bolts instrumented by the Strainsert Company) on account of their stability and consistency at cryogenic temperatures*. All gage lengths were 1/8 inch. Temperature compensation was provided by dummy gages with all lead wires cut to the same length. It was found later during the test that the iso-elastic strain gages used in the eight bolts not only gave unreliable strain reading at cryogenic temperature but were also very susceptible to mechanical failure under the combined thermal and loading test environment. At the end of the test two out of the eight gages had failed.

The many wire leads for the strain gages and thermocouple leading out of the test connector and vacuum enclosure had to be sealed against leakage under the test pressure and temperature. This presented quite a problem, particularly because of the poor weldability of the 2024T4 aluminum flange through which the wire leads went out. At first, it was planned to use Conax thermocouple glands, with lava seals, which were claimed to provide good sealing down to cryogenic temperatures. For bonding the stainless steel thermocouple gland to the aluminum flange, a special cryogenic temperature cement was used. The bond held up well, but the lava seal itself would not seal at all; not even at room temperature. Finally glass-to-metal seals, very much like the vacuum tube base, were used with stripped lead wires soldered to the connecting pins. The seal was vacuum tight but a different problem was present. After each test at the cryogenic temperature, moisture condensed at the seal and shorted the electrical connections. The moisture would not evaporate by itself for days and had to be baked out. Finally, a moisture protecting potting material (polyurethane) was deposited at the electrical terminal which solved the difficulty of water condensation. Photographs of the test fixture in various states of assembly are shown in Figures 4.2 to 4.4. Figure 4.2 shows the sealing surfaces of both the upper and lower flanges. In Figure 4.3, the two flanges are assembled with the gasket in place but the bolts have not yet been installed. Provisions for leading instrumentation wires out of the sealed chamber can be seen and the two columns used to apply a mechanical moment to the flanged connection are evident. Figure 4.4 shows the complete assembly with the vacuum chamber in place. The split ring shown in Figure 4.4 was used to position the shear "O" ring seal when it was tested with this fixture. It was found that the split ring assembling device was necessary for shear rings of large diameter since it assured proper seating of the shear ring in the two grooves provided in the flanges.

* A. Kaufman, "Investigation of Strain Gages for use at Cryogenic Temperatures," presented at Soc. for Exp. Stress Analysis Meeting, May 8-10, 1963.

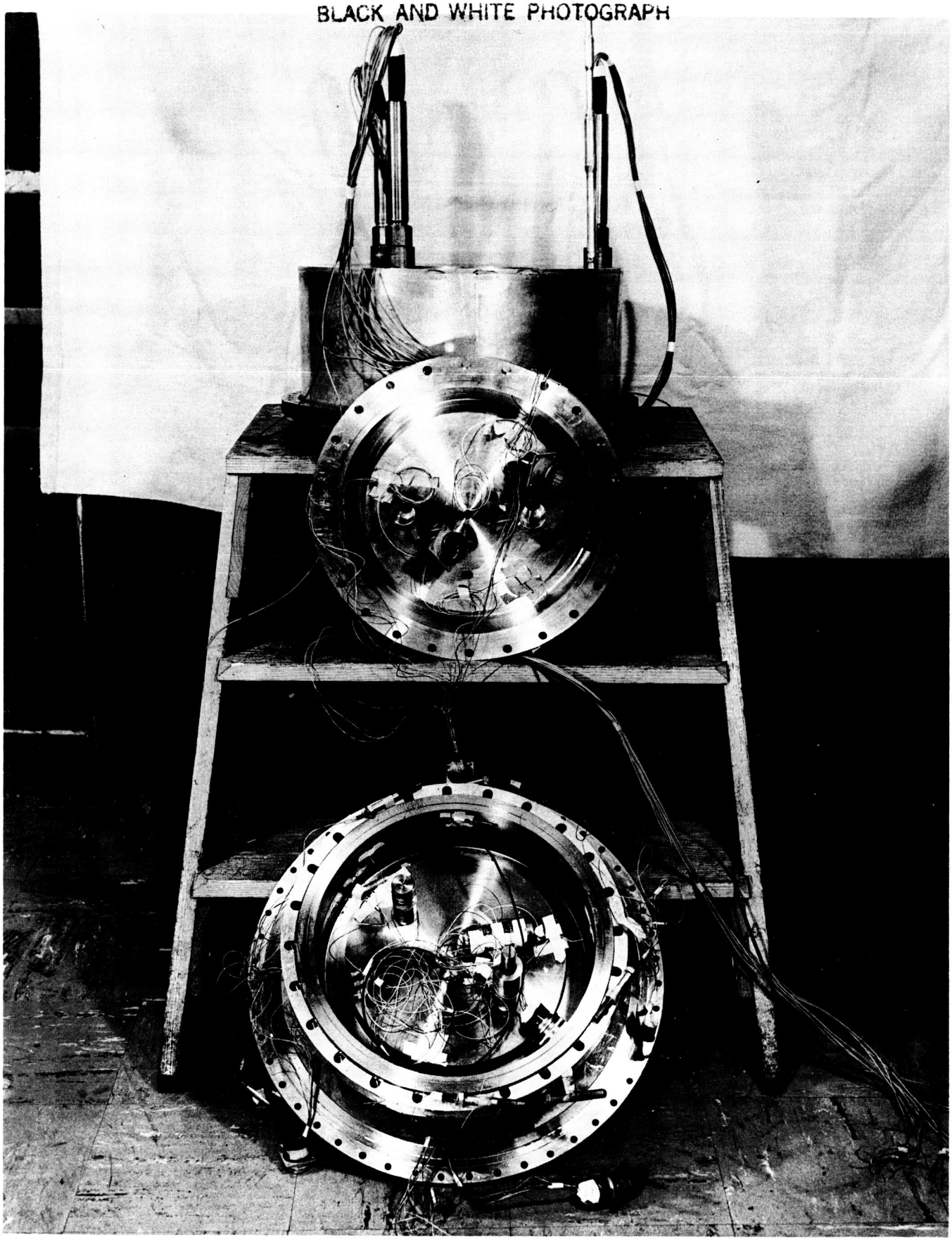

FIGURE 4.2

TWELVE INCH FLANGE TEST FIXTURE DISASSEMBLED

ORIGINAL PAGE
BLACK AND WHITE PHOTOGRAPH

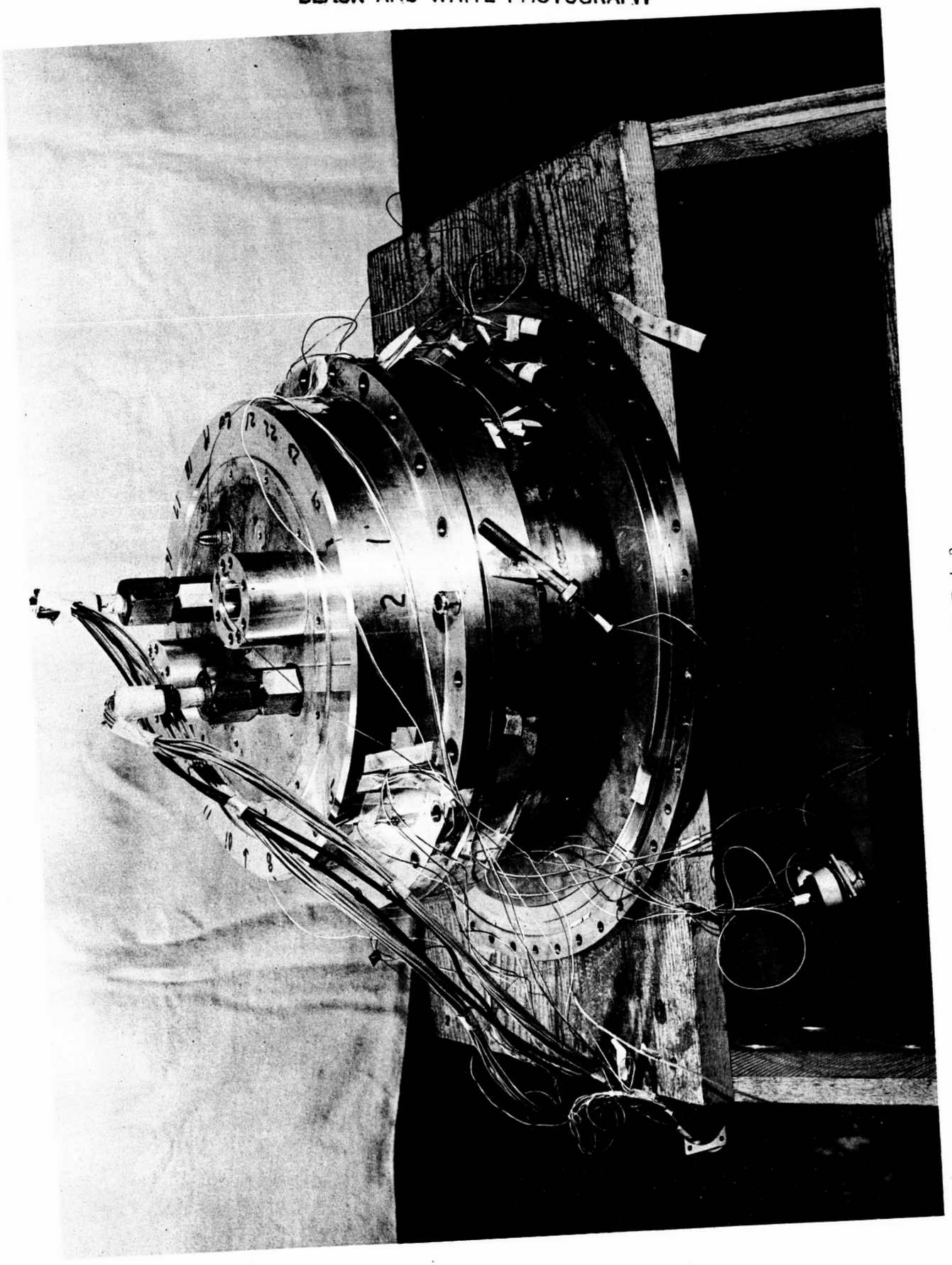

FIGURE 4.3
TWELVE INCH FLANGE TEST FIXTURE
ASSEMBLED BUT WITHOUT VACUUM CHAMBER

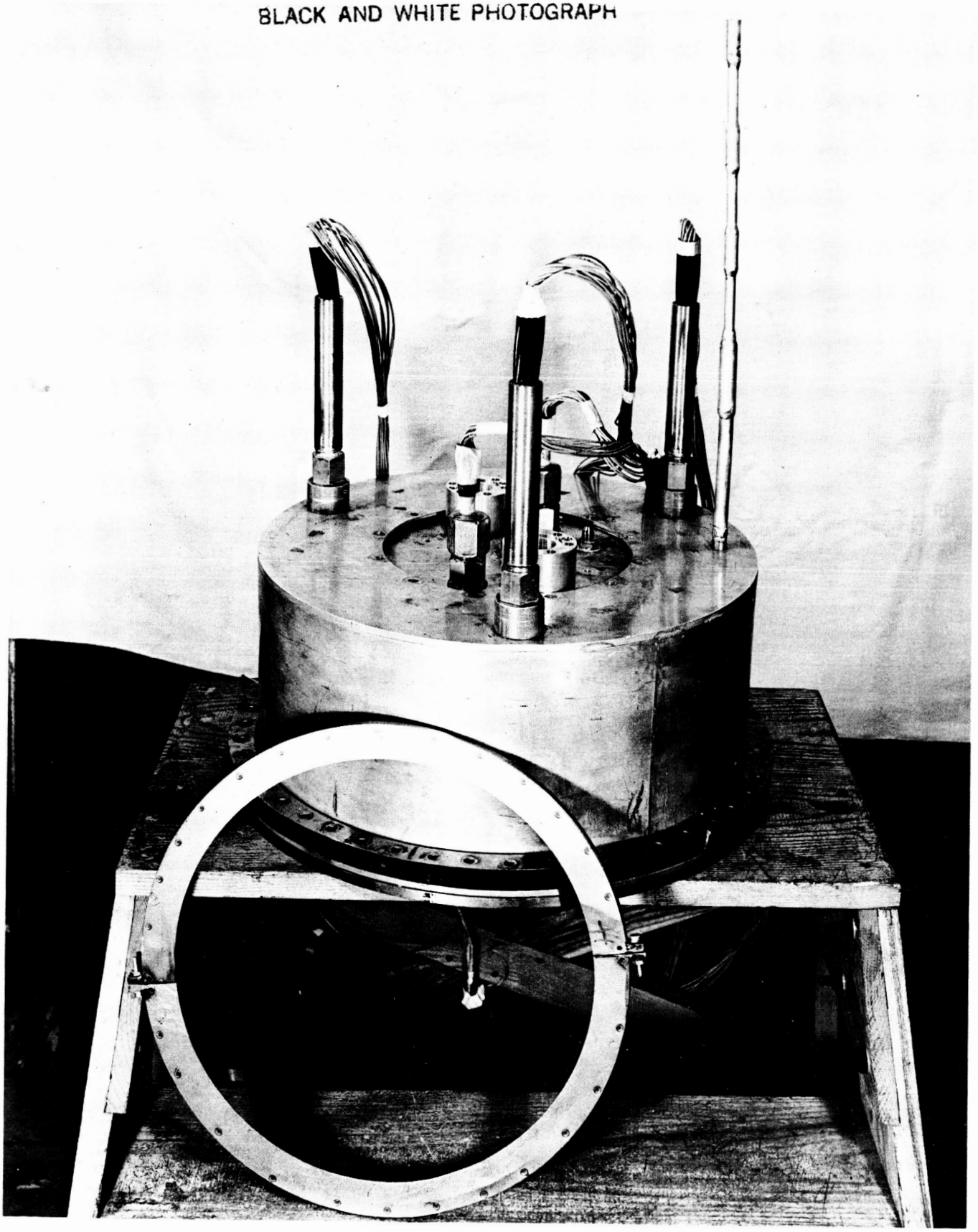

FIGURE 4.4

TWELVE INCH FLANGE
WITH VACUUM CHAMBER IN PLACE

4.5 Description of Gaskets Tested

1. Impregnated Asbestos Gaskets

   These gaskets have the following dimensions:

   13.55 in. O.D., 12.80 in. I.D., 0.062 in. thickness. They are treated for compatibility with LOX. After being compressed, part of the impregnated fluid was squeezed out. The fluid appeared dark and viscous and there was no way to determine whether or not it helped or hindered the sealing ability of the gasket.

2. LOX Grade KEL-F Gaskets

   These gaskets had the same dimensions as the asbestos gaskets.

3. Annealed Copper Shear O-Ring

   The annealed copper, shear O-ring had a mean diameter of 12.600 inches. It had a solid round cross-section with a cross-sectional diameter of $.060 \pm .003$ in.

4.6 Test

The test was to simulate the environmental conditions existing in a 12 in. LOX interconnector line. Pressurized helium gas simulated the operating pressure and also served as tracer for leakage measurements. A liquid nitrogen bath simulated the cryogenic environment of the liquid oxygen. The external moment was simulated by push-pull bolts. The test fixture and instrumentation were explained in the preceding section.

The primary objectives of the test were to measure the leakage rates at the simulated operating condition and to obtain stress and strain data in the structural components for comparison with theoretical analysis. The three kinds of gaskets described in section 4.5 were installed in the test connector, tested at room temperature, with and without a 48,000 in-lb moment and at liquid nitrogen temperature under the same conditions. Internal pressure ranged from 0 psig to 200 psig.

For a detailed, step-by-step test procedure, see Appendix VI (section 4.14).

4.7 Summary of Test Data and Comparison with Theoretical Result

4.7.1 Measured Leakage Rates

Gasket Type	Internal Pressure psig	Temperature °F	External Moment in-lb	Leakage rate atm cc/sec.
Impregnated Asbestos	200	79	0	10^{-8}
			48,000	10^{-8}
		-321	0	10^{-8}
			48,000	10^{-2}
LOX Grade KEL-F	200	79	0	10^{-6}
			48,000	10^{-6}
		-321	48,000	Excessive (see Note d)
Annealed Copper Shear O-Ring	200	86	0	10^{-8}
			48,000	10^{-8}
		-321	48,000	10^{-6} (see note e)

Notes:

a. All gaskets were assembled with an initial pre-load of approximately 52,000 lbs.

b. Some scattering of leakage rate data was observed. The leakage rate in the above table indicates only the order of magnitude.

c. At low leakage rates:

   (1) Measured leakage was not very sensitive to variations of internal pressure.

   (2) At least in the case of LOX Grade KEL-F gasket, it took hours to reach a steady leakage rate after variation of internal pressure.

d. The measured leakage rate for the LOX Grade KEL-F gasket at liquid nitrogen temperature is in the order of 10^{-1} atm cc/sec. for an internal pressure of 100 psig. The leakage rate at 200 psia became so large that it was beyond the range of the leak detector.

e. For the copper shear O-ring, the instrumentation indicated a sizable leak when the fixture was first immersed in the liquid nitrogen. However, in the several minutes required to measure the leak it had decreased to 10^{-6} atm cc/sec. After 4 hours the leak decreased to 10^{-7}. When the fixture was warmed up to room temperature, the leak returned to its original value of 10^{-8}.

4.7.2 The Rotations of the Flanges and the Hub Bending Stress as a Function of the Bolt Load are as follows:

Total Bolt Load	Rotation of Loose Flange Radian		Rotation of Integral Flange Radian		Hub Bending Stress psi	
lb.	Measured	Calculated	Measured	Calculated	Meas'd	Calc.
0	0	0	0	0	0	0
16,800	2.77×10^{-3}	3.15×10^{-3}	3.29×10^{-3}	1.40×10^{-3}	4450	3930
33,600	5.59×10^{-3}	6.30×10^{-3}	7.34×10^{-3}	2.81×10^{-3}	9330	7870
40,800	6.74×10^{-3}	7.65×10^{-3}	9.02×10^{-3}	3.51×10^{-3}	11,500	9550
52,800	8.96×10^{-3}	9.9×10^{-3}	1.16×10^{-2}	4.41×10^{-3}	14,600	12,400

Notes:

a. See section 4.8, item 5 for a discussion on the difference between the measured and calculated values for the integral flange rotations.

b. See Appendix VI (section 4.14) for a description of strain gage locations.

c. The measured data were based on one of the more reliable tests conducted when an asbestos gasket was used.

d. The measured rotations were deduced from readings of the strain gages attached to the outer circumferences of the flanges.

e. The measured hub bending stress is obtained as hub bending stress =

$$\frac{(\text{hub bending strain recorded}) \times (\text{Young's Modulus})}{1-(\text{Poisson's Ratio})^2}$$

Since it was not possible to attach the strain gage right behind the flange neck, the bending strain recorded and therefore the measured hub bending stress is slightly smaller than its actual value.

f. The total bolt loads corresponding to the measured rotations and stresses are obtained by assuming that all the uninstrumented bolts are subjected to the same load as the instrumented bolts. This is reasonable since the same torque was applied to all the non-instrumented bolts during the tightening process. This torque was equal to the average value needed on the instrumented bolts to achieve the required load.

g. The calculated rotations and stresses are based on the analysis in Appendix VII (section 4.15). Gasket reactions were assumed to act at the centerline of the gasket.

4.7.3 Measured total bolt load, flange rotations and hub bending stress as a function of the internal pressure

Internal Pressure psig	Total Bolt Load lb.	Rotation of Loose Flange(Rad)	Rotation of Integral Flange (Rad)	Hub Bending Stress psi
0	52,800	8.96×10^{-3}	1.16×10^{-2}	14,600
47.5	50,800	8.74×10^{-3}	1.18×10^{-2}	15,500
99	50,500	8.70×10^{-3}	1.20×10^{-2}	16,700
149	48,700	8.70×10^{-3}	1.20×10^{-2}	18,200
200	49,100	8.72×10^{-3}	1.25×10^{-2}	19,800

Notes a through b of the preceding section apply also to the above table.

These results are consistent with the analysis which shows that most of the stresses and deformations are due to the initial bolt load. The large increase in pressure has a small effect on these stresses and deformations.

4.7.4 Measured compression of the gaskets

	Thickness in.	
Gasket Type	Before Test	After Test
Impregnated Asbestos	0.062	0.056
LOX Grade KEL-F	0.062	0.060
*Copper Shear Ring	0.062	0.062

* An explanation of the apparent zero compression of the copper shear ring is included in section 4.7.6

4.7.5 Torque - Bolt Load Relation

Torque in-lb	Bolt Load lb/bolt
0	0
30	700
59	1400
70	1700
86	2200

Notes:

a. The bolts, nuts and washers were lubricated with Moly-Kote.

b. The torque value in the above table is the average value on the seven instrumented bolts. Variations from bolt to bolt is comparatively small with proper lubrication. A minimum of 70 in.-lb. and a maximum of 95 in-lb were used to tighten the bolts to 2,200 lb/bolt.

c. The torque bolt load relation is useful if instrumented bolts are not available. It is independent of the type of gasket used.

4.7.6 Copper Shear Ring Seal

Figure 4.5 is a sketch of a cross-section of the shear ring during the sealing operation. The grooves in the mating flanges have purposely been made smaller than the copper seal so that shearing of the metal would occur. Figure 4.6 is a micro-photograph of a cross-section of the shear ring seal after completion of the test. Note the four indentations in the cross-section made by the grooves in the mating flanges. As can be seen from the crystal structure, essentially all of the deformation of the shear ring took place in the region of these indentations. The micro-photograph shows that in this region, the crystals are distorted and are smaller due to cold working while the crystals are fairly uniform throughout the rest of the structure. Each indentation has one surface which was essentially in compression and one surface which was essentially in shear. A detail of one of the indentations is shown in Figure 4.7. Note that the sheared surface is very smooth showing that a good seal occurred here while the compressed surface is rough. This can also be seen in Figure 4.8, which is a 20X magnification of the used shear ring. Note the shine of the sheared surface showing the new metal exposed. Figure 4.9 is a micro-photograph of longitudinal section of the shear ring. The lower portion of the photograph is the copper material of the shear ring while the upper portion is nickel plating which was included prior to cutting, polishing and etching so that the surface of the copper would not be disturbed. It appears as if some intergranular corrosion was present near the surface of the copper. This is probably the result of an oxygen attack when the shear ring was fabricated and annealed. Such surface imperfections would be very detrimental to the performance of a flat gasket. Reviewing Figure 4.8, we see that the compressed surface contains most of the corrosion products, while the sheared surface is clean, showing that new material was exposed thereby making a good seal possible.

During the bolt tightening process a feeler gage was used between the flanges to measure the deformation of the upper shear ring.

The full bolt load of 52,000 pounds produced a compression of 36 mils. It is felt that the large compression would be needed in order to produce a sufficient amount of shearing to make a good seal. The gasket thickness measured the same before and after the test since all of the gasket deformation took place in the area near the four indentations.

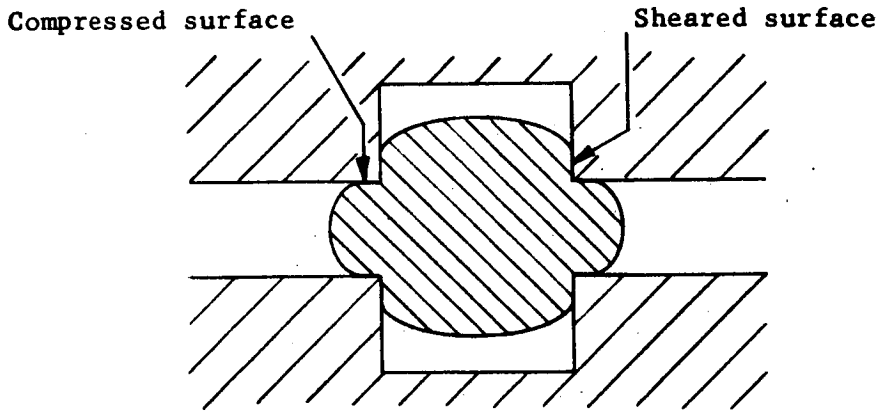

Figure 4.5 Copper Shear Ring Seal in Place Between Flange Grooves

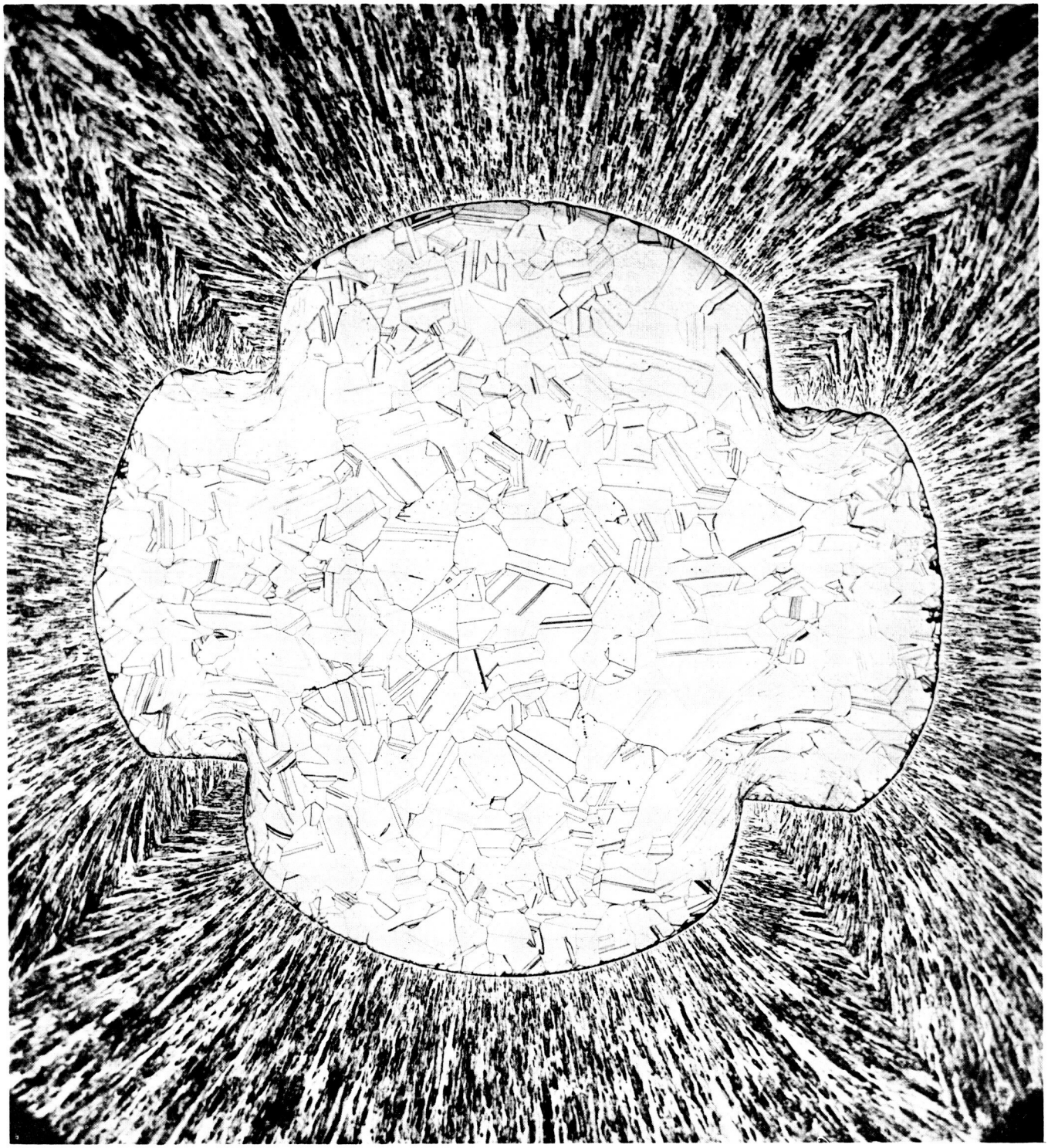

FIGURE 4.6

CROSS-SECTION OF USED COPPER SHEAR RING

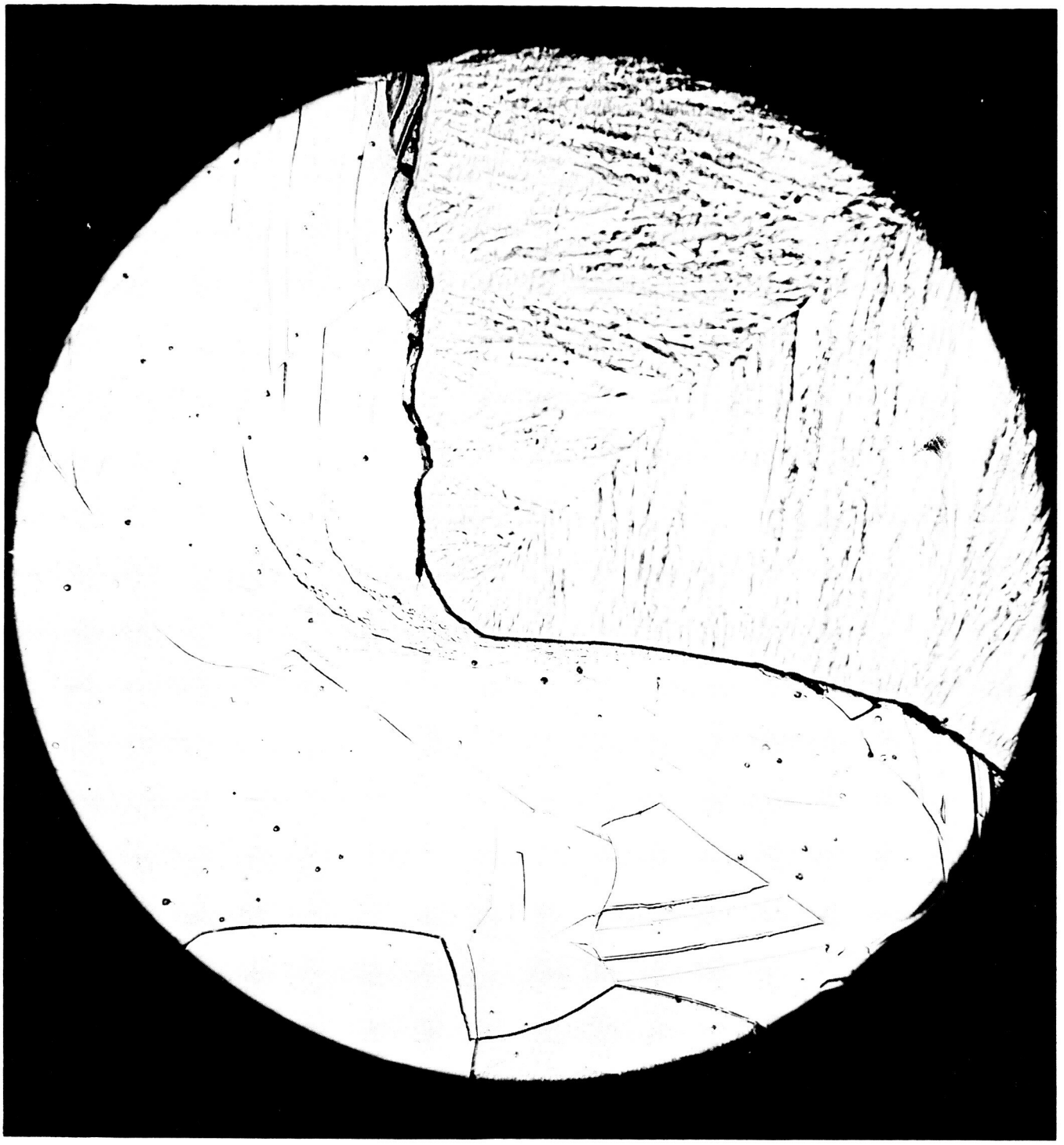

FIGURE 4.7

V-GROOVE DETAIL OF COPPER SHEAR RING.
SHEARED SURFACE IS IN HORIZONTAL POSITION HERE.

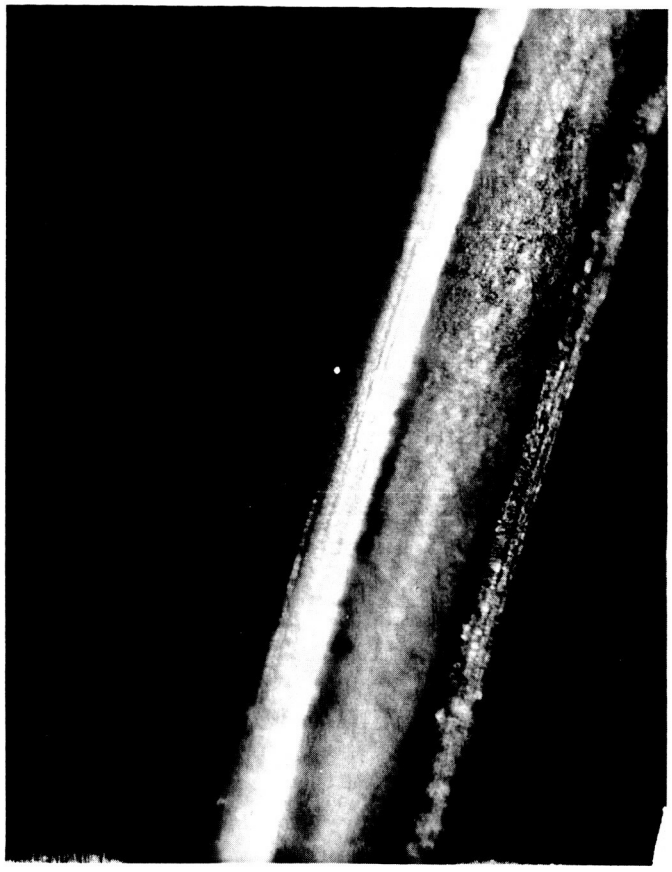

FIGURE 4.8

VIEW OF USED SHEAR RING ENLARGED TWENTY TIMES

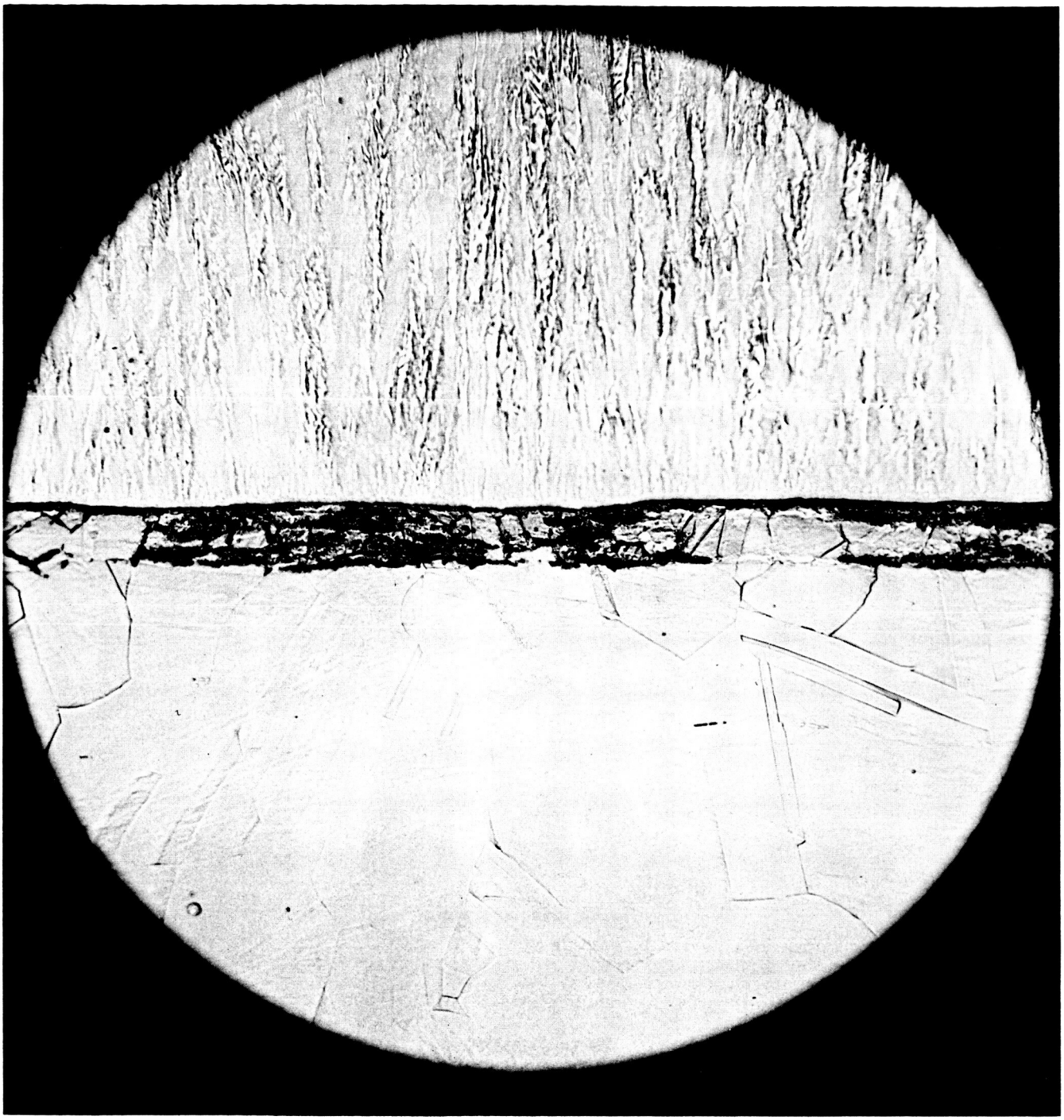

FIGURE 4.9

COPPER SHEAR RING. SHOWING SUB-SURFACE IMPERFECTIONS IN LONGITUDINAL DIRECTION

4.8 Discussion and Conclusion

1. All three types of gaskets tested sealed satisfactorily at room temperature.

2. The leakage through LOX Grade KEL-F gasket at liquid nitrogen temperature and under a 48,000 in-lb moment is excessive. The corresponding leakage through the asbestos gasket is large (10^{-2} atm cc/sec). The corresponding leakage through the annealed copper shear O-ring is small (10^{-6} atm cc/sec). This definitely demonstrates the superiority of the shear O-ring over the other two types of gaskets from the standpoint of leakage.

3. The copper shear ring does have a disadvantage that during the transient cooling down period considerable leakage occured. This is probably because the copper ring contracts much faster than the flanges and bolts. Coating of the ring with a less conductive material may help. Other soft metals such as aluminum would probably perform similiarly.

4. a. The room temperature leakage rates measured on the asbestos and LOX Grade KEL-F gaskets were smaller by orders of magnitude than the corresponding leakage rates measured on smaller specimens (see section 1).

   b. At low leakage rates:

      (1) The measured leakage rate was not very sensitive to variations of internal pressure.

      (2) At least in the case of LOX Grade KEL-F gasket it took hours to reach a steady leakage rate after each variation of internal pressure. This may not be true for other pressure ranges.

   The above facts indicate that when the sealing surfaces conform very closely to each other, the phenomenon of fluid leaking through the labyrinth of the "microscopic passages" may be quite different from that envisioned heretofore. It would be desireable to make the following investigation:

   (1) The time for the establishment of a steady leakage flow.
   (2) "Microscopic effects" such as surface tension on the retardation of flow.
   (3) A model for the flow through the "labyrinth" of the "microscopic passages".
   (4) The size effect of the gasket.

   On a microscopic scale, the above results seem to indicate that the use of a wide gasket would be advantageous. This is limited by the fact that a wider gasket results in a larger bolt circle diameter.

5. With the accuracy that can be expected of the tests, the measured rotation of the loose flange and the hub bending stress compare favorably with the theoretical prediction. However, the measured rotation of the integral flange is more than twice the predicted rotation. This may be due to inaccuracies introduced by the assumption that the flange rotates as a ring. The ring is assumed to rotate about its own cross-sectional center of gravity without any changes in shape. Of course, the flange actually has

some of the characteristics of a circular plate as well as those of a ring. It will bend into the shape indicated in the sketch. A schematic sketch of the flange which was tested is shown in section 4.14. Drawings of the actual flange are shown in section 4.13. The outer surface of the flange actually rotates through a greater angle than the CG due to the bending. Since the strain gages were located at the outer surface of the flange, their indicated rotations were high. It is also true that neglecting the effect of bending in the analysis results in an underestimation of the rotation of the CG of the flange.

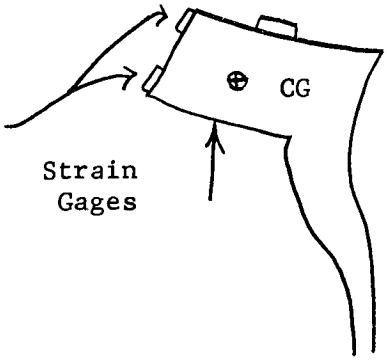

There is evidence from the test which indicates that bending of the flange does occur. When the flange test fixture was pressurized to 200 psi it was noted that the total bolt load and measured rotations of the flanges remained practically unchanged. Since the loads in the bolts did not change, this means that the gasket load must have decreased by an amount equal to the axial pressure force. This results in an increase of 8,180 in-lb for the rotating moment on the integral flange which is an increase of 37.5% over the initial moment due to bolt tightening. It is known that the increase of moment did not produce any significant change in the rotation of the outer section of the hub since the strain gages which are located there showed very little change during pressurization. A 35.6% increase in the hub bending stress was noted however, The hub bending stress can be considered to be due to two effects of the flange. First, is rotation of the flange. A bending moment produces a bending stress in the hub. The second effect is the discontinuity stress produced by the flange. Visualize the hub as being separate from the flange. When the fixture is pressurized, the hub will expand more than the flange since it is a smaller section. In order to force the hub and flange back together, it will be necessary to apply a shear force and a moment to the mating parts so that the radial and angular displacements of the two parts match. These loads produce stresses (discontinuity stresses) in the hub which oppose the stresses produced by the first effect.

It is shown in Appendix 4 that discontinuity stresses due to the second effect are negligible because of the large rigidity of the hub. The 35.6% increase in hub stress during pressurization must have been due to the first effect which is the increased rotation of the flange. This compares favorably with the 37.5% increase of moment on the flange rotated through a larger angle than the outer section. The flange therfore, must have bent in the same manner as a circular plate.

6. Bending of the bolts as a result of flange rolling does not seem to be as serious as originally thought, probably because with adequate lubrication, the clearance between the bolt and the bolt hole was able to accommodate the flange rolling.

7. With proper lubrication, the torque bolt load relation is quite consistent. Rational design specifying a certain bolt load can be applied with a reasonable degree of assurance if torque wrenches are used to assemble the connector.

8. Unfortunately, strain gage data at the liquid nitrogen temperature were judged not of sufficient accuracy for use in the analysis.

9. One experience learned during testing is that instrumentation and operation should be conducted away from the cryogenic environment as much as possible, even at the expense of increased complexity. Test experience also points out the need for improved equipment and technique of strain instrumentation at cryogenic temperatures.

4.9 Appendix I Design Procedure of Twelve Inch Cryogenic Connector

4.9.1 INTRODUCTION

A step by step design procedure is outlined in the following sections for a flanged connector which has the following appearance.

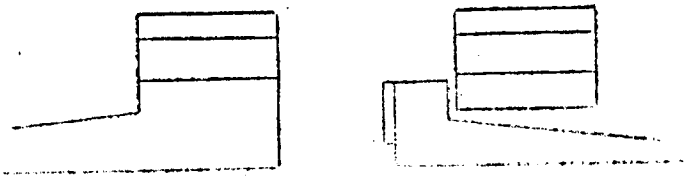

This connector is intended for operation at cryogenic temperatures and under moderate pressures. A flat gasket is used. One of the flanges is a loose flange. The two tubes to be connected are made of different materials. The design conditions are given in Section II.

For convenience and clarity the design procedure shall be treated as a typical design problem. At the same time we shall try to emphasize basic principles, so that the design procedures outlined shall have wide applicability. When applicable, the time-tested ASME Code shall be adhered to. Where deviations from the code procedure are necessary, the reason for the deviations are discussed in detail.

The ASME Code is intended for pressure vessels in steam power plants and allows large safety factors. Weight requirements of launch vehicles call for a critical design of components. A safety factor of 1.1 against the yield strength of material under proof test conditions has been used by Marshall Space Flight Center and shall also be used in the present design. The preliminary design was completed before knowing the safety factor of 1.1 used by MSFC. A safety factor of 1.0 was tentatively used. Since the difference is small no attempt is made to change the preliminary design. In the final stress analysis and refinement stage the safety factor of 1.1 should be adopted, The maximum shear stress theory should be taken as the yield criterion of the material.

The design loads depend on the moment arms and hence on the geometrical dimensions of the connector. The connector design is therefore a cut-and-try process. The procedure can be divided roughly into a preliminary design stage

and a stress analysis and refinement stage. To minimize the effort required it is imperative that the preliminary design be quite accurate. A great deal of the following will be devoted to the discussion of the principles based on which we can obtain a minimum weight design with the least effort.

The nomenclature used in this design procedure is given in Section 4.12. Whenever possible the ASME Code nomenclature is used.

4.9.2 DESIGN CONDITIONS

A. Tubes to be connected

Inside diameter = 12 in.

One tube made of 2024T4 aluminum alloy, 0.323 in. thick.

One tube made of 347 stainless steel, 0.062 in. thick.

B. Pressure

Operating pressure = 200 psi

Proof pressure = 300 psi

C. Temperature

Liquid nitrogen temperature (normal boiling point -321°F)

D. External load

48,000 lb-in moment at operating pressure

4.9.3 FLANGE MATERIAL SELECTION

Considerations are:

A. Compatibility with working fluid, corrosion resistance, etc.

B. Low temperature toughness.

C. Minimum differential thermal contraction.

D. Good strength/weight ratio

E. Ease of fabrication

F. Economy

In general, when tube materials have been chosen there is not much freedom in the flange material selection. The integral flange and ferrule material shall be the same as those of the tubes they are connected to, i.e. 2024T4 aluminum alloy and 347 stainless steel respectively. The loose flange material shall also be 2024T4 aluminum alloy so that the bolts will not be bent due to the radial differential contraction of the flanges.

4.9.4 GASKET SELECTION

Considerations are:

A. Compatibility with working fluid and cryogenic temperature.

B. Low yield point consistent with strength requirement.

C. Small amount of creep.

D. Minimum differential thermal contraction.

Requirement B of low yield point is perhaps particularly important. Since the gasket material has a different coefficient of thermal contraction from at least one of the flanges, relative displacements of the gasket and the flange surfaces are inevitable when the temperature drops from room temperature to cryogenic temperature. To prevent leakage it is imperative that the gasket be able to reseal after the relative displacement. Many materials harden at cryogenic temperature and are undesirable. Notice that we have not included the commonly accepted gasket resiliency requirement in the above. This is because for space applications where weight is of primary concern the flanges are rather critically designed and quite flexible. As a result the gasket becomes rigid in comparison anyway. In general, thinner gaskets are desirable because they can take higher bolt load as well as having less chance of gasket blow-out. Provided that there is no danger of gasket blow-out the gasket width shall be as small as possible in order to achieve a greater seating stress without requiring heavy bolt load. For high-pressure service, the gasket width should be sufficient to prevent the crushing of gaskets due to heavy bolt load. The Taylor Forge "Modern Flange Design" does not recommend a gasket stress greater than twice the gasket seating load, even though thin gaskets can sometimes take a much greater stress without being crushed.

The present design assumes the use of a treated Allpax 500 gasket of 1/16 in. thickness. According to Huntsville test data, the Allpax 500 gasket has an ultimate strength of about 5,400 psi, a Young's modulus of about 75,000 psi (another source gives considerably lower modulus) at room temperature and 1.52×10^{-6} psi at $-320^{\circ}F$. Without taking into consideration the beneficial frictional effect, the gasket width required to prevent gasket blow-out is, for the proof pressure of 300 psi, approximately

$$\text{width required} \cong \frac{(\text{internal pressure})(\text{inside radius})}{(\text{ultimate strength})}$$

$$= \frac{(300)(6)}{5400} = 0.333 \text{ in.}$$

Therefore, let us take the gasket width as 3/8 in.

Because of the neglect of frictional effect, the above method of determining gasket width may be rather conservative. However, in the absence of quantitative experimental data we shall adhere to this conservative design. An alternative method to increase the unit gasket stress by using a narrow gasket yet without the danger of gasket blow-out is to have special flange facings such as the tongue-and-groove design.

The seating stress for the 1/16 in. thick Allpax 500 gasket is determined

in the test apparatus developed by ATL as 3360 psi. The leakage rate for this stress is 2.5×10^{-5} atmospheric cc/sec for the particular test specimen. Further increase in stress does not significantly decrease the leakage rate. The total seating load required is approximately

$$W_{m2} = \pi(\frac{3}{8})(13)(3360)$$

$$= 51,500 \text{ lb.}$$

for an assumed 13 in. diameter gasket circle. The minimum design seating stress for asbestos gaskets according to ASME code is 3700 psi based on an effective gasket width of b = 3/16 in. (see the ASME Code for the definition of effective width). The minimum seating load as required by ASME code is therefore

$$\pi bGy = \pi(\frac{3}{16})(13)(3700) = 28,500 \text{ lb.}$$

which is considerably smaller than the value of 51,500 lb established in our controlled test.

Experimental data furnished by Marshall Space Flight Center show that Allpax 500 gaskets harden considerably at cryogenic temperatures. The ability for the gasket to reseal at cryogenic temperature after relative displacement has taken place is questionable. Therefore unless the relative motion due to differential thermal contraction can be prevented (this is rather difficult when the two opposing flanges and the gasket are all made of different materials) a gasket material which hardens considerably at cryogenic temperature will not be satisfactory on theoretical grounds. This may indicate that an entirely new conceptual design is required for flanged connectors in cryogenic temperature service.

Despite the question raised in the preceding paragraph we shall still tentatively design the connector for a seating load of 51,500 psi. Tests to be conducted will show us to what extent the reseal can be effected and what is the effect of seating load on the ability of the gasket to reseal.

4.9.5 BOLT SELECTION

A. Bolt material

Most of the considerations in selecting the flange material apply also to the selection of bolt material. In addition the bolt material should have a coefficient of thermal contraction that is equal to or greater than that of the flanges so that the connector will not become loose when chilled. We shall choose the bolts to be made of 2024T4 aluminum alloy with a minimum yield strength of 40,000 psi at room temperature.

B. Bolt Area

The hydrostatic end load for an assumed 13 in. diameter gasket circle is:

$H_1 = \left(\frac{\pi}{4}\right)(13)^2(200) = 26,500$ lb for the 200 psi operating pressure and

$H_2 = \left(\frac{\pi}{4}\right)(13)^2(300) = 39,800$ lb for the 300 psi proof pressure.

The gasket factor for asbestos gaskets is about 2.75 according to ASME Code. The gasket load required to maintain a tight joint under the operating pressure is

$$H_p = (2b)(\pi Gmp)$$
$$= \left(\frac{3}{8}\right)(\pi)(13)(2.75)(200) = 8430 \text{ lb.}$$

The maximum decrease in the gasket stress due to the external moment of 48,000 lb-in is approximately

$$48,000/\quad(\pi/4)(G^2)(2b)$$

if we consider the gaskets as being much stiffer than the bolts. The external moment does not cause any reduction in the <u>total</u> gasket load. For convenience, however, we shall define a fictitious reduction in gasket load as

H_m = (maximum decrease in gasket stress)(total gasket area)

$= (48,000)/G = (48,000)/13 = 14,800$ lb.

The initial bolt load required should be

(1) Greater than the hydrostatic end load under the proof pressure

$H_2 = 39,800$ lb.

(2) The larger of $W_{m2} = 51,500$ lb or

$H_1 + H_p + H_m = 26,500 + 8430 + 14,800 \cong 49,730$

Obviously, the seating load is the governing factor for the initial bolt load required. This is characteristic of low pressure connectors.

For space applications the flanges are critically designed and become quite flexible. Therefore, during pressurization the bolt load remains practically unchanged while the gasket load is considerably reduced. Allowing a possible 25% increase beyond the initial bolt load, the bolt area required is:

$$A_m = (51,500)(1.25)/40,000 = 1.61 \text{ sq. in.}$$

for a yield strength of 40,000 psi. Notice that we have not considered

(1) Possible bending stress in the bolts due to rotation of flanges.

(2) Torsional stress in the bolts due to friction in the process of bolting up. This effect can be reduced somewhat by the use of lubricants.

(3) Thermal stress due to differential contraction. This effect can probably be taken care of by the increased strength of material at cryogenic temperature.

C. Size and number of bolts

For minimum-weight design it is desirable to keep the height of the flange small for the following reasons:

(1) The moment arm of the hydrostatic end load will be smaller, resulting in a smaller flange moment.

(2) Flange thickness has much more effect than the flange height on both strength and rigidity. It is desirable to reduce the flange height while increasing the flange thickness.

The minimum flange height is controlled by the space required for bolts, bolt washers and wrench clearance. Therefore, for minimum-weight design it is desirable to use a larger number of smaller bolts. Of course, this should not be carried so far that

(1) Stress concentration at bolt holes becomes important. A minimum bolt spacing of 2 1/4 bolt diameters has been recommended.*

(2) Inadvertent overstressing of bolts is likely to occur because bolts are too small.

For minimum-weight design, fine-thread series bolts should be used. We shall tentatively choose twenty-four 3/8 in. fine series bolts, each having a stress area of 0.0876 sq. in. The total bolt area is

$$(24)(0.0876) = 2.10 \text{ sq. in.}$$

which provides a safety factor of

$$2.10/1.61 = 1.30$$

*E.O. Waters and J.H. Taylor, "The Strength of Pipe Flanges," Mechanical Engineering Vol. 49, 1927, No. 5a pp. 531-542.

The bolt spacing is, for an assumed 14 in. diameter bolt circle,

$14\pi/24 = 1.83$ in. $>$ the minimum requirement of 2 1/4 bolt diameters.

We shall check whether the bolt spacing is too large to make a tight joint when we know the flange thickness later.

4.9.6 INTEGRAL FLANGE DIMENSIONS

A. Flange Height

We have already stated that the flange height should be kept at a minimum for minimum-weight design. For 3/8 in. bolts the bolt hole diameter is 13/32 in. The narrow-gage washer has an outside diameter of $0.625\ ^{+0.020}_{-0.005}$ in. We take the distance from the bolt circle to the outer edge of the flange as 0.365 in. This insures that even at the worst misaligned position the edge of the washer would not extend beyond that of the flange. The minimum distance from the rim of the bolt hole to the edge of the flange is

$0.365 - 13/64 = 0.162$ in.

The maximum wrench outside diameter for 3/8 in. bolts is 0.885 in. If we allow a fillet radius of 1/8 in. at the junction of the flange and hub, the distance from the bolt circle to the outside of hub should be

$0.855/2 + 1/8 = 0.568$ in.

We shall take this distance as 0.55 in. With the use of washers this should provide enough wrench clearance.

Another factor which may control this distance is the height of the ferrule. The differential thermal contraction from 300^{o}K (80.6^{o}F) to 0^{o}K (-460^{o}F) between aluminum and 347 stainless steel is approximately

$(431 - 304) \times 10^{-5}$ in/in

For a 7 in. radius this corresponds to

$7\ (431-304) \times 10^{-5} = 8.9 \times 10^{-3}$ in. $\simeq 0.01$ in.

If we should provide a bearing area of 1/4 in. width between the loose flange and the ferrule ring, the distance from the bolt circle to the

outside of the tube should be, at least,

$$13/64 + 1/4 + 0.01 + 0.01 = 0.473 \text{ in.} < 0.55 \text{ in.}$$

which shows that the ferrule height is not the controlling factor.

The gasket should be located as close to the bolts as possible in order to reduce the flange moment. We shall take the distance from the center of bolt hole to the outside edge of the gasket as 0.225 in. tentatively. This leaves a clearance of approximately 0.02 in. from the edge of the bolt hole to the edge of the gasket. Since the gasket width is 3/8 in., the radial distance from the bolt circle to the gasket circle is

$$h_G = 0.225 + 3/16 = 0.413 \text{ in.}$$

Thus we have all the radial dimensions of the integral flange and the gasket provided the hub thickness is known.

B. Flange Thickness

It is more economical to use material in the hub as a source of strength than to use the same material in the flange. Therefore the flange ring of an integral flange shall be as thin as possible. The minimum flange thickness required for a tight joint is related to the bolt spacing by the following Taylor Forge empirical formula*

$$t = \frac{m + 0.5}{6} \left[\text{bolt spacing} - 2 \text{ (bolt diameter)}\right]$$

$$= \frac{2.75 + 0.5}{6} \left[1.83 - 2 \text{ (3/8)}\right] = 0.585 \text{ in.}$$

A greater thickness should probably be chosen for the following reasons

(1) The stiffer the material of the flange, the thinner it needs be in order to maintain a tight joint. The Taylor Forge empirical formula is probably based on the experience with the stiffer steel material.

(2) The leakage rate we can tolerate is smaller than that on which the Taylor Forge formula is based.

Therefore we choose a flange thickness of 0.75 in. Another factor which governs the minimum flange thickness is the radial flange stress. The flange thickness required according to this criterion is of the order of the flange hub thickness and is generally a less stringent requirement.

* "Modern Flange Design," Bulletin 502 - Fourth Edition 1961, Taylor Forge & Pipe Works, Chicago, Illinois.

C. Hub Dimensions

The aluminum tube is rather thick (0.323 in.). Under the proof pressure of 300 psi, the hoop tension is approximately

$$PB/2g_o = (300)(12)/2(0.323) = 5580 \text{ psi}$$

and the axial stress is approximately

$$H_2/\pi Bg_o = 39800/\pi(12)(0.323) = 3270 \text{ psi}$$

Since these stresses due to the internal pressure are small, the stress due to the flange moment is the controlling factor. For minimum-weight design, it is desirable to keep the bending stress at the small end of the hub equal to or slightly less than the bending stress at the large end of the hub. In other words, the hub dimensions should be such that the hub stress-correction factor f as given in ASME code is equal to or slightly less than unity. This requirement fixes the hub length once the hub thickness at the large end is known.

The flange moment due to the initial tightening of bolts is

$$(W_{m2})(h_G) = (51,500)(0.413) = 21,300 \text{ lb-in}$$

Because of the flexibility of the flanges, we shall assume that under pressurization the bolt load remains practically unchanged. The additional flange moment due to pressurization then becomes approximately

$$H_2(h_D - h_G)$$

h_D is still unknown; we shall approximate it by distance from bolt circle to outside of hub + $g_o/2$

$$= 0.55 + 0.323/2 = 0.712 \text{ in.}$$

It is clear that this underestimates h_D. The total flange moment under the proof pressure is, therefore, approximately

$$M_o = 21,300 + 39,800\ (0.712 - 0.413) = 33,200 \text{ lb-in.}$$

Let us assume that this moment is completely transmitted to the hub. The hub thickness required is approximately

$$g_1 = \sqrt{6M_o/\pi BS_f}$$

$$= \sqrt{6(33,200)/\pi(12)(40,000)} = 0.363 \text{ in.}$$

Let us choose $g_1 = 0.375$ in. Notice that we may have underestimated the flange moment somewhat but compensating it by overestimating the moment transmitted to the hub.

The factor $h_o = \sqrt{Bg_o} = \sqrt{12(0.323)} = 1.97$ and $g_1/g_o = 0.375/0.323 = 1.16$. Fig. UA-51.6 in the ASME Code indicates that in order to have the stress-correction factor f equal to or slightly less than unity, we need a hub length of

$$h = 0.15\, h_o = (0.15)(1.97) = 0.296 \text{ in.}$$

Let us take h = 0.3 in. This gives a hub taper of

$$\frac{0.375-0.323}{0.3} \simeq 1 \div 6$$

less than the 1:3 maximum ratio allowed by ASME Code.

D. Summary of Flange Dimensions and Determination of its Characteristics

We have now the following tentative dimensions for the integral 2024T4 aluminum flange.

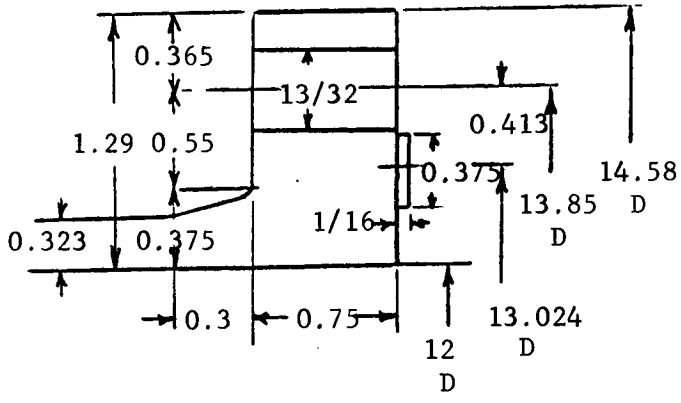

Notice that the bolt-circle and gasket-circle diameters are close to the values of 13 in. and 14 in. assumed previously in the calculations. Therefore it is unnecessary to revise these calculations until the more exact stress analysis to be performed later. We can now determine some of the characteristics of the flange which will be of use later on. We have,

$g_1/g_o = 1.16$

$h/h_o = 0.152$

$K = 14.58/12 = 1.215$

$T = 1.83$

$Z = 5.20$

$Y = 10.08$

$U = 11.07$

$F = 0.904$

$V = 0.50$

$e = F/h_o = 0.904/1.97 = 0.459$

$d = h_o g_o^2 U/V = (1.97)(0.323)^2(11.07)/0.5 = 4.55$

$t = 0.75$

$L = (te + 1)/T + t^3/d = \left[(0.75)(0.459) + 1\right]/1.83 + (0.75)^3/4.55$

$= 0.734 + 0.0927 = 0.827$

$E = 10.6 \times 10^{-6}$ psi

$\mu = 0.33$

The rotational rigidity of the flange is

$$Lh_o g_o^2 E(1 - \mu^2)V = (0.827)(1.97)(0.323)^2(10.6 \times 10^6)/(1-0.33^2)(0.5)$$
$$= 4.05 \times 10^6 \text{ lb-in/rad.}$$

The stresses in terms of the flange moment M_o are

Longitudinal hub stress $S_H = fM_o/Lg_1^2B$

$= M_o/(0.827)(0.375)^2(12) = 0.717\ M_o$

Radial flange stress $S_R = (4te/3 + 1)M_o/Lt^2B$

$= M_o\left[(14)(0.75)/3 + 1\right)/(0.827)(0.75)^2(12)]$

$= 0.359\ M_o$

Tangential flange stress $S_y = YM_o/t^2B - ZS_R$

$= M_o\left[10.08/(0.75)^2(12) - (5.2)(0.359)\right]$

$= -0.38\ M_o$

The ASME Code allows the hub stress to be as high as 1.5 S_f, because slight yielding in the hub would only cause a shifting of load from the hub to the flange which has the capacity to absorb the additional load. For the less ductile material such as the 2024T4 aluminum and with the use of yield strength as S_f, it seems desirable not to let the hub stress exceed S_f. Therefore our design requirement becomes

$$S_H,\ S_R,\ S_T,\ (S_H + S_R)/2,\ (S_H + S_T)/2 \leq S_f$$

Obviously $S_H = 0.717\ M_o \leq S_f$ is the most critical requirement. This shows, a posteriori, the correctness of our procedure in basing the flange design on the most critical section, the hub at its large end.

From the equation for the longitudinal hub stress we can derive the moment transmitted to the large end of the hub as, approximately

$$M \cong (\pi/6L)M_o = M_o\left[\pi/(6)(0.827)\right]$$

$$= 0.633\ M_o$$

This shows that by assuming the flange moment as completely transmitted to the hub we have used a hidden factor of safety of magnitude

$$1/0.633 = 1.58$$

This is perhaps much too conservative even when the flange moment is somewhat underestimated. But we shall not go back and change the hub thickness now until later when a more exact stress analysis is conducted.

4.9.7 FERRULE DIMENSIONS

A. Hub Thickness

The ferrule material is 347 stainless steel with a minimum yield strength of 30,000 psi at room temperature. The outside diameter of the ferrule ring is taken to be the same as the gasket outside diameter, i.e. 13.40 in.

An estimate of the moment on the ferrule can be made as follows,

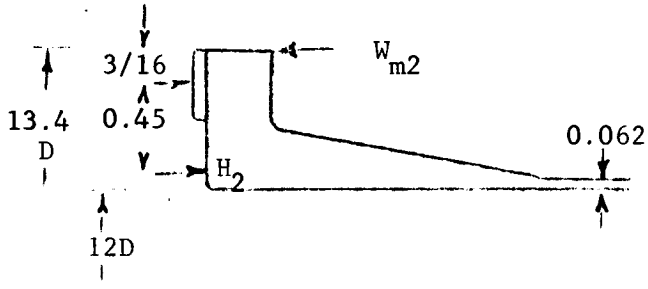

Let us assume that the loads act at the positions as shown and that the bolt load changes insignificantly during pressurization, then the moment on the ferrule is approximately

$$W_{m2}(3/16) + H_2\ (0.45) = (51,500)(3/16) + (39,800)(0.45)$$

$$= 27,000\ \text{lb-in.}$$

If 80% of this moment is transmitted to the hub, the hub thickness required becomes approximately

$$g_1 = \sqrt{6M/\pi BS_f}$$

$$= \sqrt{(6)(0.8)(27,500)/\pi(12)(30,000)} = 0.324 \text{ in.}$$

Let us take $g_1 = 0.35$ in.

B. Hub Length

The 347 steel tube is quite thin (0.062 in.). Under the proof pressure of 300 psi the hoop tension is approximately

$$PB/2g_o = (300)(12)/(2)(0.062) = 29,000 \text{ psi}$$

and the axial stress approximately

$$H_2/\pi Bg_o = 39,800/\pi(12)(0.062) = 17,000 \text{ psi}$$

These are large stresses. Therefore the minimum hub length should be such that only negligible bending is transmitted to the tube. It is known from the early work of Waters and his associates* that this length is approximately

$$h = \sqrt{B\,(g_o + g_1)/2} = \sqrt{(12)(0.062 + 0.35)/2}$$

$$= 1.57 \text{ in.}$$

Therefore, let us take $h = 1.60$ in.

C. Ring Thickness

The ring thickness required is governed by the radial flange stress. A good estimate** is to take the thickness the same as the hub thickness, which is 0.35 in. for the present case. We now have, for the ferrule,

$$h_o = \sqrt{Bg_o} = \sqrt{(12)(0.062)} = 0.863$$

$$h/h_o = 1.60/0.863 = 1.85$$

$$g_1/g_o = 0.35/0.062 = 5.64$$

$$K = 13.4/12 = 1.117$$

$$T = 1.87$$

---

* E.O. Waters, D.B. Rossheim, D.B. Wesstrom and F.S.G. Williams, "Development of General Formulas For Bolted Flanges," Taylor Forge and Pipe Works, Chicago, Illinois.

** A somewhat better estimate can be obtained if we note that the radial flange stress is approximately given by

$$S_R = M_o T/t^2 B$$

$$Z = 9.07$$

$$Y = 17.54$$

$$U = 19.27$$

Notice that the ratio $g_1/g_o = 5.64$ is already beyond the range of the design chart given by ASME code. By extrapolating from these charts we obtain

$$F \cong 0.51$$

$$V \cong 0.022$$

Therefore

$$e = F/h_o = 0.51/0.863 = 0.591$$

$$d = h_o g_o^2 U/V = (0.863)(0.062)^2(19.27)/0.022 = 2.91$$

$$L = (te + 1)/T + t^3/d = \left[(0.35)(0.591) + 1\right]/1.87 + (0.35)^3/2.91$$

$$= 0.645 + 0.0147 = 0.660$$

The radial flange stress in the ring is

$$S_R = \left[(4te/3) + 1\right] M_o/Lt^2B$$

$$= \left[(4)(0.35)(0.591)/3 + 1\right] \quad M_o/(0.66)(0.35)^2(12)$$

$$= 1.32\ M_o = (1.32)(27,500) = 36,200 \text{ psi}$$

$$> S_f = 30,000 \text{ psi}$$

This indicates that the assumed thickness of 0.35 in. is insufficient. Since the maximum stress is inversely proportional to the square of the ring thickness we have the revised value of the thickness required as

$$t = 0.35\sqrt{36,200/30,000} = 0.385 \text{ in.}$$

Let us take the flange thickness as t = 0.4. The factor L is now recalculated as

$$L = \left[(0.4)(0.591) + 1\right]/1.87 + (0.4)^3/2.91 = 0.683$$

Now the radial flange stress in the ring is

$$S_R = \left[4(0.4)(0.591)/3 + 1\right] M_o/(0.683)(0.4)^2(12)$$

$$= 1.00\ M_o = 27,500 \text{ psi}$$

The longitudinal hub stress

$$S_H = fM_o/Lg_1^2B = (1)\ (M_o)/(0.683)(0.35)^2(12) = 0.996\ M_o$$

$$= 27,400 \text{ psi}$$

and the tangential flange stress

$$S_T = YM_o/t^2B - ZS_R$$

$$= M_o\left[17.54/(0.4)^2(12) - (9.07)(1)\right] = 0.06\ M_o = 1,650 \text{ psi}$$

D. Summary of Ferrule Dimensions and Characteristics

We have now the following tentative dimensions for the 347 stainless steel ferrule

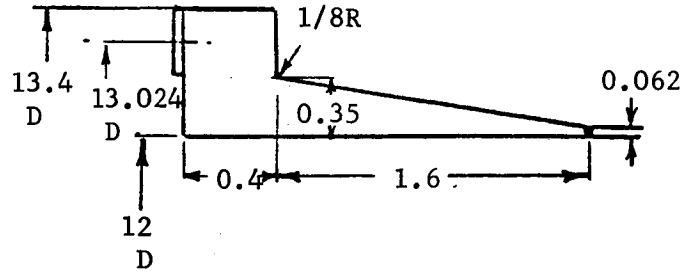

The rotational rigidity of the ferrule is:

$$Lh_o g_o E/(1-\nu^2)V = (0.683)(0.863)(0.062)^2(29 \times 10^6)/(1-0.3^2)(0.022)$$
$$= 3.35 \times 10^6 \text{ lb-in/rad.}$$

The moment transmitted from the ring to the hub is approximately

$$M = (\pi/6L)M_o = \left[\pi/(6)(0.683)\right] M_o = 0.767\ M_o$$

which is very close to the value of $0.8\ M_o$ assumed previously.

4.9.8 LOOSE FLANGE DIMENSIONS

The loose flange is made of 2024T4 aluminum alloy. The outside diameter of the loose flange can be taken the same as that of the integral flange, i.e. 14.58 in. The inside diameter of the loose flange can be taken as 12.9 in. This provides a bearing area of 1/4 in. width between the flange and the ferrule ring and leaves a radial clearance of 0.1 in. between the edges of the ferrule and the flange.

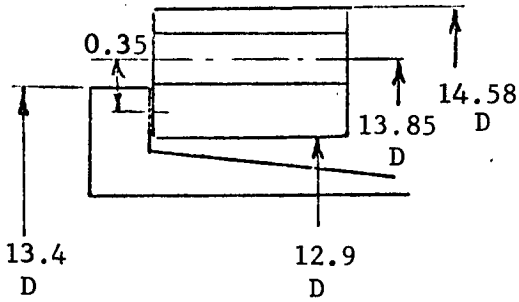

The flange thickness is governed by strength and rigidity considerations. The flange moment due to initial bolting up is

$$M = W_{m2} h_G = (51,500)(0.35) = 18,100 \text{ lb-in.}$$

For a possible 25% increase in bolt load during pressurization, the maximum flange moment is

$$M_o = 1.25\ M = (1.25)(18,100) = 22,600 \text{ lb-in.}$$

The loose flange is relatively flexible. It will tend to bear on the outer edge of the ferrule under the moment load. The flange moment determined above is on the conservative side. Notice that in determining the ferrule moment previously, we have assumed that the bolt load is transmitted from the loose flange to the ferrule at the outer edge of the ferrule ring. That assumption is conservative for the ferrule but unconservative for the loose flange. The only stress component of consequence in the loose flange is the tangential flange stress

$$S_T = YM_o/t^2B$$

With $K = A/B = 14.58/12.9 = 1.13$ the factor $Y = 15.91$ from ASME code. The flange thickness required for strength is obtained from the above equation as

$$t = \sqrt{YM_o/BS_f} = \sqrt{(15.91)(22,600)/(12.95)(40,000)}$$
$$= 0.835 \text{ in.}$$

Besides strength we also need to investigate the rigidity of the flange so that the totation of the flanges does not cause excessive bolt bending. The rotational rigidity of the loose flange is given by the expression

$$(2\pi E)(1/12)(A-B)(t^3)/(A + B)$$
$$= (2\pi)(10.6 \times 10^6)(1/12)(14.58 - 12.9)(1)^3/(14.58 + 12.9)$$
$$= 6.79 \times 10^5 \text{ lb-in/rad.}$$

for a flange thickness of 1 in. Notice that this amounts to only about one sixth of the rigidity of the integral flange. The rotation of the flange under the moment, $M_o = 22,600$ lb-in is

$$22,600/6.79 \times 10^5 = 3.33 \times 10^{-2} \text{ rad.}$$

Likewise, the rotation of the integral flange under the assumed moment of $M_o = 33,200$ lb-in is

$$33,200/4.05 \times 10^6 = 8.20 \times 10^{-3} \text{ rad.}$$

If, as a first approximation, the bolt is assumed to bend uniformly due to the rotation of flanges, the bolt will have a radius of curvature

ρ = length of bolt/total rotation of flanges

and a maxim bending stress of

(Bolt radius) x E/ρ

Therefore the maximum bending stress in the bolts becomes approximately

$(10.6 \times 10^6)(3/16)(3.33 \times 10^{-2} + 8.20 \times 10^{-3})/(0.75 + 0.40 + 1.00) = 38{,}300$ psi

This bending stress, added to the axial stress in the bolts, would have exceeded the yield strength of the bolts. Of course, some free play exists between the bolt and the bolt hole and improves the situation somewhat. Since the loose flange assumed above is much more flexible than the integral flange, the most effective way of reducing the flange rotation and hence the bolt bending is to increase the thickness of the loose flange. An increase of the loose flange thickness to 1.6 in. increases its rigidity to

$(6.79 \times 10^5)(1.6/1)^3 = 2.78 \times 10^6$ lb-in/rad.

and reduces its rotation to

$3.33 \times 10^{-2}/(1.6)^3 = 8.13 \times 10^{-3}$ rad.

The maximum bending stress in the bolt is now reduced to

$(10.6 \times 10^6)(3/16)(8.13 \times 10^{-3} + 8.20 \times 10^{-3})/(0.75 + 0.40 + 1.60) = 11{,}800$ psi

In addition to the flange rotation considered above there will also be additional rotation of the integral flange due to the barreling effect of the internal pressure. The above treatment is rather crude. We still need more information from experimental tests to reveal

(1) How much bending of the bolts can be tolerated.

(2) To what extent the free play between the bolt and the bolt hole can reduce the bending of bolts.

This example shows that probably for most cases the loose flange should be designed on the basis of rigidity requirement. The resulting design will generally have more than enough strength.

This completes our preliminary design of the flanged connector. The dimensions of the connector are summarized in the following drawing.

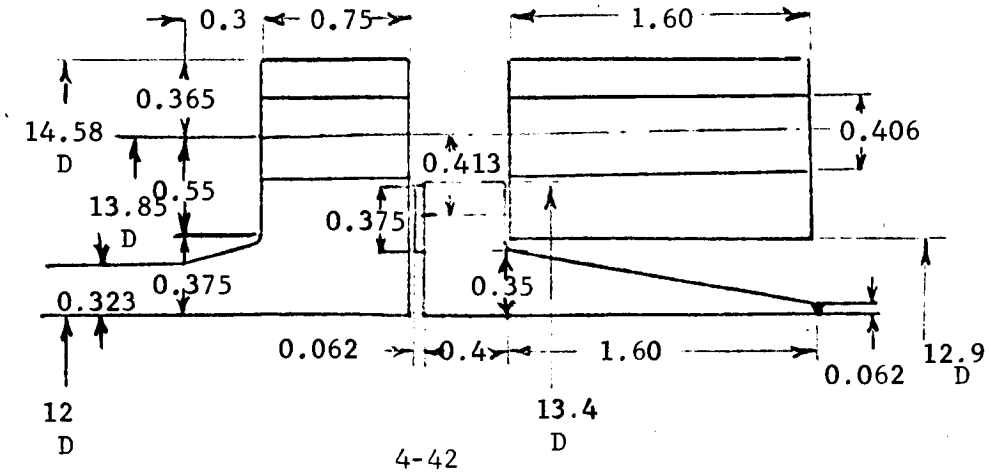

Notice that we have based our design mainly on the room temperature properties of the material. The reasons for this are:

(1) The connector is to be proof-tested at room temperature.

(2) During the transient cooling down period the load will be in full load while the material has not completely gained its increased strength at cryogenic temperature.

4.9.9 DETERMINATION OF THE STIFFNESS OF CONNECTOR COMPONENTS

Expressions for the stiffness of connector components are given explicitly by the appropriate equations in Section 4.10. Their numerical values are determined in this section.

A. Integral Flange

The rotational rigidity of the integral flange has been obtained in Section 4.9.6D as

$$c = 4.05 \times 10^6 \text{ lb-in/rad.}$$

The barreling rigidity of the flange is given by Eq. (B.18) in Section 4.10. There are two alternatives in evaluating Eq. (B.18) for hubbed flanges:

(1) By considering the hub as a part of the tube.

(2) By considering the hub as a part of the flange.

The first approach is slightly simpler. For a stocky and short hub, however, the second approach is more accurate. The present hub is comparatively thin. The first approach would be more accurate. To illustrate the procedures we shall calculate the rigidity by both methods.

In method (1) we consider the tube as having an effective thickness which is the average thickness of the hub and tube extending to a distance of $\sqrt{B(g_o + g_1)/2}$ behind the flange. For the present flange

$$\sqrt{B(g_o + g_1)/2} = \sqrt{(12)(0.323 + 0.375)/2} = 2.05 \text{ in.}$$

Therefore the effective thickness of tube is

$$g_{eff} = g_o + h\,(g_1 - g_o)/2(2.05) = 0.323 + (0.3)(0.375 - 0.323)/2\ (2.05)$$
$$= 0.327 \text{ in.}$$

We take it as 0.33 in. because the above method underestimates the effective thickness somewhat. We now have

$$E = 10.5 \times 10^6 \text{ psi}$$
$$g_{eff} = 0.33 \text{ in.}$$
$$\mu = 0.33$$
$$r_o = (B + g_{eff})/2 = (12 + 0.33)/2 = 6.16 \text{ in.}$$
$$r_c = (A + B)/4 = (14.58 + 12)/4 = 6.65 \text{ in.}$$
$$z = t/2 = 0.75/2 = 0.375 \text{ in.}$$
$$A_F = t(A - B)/2 = (0.75)(14.58 - 12)/2 = 0.968 \text{ in}^2$$

$$I = g_{eff}^3/12\,(1-\mu^2) - (0.33)^3/12(1-0.33^2) = 3.36 \times 10^{-3}\ in^3$$

$$I_y = t^3(A-B)/24 = (0.75)^3(14.58-12)/24 = 4.54 \times 10^{-2}\ in^4$$

$$\beta^4 = 3(1-\mu^2)/(r_o g_{eff})^2 = 3(1-0.33^2)/\left[(6.16)(0.33)\right]^2 = 0.648/in^4$$

$$\beta^3 = 0.722/in^3$$

$$\beta^2 = 0.805/in^2$$

$$\beta = 0.897/in$$

$$h_f = (A-B)/2 = (14.58 - 12)/2 = 1.29\ in.$$

Also,

$$z/\beta = 0.375/0.897 = 0.418\ in^2$$

$$1/2\beta^2 = 1/2\,(0.805) = 0.622\ in^2$$

$$1/2\,\beta^3 z = 1/2(0.722)(0.375) = 1.85\ in^2$$

$$r_o r_c I/zA_F = (6.16)(6.65)(3.36 \times 10^{-3})/(0.375)(0.968) = 0.379\ in^2$$

$$r_o r_c zI/I_y = (6.16)(6.65)(0.375)(3.36 \times 10^{-3})/4.54 \times 10^{-2} = 1.14\ in^2$$

Therefore the factor

$$X = (z/\beta + r_o r_c zI/I_y)(1/2\beta^3 z + r_o r_c I/zA_F + r_o r_c zI/Iy) - (1/2\beta^2 - r_o r_c zI/Iy)^2$$

$$= (0.418 + 1.14)(1.85 + 0.425 + 1.14) - (0.622 - 1.14)^2$$

$$= 5.05\ in^4$$

and the barreling rigidity is, according to Eq. (B.18) of Appendix B,

$$c_p = XEg_1 I_y/\left[r_o^4 I\,(1-\mu/2-g_1/h_a)(1/2\beta^2 + z/\beta)\right]$$

$$= (5.05)(10.6 \times 10^6)(0.375)(4.54 \times 10^{-2})/\left[(6.16)^4(3.36 \times 10^{-3})\right.$$
$$\left.(1-0.33/2 - 0.375/1.29)(0.622 + 0.418)\right]$$

$$= 3.33 \times 10^5\ psi/rad.$$

It is also of interest to calculate the rotational rigidity of the flange according to Eq. (B.16b) of Section 4.10, i.e.

$$c = 2\pi\beta IyEX/r_c a(r_o r_c I/zA_F + 1/4\ \beta^3 z)$$

$$= (2\pi)(0.897)(4.54 \times 10^{-2})(10.6 \times 10^6)(5.05)/(6.65)(0.375)(0.379 + 1.85/2)$$

$$= 4.20 \times 10^6\ lb\text{-}in/rad.$$

which agrees to within 4% of the value obtained previously from Eq. (B.16a) of Section 4.10.

In Method (2) we consider the hub as a part of the flange. We shall first determine the centroid of the flange and hub cross section.

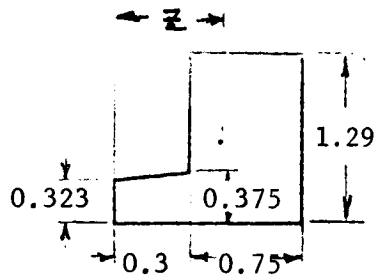

The area of the flange-hub cross section is

$$A_F = (1.29)(0.75) + (0.3)(0.375 + 0.323)/2$$

$$= 0.968 + 0.105 = 1.07 \text{ in}^2$$

The average height of the flange-hub cross section is

$$h_f = A_F/(0.3 + 0.75) = 1.07/1.05 = 1.02 \text{ in.}$$

The distance z that locates the centroid of the flange-hub cross section can be obtained as

$$z = \left[(0.968)(0.75/2 + 0.3) + (0.105)(0.15)\right] /1.07$$

$$= 0.625 \text{ in.}$$

The moment of inertia of the cross section about a radial axis through the centroid is

$$I_y = (1.29)(0.75)^3/12 + (0.968)(0.75/2 + 0.3 - 0.625)^2$$

$$= 7.23 \times 10^{-2} \text{ in}^4$$

Notice that in finding the centroid and evaluating the moment of inertia we have to good accuracy, approximated the trapezoidal hub cross section by a rectangle. Notice also that no attempt is made here to determine the radial centroidal position since we are only interested in the radial distance r_c which changes only insignificantly with the addition of the hub. We now have

$$A_F = 1.07 \text{ in}^2$$

$$z = 0.625 \text{ in.}$$

$$h_f = 1.02 \text{ in.}$$

$$I_y = 7.23 \times 10^{-2} \text{ in}^4$$

$$g_o = 0.323 \text{ in.}$$

$$I = g_o^3/12(1-\mu^2) = (0.323)^3/12(1-0.33^2) = 3.15 \times 10^{-3} \text{ in}^3$$

$$\beta^4 = 3(1-\mu^2)/(r_o g_o)^2 = 3(1-0.33^2)/\ (6.16)(0.323)^{\ 2} = 0.676 \text{ in}^4$$

$$\beta^3 = 0.747/\text{in}^3$$

$$\beta^2 = 0.823 /\text{in}^2$$

$$\beta = 0.907/\text{in}$$

Also,

$$z/\beta = 0.625/0.907 = 0.689 \text{ in}^2$$

$$1/2\beta^2 = 1/(2)(0.823) = 0.608 \text{ in}^2$$

$$1/2\beta^3 z = 1/(2)(0.747)(0.625) = 1.07 \text{ in}^2$$

$$r_o r_c I/zA_F = (6.16)(6.65)(3.15 \times 10^{-3})/(0.625)(1.07) = 0.193 \text{ in}^2$$

$$r_o r_c zI/I_y = (6.16)(6.65)(0.625)(3.15 \times 10^{-3})/(7.23 \times 10^{-2}) = 1.12 \text{ in}^2$$

Therefore,

$$X = (z/\beta + r_o r_c zI/I_y)(1/2\beta^3 z + r_o r_c I/zA_F + r_o r_c zI/I_y) - (1/2\beta^2 - r_o r_c zI/I_y)^2$$

$$= (0.689 + 1.12)(1.07 + 0.193 + 1.12) - (0.608 - 1.12)^2$$

$$= 4.03 \text{ in}^4$$

and the barreling rigidity is, according to Eq. (B.18)

$$c_p = XEg_o I_y / \left[r_o^4 I(1-\mu/2-g_o/h_o)(1/2\beta^2 + z/\beta)\right]$$

$$= (4.03)(10.6 \times 10^6)(0.323)(7.23 \times 10^{-2}) / \left[(6.16)^4 (3.15 \times 10^{-3})\right.$$

$$\left.(1 - 0.33/2 - 0.323/1.02)(0.608 + 0.689)\right]$$

$$= 3.28 \times 10^5 \text{ psi/rad.}$$

which is very close to the rigidity obtained by method (1). The rotational rigidity according to the method is

$$c = 2\pi\beta I_y EX/r_c z(r_o r_c I/zA_F + 1/4\beta^3 z)$$

$$= (2\pi)(0.907)(7.23 \times 10^{-2})(10.6 \times 10^6)(4.03)/(6.65)(0.625)(0.193 \times 1.07/2)$$

$$= 5.82 \times 10^6 \text{ lb-in/rad.}$$

almost 40% greater than that obtained by method (1).

B. Loose Flange

The rotational rigidity of the loose flange has been obtained in Section VIII as

$$c = 2.78 \times 10^6 \text{ lb-in/rad.}$$

C. Ferrule

The rotational rigidity of the ferrule has been obtained in Section VII. D as

$$c = 3.35 \times 10^6 \text{ lb-in/rad.}$$

The barreling rigidity can be obtained from Eq. (B.18) of Section 4.10. In order to apply Eq. (18) we shall approximate the tapered hub of the ferrule by an equivalent constant thickness cylinder. Since the hub taper is long we would not expect to get good results by simply taking the average thickness of the taper as the equivalent thickness. A more accurate equivalent thickness is given by Eq. (C.1) of Section 4.11. For the present case Eq. (C.1) can be integrated to give

$$g_{eqv.} = g_1 \left(1 - \frac{g_1 - g_o}{g_1 h} \left[\frac{e^{-\beta h}(1 + \beta h) - 1}{e^{-\beta h} - \beta} \right] \right)$$

This equation can be solved easily by the method of successive approximations to give

$$g_{eqv.} = 0.246 \text{ in.}$$
$$\beta = 1.05$$

We now have

$$\beta^2 = 1.10$$
$$\beta^3 = 1.16$$
$$r_o = (B + g)/2 = (12 + 0.246)/2 = 6.12 \text{ in.}$$
$$r_c = (A + B)/4 = (13.4 + 12)/4 = 6.35 \text{ in.}$$
$$z = t/2 = 0.4/2 = 0.2 \text{ in.}$$
$$A_F = t(A - B)/2 = (0.4)(13.4 - 12)/2 = 0.28 \text{ in}^2$$
$$I = g^3/12\,(1-\mu^2) = (0.246)^3/12(1 - 0.3^2) = 1.35 \times 10^{-3} \text{ in}^3$$
$$I_y = t^3\,(A-B)/24 = (0.4)^3(13.4 - 12)/24 = 3.73 \times 10^{-3} \text{ in}^4$$
$$E = 29 \times 10^6 \text{ psi}$$
$$h_f = (A-B)/2 = (13.4 - 12)/2 = 0.7 \text{ in.}$$

Also,

$$z/\beta = 0.2/1.05 = 0.191 \text{ in}^2$$
$$1/2\beta^2 = 1/2(1.10) = 0.455 \text{ in}^2$$
$$1/2\beta^3 z = 1/2(1.16)(0.2) = 2.15 \text{ in}^2$$
$$r_o r_c I/zA_F = (6.12)(6.35)(1.36 \times 10^{-3})/(0.2)(0.28) = 0.911 \text{ in}^2$$
$$r_o r_c zI/I_y = (6.12)(6.35)(0.2)(1.36 \times 10^{-3})/3.73 \times 10^{-3} = 2.84 \text{ in}^2$$

Therefore,

$$X = (z/\beta + r_o r_c zI/I_y)(1/2\beta^3 z + r_o r_c I/zA_F + r_o r_c zI/I_y) - (1/2\beta^2 - r_o r_c zI/I_y)^2$$
$$= (0.191 + 2.84)(2.15 + 0.911 + 2.84) - (0.455 - 2.84)^2$$
$$= 12.2 \text{ in}^4$$

and the barreling rigidity is

$$c_p = XEg_1 I_y / \left[r_o^4 I (1-\mu/2-g_1/h_a)(1/2\beta^2 + z/\beta) \right]$$
$$= (12.2)(29 \times 10^6)(0.35)(3.73 \times 10^{-3}) / \left[(6.12)^4 (1.36 \times 10^{-3})(1-0.3/2 - 0.35/0.7)(0.455 + 0.191) \right]$$
$$= 1.07 \times 10^6 \text{ psi/rad.}$$

The rotational rigidity according to Eq. (B.16b) of Section 4.10 is

$$c = 2\pi\beta I_y EX/r_c z(r_o r_c I/zA_F + 1/4\beta^3 z)$$

$$= (2\pi)(1.05)(3.73 \times 10^{-3})(29 \times 10^6)(12.2)/(6.35)(0.2)(0.911 + 2.15/2)$$

$$= 3.45 \times 10^6 \text{ lb-in/rad.}$$

which agrees within 3% of the rigidity obtained previously by ASME Code method. On the other hand, it can be shown that if we were to take the average thickness of the hub as the equivalent thickness an error of -22% would result.

D. Bolts-Gasket System

The stiffness of the bolts is, from Eq. (B2a),

$$k_B = A_B E_B/\ell_B = (24)(\pi/4)(3/8)^2(10.6 \times 10^6)/(0.75 + 0.062 + 0.4 + 1.60 + 3/16)$$

$$= 9.37 \times 10^6 \text{ lb/in}$$

where the effective bolt length ℓ_B = integral flange thickness + gasket thickness + ferrule thickness + loose flange thickness + bolt radius.

The stiffness of the gasket is from Eq. (B.2b)

$$k_G = A_G E_G/\ell_G$$

$$= \begin{cases} \pi(13.024)(0.375)(7.5 \times 10^4)/0.062 = 1.86 \times 10^7 \text{ lb/in at room temperature} \\ \pi(13.024)(0.375)(1.52 \times 10^6)/0.062 = 3.76 \times 10^8 \text{ lb/in at } -320^\circ\text{F} \end{cases}$$

The rotational rigidity of the gasket-bolt system is, according to Eq. (B.8),

$$c = k_B k_G h_G^2/(k_G + k_G)$$

$$= \begin{cases} (9.37 \times 10^6)(1.86 \times 10^7)(0.413)^2/(0.937) + 1.86) \times 10^7 \\ = 1.06 \times 10^6 \text{ lb in/rad. at room temperature} \\ (9.37 \times 10^6)(3.76 \times 10^8)(0.413)^2/(0.937 + 37.6) \times 10^7 \\ = 1.56 \times 10^6 \text{ lb. in/rad. at } -320^\circ\text{F} \end{cases}$$

The thermal rotation stiffness is, by modifying Eq. (B.12b) in Section 4.10 to include the ferrule,

$$c_T = h_G/\left[\alpha_G \ell_G - (\alpha_B \ell_B - \alpha_{F1} t_{F1} - \alpha_{F2} t_{F2} - \alpha_{F3} t_{F3})\right]$$

Since the bolts and the flanges are made of the same material, this becomes

$$c_T = h_G/\left[\ell_G(\alpha_G - \alpha_B) + t_{F3}(\alpha_{F3} - \alpha_B)\right]$$

For a temperature drop from 68°F to -320°F the average coefficients of linear thermal expansion of the 2024T4 aluminum bolts and the 347 stainless steel ferrule are

$$\alpha_B = 9.8 \times 10^{-5} \text{ in/in}^\circ\text{F}$$

$$\alpha_{F3} = 7.22 \times 10^{-5} \text{ in/in}^\circ\text{F}$$

No experimental data is available for the coefficient of expansion of the asbestos gasket material at cryogenic temperatures. Therefore we shall take its room temperature value of

$$\alpha_G = 2 \times 10^{-6} \text{ in/in}^{\circ}\text{F}$$

This uncertainty does not introduce a significant error because the gasket thickness ℓ_G is small in comparison with the ferrule thickness t_{F3}. Therefore, we have the thermal rotational stiffness of the bolt-gasket system

$$c_T = (0.413)/\left[0.062(2 \times 10^{-6} - 9.8 \times 10^{-5}) + 0.4\ (7.22 \times 10^{-5} - 9.8 \times 10^{-5})\right]$$

$$= -1.03 \times 10^{5} \ ^{\circ}\text{F/rad.}$$

4.9.10 ANALYSIS OF THE PRELIMINARY DESIGN CONNECTOR

A. The connector under assembled conditions

The initial bolt load is

$$W_{m2} = 51,500 \text{ lb.}$$

The moments on the flanges are

$$M_1 = (W_{m2})\ (h_G) = (51,500)\ (0.413) = 21,300 \text{ lb-in}$$

$$M_2 = (W_{m2})\ (h_L) = (51,500)\ (0.225) = 11,600 \text{ lb-in}$$

$$M_3 = (W_{m2})\ (h_G - h_L) = (51,500)\ (0.413-0.225) = 9,680 \text{ lb-in}$$

The rotations of the flanges are:

$$\theta_1 = M_1/C_1 = 21,300/4.05\text{x}10^6 = 5.26\text{x}10^{-3} \text{ rad.}$$

$$\theta_2 = M_2/C_2 = 11,600/2.78\text{x}10^6 = 4.17\text{x}10^{-3} \text{ rad.}$$

$$\theta_3 = M_3/C_3 = 9,680/3.35\text{x}10^6 = 2.89\text{x}10^{-3} \text{ rad.}$$

where the subscripts 1, 2 and 3 denote the integral flange, the loose flange and the ferrule respectively.

The fact that the loose flange rotates more than the ferrule justifies our taking $h_L = 0.225$ in., i.e., considering the bolt load transmits from the loose flange to the ferrule at the top of the ferrule.

Since the moments are smaller than the moments we have been considering in our preliminary design, none of the flanges will be overstressed during initial assembly.

B. The connector under proof test condition

The connector is to be proof-tested at 300 psi and at room temperature. The total hydrostatic end force is

$$H = 0.785\ G^2P = (0.785)\ (13.024)^2\ (300) = 39,900 \text{ lb.}$$

and the hydrostatic end force on area inside of flange is

$$H_D = 0.785\ B^2P = (0.785)\ (12)^2\ (300) = 33,900 \text{ lb.}$$

Following the procedure of Section 4.10 we shall resolve the hydrostatic end force on the flange into a force passing through the gasket circle and a moment. This moment is

$$M_1 = H_D\ (h_D - h_G) + (H - H_D)\ (h_T - h_G)$$

$$= 33,900\ (0.325) + (39,900 - 33,900)\ (0.256)$$

$$= 12,500\ \text{lb-in.}$$

on the integral flange and

$$M_3 = 33,900\ (0.337) + (39,900 - 33,900)\ (0.256)$$

$$= 12,900\ \text{lb-in}$$

on the ferrule.

In addition to these external moments on the flanges there is also the internal moment M_4 due to the gaskets and bolt reaction. If the location of the load reaction between the loose flange and the ferrule remains unchanged, M_4 can be determined in a straightforward way from Eq. (B.29) of Section 4.10. We have shown that initially the loose flange more or less bears on the tip of the ferrule ring. Under pressure, however, the ferrule will tend to rotate more than the loose flange, and the location of the load reaction will tend to move inward. Under this circumstance, the determination of M_4 becomes much more complicated. We would have to

(1) Assume a location of the load reaction, h_L.

(2) Solve for M_4 from Eq. (B.31)

(3) Calculate the moments on the loose flange and the ferrule and from the moments find the rotations. If the rotations are compatible, we have the correct answer. If not, assume another value of the location of the load reaction and repeat the procedure until we have the correct answer.

We shall illustrate this procedure in the following. Assume now that the load reaction moves slightly inward from $h_{L0} = 0.225$ in. to $h_L = 0.3$ in. This assumes the load reaction is still closer to the top than the neck of the ferrule.

Now,

$$\gamma = h_L/h_G = 0.3/0.413 = 0.727$$

$$h_L/h_{L0} = 0.3/0.225 = 1.33$$

ΔF = H = 39,000 lb.

ΔT = 0

P = 300 psi

M_1 = 12,500 lb-in.

M_3 = 12,900 lb-in.

M_{20} = initial moment on the loose flange = 11,600 lb-in.

Substitution of these values and the stiffness of components obtained in Section 4.9.9 into Eq. (B.31), we obtain

$$M_4 \left[1 / 4.05 \times 10^6 + (0.727)^2 / 2.78 \times 10^6 + (1-0.727)^2 / 3.35 \times 10^6 + 1 / 1.06 \times 10^6\right]$$

$$= 12{,}500 / 4.05 \times 10^6 + (1-0.727)(12{,}900) / 3.35 \times 10^6$$

$$+ 11{,}600\ (1.33-1)\quad 0.727 / 2.78 \times 10^6 - (1-0.727) / 3.35 \times 10^6$$

$$+ 300 \left[1 / 3.33 \times 10^5 + (1-0.727) / 1.07 \times 10^6\right] - 39{,}000 / 7.68 \times 10^6$$

or

$$M_4 = 442 \text{ lb-in.}$$

The total moments on the loose flange and the ferrule are

$$(M)_{\text{loose flange}} = M_2 + M_{2_o}\ (h_L/h_{L0}) = - \gamma M_4 + M_{20}\ (h_L/h_{L0})$$

$$= - (0.727)(442) + 11{,}600\ (1.33) = 15{,}100 \text{ lb-in.}$$

$$(M)_{\text{ferrule}} = M_3 - M_4\ (1-\gamma) - M_{20}\ (h_L/h_{L0} - 1) + \text{initial assembly moment}$$

$$= 12{,}900 - 442\ (1-0.727) - 11{,}600\ (1.33-1) + 9{,}680$$

$$= 18{,}700 \text{ lb-in.}$$

The rotations of the loose flange and the ferrule are

$$(\theta)_{\text{loose flange}} = (M)_{\text{loose flange}}/c_2 = 15,100 \;/\; 2.78 \times 10^6 = 5.43\times10^{-3} \text{ rad.}$$

$$(\theta)_{\text{ferrule}} = (M)_{\text{ferrule}}/C_3 + P/c_{3p} = 18,700 \;/\; 3.35\times10^6 + 300 \;/1.07\times10^6 = 5.86\times10^{-3} \text{ rad.}$$

The fact that the loose flange rotates less than the ferrule indicates that the load reaction is near the neck of the ferrule and this contradicts our originally assumed location of the load reaction. Since these rotations are nearly equal we know that the location of load reaction assumed is quite close to the true value. An improved value of the location of the load reaction h_L can be found as follows. From our previous calculations we know that for a slight change in h_L, M_4 will not change very much and the total moments on the loose flange and the ferrule will be approximately given by

$$(M)_{\text{loose flange}} = -(0.727)(442) + 11,600\ (h_L/h_{LO}) = -321 + 11,600\ (h_L/h_{LO})$$

$$(M)_{\text{ferrule}} = 12,900 - 442\ (1-0.727) - 11,600(h_L/h_{LO}-1) + 9,680$$
$$= 34,100 - 11,600(h_L/h_{LO}$$

Equating the rotations of the loose flange and the ferrule, we obtain

$$\left[-321 + 11,600\ (h_L/h_{LO})\right] \;/2.78\times10^6 = \left[34,100-11,600\ (h_L/h_{LO})\right] \;/3.35\times10^6 + 300 \;/\; 1.07\times10^6$$

or

$$h_L/h_{LO} = 1.39$$

Therefore $h_L = (0.225)(1.39) = 0.313$ in. and $h_L/h_G = 0.313/0.413 = 0.758$

Now Eq. (B.31) becomes

$$M_4 \left[1 \;/\; 4.05\times10^6 + (0.758)^2/2.78\times10^6 + (1-0.758)^2/3.35\times10^6 + 1 \;/\; 1.06\times10^6\right]$$
$$= 12,500/4.05\times10^6 + (1-0.758)(12,900)/3.35\times10^6$$
$$+ 11,600\ (1.39-1)\left[0.758/2.78\times10^6 - (1-0.758)/3.35\times10^6\right]$$
$$+ 300\left[1 \;/\; 3.33\times10^5 + (1-0.758(/1.07\times10^6\right] - 39,900/7.68\times10^6$$

or

$$M_4 = 420 \text{ lb-in.}$$

The total moments on the loose flange and the ferrule are

$$(M)_{\text{loose flange}} = M_2 + M_{20}\,(h_L/h_{LO}) = -\gamma\, M_4 + M_{20}\,(h_L/h_{LO})$$

$$= -(0.758)(420) + 11{,}600\,(1.39) = 15{,}800 \text{ lb-in.}$$

$$(M)_{\text{ferrule}} = M_3 - M_4\,(1-\gamma) - M_{20}\,(h_L/h_{LO}-1) + \text{initial assembly moment}$$

$$= 12{,}900 - 420\,(1-0.758) - 11{,}600\,(1.39-1) + 9{,}680$$

$$= 18{,}000 \text{ lb-in.}$$

The corresponding rotations are

$$(\theta)_{\text{loose flange}} = (M)_{\text{loose flange}}/C_2 = 15{,}800/2.78\times10^{6} = 5.68\times10^{-3} \text{ rad.}$$

$$(\theta)_{\text{ferrule}} = (M)_{\text{ferrule}}/C_3 + P/c_{3p} = 18{,}000/3.35\times10^{6} + 300/1.07\times10^{6}$$

$$= 5.68\times10^{-3} \text{ rad.}$$

which indicate the location of load reaction assumed is correct. The total moment on the integral flange is

$$(M)_{\text{integral flange}} = M_1 - M_4 + \text{initial assembly moment}$$

$$= 12{,}500 - 420 + 21{,}300 = 33{,}400 \text{ lb-in.}$$

The rotation of the integral flange is

$$(M)_{\text{integral flange}}/C_1 + P/c_{1p} = 33{,}400/4.05\times10^{6} + 300/3.33\times10^{5}$$

$$= 9.15\times10^{-3} \text{ rad.}$$

The increase in the bolt load can be obtained from Eq. (B.22b) as

$$\Delta F_B = -M_4/h_G = -420/0.413 = -1020 \text{ lb.}$$

or actually a slight decrease of about 1,000 lb. The decrease in the gasket load is, from Eq. (B.22a),

$$2F_G = \Delta F - \Delta F_B = 39{,}900 + 1{,}020 = 40{,}900 \text{ lb.}$$

C. The Connector Under Operating Condition

The operating pressure is 200 psi and the operating temperature -321°F. Following the procedure of the preceding section we shall resolve the hydrostatic end force on the flanges into a force passing through the gasket circle

and a moment. Since these moments are proportional to the pressure we have

$$M_1 = 12,500\ (200/300) = 8,330\ \text{lb-in.}$$

on the integral flange and

$$M_3 = 12,900\ (200/300) = 8,600\ \text{lb-in.}$$

on the ferrule.

Let us assume that under the operating pressure and temperature the load reaction between the loose flange and the ferrule is at $h_L = 0.3$ in. Then

$$\gamma = h_L/h_G = 0.3/0.413 = 0.727$$

$$h_L/h_{LO} = 0.3/0.225 = 1.33$$

$\Delta F = H = 39,900\ (200/300) = 26,600$ lb .

ΔT = temperature increment from $80^{\circ}F$ to $-321^{\circ}F = -401^{\circ}F$

$P = 200$ psi

$M_1 = 8,300$ lb-in.

$M_3 = 8,600$ lb-in.

M_{20} = initial moment on the loose flange = 11,600 lb-in.

Substitution of these values into Eq. (B.31), and taking into consideration the increased stiffness of the gasket at the cryogenic temperature, we obtain

$$M_4 \left[1 / 4.05\text{x}10^6 + (0.727)^2/2.78\text{x}10^6 + (1-0.727)^2/3.35\text{x}10^6 + 1 / 1.56\text{x}10^6\right]$$

$$= 8,330/4.05\text{x}10^5 + (1-0.727)(8,600)/3.35\text{x}10^6$$

$$+ 11,600\ (1.33-1)\ \left[0.727/2.78\text{x}10^6 - (1-0.727)/3.35\text{x}10^6\right]$$

$$+ 200\ \left[1 / 3.33\text{x}10^5 + (1-0.727)/1.07\text{x}10^6\right] \quad -26,600/1.55\text{x}10^8$$

$$- (-401)/\ (-1.03\text{x}10^5)$$

or

$$M_4 = 200\ \text{lb-in.}$$

The total moments on the loose flange and the ferrule are

$$(M)_{\text{loose flange}} = -\gamma\ M_4 + M_{20}\ (h_L/h_{L_o})$$

$$= -\ (0.727)(200) + 11{,}600\ (1.33) = 15{,}300\ \text{lb-in.}$$

$$(M)_{\text{ferrule}} = M_3 - M_4\ (1-\gamma\ ) - M_{20}\ (h_L/h_{LO}-1) + \text{initial assembly moment}$$

$$= 8{,}600 - 200\ (1-0.727) - 11{,}600\ (1.33-1) + 9{,}680$$

$$= 14{,}400\ \text{lb-in.}$$

Since the loose flange is more flexible than the ferrule, it is evident that for these moments the loose flange will rotate more than the ferrule. This indicates that the assumed location of the load reaction h_L=0.3 is still too large because there will be some $h_L < 0.3$ which will also cause the loose flange to rotate more than the ferrule. Following the method of the preceding section we find an improved value of the location of the load reaction as $h_L = 0.27$ in. Therefore

$$\gamma = h_L/h_G = 0.27/0.413 = 0.654$$

$$h_L/h_{LO} = 0.27/0.225 = 1.20$$

and Eq. (B.31) becomes

$$M_4\ \left[1\ /\ 4.05\text{x}10^6 + (0.654)^2/2.78\text{x}10^6 + (1-0.654)^2/3.35\text{x}10^6 + 1\ /\ 1.56\ \text{x}\ 10^6\right]$$

$$= 8{,}330/4.05\text{x}10^6 + (1-0.654)(8{,}600)/3.35\text{x}10^6$$

$$+ 11{,}600\ (1.20-1)\ \left[0.654/2.78\text{x}10^6 - (1-0.654)/3.35\text{x}10^6\right]$$

$$+ 200\ \left[1\ /\ 3.33\text{x}10^5 + (1-0.654/1.07\text{x}10^6\right]\ -26{,}600/1.55\text{x}10^8$$

$$-\ (-401)/(-1.03\text{x}10^5)$$

or

$$M_4 = 340\ \text{lb-in.}$$

The total moments on the loose flange and the ferrule are

$$(M)_{\text{loose flange}} = -\ \ M_4 + M_{20}\ (h_L/h_{LO})$$

$$= -\ (0.654)(340) + 11{,}600\ (1.20) = 13{,}700\ \text{lb-in.}$$

$$(M)_{\text{ferrule}} = M_3 - M_4\ (1-\gamma\ ) - M_{20}\ (h_L/h_{LO}-1) + \text{initial assembly moment}$$

$$= 8{,}600 - (340)(1.0654) - 11{,}600\ (1.20-1) + 9{,}680$$

$$= 15{,}900\ \text{lb-in.}$$

The corresponding rotations are

$$(\theta)_{\text{loose flange}} = (M_{\text{loose flange}})/C_2 = 13,700/2.78\text{x}10^6 = 4.93\text{x}10^{-3} \text{ rad.}$$

$$(\theta)_{\text{ferrule}} = (M_{\text{ferrule}})/C_3 + P/C_{3p} = 15,900/3.35\text{x}10^6 + 200/1.07\text{x}10^6$$

$$= 4.94\text{x}10^{-3} \text{ rad.}$$

The total moment on the integral flange is

$$(M)_{\text{integral flange}} = M_1 - M_4 + \text{initial assembly moment}$$

$$= 8,330 - 340 + 21,300 = 29,300 \text{ lb-in.}$$

The decrease in the bolt load is

$$-\Delta F_B = M_4/h_G = 340/0.413 = 824 \text{ lb.}$$

The decrease in the gasket load is

$$\Delta F_G = \Delta F - \Delta F_B = 26,600 + 824 = 27,400 \text{ lb.}$$

In addition to the hydrostatic and thermal load we also have the external moment of 48,000 lb-in. According to the simple flexural formula this moment will cause a maximum bending stress of approximately

$$48,000/3.2\,\gamma_o^2 g_o = 48,000/(3.2)(6.03)^2(0.062) = 6,650 \text{ psi}$$

in the stainless steel tube. The corresponding stresses in the flanges and the aluminum tube are much smaller. This external moment will also cause a maximum decrease in gasket load of magnitude*

$$(\Delta F_G)_{max} = M \Big/ (\pi/4)G^2 \left[1 + \left[(1+2h_G/G)^2 (k_b/k_g)\right]\right]$$

$$= 48,000 \Big/ \left(\frac{\pi}{4}\right)(13.024)^2 \left[1 + (1+0.826/13.024)^2 (9.37\text{x}10^6/3.76\text{x}10^8)\right]$$

$$= 350 \text{ lb/in.}$$

and a maximum increase in bolt load of

$$(\Delta F_B)_{max} = (K_B/K_G)(\Delta F_G)_{max} = (9.37\text{x}10^6/3.76\text{x}10^8)(350)$$

$$= 8.72 \text{ lb/in.}$$

which corresponds to a negligible increase of

$$(8.72)(\pi)(G+2h_G)/A_B$$

$$= (8.72)(\pi)(13.024+0.826)/2.10 = 181 \text{ psi}$$

*See Final Report for First Contract Period, Section 47, Design Criteria

in the maximum bolt stress. The above shows that because the gasket becomes very much stiffer at cryogenic temperatures, the external moment is mainly taken by the gasket.

The minimum gasket load under the combined operating pressure, temperature, and external moment environment is

$$51,500 - 27,400 - (350)(\pi)(13.024) = 9,800 \text{ lb.}$$

Since this is greater than the gasket load

$$H_D = (2b)(\pi GmP) = (3/8)(\pi)(13.024)(2.75)(200) = 8,450$$

required to maintain a tight joint under the operating pressure, leakage is not likely to occur.

D. Discussions

(1) In the preliminary design we considered the stresses due to flange moments alone and did not consider any stresses due to the barrelling effect. With the result of this section we could have calculated the stresses due to the barreling effect if we so wished even though this would be a somewhat tedious process. In general, the barreling effect is to relieve the maximum stresses due to flange moment. Waters* stated that "If the maximum longitudinal hub stress due to bolt pull alone occurs at the large end of the hub, it is considered unlikely that a much greater longitudinal stress, due to combined bolt pull and internal pressure, occurs at any point whatever." Therefore, we shall not consider the stresses due to barreling effect here. Since the maximum stresses due to barreling effect are generally of the same order of magnitude as the axial tensile stress due to hydrostatic end force* and are of secondary importance, flanges designed on the basis of the flange moments alone will not be overly conservative, either.

(2) Of the moments assumed in the preliminary design, the moment on the ferrule seems to be overestimated. This is because we assumed the load reaction between the loose flange and the ferrule acted at the top of the ferrule ring. If we are only interested in a satisfactory design with a minimum of time and effort, this procedure is recommended. However, if we are interested in a minimum weight design, it will save us some effort to assume, in the preliminary design stage, that the location of the load reaction is at the middle of the width of area of contact between the loose flange and the ferrule.

*Waters, op cit.

4.9.11 OPTIMIZATION OF THE PRELIMINARY DESIGN

The preliminary design connector was analyzed in Section 4.9.10 and found to be satisfactory. The connector will retain enough gasket compression to provide leak-tightness under the operating conditions. The maximum bolt load and flange moments existing in the connector are not greater than those assumed in the preliminary design and therefore will not be overstressed. But there is still room for improvement to achieve a lighterweight design. We shall discuss some possible refinements of the preliminary design in this section.

A. Bolts.

The bolt area chosen in the preliminary design is based on an anticipated bolt load of 1.25 W_{M2}. We found in Sect. 4.9.10, that the actual maximum bolt load is W_{M2}. Therefore the bolt area required may be reduced by one fifth. This may be achieved by, say, reducing the number of bolts from twenty four to twenty. This, however, would increase the bolt spacing to

$$\pi\ (G+2h_G)\ /\ 20 = 2.17 \text{ in.}$$

Even according to the Taylor Forge empirical formula, which was considered not conservative for the present connector, the flange thickness required for this bolt spacing is

$$t = \frac{2.75 + 0.5}{6}\left[2.17 - 2\ (3/8)\right] = 0.77 \text{ in.}$$

greater than the 0.75 in. thickness chosen. This shows that by merely decreasing the number of bolts will not result in a more economical design. An alternative would be to choose smaller size bolts. If we choose twenty-eight 5/16 in. fine series bolts each having a stress area of 0.0579 sq in., the maximum stress in the bolts will be approximately

$$W_{m2}\ /\ A_B = 51{,}500\ /\ (28)(0.0579), = 31{,}700 \text{ psi}$$

$$\simeq S_f = 40{,}000\ /\ 1.1 = 36{,}400 \text{ psi}$$

not including any torsional stress during bolting-up or bending stress due to flange rotations. The bolt spacing now becomes

$$\pi\ (13.85)\ /\ 28 = 1.55 \text{ in.}$$

greater than the minimum requirement of 2-1/4 bolt diameters. The flange thickness required to distribute the bolt load evenly is

$$t = \frac{2.75 + 0.5}{6}\left[1.55 - 2\ (5/16)\right] = 0.501 \text{ in.}$$

according to the Taylor Forge empirical formula. This, in comparison with the original thickness requirement of 0.585 in for the twenty-four 3/8 in. bolts indicate that a thinner flange, say, t = 0.6 in. may be used. This will result in considerable savings in weight. Furthermore, with the use of smaller bolts, the flange height can also be reduced accordingly.

In spite of the advantages of the smaller size bolts stated above, it is perhaps best not to change from the original twenty-four 3/8 in. bolts to the twenty-eight 5/16 in. bolts for the following reason. Because of the uncertain frictional effect it is difficultto install a correct tension in a bolt even with the use of a torque wrench. The 2024T4 aluminum bolt does not have much reserve strength beyond its yield point and overstressing is likely to occur if a small safety factor is used.

B. Integral Flange

The maximum moment on the integral flange is obtained in Section 4.9.10 as 33,400 lb-in. The maximum longitudinal hub stress was obtained in Section 4.9.6D as

$$S_H = 0.717\ M_o$$

$$= (0.717)(33,400) = 23,800 \text{ psi.} \quad \text{<} \quad S_f = 40,000 / 1.1 = 36,400 \text{ psi}$$

Since the stress S_H is inversely proportional to the square of the hub thickness while slight change in hub thickness will not change very much either M_o or the coefficient 0.717, we have a refined hub thickness as

$$\left(\sqrt{23,800/36,400}\right) \quad g_1 = \left(\sqrt{23,800/36,400}\right) \quad (0.375) = 0.304 \text{ in.}$$

Since this is smaller than the tube thickness of $g_o = 0.323$ in, no hub is required on the integral flange.

C. Loose Flange

We have stated that the loose flange is to be designed on the basis of rigidity rather than strength in order to prevent excessive bending of the bolts. A total rotation of

$$(\theta)_{\text{integral flange}} + (\theta)_{\text{loose flange}} = 8.13\text{x}10^{-3} + 8.20\text{x}10^{-3}$$

$$= 1.63\text{x}10^{-2} \text{ rad.}$$

was assumed in the preliminary design. The actual maximum rotation was found in Section 4.9.10 to be

$$(\theta)_{\text{integral flange}} + (\theta)_{\text{loose flange}}$$

$$= 9.15\text{x}10^{-3} + 5.68\text{x}10^{-3} = 1.48\text{x}10^{-2} \text{ rad.}$$

Since this is only slightly less than the assumed value and since the changes in the integral flange dimensions proposed in Paragraph B above will likely

increase the actual rotation, no reduction in the loose flange dimensions is recommended.

D. Ferrule

The maximum moment on the ferrule is obtained in Sect. 4.9.10 as $M_o = 18,000$ lb-in. The radial flange stress in the ferrule ring is

$$S_R = 1.00\ M_o$$

$$= (1)(18,000) = 18,000 \text{ psi}$$

for a 0.4 in. ring thickness. Since to a first approximation, the stress S_R is inversely proportional to the square of the hub thickness, a revised value of the ring thickness can be obtainable as

$$\left(\sqrt{18,000/S_f}\right)\ (0.4) = \left(\sqrt{18,000 \ /\ (30,000 \ /\ 1.1)}\ \right)\ (0.4)$$

$$= 0.325 \text{ in.}$$

We shall take the ring thickness as t = 0.35 in. since with the reduction in ferrule dimensions a somewhat greater moment will be transmitted to the ring.

The longitudinal hub stress is approximately

$$S_H = 0.996\ M_o = (0.996)(18,000) = 18,000 \text{ psi}$$

for a hub thickness of $g_1 = 0.35$ in. A revised value of the hub thickness can be obtained as

$$\sqrt{(18,000) \ /\ (30,000 \ /\ 1.1)}\ \ (0.35) = 0.285 \text{ in.}$$

Let us take it as $g_1 = 0.3$ in.

E. Summary of Dimensions of the Connector According to the Refined Design

The following drawing shows the refined version of our connector.

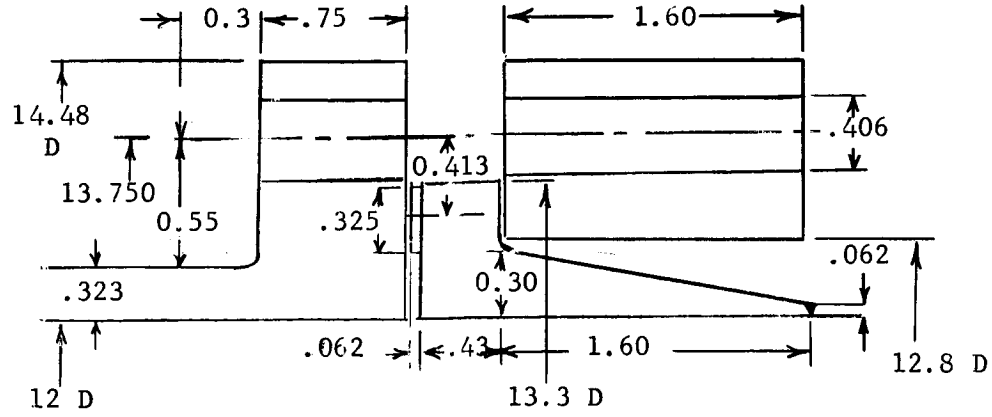

We have to go through the procedure of Section 4.9.9 and 4.9.10 again to determine if this refined design is satisfactory. It is believed that this design will most likely be safe as far as stresses are concerned. However, with the reduced dimensions the flanges will be more flexible. The result is that the reduction in gasket stress will be greater under the operating condition. Since the minimum gasket stress for the sturdier preliminary design connector under the operating condition is not much greater than the gasket stress required to maintain a tight joint there is some reason to doubt whether the present refined design will maintain enough gasket load under the operating condition. Should we find out this were the case as we went through the procedure of Sect.4.9.10, we could increase the initial bolt load somewhat. This would in turn increase the flange moment and might require us to restore some of the flange thickness.

It is clear from the above that the connector design is a tedious cut-and-try process. However, with a well chosen preliminary design, usually a single refinement is sufficient to achieve an optimum, minimum weight design.

4.10 **APPENDIX II - A SIMPLIFIED METHOD OF ANALYSIS OF FLANGED CONNECTORS WITHOUT CONTACT OUTSIDE BOLT CIRCLE**

It is well known* that design calculations based on ASME Code do not indicate conditions that actually exist in a flanged joint, but merely represent some arbitrary stage in the tightening of bolts. Yet to determine the variations in load, moment and stress that take place in a connector from initial tightening to proof testing, and to the service temperature and pressure becomes a complex task because the bolt load, gasket load and the flange moments are all interrelated. In the following we shall present a simple, "building block" approach for the analysis of flanged connectors without contact outside the bolt circle. It is believed that this method is conceptually clear and easy to apply.

A. When Both Flanges Are Integral Flanges

In analyzing a connector with integral flanges it is most convenient to follow Dudley** by decomposing the external load on the flanges into a force passing through a certain point and a moment. The force will separate the flanges without causing rotation of the flanges. Similarly the moment will rotate the flanges without separating them. The possibility of this decomposition will be shown in the succeeding paragraphs.

(1) Analysis of the bolts and gasket system

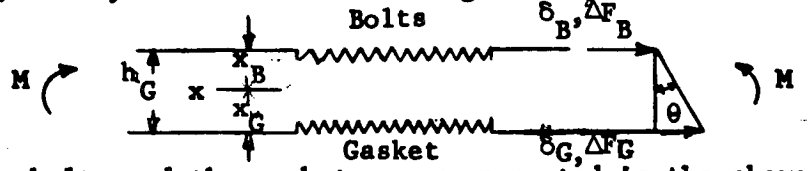

The bolts and the gasket are represented in the above figure by linear springs. ΔF_B and ΔF_G are the bolt load and gasket load increments, tension being considered positive. δ_B and δ_G are the extensions of the bolt and the gasket. These are all measured from the initially assembled condition.

We can define the stiffnesses of the bolts and gasket as

$$k_B = \Delta F_B/\delta_B \qquad \text{(B.1a)}$$

$$k_G = \Delta F_G/\delta_G \qquad \text{(B.1b)}$$

If Hooke's law holds for the bolts and the gasket we have

$$k_B = A_B E_B/\ell_B \qquad \text{(B.2a)}$$

$$k_G = A_G E_G/\ell_G \qquad \text{(B.2b)}$$

where A_B and A_G are the total bolt and gasket areas, E_B and E_G are Young's modulus of the bolt and gasket material, ℓ_G is the gasket thickness, and ℓ_B the effective length of the bolt extending one-half bolt diameter beyond the base of the nut.

* "Pressure Vessel and Piping Design - Collected Papers 1927-1959," ASME, New York 1950, p. 122.

**"Deflection of Heat Exchanger Flanged Joints as Affected by Barreling and Warping" by W.M. Dudley, Journal of Engineering for Industry, Nov. 1961, pp 460-466.

From the individual stiffnesses we can define a combined axial stiffness of the bolts and gasket system by the following equation

$$k = k_B + k_G = \Delta F/\delta = (\Delta F_B + \Delta F_G)/\delta = (k_B\delta_B + k_G\delta_G)/\delta \qquad (B.3)$$

From this equation we can see that δ is the extension of a point x which is at a distance of

$$x_G = k_B h_G/(k_B + k_G) \qquad (B.4a)$$

$$x_B = k_G h_G/(k_B + k_G) \qquad (B.4b)$$

from the gasket circle and the bolt circle. We can also define a rotational rigidity of the bolts and gasket system as

$$c = M/\theta \qquad (B.5)$$

where $M = \Delta F_G x_G - \Delta F_B x_B = k_B k_G h_G(\delta_G - \delta_B)/(k_B + k_G)$ (B.6)

is the moment about the point x and

$$\theta = (\delta_G - \delta_B)/h_G \qquad (B.7)$$

Therefore, the rotational rigidity

$$c = k_B k_G h_G^2/(k_B + k_G) \qquad (B.8)$$

In addition to extension and rotation due to load variation there are also the extension and rotation due to temperature variation. The thermal extension of the bolts and the gasket are $\alpha_B \ell_B \Delta T_B$ and $\alpha_G \ell_G \Delta T_G$ respectively. The α's are linear coefficients of thermal expansion and the ΔT's are temperature increments. In our previous representation of bolts by a linear spring, the effective length (almost identical to the full length) of the bolt is considered. This is meaningful because the flange thickness is almost invariant under load. The flange thickness certainly will change under temperature variations. Therefore the apparent extension of a bolt is

$$\delta_{BT} = \alpha_B \ell_B \Delta T_B - \alpha_{F1} \ell_{F1} \Delta T_{F1} - \alpha_{F2} \ell_F \ell \Delta T_{F2} \qquad (B.9)$$

where the subscripts F1 and F2 refer to the two flanges connected by the bolts and ℓ_{F1} and ℓ_{F2} are flange thicknesses. From δ_{BT} and the thermal extension of the gasket $\delta_{GT} = \alpha_G \ell_G \Delta T_G$ we can define the thermal extension of the gasket bolt system as

$$\delta_T = (k_G\delta_{GT} + k_B\delta_{BT})/(k_B + k_G)$$

$$= \left[k_G\, \alpha_G \ell_G \Delta T_G + k_B(\alpha_B \ell_B \Delta T_B - \alpha_{F1} \ell_{F1} \Delta T_{F1} - \alpha_{F2} \ell_{F2} \Delta T_{F2})\right]/(k_B + k_G) \qquad (B.10)$$

and the thermal rotation as

$$\theta_T = (\delta_{GT} - \delta_{BT})/h_G = \left[\alpha_G \ell_G \Delta T_G - (\alpha_B \ell_B \Delta T_B - \alpha_{F1} \ell_{F1} \Delta T_{F1}) - (\alpha_{F2} \ell_{F2} \Delta T_{F2})\right] / h_G \quad \text{(B.11)}$$

In particular, for uniform temperature increments, $\Delta T_G = \Delta T_B = \Delta T_{F2} = \Delta T$ we can define thermal stiffnesses

$$k_T = (k_B + k_G) / \left[k_G \alpha_G \ell_G + k_B (\alpha_B \ell_B - \alpha_{F1} \ell_{F1} - \alpha_{F2} \ell_{F2})\right] \quad \text{(B.12a)}$$

$$c_T = h_G / \left[\alpha_G \ell_G - (\alpha_B \ell_B - \alpha_{F1} \ell_{F1} - \alpha_{F2} \ell_{F2})\right] \quad \text{(B.12b)}$$

such that

$$\delta_T = \Delta T / k_T \quad \text{(B.13a)}$$

$$\theta_T = \Delta T / c_T \quad \text{(B.13b)}$$

The thermal stiffnesses reduce to the following simple forms when the flanges and bolts are made of the same material

$$k_T = (k_B + k_G) / \ell_G (k_G \alpha_G + k_B \alpha_B) \quad \text{(B.14a)}$$

$$c_T = h_G / \ell_G (\alpha_G - \alpha_B) \quad \text{(B.14b)}$$

(2) Analysis of the Flange

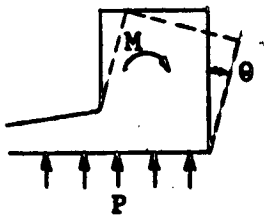

The rotation of the flange under the moment M is given by

$$\theta = M/c \quad \text{(B.15)}$$

where the stiffness is

$$c = L h_o g_o^2 E / (1 - \mu^2) V \quad \text{(B.16a)}$$

according to ASME Code procedure or

$$c = 2\pi\beta I_y E X / r_c z (r_o r_c I / z A_F + 1/4\beta^2 z) \quad \text{(B.16b)}$$

by Dudley's* method. There is some minor difference between the stiffnesses given by Eqs. (B.16a) and (B.16b). Eq. (B.16a) is preferred because it can be readily determined from design charts in the ASME Code.

* Dudley, op. cit.

The rotation of the flange under the internal pressure P (barreling effect) is given by

$$\theta = P/c_p \qquad (B.17)$$

where the stiffness c_p is approximately

$$c_p = XEgIy/\ r_o^4 I(1 - \mu/2 - g/h_f)(1/2\beta^2 + z/\beta) \qquad (B.18)$$

where h_f is the average flange height and $g = g_o$ if the hub is considered as part of the flange and $g = g_1$ if the hub is considered as part of the tube.

With this information we are now ready to study the overall behavior of a flanged connector.

(3) Over-all Behavior of the Connector

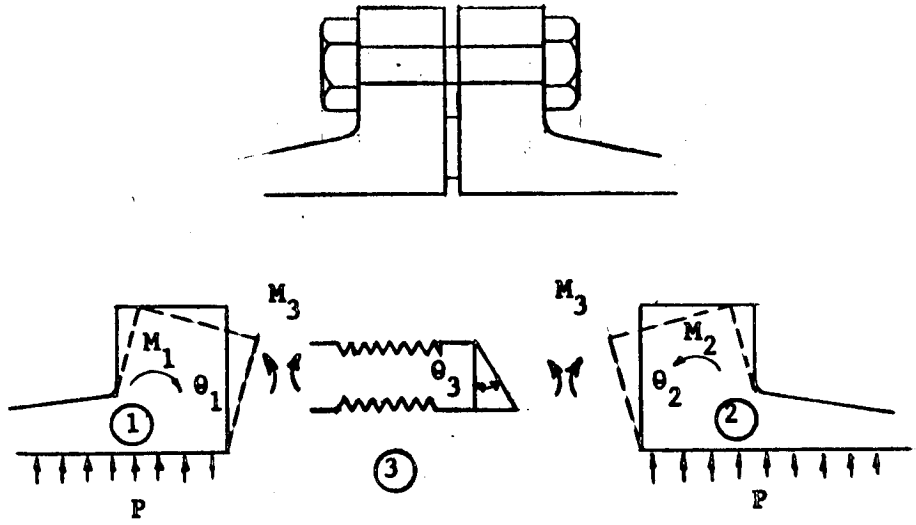

Following Section A.(1) we shall resolve the load on the bolts-gasket system into a force ΔF passing through the point x and a moment M_3 about the same point. The force will cause stretching but not rotation of the bolts-gasket system. Similarly the moment will cause rotation but not stretching of the system. To take advantage of this property we shall find it convenient to resolve any external axial force and moment on the flange also into a force ΔF passing through x and a moment M_1 (or M_2) about x. By external axial force we mean the hydrostatic end force, the force arising from constrained thermal expansion and anything other than the bolts and gasket reactions. Equilibrium requires that the resultant of these external forces be equal to the total force on the bolts-gasket system. This is why we have used ΔF indiscriminately in the above. The advantage of our scheme is now clear. The external axial force ΔF thus defined will only cause stretching of the bolts-gasket system or separation of the flanges by the amount $\Delta F/k$. It will

not cause any rotations and need not be considered any further. The net moment on the flange is now the sum of the external moment about the point x and the internal moment of the bolts-gasket system, or equal to M_1 (or M_2) - M_3 as shown in the above figure.

Recalling the definitions of the individual stiffnesses of the components we can write down immediately

$$(M_1 - M_3)/c_1 + P/c_{1P} = \theta_1 \qquad \text{(B.19a)}$$

$$(M_2 - M_3)/c_2 + P/c_{2P} = \theta_2 \qquad \text{(B.19b)}$$

$$M_3/\theta_3 + \Delta T/c_T = \theta_3 \qquad \text{(B.19c)}$$

The last equation assumes that all the components are at the same temperature increment ΔT. Compatibility of rotation gives us

$$\theta_1 + \theta_2 = \theta_3 \qquad \text{(B.20)}$$

Therefore

$$(M_1 - M_3)/c_1 + P/c_{1P} + (M_2 - M_3)/c_2 + P/c_{2P} = M_3/c_3 + \Delta T/c_T$$

or

$$M_3 = (1/c_1 + 1/c_2 + 1/c_3)^{-1}\left[M_1/c_1 + M_2/c_2 + P(1/c_{1P} + 1/c_{2P}) - T/C_T\right] \qquad \text{(B.21b)}$$

The moments M_1 and M_2 on the flanges, the pressure P, the temperature increment ΔT, and the axial force ΔF are known quantities. Eq. (B.21b) is a very simple algebraic equation which gives the moment M3 in terms of the known quantities. When M3 is known, the rotation of the flanges on the bolts-gasket system and the stresses in the flanges can be readily calculated. The bolt load and gasket stress are given by Eqs. (B.3) and (B.6) in terms of ΔF and M_3.

B. When One of the Flanges is a Floating Flange

In problem A when both flanges are integral flanges we were able to decompose the external load on the flanges into a force passing through a certain point and a moment. The force will separate the flanges without causing rotations of the flanges. Similarly the moment will rotate the flanges without causing separation of the flanges. In the present problem such a decomposition is not possible. This can be seen from the fact that if a force tends to separate the flanges, the bolt load will increase and this invariably increases the rotation of the floating flange. The result is that there are cross couplings among forces, moments, flange separation and rotation.

In the present problem we shall find it convenient to decompose the external load on the flanges into a force at the gasket circle and a moment about the gasket circle. The advantageof this decomposition will be clear later on even though the cross coupling mentioned above still exists.

(1) Analysis of the Bolts and Gasket System

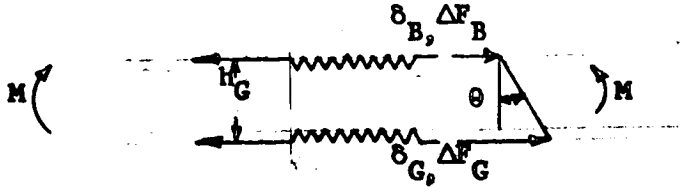

The resultant force and moment on the bolt-gasket system are defined as:

$$\Delta F = \Delta F_B + \Delta F_G \qquad \text{(B.22a)}$$

$$M = -\Delta F_B h_G \qquad \text{(B.22b)}$$

The rotation of the bolt-gasket system is

$$\theta = (\delta_G - \delta_B)/h_G = (\Delta F_G/k_G - \Delta F_B/k_B)/h_G = \Delta F/k_G h_G + M/C \qquad \text{(B.23)}$$

where

$C = k_G k_B h^2 G/(k_B + k_G)$ as defined previously.

Similarly the stretching of the gasket is

$$\delta_G = \Delta F_G/k_G = (\Delta F - \Delta F_B)/k_G = \Delta F/k_G + M/k_G h_G \qquad \text{(B.24a)}$$

and the stretching of the bolt is

$$\delta_B = \Delta F_B/k_B = M/k_B h_G \qquad \text{(B.24b)}$$

The thermal rotation of the bolt-gasket system is given, as before, by Eq. (B.13b) for the case of uniform temperature.

(2) Analysis of the Flanges

The integral flange has been analyzed in Part A. The only difference now is that we shall decompose the external load on the flange into a force passing through the gasket circle and a moment about the gasket circle. A loose flange is shown

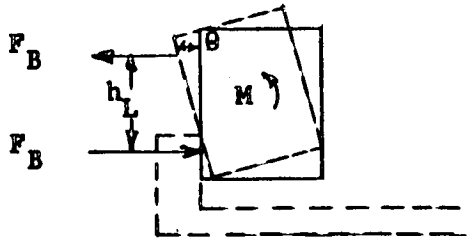

in the figure. The resultant load on the flange is a moment $M = F_B h_L$. The rotation of the flange under the moment is

$$\theta = M/c \qquad \text{(B.25)}$$

where the rotational rigidity of the flange is

$$c = 2\pi EI_y/r_c \qquad \text{(B.26)}$$

(3) Over-all Behavior of the Connector

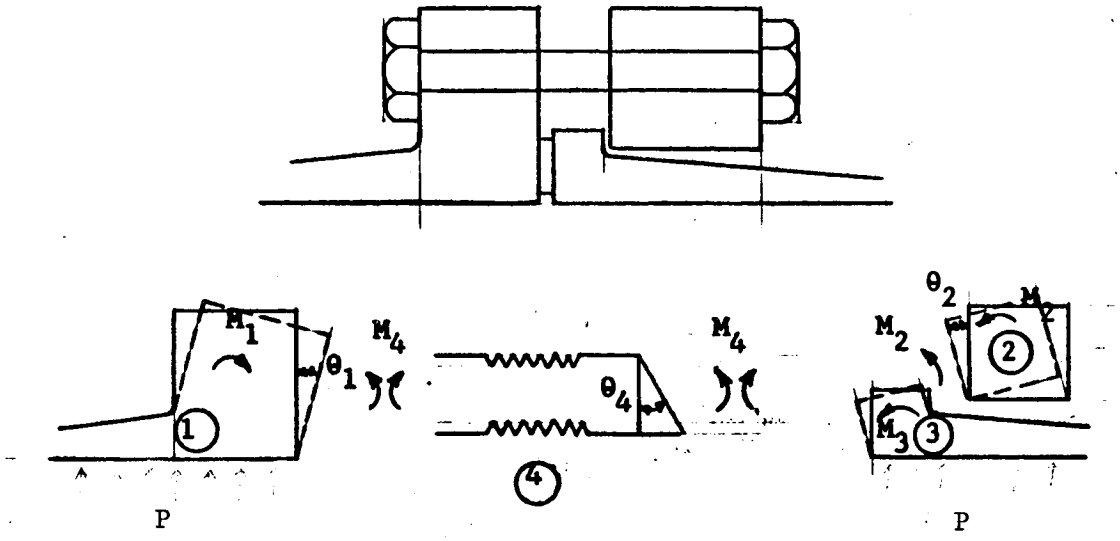

For the integral flange we have

$$(M_1 - M_4)/c_1 + P/c_{1P} = \theta_1 \qquad \text{(B.27a)}$$

For the loose flange

$$M_2/c_2 = \theta_2, \qquad \text{(B.27b)}$$

$$M_2 + \Delta F_B h_L = -(h_L/h_G)\, M_4 \qquad \text{(B.27c)}$$

For the ferrule

$$(M_3 - M_2 - M_4)/c_3 + P/c_{3P} = \theta_3$$

or

$$\left[M_3 - M_4(1 - h_L/h_G)\right]/c_3 + P/c_{3P} = \theta_3 \qquad \text{(B.27d)}$$

Compatibility of deformation requires that

$$\delta_G - h_G\theta_1 - h_L\theta_2 - \theta_3(h_G - h_L) = \delta_B \qquad \text{(B.28a)}$$

or

$$\theta_4 - \theta_1 - (h_L/h_G)\theta_2 - (1 - h_L/h_G)\theta_3 = 0 \qquad \text{(B.28b)}$$

Substituting in the loads and stiffnesses we obtain

$$M_4 \left\{1/c_1 + 1/c_4 + (1 - \gamma)^2/c_3 + \gamma^2/c_2\right\}$$

$$= M_1/c_1 + (1 - \gamma)M_3/c_3 + P\left[1/c_{1P} + (1 - \gamma)/c_{3P}\right] - \Delta F/k_G h_G - \Delta T/c_T \qquad \text{(B.29)}$$

where

$$\gamma = h_L/h_G.$$

Eq. (B.29) is a simple algebraic equation which gives the moment on the bolt-gasket system M_4 in terms of the known axial force ΔP, temperature ΔT, moment on the integral flange M_1 and moment on the ferrule M_3. When M_4 is known the stresses and deflections of interest to us can be readily calculated.

Sometimes the location of the load reaction between the loose flange and the ferrule changes with load. Under this circumstance, instead of Eq. (27b), we have

$$\left[M_2 + M_{20}\,(h_L/h_{L0} - 1)\right]/c_2 = \theta_2 \qquad \text{(B.30a)}$$

Similarly, Eq. (27d) is replaced by

$$\left[M_3 - M_4\,(1 - h_L/h_G) - M_{2o}\,(h_L/h_{L0} - 1)\right]/c_3 + P/c_{3P} = \theta_3 \qquad \text{(B.30b)}$$

where M_{2o} is the initial moment on the loose flange and h_{L0} is the initial location of the load reaction between the loose flange and the ferrule. Notice that the terms in the brackets of Eqs. (B.30) represent the increase in moment on the loose flange and the ferrule respectively. Substitution of Eqs. (B.30) into Eq. (B.28b) we obtain instead of Eq. (B.29),

$$\begin{aligned} M_4 &\left[1/c_1 + \gamma^2/c_2 + (1 - \gamma)^2/c_3 + 1/c_4\right] \\ &= M_1/c_1 + (1 - \gamma)\,M_3/c_3 + M_{20}(h_L/h_{L0} - 1)\left[\gamma/c_2 - (1 - \gamma)/c_3\right] \\ &\quad + P\left[1/c_{1p} + (1 - \gamma)/c_{3P}\right] - \Delta F/k_G h_G - \Delta T/c_T \end{aligned} \qquad \text{(B.31)}$$

C. Note

(1) Since the flanged connector is tightened by advancing the nut on the bolt, the above analysis does not apply to the initial bolt-tightening period. The loads and deflections referred to above should be understood to be those beyond the initial assembled condition. However, with the stiffness of the components given it is a simple matter to calculate the initial stresses and deflections.

(2) Frictional effect has not been included in the above analysis.

4.11 APPENDIX III EQUIVALENT THICKNESS OF A TAPERED HUB-TUBE

Oftentimes it is desirable to represent a tapered hub-tube by a uniform thickness tube in order to obtain an approximate solution / to its stiffness characteristics. To a first approximation, we may take the average thickness of the tapered hub-tube as the equivalent uniform-tube thickness. Obviously this is not very satisfactory because we know that the material closer to the load has greater effect. Therefore as the tapered hub becomes long the accuracy of this procedure deteriorates. In order to obtain an improved approximation we note that the solution for uniform thickness tube decays exponentially from the loaded end approximately. This suggests the following exponentially weighted equivalent thickness

$$g_{eqv.} = \frac{\int_0^\infty g e^{-\beta} dx}{\int_0^\infty e^{-\beta} dx} \qquad (C.1)$$

where x = 0 is the loaded end and

$$\beta = \sqrt[4]{3(1 - \mu^2)}/\sqrt{rg}$$

The integrals in Eq. (1) converge fast and it is usually sufficient to carry out the integration to $x = \sqrt{B(g_1 + g_o)/2}$. If the hub taper varies in a more complex manner the integral in the numerator of Eq. (C.1) can be integrated graphically or numerically.

APPENDIX IV NOMENCLATURE

The nomenclature used in the design procedure is presented in the following. Whenever possible the ASME code nomenclature is used.

A = outside diameter of flange

A_B = total cross-sectional area of bolts

A_F = cross-sectional area of flange

A_G = face area of gasket

A_m = total required cross-sectional area of bolts

B = inside diameter of flange

b = effective gasket seating width

b_o = basic gasket seating width

C = bolt-circle diameter

c = rotational rigidity, lb-in/rad.

c_P = barreling rigidity, psi/rad.

c_T = thermal rotational rigidity, ^oF/rad.

d = factor $h_o g_o^2 U/V$

E = modulus of elasticity

e = factor = F/h_o

F = factor, for integral-type flanges obtain from Fig. UA-51.2 ASME code
for loose-type flanges obtain from Fig. UA-51.4 ASME code

f = hub stress correction factor, obtain from Fig. UA-51.6 ASME Code

G = diameter at location of gasket load reaction

g_o = thickness of hub at small end

g_1 = thickness of hub at back of flange

H = total hydrostatic end force = $0.785G^2P$

H_D = hydrostatic end force on area inside of flange = $0.785\ B^2P$

H_m = fictitious decrease in gasket force due to external moment

H_D = gasket force required under operating pressure = 2b x 3.14 GmP

H_T = difference between total hydrostatic end force and the hydrostatic end force on area inside of flange = $H - H_D$

h = hub length

h_D = radial distance from the bolt circle to the circle on which H_D acts as prescribed in Par. UA-49, ASME Code

h_f = average flange height

h_G = radial distance from gasket load reaction to the bolt circle, (C - G)/2

h_L = radial distance from the bolt circle to the load reaction between the loose flange and the ferrule.

h_o = factor = $\sqrt{Bg_o}$

h_T = radial distance from the bolt circle to the circle on which H_T acts as prescribed in Par. UA-49, ASME code.

I = bending rigidity of tube = $g_o^3/12(1 - \mu^2)$

I_y = moment of inertia of flange cross section about the radial axis through its centroid.

K = ratio of outside diameter of flange to inside diameter of flange = A/B

k_B, k_G, k = stiffnesses of bolts, gasket and bolts-gasket system

L = factor = $(te+ 1)/T + t^3/d$

ℓ_B, ℓ_G = Effective length of bolt and thickness of gasket

M = moment

m = gasket factor, obtain from Table UA-47.1, ASME Code

P = pressure

Q = radial shearing force

r_o = mean radius of tube

r_c = radial distance to the centroid of the flange cross section

S_f = design stress

S_H = longitudinal stress in hub

S_R = radial stress in flange

S_T = tangential stress in flange

T = factor involving K, obtain from Fig. UA-51.1, ASME Code

t = flange thickness

U = factor involving K, obtain from Fig. UA-51.1, ASME Code

V = factor, obtain from Fig. UA-51.3 for integral-type flanges
from Fig. UA-51.5 for loose-type flanges

W_B, W_G = total bolt load and gasket load

W_{m2} = required seating load

X = factor, see Eq. (13), Reference 2.

Y = factor involving K, obtain from Fig. UA-51.1, ASME Code

Z = factor involving K, obtain from Fig. UA-51.1, ASME Code

z = distance from end of tube to the centroid of the flange cross section

$\alpha_B, \alpha_F, \alpha_G$ = linear coefficients of thermal expansion of bolt, flange, and gasket material

β = shell constant = $\sqrt[4]{3(1 - \mu^2)} / \sqrt{r_o g_o}$

γ = h_L / h_G

ΔF = increase in tension in the bolts-gasket system = $\Delta F_B + \Delta F_G$

ΔF_B = increase in bolt tension

ΔF_G = decrease in gasket compression

ΔT = temperature increment

δ = length or thickness increment

θ = angle of rotation

μ = Poisson's ratio

4.13 APPENDIX V Drawings of Test Section

1) 544E533 Sheet 1

2) 544E533 Sheet 2

FOLDOUT FRAME

FOLDOUT FRAME 2

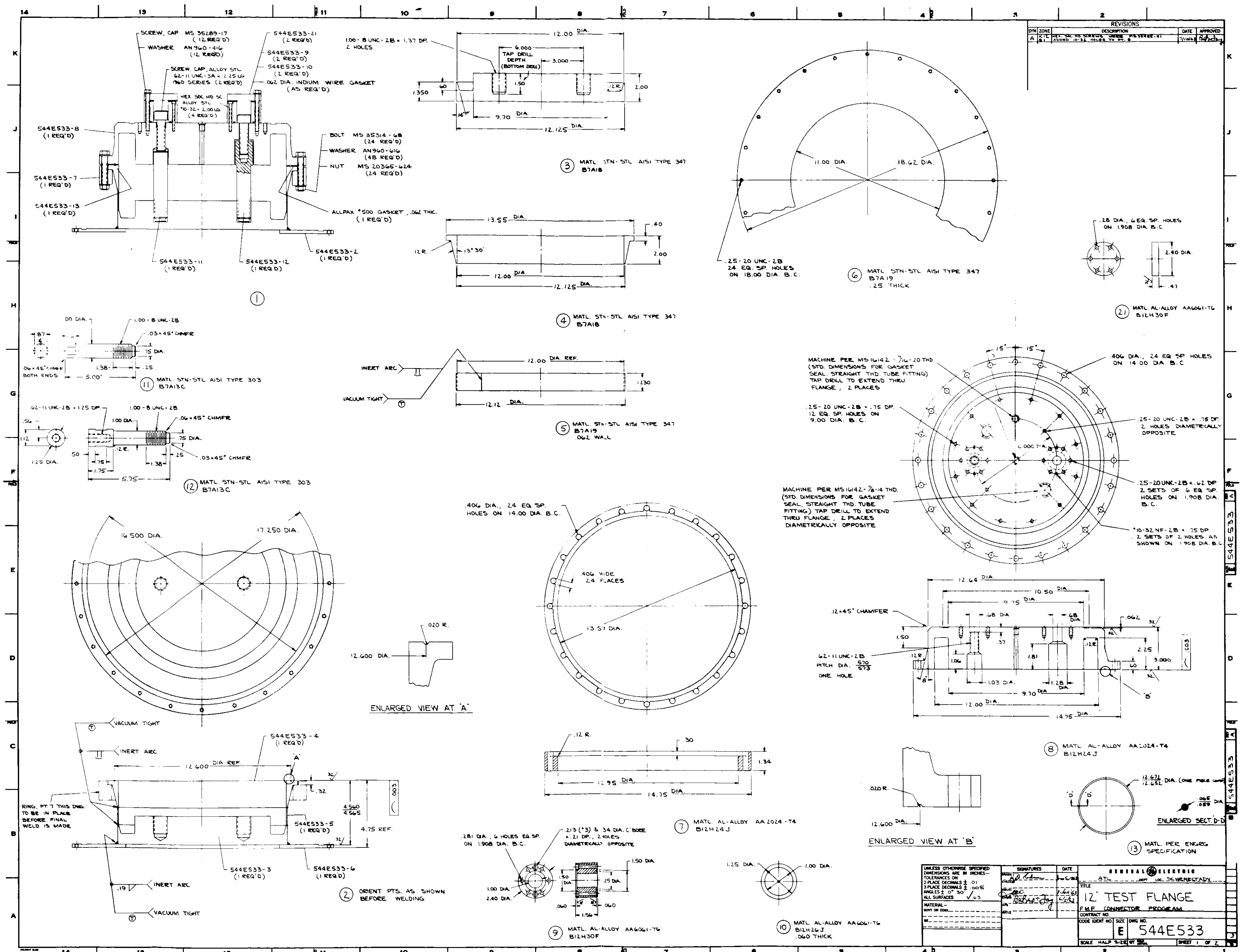

ORIGINAL PAGE IS OF POOR QUALITY

ORIGINAL PAGE IS OF POOR QUALITY

FOLDOUT FRAME

FOLDOUT FRAME 2

REVISIONS			
SYM	ZONE	DESCRIPTION	DATE	APPROVED

END FITTING PER MS33656-4 WITH .25 O.D. TUBING × 6.00 LG. (2 REQ'D)

LIFTING EYE BOLT, .25-20 (2 REQ'D)

CONAX THERMOCOUPLE GLAND CAT.# TG 20-A16 WITH MOUNTING THD. PER MS33656-10 (O-RING MTG) 5 PLACES

SCREW, CAP MS35289-3 (24 REQ'D)

WASHER AN960-416 (24 REQ'D)

SCREW, CAP MS35289-8 (12 REQ'D)

WASHER AN960-416 (12 REQ'D)

.50 DIA., ONE HOLE IN PT. 18 FOR PT. 17

INERT ARC

VACUUM TIGHT

(17) MATL. AL-ALLOY TUBING AA6061-T6 B12H6G 500 O.D. × .049 WALL × 6.00 LG.

.12

SECTION E-E

7.25 R

.28 DIA., 24 EQ. SP. HOLES ON 18.00 DIA. B.C.

.28 DIA., 12 EQ. SP. HOLES ON 9.00 DIA. B.C.

15°

MACHINE PER MS16142-7/8-14 THD. (STD. DIMENSIONS FOR GASKET SEAL, STRAIGHT THD. TUBE FITTING) 3 EQ. SP. HOLES 1.25 HOLES IN PT. 18 FOR PT. 16

INERT ARC

VACUUM TIGHT

S44E533-15 (1 REQ'D)

S44E533-1 (1 REQ'D)

(14)

(18) MATL. AL-ALLOY AA6061-T6 B12H26J

S44E533-16 (3 REQ'D)

(19) MATL. AL-ALLOY AA6061-T6 B12H26J .188 WALL

16.87 DIA.

8.50 DIA.

.070

.25

9.78 DIA.

10.00 DIA.

10.25 DIA.

10.47 DIA.

13.00 DIA.

7.312

INERT ARC 3 PLACES

VACUUM TIGHT

INERT ARC

VACUUM TIGHT

TACK WELD AS REQ'D TO MAINTAIN MINIMUM DISTORTION

.070

.25

16.12 DIA.

16.53 DIA.

16.75 DIA.

17.00 DIA.

17.22 DIA.

18.62 DIA.

(20) MATL. AL-ALLOY AA6061-T6 B12H26J

(15)

1.50 DIA.

1.06

1.19

1.25 DIA.

(16) MATL. AL-ALLOY AA6061-T6 B12H30F

UNLESS OTHERWISE SPECIFIED DIMENSIONS ARE IN INCHES— TOLERANCES ON: 2-PLACE DECIMALS ± .01 3-PLACE DECIMALS ± .005 ANGLES ± 0°30' ALL SURFACES √63 MATERIAL — GOVT OR COML —	SIGNATURES	DATE

GENERAL ELECTRIC

ATC DEPT LOC. SCHENECTADY

TITLE 12" TEST FLANGE

FMF CONNECTOR PROGRAM

CONTRACT NO.

CODE IDENT NO. | SIZE | DWG NO.

E | 544E533

SCALE HALF SIZE | WT | SHEET 2 OF 2

544E533 REV E

ORIGINAL PAGE IS OF POOR QUALITY

ORIGINAL PAGE IS OF POOR QUALITY

4.14 Appendix VI - Test Procedure

4.14.1 Description of Test Set-Up

A. Schematic of Test Set-Up

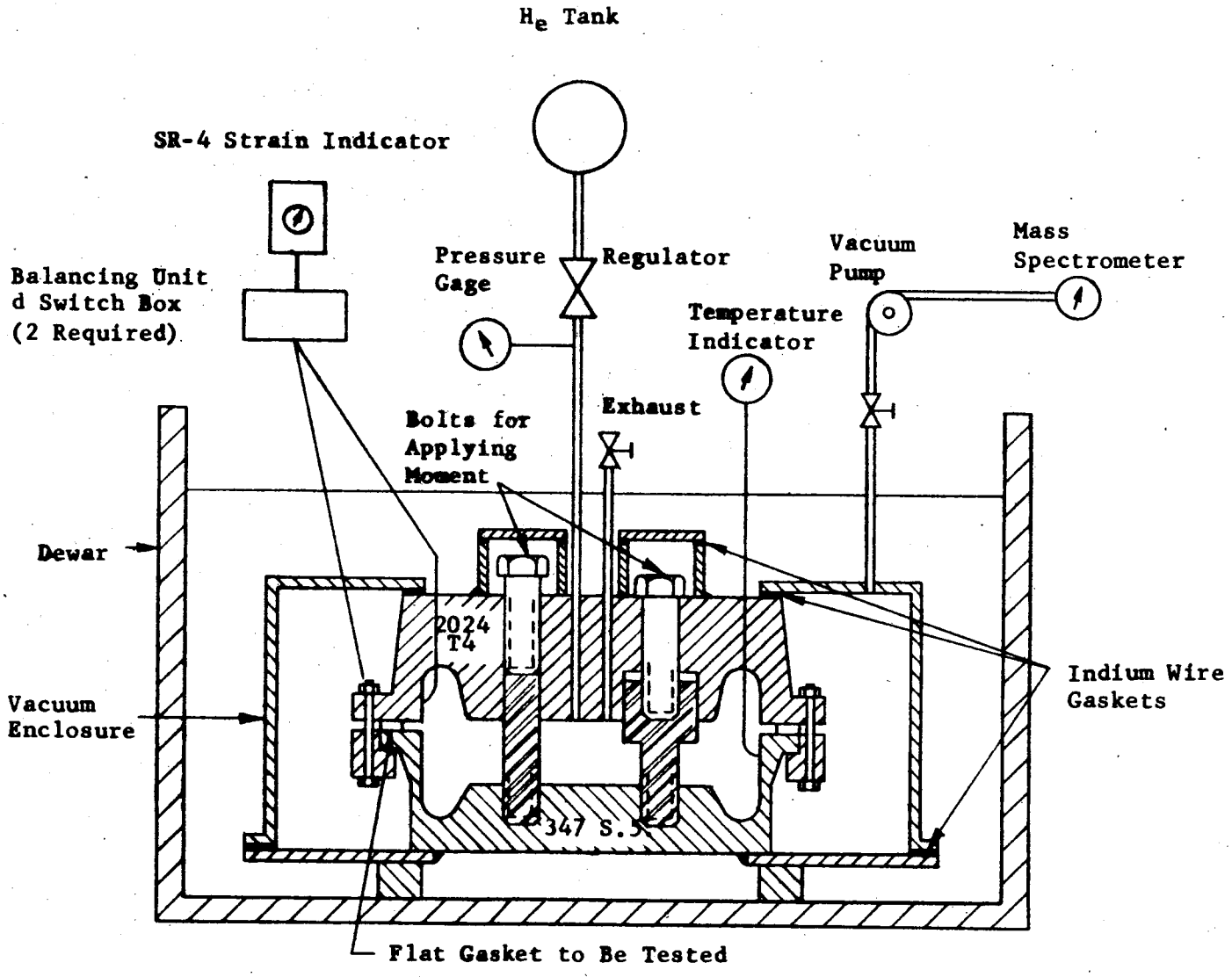

B. Bolt Numbering and Torque Sequence

● Strain gage Bolts

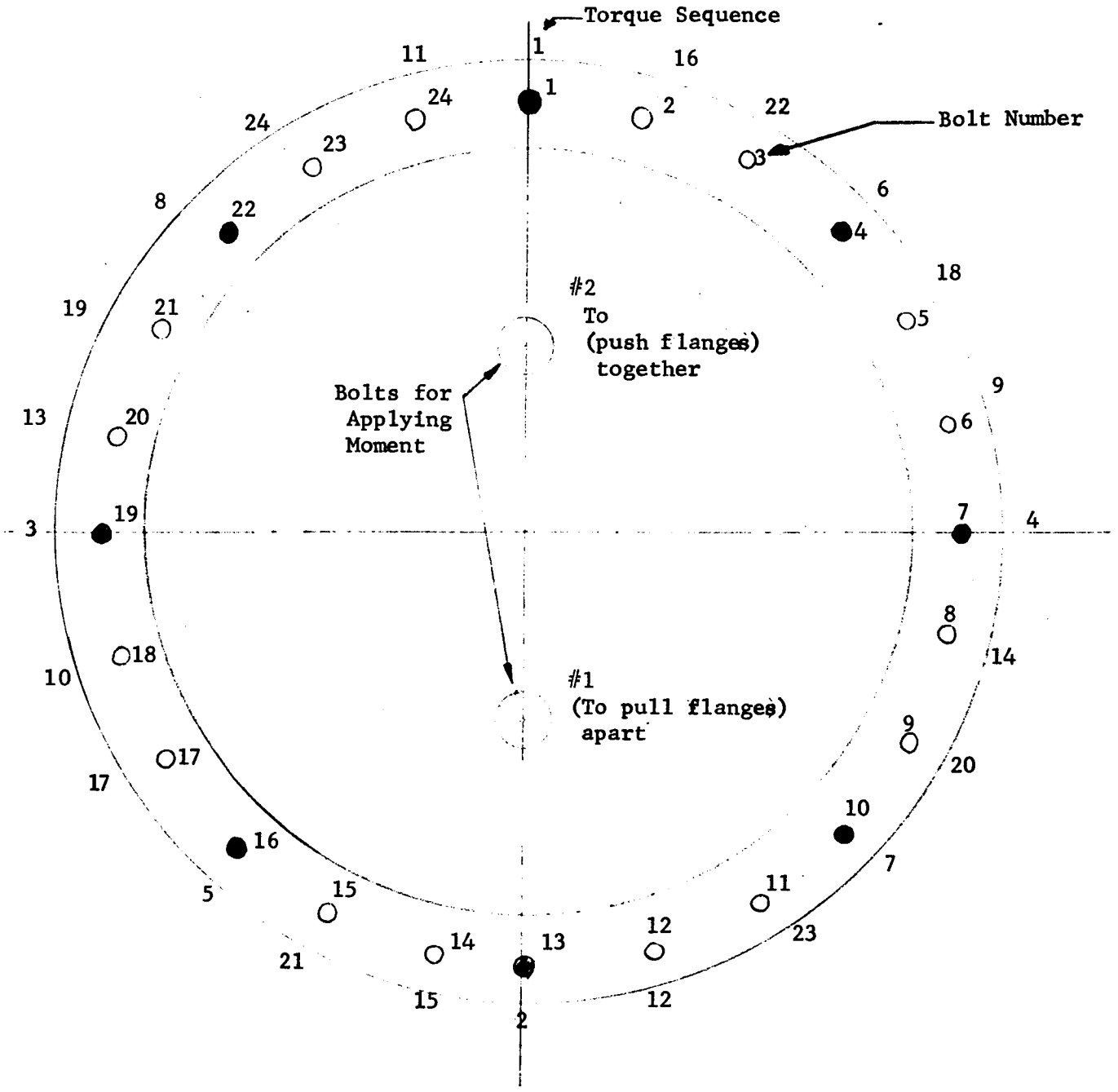

Torque Sequence for Each Specified Torque Increment

C. Strain Gage Location and Numbering

(1) Strain gages in bolts

Bolts #1, 4, 7, 10, 13, 16, 19, 22 have built-in strain gages. Their leads are numbered 1, 2, 3, 4, 5, 6, 7, 8 respectively. The dummy gage for these is to be labeled as B.

(2) Strain gages on the integral aluminum flange and hub.

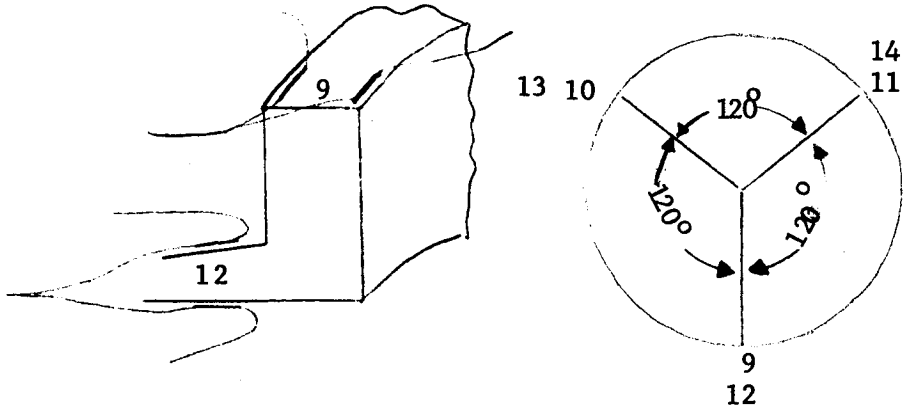

The strain gages are located 120° apart and connected as shown in order to measure bending strains. The leads are numbered as 9, 9c, 10, 10c, 11, 11c, 12, 12c, 13, 13c, 14, 14c respectively. The letter c denotes the common point of the two pairs of gages. Notice that there are only three (3) leads for the gages on the flange (for instance two (2) #9's and one (1) #9c), while there are four (4) leads for the gages on the hub (for instance two (2) 12's and two (2) #12c's).

Notice that no dummy gage is needed.

(3) Strain gages on the floating flange

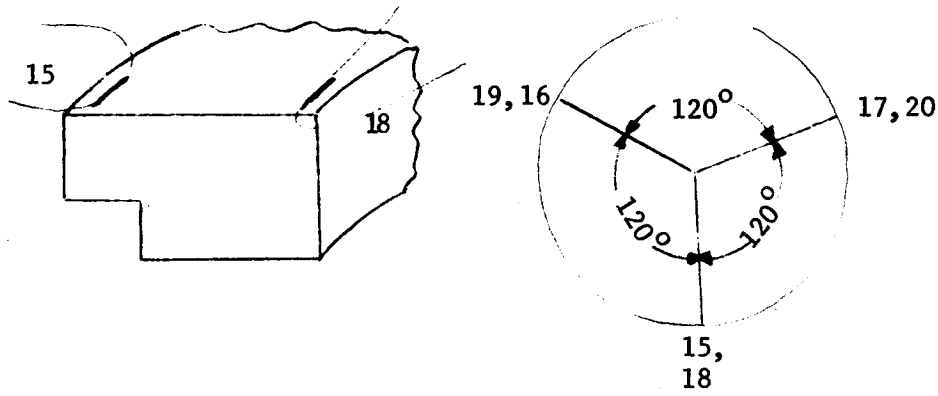

The leads are numbered

15, 16, 17, 18, 19, 20

There are, of course, two identically numbered leads for each gage. The dummy gage is labeled F.

(4) Strain gages on the ferrule

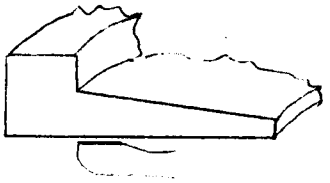

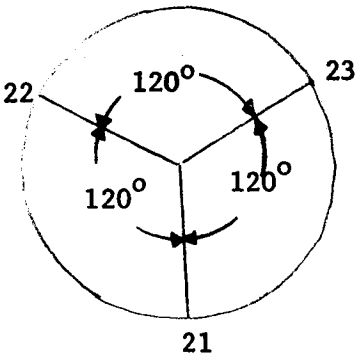

The leads are numbered

21, 22, 23

The dummy gage is labeled S

(5) Strain gages on the Moment Applying Columns

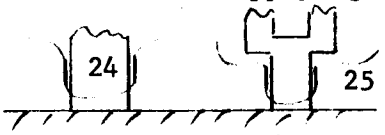

The strain gages are connected in series to measure axial strains. The leads are numbered 24 and 25. The dummy gage is labeled C.

(6) The total number of gages required are:

12 for integral flange
6 for floating flange
3 for ferrule
4 for column
1 for floating flange dummy gage
1 for ferrule dummy gage
2 for column dummy gage

total 29 gages, Plus two for calibrating floating flange and ferrule dumay gages. Unless otherwise specified Nichrome V, uncompensated, 1/8" gage length gages will be used.

(7) (a) No. of gages going out of the vacuum chamber

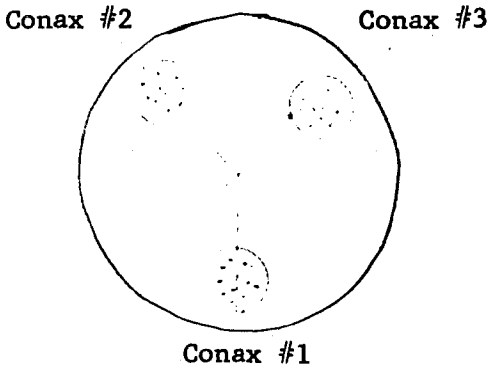

15 for the integral flange
12 for the floating flange
16 for the bolts
2 for the bolt dumay gage
2 for the floating flange dummy gage

total 47 leads

Now, let

Leads 9, 9c, 12, 12c, 15, 18, 4, 5, 6

go thru Conax #1 (total of 15 leads)

Leads 10, 10c, 13, 13c, 16, 19, 7, 8, 1, one lead of F

go thru Conax #2 (total of 16 leads)

Leads 11, 11c, 14, 14c, 17, 20, 2, 3, 2, 3, B, one lead of F

go thru Conax #3 (total of 16 leads)

(b) No. og gages going out of the pressure chamber

6 for integral flange
6 for ferrule
4 for column
2 for columm dummy gage
2 for ferrule dummy gage
2 for thermal couple
total 22 leads

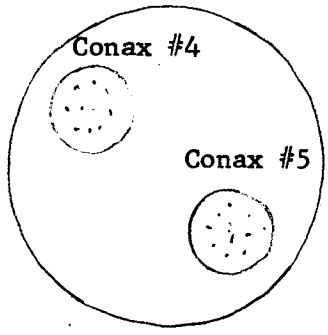

Leads C, S, T (thermal couple leads)

A total of six leads going thru conax #5

The rest go through Conax #4

4.14.2 Inspection

A. Assure that all torque wrenches, pressure gages and thermocouples have been recently calibrated.

B. The following inspection is required prior to and after testing.

(1) Visually inspect flange surfaces and gasket for evidence of damage, irregularities or radial scratches.

(2) Check thickness of gasket at six equally spaced points and record.

4.14.3 Setting up Instrumentation

A. Number the strain gage bolts. Calibrate them.

B. Mounting strain gages:

The active gages are to be mounted at the locations indicated in 4.14.1.C. The dummy gages (other than those for bolts) are to be mounted on 5" long, 1/4", 1/8" thick beams which can be used later for calibration purposes. Detailed procedures for mounting the gages are as follows:

(1) Remove the gage from the protective cardboard case, lay the gage in the teflon wrapper on a piece of glass, turn back the top part of the teflon wrapper and shear off with a razor blade. Take a strip of scotch tape and press the tape on the foil gage, turn tape upside down and use tweezers to take off the teflon back and then very carefully, by using tweezers, peel back the plastic backing in a horizontal manner, doing this very slowly. The gage is now ready to press on to the surface of the work to be gaged.

(2) The surface that is to receive the gage should be sand blasted.

(3) Clean and scribe lines where the gage is to be mounted.

(4) Clean surface with trichlorethelyne.

(5) Apply .001 of an inch of Mithra #200 cement, and bake for one hour.

(6) Sand lightly with #400 emery paper, so as to have a smooth surface, and clean.

(7) Apply .001 of an inch of Mithra #200 over scribed lines, just enough surface for gage.

(8) The foil gage on the scotch tape is now ready to press on to the wet Mithra cement directly over the scribe lines, which is the location for mounting the gage.

(9) Press with finger directly over gage to squeeze out excess cement.

(10) Apply silicon rubber pad about one-half inch square directly over gage and clamp with small pressure, about 5 lb., and bake in oven for two hours at 300°C.

(11) Remove work from oven and let cool.

(12) Remove clamp and rubber pad.

(13) Remove scotch tape with tweezers, use trichlorethelyne to soften the sticky part of the scotch tape and pull tape slowly in a horizontal direction applying trichloethelyne at the same time. After scotch tape is removed, clean gage carefully with trichlorethelyne.

(14) After gages are wired, coat the gages with GA-5 cement and bake in oven 60 minutes at 200°F.

C. Mounting Thermocouple

The thermocouple is to be mounted to the less conductive stainless steel flange. #20 wires are to be used. Thermocouple leads are to be labeled T.

D. Installing Conax plugs and threading wire leads through them:

(1) Screw in the two columns into the stainless steel bottom.

(2) Install conax plugs 1,2,3,4 and 5. Put low temperature cement around the thread and cure it at prescribed temperature to ensure the conax plus will be leak tight at LN_2 temperature.

(3) Put dummy gages F and C on top of the steel bottom plate.

(4) Thread wire leads originating inside the flanges through conax plugs #4 and #5 in the order indicated in 4.14.1C. Insert pieces of "free" 20 wires into the ten unused holes.

(5) Install gasket to be tested. Care should be taken not to damage the flange surfaces or gasket.

(6) Put the aluminum flange on top of the steel flange, separated by the gasket. Put the bolts through the bolt holes. Be sure the strain gage bolts are put into the correct bolt holes.

(7) Thread wire leads through conax plugs #1, 2, 3, as indicated in 4.14.1C. Count the total number of wire leads and be sure that all leads go through, including the dummy gage leads B and F. Insert a piece of "free" #20 wire in the remaining hole.

E. Balancing the strain gage bridge circuit:

(1) Connect the leads to the switch box and balancing unit as indicated in 4.14.1C. Double check to be sure that the active and dummy gages are correctly connected.

(2) Balance the bridge circuit.

F. Have mass spectrometer calibrated and ready for connection to vacuum chamber. Have thermocouple temperature indicator, Helium gas tank, LN_2 tank and necessary pipes and fittings ready for installation.

4.14.4 Assembly

A. Assemble the flanges according to the torque sequence indicated in 4.14.1B. "Snug" all bolts using cross torque to 30 in-lb torque. Record strains.

B. Using cross torque method, increase bolt torque in three steps until the required bolt load is obtained. Record strains at each step and use the instrumented bolts to control the bolt load. Watch possible bolt yielding and bent bolts. Record date of assembly.

C. 24 hours after assembly check bolt strain for bolt relaxation due to gasket set. Retorque to strains recorded previously at 190 in-lb, if necessary. Record torque wrench readings. Repeat this step in 24 hr. intervals until no bolt relaxation occurs. Record number of retorquings needed.

D. Install the vacuum enclosure. Be sure that dummy gages B and F are not left outside.

E. Tighten the conax plugs according to instructions. The wires should be at the two ft. marks.

F. Tighten the two caps which cover the bolts for applying the moment. Close the helium inlet and exhaust.

G. Evacuate the vacuum chamber. Put sniffers around the indium wire vacuum seal. Read the mass spectrometer and be sure that the rate of leakage is under 10^{-8} cc/sec.

4.14.5 Test

A. Room temperature test (without moment)

(1) Evacuate the vacuum chamber and pressure chamber

(2) Record strains

(3) Pressurize to 50, 100, 150 and finally to 200 psig. Record leakages and strains at each step.

(4) Depressurize and record residual strains (shut inlet valve, then open exhaust valve)

B. Room temperature test (with moment)

(1) Remove the two caps (be sure that fixture is depressurized already)

(2) Apply lubricant to the bolt thread and tighten the two bolts until a compressive strain of 350 μ in. is recorded in column #1 and a tensil strain of 350 μ in. is recorded in column #2. This applies a moment of 48,000 lb-in on the flanges.

(3) Evacuate the pressure chamber.

(4) Record strains.

(5) Pressurize to 50, 100, 150 and finally to 200 psig. Record leakages and strains at each step.

(6) Depressurize and record residual strains.

C. LN_2 temperature test (without moment)

(1) Remove the two caps and loosen the two bolts (be sure fixture is depressurized).

(2) Tighten the two caps.

(3) Lower the assembled flanges into the dewar.

(4) Evacuate the pressure chamber.

(5) Pressurize to 140 psig.

(6) Pour in LN_2.

(7) Record temperature and leakage rate continuously until temperature stabilizes.

(8) Record strains.

(9) Pressurize at 200 psig. Record strains and leakage rate.

(10) Depressurize and record residual strains.

D. LN_2 temperature test (with moment)

(1) Remove some amount of LN_2 until LN_2 level just covers the test fixture.

(2) Remove the two caps and tighten the bolts to a strain of 350 μ in.

(3) Tighten the two caps.

(4) Evacuate the pressure chamber.

(5) Pressurize to 140 psig.

(6) Pour back the LN_2 previously removed.

(7) Repeat steps (7) - (10) in C.

4.14.6 Disassembly

A. Be cetain that the fixture is depressurized. Remove some LN_2 until LN_2 level just covers the test fixture. Remove the two caps and loosen the two bolts. Lift the fixture out of the dewar.

B. Loosen the vacuum enclosure. Lift it up not to exceed 1 ft. to avoid breaking the strain gage connections.

C. Loosen the bolts. Remove the gasket. Visually inspect flange surfaces and gasket for evidence of irregularities. Inspect bolts for possible bend and measure residual strain in the bolts.

4.14.7 Other tests

A. The test procedure outlined in the above, is for the Allpax #500 gasket. It is desired that every step in the above test be thoroughly carried out. For other gaskets:

(1) Different initial seating bolt load will be required.

(2) Depending on time and money available we probably will not carry out every test outlined above. It is planned that at least test VD (LN_2 temperature with moment) should be conducted.

B. Repeat inspection procedure 4.14.2B, after all tests are completed.

4.14.8 Safety Precautions

A. Protective gloves and safety glasses shall be worn at all times during the test.

B. Be sure that the test fixture is depressurized before attempting to change anything in the test set-up.

4.15 Appendix VII Analysis of the Test Connector

4.15.1 Loose Flange

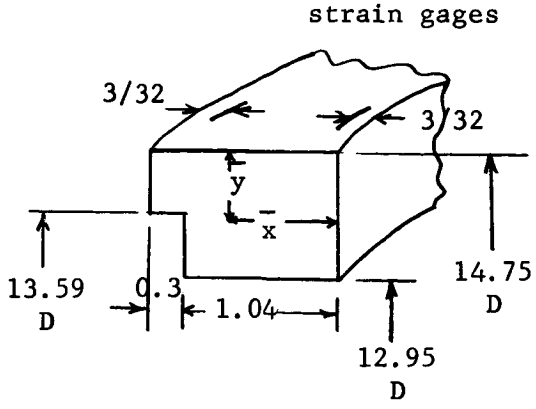

The centroidal distance $\bar{x}$ and $\bar{y}$ of the flange cross-section can be determined as

$$\bar{x} = 0.770 \text{ in.}$$

$$\bar{y} = 0.424 \text{ in.}$$

The moment of inertia of the cross-section about a radial axis through the centroid can be determined as

$$I_q = 0.175 \text{ in}^4$$

The rotation rigidity of the flange is

$$C = 2E\pi I_q / r_c$$

$$= (2\pi)(10.6 \times 10^6)(0.175)/(14.075/2 - 0.424)$$

$$= 1.68 \times 10^6 \text{ in-lb/rad}$$

If it is assumed that the reaction between the flange and the ferrule is located at the midline of the area of contact the moment arm of the bolt load is

$$h_L = 0.315 \text{ in.}$$

Then each 10,000 lb. of total bolt load will cause a flange relation of

$$(10{,}000)(0.315)/1.68 \times 10^6 - 1.82 \times 10^{-3} \text{ rad}$$

The rotation of the flange can also be determined experimentally from the strain gage readings as

flange rotation - (right strain gage reading - left strain gage reading)(radial distance of gages/distance between two gages)

Comparisons between the measured and theoretical values of the flange rotations are given in section 1.7.2

4.15.2 Integral Flange

The dimensions of the integral flange are shown in the following drawing:

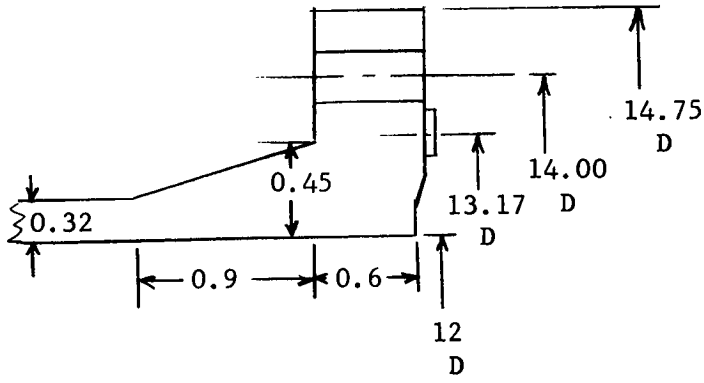

In the notation of Appendix IV (section 4.12) we have now

$g_{1/g_o} = 0.45/_{0.32} = 1.41$

$h/_{h_o} = 0.9/_{(12)(0.32)} = 0.459$

$K = 14.75/_{12} = 1.23$

$T = 1.83$

$Z = 4.90$

$Y = 9.50$

$U = 10.44$

$F = 0.86$

$V = 0.35$

$e = F/_{h_o} = 0.86/1.96 = 0.439$

$d = h_o g_o U/V = (1.96)(0.32)^2(10.44)/0.35 = 5.98$

$t = 0.6$

$L = \left[(te + 1)/_T\right] + t^3/d = 0.726$

$E = 10.6 \times 10^6$

$\mu = 0.33$

C-3

The rotational rigidity of the flange is

$$Lhog_o^2/(1-\mu^2)EV = (0.726)(1.96)(0.32)^2(10.6 \times 10^6)(1-0.3^2)(0.35)$$

$$= 4.95 \times 10^6 \text{ lb-in/rad}$$

If the gasket load is assumed to be acting at the gasket circle, then $h = 0.413$ in., and each 10,000 lb. of total bolt load will cause a flange rotation of

$$(10,000)(0.413)/4.95 \times 10^6 = 8.35 \times 10^{-4} \text{ rad.}$$

The average thickness of the tapered hub-tube is

$$g_{ave} = 0.356$$

We now have, in the notation of Appendix IV

$$r_o = (B + g_{ave})/2 = (12 + 0.356)/2 = 6.18 \text{ in.}$$

$$r_c = (A + B)/4 = (14.75 + 12)/2 = 6.69 \text{ in.}$$

$$z = t/2 = 0.6/2 = 0.3 \text{ in.}$$

$$A_F = t(A-B)/2 = (0.6)(14.75-12)/2 = 0.824 \text{ in}^2$$

$$I = g_{ave}^3/12(1-\mu^2) = (0.356)^3/12(1-0.3^2) = 4.22 \times 10^{-3} \text{ in}^3$$

$$I_y = t^3(A-B)/24 = (0.6)^3(14.75-12)/24 = 2.48 \times 10^{-2} \text{ in}^4$$

$$\beta^4 = 3(1-\mu^2)/(r_o G_{ave})^2 = 3(1-0.33^2)/(6.18)^2(0.356)^2 = 0.552/\text{in}^4$$

$$\beta^3 = 0.640/\text{in}^3$$

$$\beta^2 = 0.743/\text{in}^2$$

$$\beta = 0.862/\text{in}$$

$$Z/\beta = 0.3/0.862 = 0.348 \text{ in}^2$$

$$h_f = (A-B)/2 = (14.75-12)/2 = 1.38 \text{ in.}$$

$$1/2\beta^2 = 0.673 \text{ in}^2$$

$$1/2\beta^3 Z = 2.61 \text{ in}^2$$

$$r_o r_c I/ZA_f = (6.18)(6.69)(4.22 \times 10^{-3})/(0.3)(0.824) = 0.706 \text{ in}^2$$

$$r_o r_c ZI/I_y = (6.18)(6.69)(0.3)(4.22 \times 10^{-3})/2.48 \times 10^{-2} = 1.89 \text{ in}^2$$

Therefore the factor

$$X = (Z/\beta + r_o r_c ZI/I_y)(1/2\beta^3 Z + r_o r_c I/ZA_F + r_o r_c ZI/I_y) - (1/2\beta^2 - r_o r_c ZI/I_y)^2$$

$$= (0.348 + 1.89)(2.61 + 0.706 + 1.89) - (0.673-1.89)^2$$

$$= 10.2 \text{ in}^4$$

The barreling rigidity of the flange is

$$C_p = XEg_1 I_y / [r_o^4 I(1-\mu/2 - g_1/h_a)(1/2\beta^2 + Z/\beta)]$$

$$= (10.2)(10.6 \times 10^6)(0.45)(2.48 \times 10^{-2}) / [(6.18)^4 (4.22 \times 10^{-3}) (1-0.33/2 - 0.45/1.38)(0.673 + 0.348)]$$

$$= 3.78 \times 10^5 \text{ psi/rad}$$

4.15.3 Bolts-Gasket System

The stiffness of the bolts is

$$k_B = A_B E_B / \ell_B = (24)(\pi/4)(3/8)^2 (10.6 \times 10^6)/(0.6 + 0.062 + 0.4 + 1.04 + 3/16)$$

$$= 1.23 \times 10^7 \text{ lb/in}$$

the stiffness of the gasket was obtained in Appendix A as

$$k_G = 1.86 \times 10^7 \text{ lb/in}$$

the rotational rigidity of the gasket-bolt system is

$$C = k_B k_G h^2 / (k_B + k_G)$$

$$= (1.23 \times 10^7)(1.86 \times 10^7)(0.413)^2/(1.23 + 1.86) \times 10^7$$

$$= 1.26 \times 10^6 \text{ lb-in/rad}$$

4.15.4 Hub Bending Stress

The hub bending stress

$$S_H = fM_o/Lg_1^2 B = (1)(M_o)/(0.726)(0.45)^2(12)$$

$$= 0.567 M_o$$

Assuming that the gasket reaction acts at the gasket circle, $h_G = 0.413$ and

$$S_H = (0.567)(0.413)(\text{total bolt load})$$

or, for each 10,000 lb of total bolt load the hub bending stress amounts to $S_H = 2,340$ psi.

5. THREADED TUBE CONNECTOR

by

John Wallach

5.0 Summary

This section deals with the design and test of a typical separable connector for tubing of one-inch size and smaller. The design requirements call for a leak-tight connection for high pressure fluid service. The operating conditions include high, low and room temperatures and an externally applied transverse moment.

A threaded connector was designed for a one-inch stainless steel tube. It consists of a union, flanged-section, nut, and gasket, Fig. 5.1 and 5.3. The seal is effected by the action of the knife edges on the union and flanged-section cutting axially into the gasket, Fig. 5.2. This connector is referred to as the welded knife-edge connector as it is welded to the tubing. Two other connectors designed, but not tested, are a flared knife-edge and metallic O-ring connector. These will be tested at a later date. Drawings for all three are in Section 5.4.4.

The welded knife-edge connector was tested at room temperature, 500°F and -300°F. At each temperature, the connector was pressurized with helium to 1500 psi and a transverse moment of 450 inch pounds was applied. The leakage measured never exceeded 1×10^{-5} atm cc/sec. except in the reassembly tests. In the reassembly tests reuse of the same gasket sometimes resulted in leakage less than 1×10^{-5} atm cc/sec. and sometimes resulted in leakage larger than 1×10^{-2} atm cc/sec. The connector was designed with a disposable gasket and the test results showed the connector to perform very satisfactorily if the gasket is replaced at every assembly.

5.1 Design Requirement

The threaded tube connector program was to design, manufacture and test a high-pressure-gas tube connector. The testing was primarily intended to measure leakage to determine the effectiveness of the connector design under conditions of high internal pressure, high, low, and room temperatures, and static loading.

The connector requirements were defined to correspond to the requirements of the MC Flared Tube Connectors Program of the George C. Marshall Space Flight Center. However, the cyclic loading was simulated by static loading in order to allow taking leakage measurements while the load is applied. No design requirement was available for the amount of static load applied to the connector. Therefore, a moment was chosen which results in a maximum axial tensile stress in the tube equal to the hoop stress in the tube due to the 3000 psi pressure. The design pressure was reduced from 3,000 psi to 1,500 psi, because at the time of the tests, there was no gas available at a higher pressure.

The design requirements for the tube connector were:

1. Connector must be separable.

2. Connector must be compatible with most fluids encountered during operation.

3. "Zero" leakage under the following operating conditions.

    a) Room temperature with a pressure of 1500 psi and a moment of 450 inch lb.
    b) Five reassemblies using the same seal and performing satisfactorily under the conditions specified in (a).
    c) Conditions (a) for 72 hours.
    d) 500^{o}F with a pressure of 1500 psi and a moment of 450 inch lb.
    e) -320^{o}F with a pressure of 1500 psi and a moment of 450 inch lb.

5.2 Design Results

The tube connector designed and tested in accordance with the design requirements is a threaded connector consisting of a flanged-section, union, nut, and gasket, Fig. 5.1. The seal consists of a set of knife-edges which axially cut into a soft copper gasket, Fig. 5.2. The gasket, part number 115A4752-1 (see Sec. 5.4.4 for all drawings), fits snugly over the protruding cylindrical section of the flanged-section, part number 544E540-26. The protruding section of the flanged-section slides into the counter-bored diameter of the union, part number 544E540-22. Then the nut, part number MC124C16U, slides over the flanged-section and threads into the union. As the nut is tightened on the union, the knife-edges on the union and flanged-section cut into the gasket. At a sufficiently large torque on the nut, the protruding section of the flanged-section contacts the counter-bore of the union and limits the depth of cut of the knife-edges into the gasket.

The gasket is made of soft oxygen-free 121 copper. The flanged-section is made of 321 stainless steel and the nut and union are made of 316 stainless steel. The "V" shaped knife-edges were machined into the union and flanged-section without any special tools or methods. The gasket was machined from flat copper stock. The manufacture of the connector does not require any super-fine finishing or special machining.

A one-inch tube size was chosen because of the greater ease in instrumenting a larger size and the ease in measuring the larger external loads which could be applied. Stainless steel was chosen because of its compatibility with most of the operating fluids that might be used in the piping system. Standard MC parts were used where possible to reduce the design time and reduce manufacturing costs. The connector is welded to the tubing.

The connector was tested under all the conditions given in Section 5.1 and performed satisfactorily. Under all operating conditions, leakage was below 1×10^{-5} atm cc/sec. of helium.

Two other connectors were designed but not tested. One is a modified MC connector. The flare is extended and a knife-edge is machined on the lip, part number 662B903-1. A knife-edge is cut into the union, part number 544E540-16 and a metallic gasket is used, part number 115A4752-1 or -2. The other connector is the flanged type and uses a metallic O-ring for a gasket. The union, part number 544E540-21, has a semi-circular groove cut into it. The flanged-section, part number 544E540-24, has a similar groove. The metallic O-ring has the same mean diameter as the grooves, but has a cross-sectional diameter of .062 inches, about 1-1/2 times that of the grooves. The flared knife-edge connector is shown in Fig. 5.4 and the metal O-ring connector is shown in Fig. 5.5.

ORIGINAL PAGE
BLACK AND WHITE PHOTOGRAPH

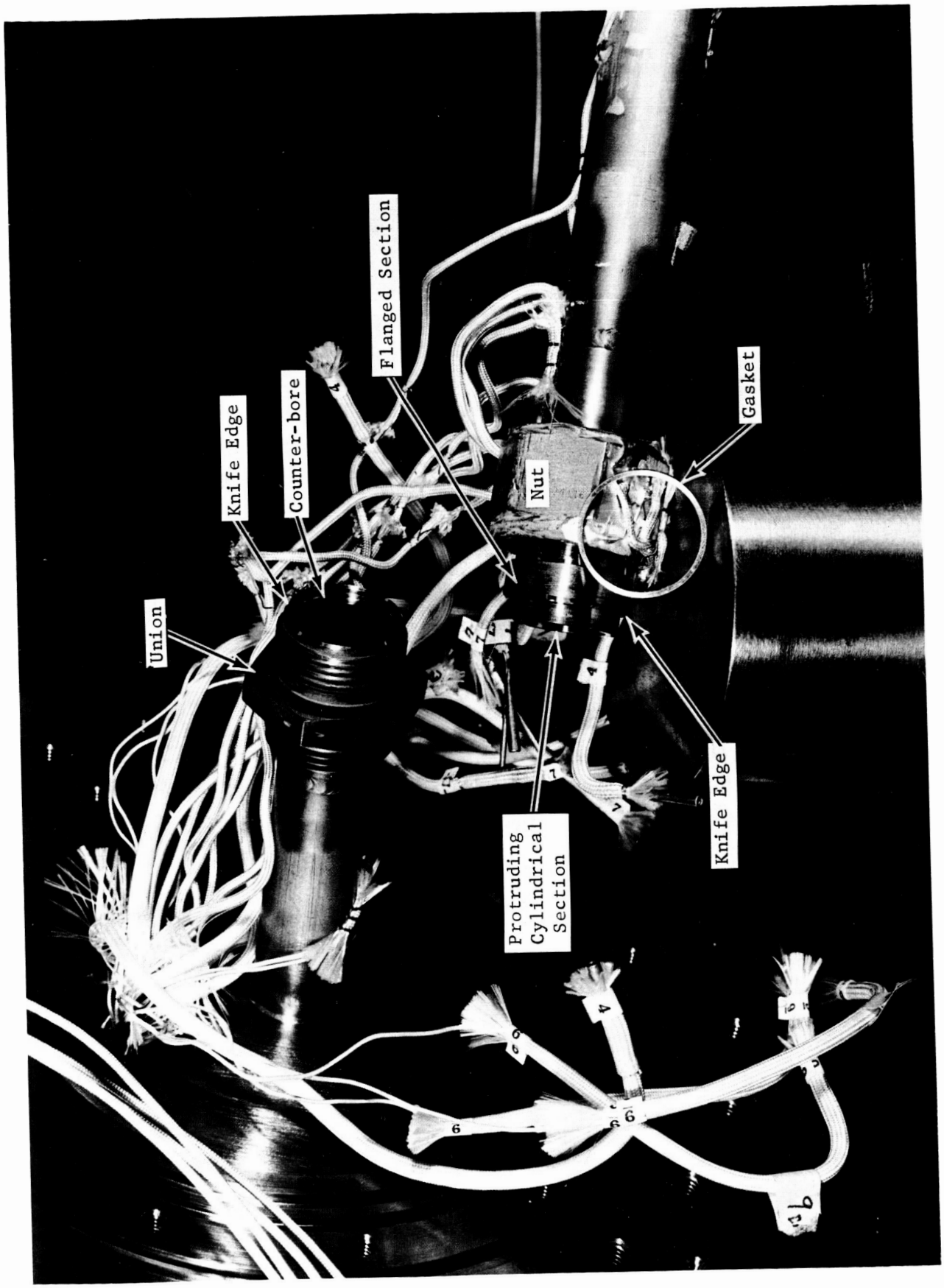

FIG. 5.1 WELDED FLANGED CONNECTOR

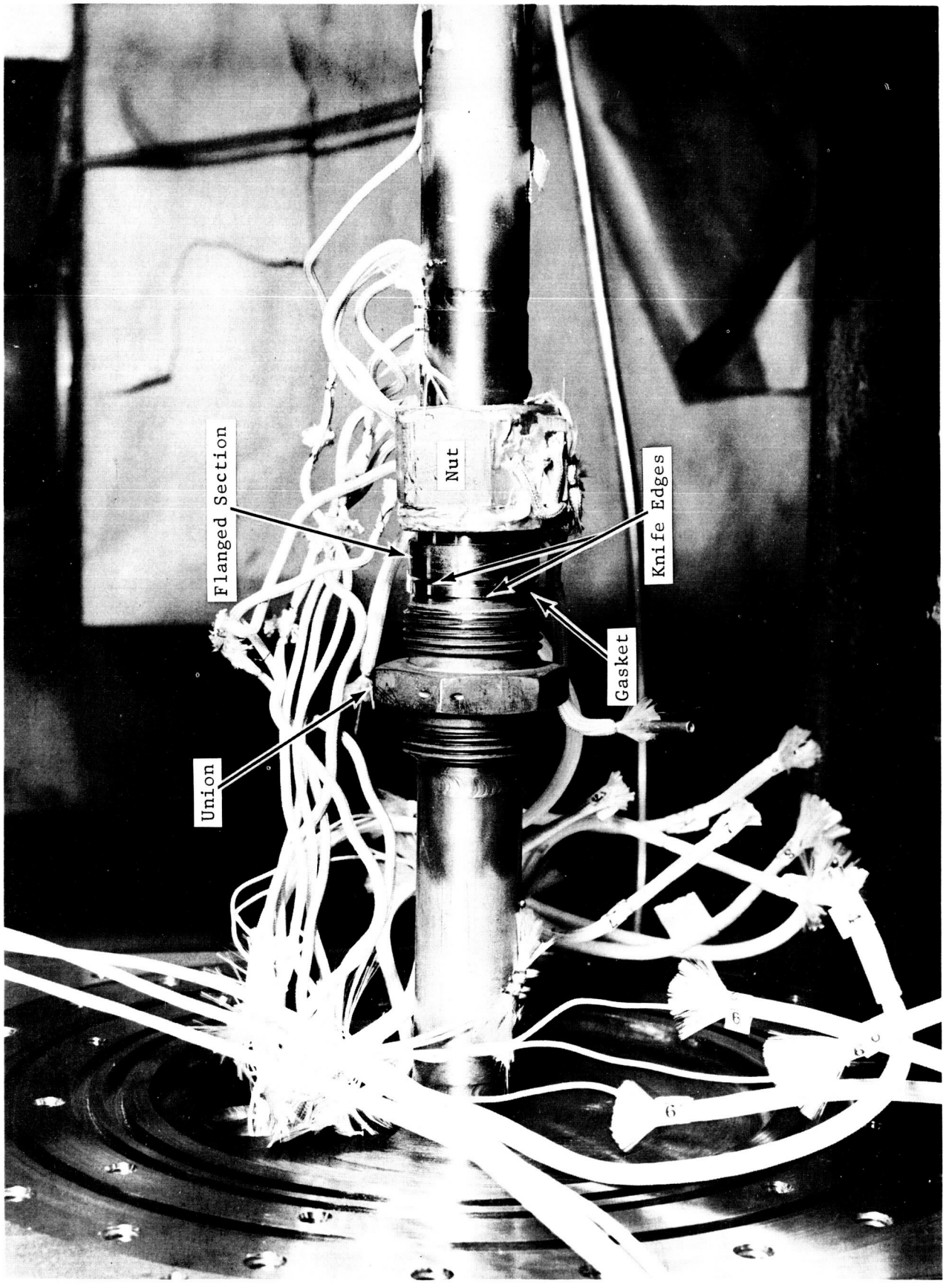

FIG. 5.2 ASSEMBLY OF WELDED-KNIFE-EDGE CONNECTOR

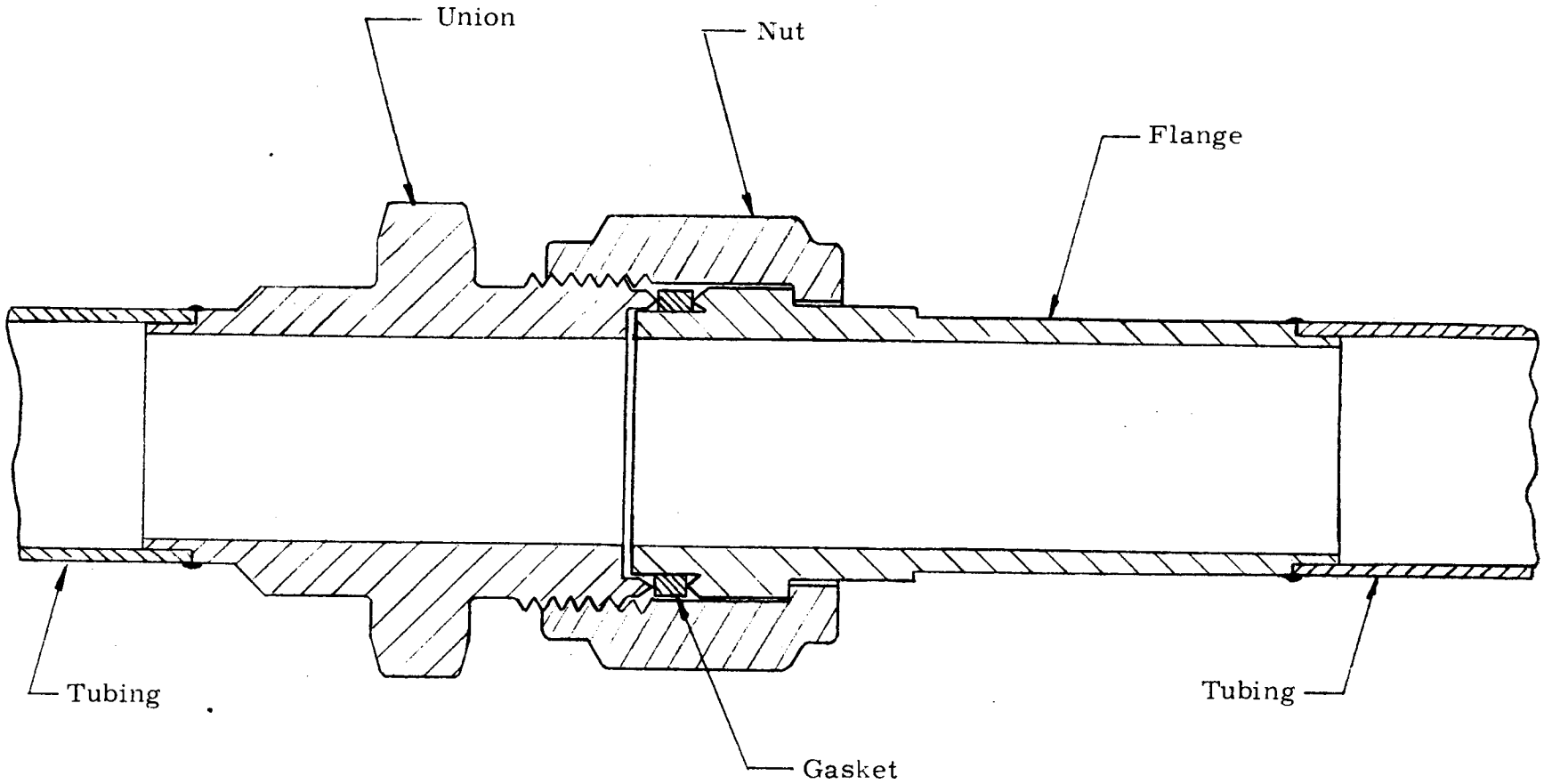

FIG. 5.3 WELDED KNIFE-EDGE CONNECTOR

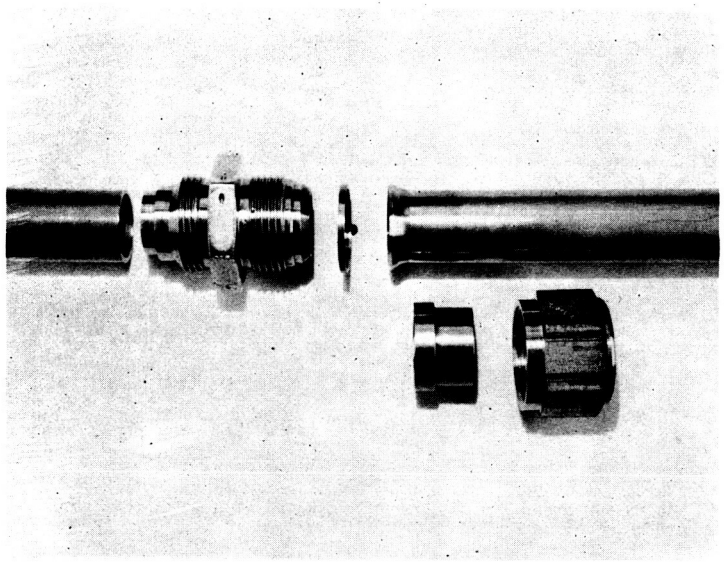

FIG. 5.4

ATL FLARED KNIFE-EDGE CONNECTOR AND
TUBING PRIOR TO ASSEMBLY

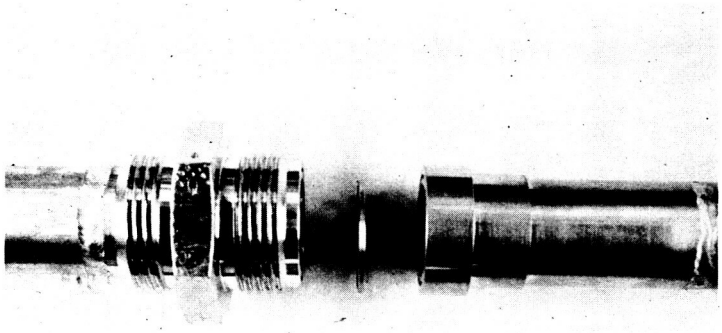

FIG. 5.5

ATL METAL O-RING CONNECTOR PRIOR TO
ASSEMBLY. NUT NOT SHOWN.

5.3 Design Testing

The purpose of the tests was to determine whether the welded knife-edge connector met the design requirements. It was therefore necessary to duplicate the environmental conditions, pressurize the connector and measure the leakage. The design requirements are described in Sec. 5.1, the test equipment is described in Sec. 5.4.2 and the test procedure and results are described in this section.

5.3.1 Preliminary Tests

The performance of the connector depends upon the preload put in at assembly. Because the calculation of the preload from the torque applied to the nut is inaccurate the nut was calibrated. A set of strain gages was mounted on opposite flats of the nut and wired to read only pure axial strain. Then the nut was loaded in a universal testing machine in a manner that duplicates the nut loading in the connector. The strain versus load reading gave a straight line calibration curve. Then with the use of this curve it was possible to accurately set the preload during assembly by measuring the strain in the nut.

Another test which should have been performed before the other connector tests, but was not, was an assembly test to determine if the flanged-section actually seats on the union. Because of the low yield stress of annealed copper and the high preload it was assumed that the flanged-section would seat on the union during assembly. However, the annealed copper raw material was not as soft as expected and during the sequence of tests run it became questionable whether the flanged-section did seat on the union. Therefore, the flanged-section was coated with a bluing compound and the connector was assembled with an increasing sequence of preloads. The results showed that the flanged-section did not seat on the union at assembly and probably not at anytime during the tests.

Therefore, the tests did not take full advantage of the independent load path built into the connector. If the flanged-section had seated on the union and created the independent load path the seal would have been less sensitive to externally applied loads. This would have meant a lower level of leakage, but as there was no measurable leakage in most of the tests the improved sealing could not have been measured. Therefore, the results of the leakage testing would have changed very little.

The results of the test to determine seating does indicate a need for a softer gasket, smaller included angle on the knife-edge, less depth of cut of the knife-edge prior to seating of the flanged-section on the union, and a containment of the gasket that does not interfere with the seating of the flanged-section. These changes to the sealing area of the connector should be made and tested before the connector design is considered final.

5.3.2 Room Temperature Test

5.3.2.1 Test Procedure

This test was performed at room temperature. The connector was assembled with a preload of 2300 lb. Leakage readings were taken at each of a sequence of internal pressure and external moment settings.

5.3.2.2 Test Results

The test pressure, moment settings, and leakage readings are tabulated below:

Helium Pressure Psig	Transverse Moment Inch lb	Helium Leakage atm cc/sec
0	0	n.m.*
300	0	n.m.
600	0	n.m.
910	0	n.m.
1190	0	n.m.
1500	0	n.m.
475	0	n.m.
475	150	n.m.
475	300	n.m.
475	450	n.m.
1000	0	n.m.
1000	150	n.m.
1000	300	n.m.
1000	450	n.m.
1500	0	n.m.
1500	150	n.m.
1500	300	n.m.
1500	450	n.m.

*n.m. - none measurable.

The sensitivity of the mass spectrometer leak detector varied due to the cleanliness of the vacuum system and other factors. Therefore, it is only possible to say that there was no measurable leakage and to state the level of leakage which was measurable. It can then be concluded that if there was any leakage

it was below this measurable level. The level of leakage measurable was determined by placing a sequence of known leaks in the system and measuring the leakage.

n.m. for this test was below 9×10^{-7} atm cc/sec.

5.3.3 Reassembly Test

5.3.3.1 Test Procedure

This sequence of tests was run at room temperature. A new gasket was installed in the connector and tested for leakage at internal pressure to 1500 psig and external moments to 450 inch lb. The connector was then disassembled, the gasket was removed and remounted on the connector, the connector was reassembled, and the connector was tested for leakage as before. In this way a total of six tests were run using the same gasket.

5.3.3.2 Test Results

For each test the gasket orientation, preload, test points and leakage are tabulated.

5.3.3.2.1 First Test - New Gasket

Preload = 2300 lb

Helium Pressure Psig	Transverse Moment Inch lb	Helium Leakage atm cc/sec
0	0	n.m.
310	0	n.m.
600	0	n.m.
900	0	n.m.
1200	0	n.m.
1500	0	n.m.
1500	150	n.m.
1500	300	n.m.
1500	450	n.m.

n.m. $< 3 \times 10^{-6}$ atm cc/sec.

5.3.3.2.2 First Reassembly

Gasket removed and remounted backwards and rotated 90°.

Preload = 2200 lb.

Helium Pressure Psig	Transverse Moment Inch lb	Helium Leakage atm cc/sec
0	0	n.m.
300	0	n.m.
600	0	n.m.
900	0	n.m.
1210	0	n.m.
1500	0	n.m.
1500	150	n.m.
1500	300	n.m.
1500	450	n.m.

n.m. $< 9 \times 10^{-7}$ atm cc/sec

5.3.3.2.3 Second Reassembly

Gasket rotated 90° clockwise.

Preload = 2200 lb.

Helium Pressure Psig	Transverse Moment Inch lb	Helium Leakage atm cc/sec
0	0	n.m.
310	0	n.m.
600	0	n.m.
900	0	n.m.
1200	0	n.m.
1500	0	n.m.
1500	150	n.m.
1500	300	n.m.
1500	450	3×10^{-4}

n.m. $< 3 \times 10^{-6}$ atm cc/sec

5.3.3.2.4 Third Reassembly

Gasket rotated 90° clockwise.

Preload = 2200 lb.

Helium Pressure Psig	Transverse Moment Inch lb	Helium Leakage atm cc/sec
0	0	n.m.
310	0	n.m.
610	0	n.m.
900	0	n.m.
1200	0	n.m.
1500	0	2×10^{-5}
1500	150	5×10^{-4}
1500	300	$> 1 \times 10^{-2}$
1500	450	not attempted

n.m. $< 3 \times 10^{-6}$ atm cc/sec

5.3.3.2.5 Fourth Reassembly

Gasket removed and remounted backwards.

Preload = 2200 lb.

Helium Pressure Psig	Transverse Moment Inch lb	Helium Leakage atm cc/sec
0	0	n.m.
300	0	n.m.
600	0	n.m.
900	0	n.m.
1200	0	n.m.
1500	0	n.m.
1500	150	n.m.
1500	300	n.m.
1500	450	n.m.

n.m. $< 3 \times 10^{-6}$ atm cc/sec

5.3.3.2.6 Fifth Reassembly

Gasket rotated 180°.

Preload = 2200 lb.

Helium Pressure Psig	Transverse Moment Inch lb	Helium Leakage atm cc/sec
0	0	n.m.
300	0	n.m.
610	0	n.m.
900	0	n.m.
1200	0	n.m.
1500	0	2×10^{-4}
1500	150	6×10^{-4}
1500	300	4×10^{-3}
1500	450	$>8 \times 10^{-3}$

n.m. $< 3 \times 10^{-6}$ atm cc/sec

5.3.4 Extended Time Test

5.3.4.1 Test Procedure

This test was run at room temperature. The connector was assembled with a preload of 2200 lb. The connector was pressurized to 1500 psig of helium and loaded with an external moment of 450 inch lb. Then leakage readings were taken periodically for 72 hours.

5.3.4.2 Test Results

Time Since First Reading Hours	Helium Leakage atm cc/sec
0:00	n.m. ($< 3 \times 10^{-6}$)
0:15	"
0:30	"
1:00	"
1:30	"
2:30	"
3:30	"
4:30	"

(continued on following page)

Time Since First Reading Hours	Helium Leakage atm cc/sec
(continued)	
5:30	n.m.
6:30	"
9:50	n.m. ($< 4 \times 10^{-5}$)
25:05	n.m. ($< 4 \times 10^{-5}$)
35:35	n.m. ($< 1 \times 10^{-5}$)
51:15	n.m. ($< 4 \times 10^{-5}$)
72:00	n.m. ($< 1 \times 10^{-5}$)

5.3.5 High Temperature Test

5.3.5.1 Test Procedure

The connector was assembled with a preload of 2200 lb. The connector was then heated to 500°F with no internal pressure or external moment applied. When the connector was at temperature the leakage was measured at a sequence of internal pressures and external moment settings.

5.3.5.2 Test Results

Helium Pressure Psig	Transverse Moment Inch lb	Connector Temperature °F	Helium Leakage atm cc/sec
0	0	510	n.m.
300	0	510	n.m.
600	0	510	n.m.
900	0	500	n.m.
1200	0	500	n.m.
1500	0	500	n.m.
500	0	500	n.m.
500	150	490	n.m.
500	300	490	n.m.
500	450	490	n.m.
1000	0	490	n.m.
1000	150	490	n.m.
1000	300	500	n.m.
1000	450	500	n.m.
1500	0	500	n.m.
1500	150	500	n.m.
1500	300	500	n.m.
1500	450	500	n.m.*
1500	500	490	8×10^{-5}

n.m. $< 2 \times 10^{-6}$ atm cc/sec

* At this point there was a momentary leak which closed-up before it could be read. Therefore, the moment was increased above the design requirement and the next test point was taken.

5.3.6 Low Temperature Test

5.3.6.1 Test Procedure

The connector was assembled with a preload of 2300 lb. The connector was then cooled to -300°F with no internal pressure or external moment applied. When the connector was at temperature the leakage was measured at a sequence of internal pressures and external moment settings.

5.3.6.2 Test Results

Helium Pressure Psig	Transverse Moment Inch lb	Connector Temperature °F	Helium Leakage atm cc/sec
0	0	-300	n.m.
300	0	-300	n.m.
600	0	-300	n.m.
900	0	-300	n.m.
1220	0	-300	n.m.
1500	0	-300	n.m.
500	0	-300	n.m.
490	150	-300	n.m.
1020	150	-300	n.m.
1500	150	-300	n.m.
500	300	-300	n.m.
1000	300	-300	n.m.
1500	300	-300	n.m.
520	450	-300	n.m.
1000	450	-300	n.m.
1500	450	-300	n.m.

n.m. $< 6 \times 10^{-6}$ atm cc/sec

5.4 Appendix

5.4.1 Design Procedure

5.4.1.1 Three Connectors

The tube connector design began with a redesign of the present MC fitting, Fig. 5.7. It was shown in Ref. 2 that, in general, the leakage level of the MC flared connector when pressurized with helium to 1500 psi is 10^{-4} to 10^{-2} cc/sec. It was also shown that the use of Voi-Shan crush washers decreased the leakage but did not result in sealing in many cases. Therefore, it was deemed necessary to redesign the MC connector. Because of the present wide use of the MC connector, the redesign was held to a minimum and only a gasket was added and knife-edges were cut on the tube and union. The modified fitting is referred to as the flared knife-edge connector in this report.

The nut, union, flared-tube and gasket are part numbers MC124C16U, 544E540-16, 662B903-1, and 115A4752 respectively. The nut is a standard MC nut. The union is an MC160C16 union with a knife-edge cut into it. The flared-tube is flared to the same specifications as the MC flared-tubing, but the final diameter of the flare is slightly larger and a knife-edge is machined on the lip. The gasket is a simple ring of rectangular cross-section.

The knife-edges on the flared-tube and union axially cut into the gasket when the nut is tightened. The seal thus formed has been shown to seal to well below 1×10^{-4} atm cc/sec. of helium for an internal pressure of 1120 psi, Ref. 2. Also, the results of testing a similar connector included in this section show that this type of seal will perform satisfactorily. The flared knife-edge connector, however, was not tested.

Besides improving the sealing abilities of the MC connector, the above modification will also considerably reduce the cost. Eliminated is the need for a super-fine finish on the union and flare. Standard machine shop practice will be sufficient throughout. All the parts of the connector have been manufactured using standard machine shop practices.

Even after this modification, the MC connector still had some undesirable features and further modifications were made to eliminate these. The flared tubing is subject to fatigue failures in the bend of the flare, Ref. 3. Therefore, the tube-to-connector connection was changed to a weld. A butt weld was used for the connector tested. However, the production design should have the type of weld described in Ref. 4. In the production design, the tube fits snugly into the connector and the weld is in the double thickness area. In this way, the weld strength is comparable to that of the

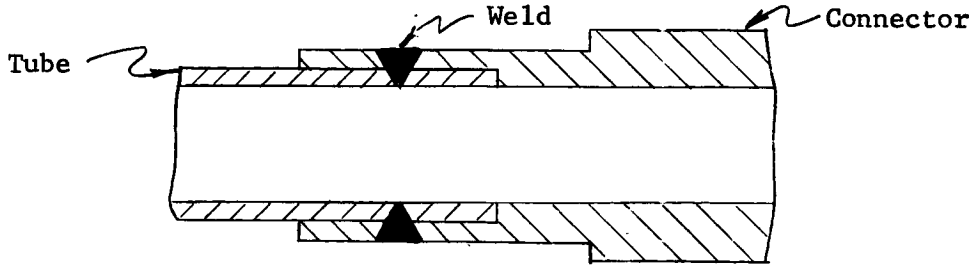

Fig. 5.6

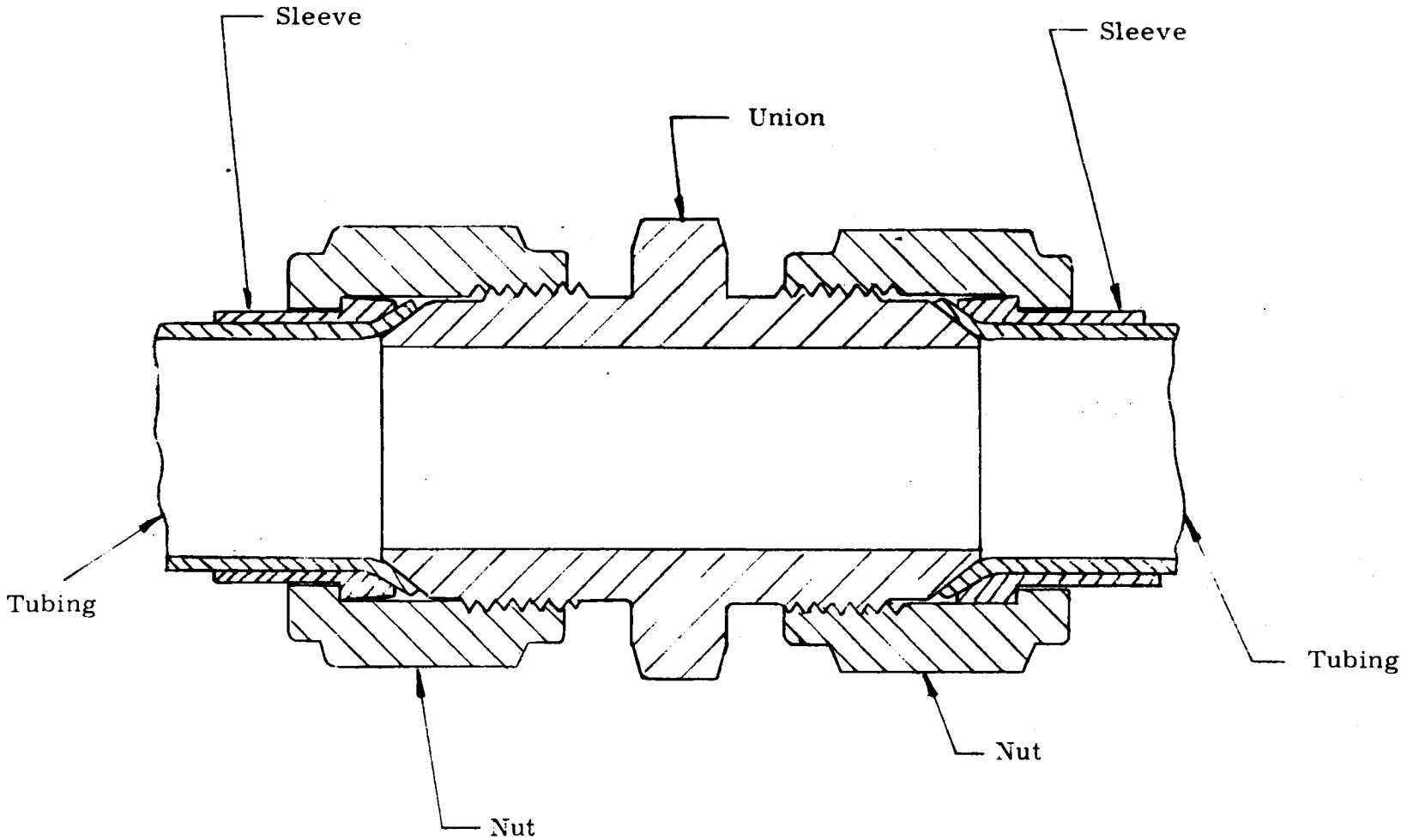

FIG. 5.7 MC TUBE CONNECTOR

tube because of the double thickness of the material.

The location of the weld has the added feature in that the connection of the tube to the connector is separated from the sealing surface. In the MC fitting the flared-tube form part of the seal, is the connection of the tube to the connector, and is part of the load path. Combining these three functions is undesirable, Ref. 5. The modified fitting, referred to in the report as the welded knife-edge connector, has the three functions separated.

A third design has two of the functions combined. The sealing and load path are combined. This connector, referred to in this report as the metallic-O-ring connector, consists of a union, flanged-section, nut, and O-ring; part numbers 544E540-21, 544E540-24, MC124C16U, and United Aircraft Products catalogue number U-42XX-01063-NPX. The seal consists of two semi-circular grooves, one each in the opposite faces of the union and flanged-section, and a metallic-O-ring which is clamped between these faces. The grooves and O-ring have the same mean diameter, but the diameter of the circular cross-section of the groove is about 2/3 that of the O-ring. Therefore, when the O-ring is crushed between the union and flanged-section, the edges of the semi-circular grooves cut into the O-ring and form a seal.

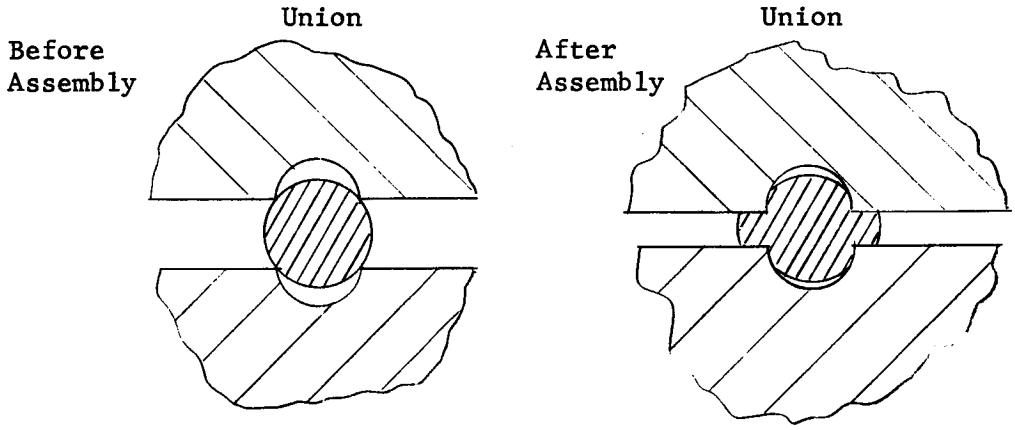

As the welded knife-edge connector, the metallic-O-ring connector is attached to the tubing by welding.

Combining the seal and load path makes the seal more sensitive to variations in the load, and any relative motion between the union and flanged-section. The welded knife-edge connector has these functions separated and the metallic-O-ring connector could also be designed likewise. However, this becomes difficult for tube connectors of small sizes. The cross-sectional diameter of the O-ring either becomes so small that the ring is very fragile or the over-all size of the connector becomes too large.

5.4.1.2 Design of Welded Knife-edge Connector

The design of this connector is based on the principles set forth in Chapter 2 of Ref. 5. The steps were not necessarily taken in the same order because there were three connectors designed somewhat simultaneously. However, the manner in which the connector was designed is more easily

explained by following an orderly procedure. The procedure begins with the choice of connector.

5.4.1.2.1 Choice of Connector

The design requirements called for a connector for tube sizes of one-inch or less. This eliminated the use of a bolted flanged connector. For such small tube sizes a bolted flanged connector design uses a number of very small bolts in order to obtain a close bolt spacing. This leads to an assembly problem, because it is very easy to break the bolts by overtorquing them. The use of a threaded connector with a single nut provides the uniform compression of the seal without the assembly problem. The design requirements called for a connector design with a wide range of possible applications. This led to the selection of the threaded connector. The threaded connector allows quick assembly and disassembly using standard tools, can be designed for high pressure service, and will perform well under the prescribed environmental conditions.

5.4.1.2.2 Method of Sealing

The knife-edges and gasket method was chosen because of the positive sealing obtained by the knife-edges cutting into the gasket. The knife-edges are machined on the union and flanged-section which are made of stainless steel. The gasket is made of annealed copper. The knife-edges cut into the soft gasket by a combination of shearing action and bulk plastic flow of the material. This plastic flow of the copper allows the copper to fill in all of the leakage paths in the knife-edge to gasket interface. The knife-edge is not plastically deformed.

The seal was tested prior to its use in a connector, Ref. 2. In the tests, a soft aluminum gasket was used between two stainless steel knife-edges. The tests showed that the leakage rate dropped to a very low level at an extremely low force on the gasket. Further increases in the axial force brought only a slight decrease in the leakage level. Decreasing the force on the gasket caused no increase in leakage until about 30% of the load was removed. Then an increase in leakage was noted. The test was conducted at room temperature with helium gas pressurized to 1120 psi.

The test showed that the method of sealing was satisfactory. The aluminum gasket was used because at this stage of the design both an aluminum gasket and copper gasket were under consideration. The yield strength of the copper gasket is not sufficiently larger than that of the aluminum gasket to make much difference in the test results. The copper gasket was later chosen because of its slightly higher yield strength at 500°F. The test also showed that there was no permanent deformation of the knife-edges, but the gasket was permanently deformed. Therefore, it was decided against reuse of the gasket.

5.4.1.2.3 Material and Geometry

The primary goal of the connector design was the seal. Therefore, the design effort for the remainder of the connector was a modification of a proven design. The design chosen was the MC one-inch stainless steel connector. The nut was retained without any modification, the union was retained with modification, and the sleeve and flared-tubing were replaced by a flanged-section.

The nut and union material are AISI 316 stainless steel. This is used because of its resistance to corrosion and compatibility with many fluids which may be used in the piping system. For the same reasons the flanged-section was made of AISI 321 stainless steel. In fact, AISI 321 stainless steel was used for the tubing and test fixture also. This made it easier to weld the flanged-section and union to the tubing.

The seal (consisting of the gasket and two knife-edges) was located between the union and flanged-section at the outer radius of the two latter members. In this way, the seal was moved away from the fluid contained in the connector and there was enough space between the seal and inside diameter to put a bearing surface between the union and flanged-section. This bearing surface between the union and flanged-section limits the depth to which the knife-edges cut into the gasket and provides a load path for the transmission of compressive loads through the connector which is separate from the seal. The tensile load path is through the nut. The seal receives only sufficient load to force the knife-edges into the gasket. Then the flanged-section bottoms on the union and nearly all of the compressive load is transferred directly from the union to the flanged-section. The seal sees very little of any changes in external load.

The bearing surface on the union is countersunk beneath the level of the knife-edge. This was done for ease in manufacture and is intended for use only on the connector tested in the laboratory. Leaving the knife-edge exposed invites damage. A better design is to leave a protruding section on both the union and flanged-section.

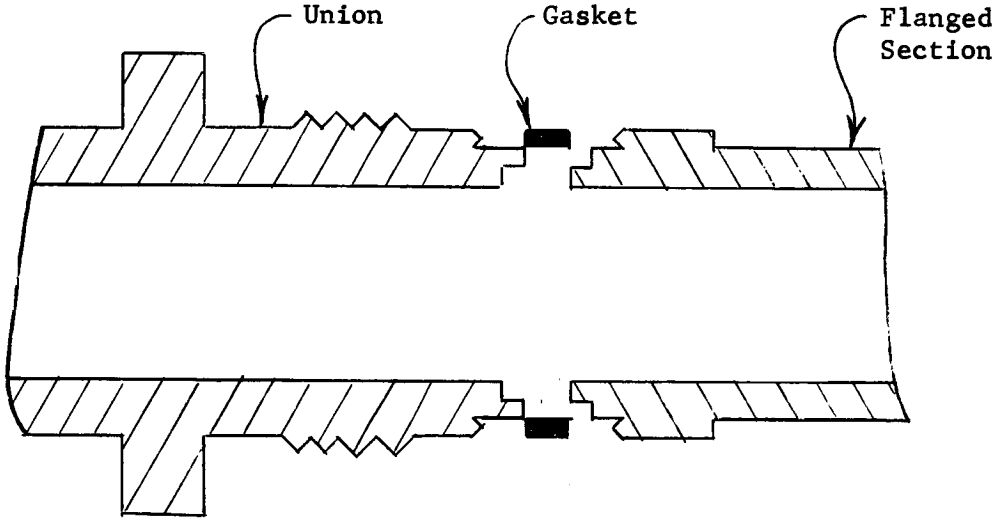

Fig. 5.8

The inter-locking feature is used to positively align the parts during assembly and to prevent relative radial motion between the union and flanged-section.

The flanged-section has the protruding section through which the load is transmitted to the union, the knife-edge which cuts into one side of the gasket and a shoulder which engages the nut. Like the union, the flanged-section is welded to the tubing. For the test connector, butt-welds were specified for joining the connector to the tubing. For the production design the welds specified would be similar to those described in Ref. 4. Also, the weld side of the union would not be threaded and be prepared differently for welding.

5.4.1.2.4 Environmental Conditions

The environmental conditions important in this design are the various temperatures and external loads. The connector must perform satisfactorily at room temperature, $-320^{\circ}F$ and $+500^{\circ}F$ with an axial tensile force and a transverse moment. The axial force is equal to the maximum internal pressure of 1500 psi times the inside cross-sectional area of the tubing, 890 lbs. and the moment is 450 inch lb. The temperatures are steady-state conditions at which the whole connector will be at approximately the same temperature. Heating and cooling of the connector will be slow and controlled.

5.4.1.2.5 Preload Determination

The preload is the tension put in the nut at assembly. Its only purpose is to keep the seal from opening up under all operating conditions. This means keeping the load on the seal above some allowable minimum and preventing any relative motion between the knife-edges and gasket. These objectives are accomplished by bringing the union and flanged-section into direct contact and maintaining a minimum compressive load on the union to flanged-section interface.

The connector has two load paths in compression and one in tension. The seal and union to flanged-section interface form the two parallel compressive load paths. The nut is the tensile load path. The members of the connector which make up these load paths can be represented as an elastic spring. The three load paths are three springs in parallel. External loads are shared by the springs and distributed among them in proportion to their respective spring constants.

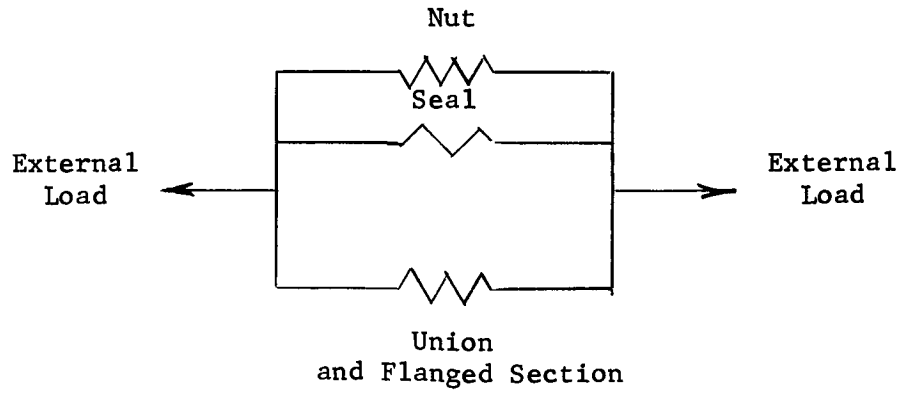

However, the spring constant for the seal is so much smaller than that for the union and flanged-section that it can be neglected in the preload calculation.

The initial load applied to the seal during assembly must be sufficient to push the knife-edges into the gasket and make a leak-tight seal. It was shown in the knife-edge tests reported on in Ref. 2 that a depth of cut of approximately 4 mils for each knife-edge was sufficient to make a seal and this was achieved with a load of approximately 260 lb/inch of seal circumference. Therefore, in order to initially seal the connector during assembly, each knife-edge must cut into the gasket at least 4 mils. This was accomplished by using a more than adequate preload (the evaluation of which follows in this section) and choosing the dimensions so that the flanged-section will not bottom on the union before a sufficiently deep cut is obtained in the gasket. The depth of cut allowed by the geometry of the connector is a minimum of 17.5 mils per knife-edge.

Once the desired level of leakage is reached, it was shown in the knife-edge test of Ref. 2 that the seal leakage will not noticeably increase until the load on the seal is decreased by more than 30%. Therefore, as the springs representing the seal and union to flanged-section are in parallel, it is only necessary to prevent the compressive force on the union to flanged-section from decreasing by more than 30% from the force applied during assembly. Then, if the preload is large enough to effect a seal with the desired level of leakage, there should be no noticeable increase in leakage during all operating conditions.

The preload can be calculated explicitly by setting the condition that the force on the union during the most severe operating condition is v of the force of the preload.

$$f_u = - v P$$

Substituting in equation 5-15 of Section 5.4.3 and solving for P gives:

$$(1-v)P = .749F_T - E \left\{ .0915a_U T_U + .0928a_F T_F - .1843a_N T_N \right\} + 1.42M_T$$

The maximum values of F_T and M_T are 890 and 450 respectively. F_T is the axial force due to the internal pressure of 1500 psi and M_T is the externally applied transverse moment.

Using the room temperature conditions as the most severe:

$$P\ (70^{\circ}F) = \frac{1305}{1-v}\ \text{lb.}$$

Using $500^{\circ}F$ conditions as the most severe:

$$a_U = a_N = 8.82 \times 10^{-6}\ \text{in/in}^{\circ}F \text{ and } a_F = 9.48 \times 10^{-6}\ \text{in/in}^{\circ}F$$

$$E = 26 \times 10^{6}\ \text{psi}$$

$$P\ (500^{\circ}F) = \frac{621}{1-v}\ \text{lb.}$$

Using $-320^{\circ}F$ conditions as the most severe:

$$a_U = a_N \quad \text{and} \quad T_U = T_F = T_N = -390$$

$$E = 29.5 \times 10^6 \text{ psi}$$

$$P\ (-320^{\circ}F) = \frac{1305}{1-\nu} - \frac{106.8}{1-\nu}\left(10^7\right)\left(a_N - a_F\right)$$

Best available data shows $a_N = a_F$

$$P\ (-320^{\circ}F) = \frac{1305}{1-\nu} \text{ lb.}$$

Therefore, a preload of $\frac{1035}{1-\nu}$ lb. should be used. However, the value of ν is not well defined. The results for the knife-edge tests reported on in Ref. 2 show a maximum load of 633 lb/inch. On unloading, the leakage started to increase at 440 lb/inch and was up to 1×10^{-5} atm cc/sec. at 256 lb/inch. If ν is based on the point that the leakage increased, then $\nu = .7$. If ν is based on the point where the leakage is 1×10^{-5} atm cc/sec. (which is well below the design point of 1×10^{-4} atm cc/sec.) then $\nu = .4$. Using $\nu = .7$, the calculated value of P = 4350 lb. This is more than twice the value used in the standard MC fitting.

If $\nu = .4$ is used, then P = 2180 lb.

A preload of 2,200 lb. was chosen. This is close to the preload used in the testing of the MC fittings and avoids the ultra-conservatism of using $\nu = .7$.

5.4.1.2.6 Structural Integrity

The structural integrity of the connector is its ability to function properly under all operating conditions without being damaged. There should not be sufficient creep in the connector to allow the load on the seal to drop below the minimum value. The connector should not grossly deform due to yielding. There should be no structural static or fatigue failure. Also, the environmental conditions should not cause any deterioration of the connector.

In this design, the only item of importance is the prevention of gross deformation due to yielding or failure due to static loading. The time period set forth in the connector requirements is not long enough to consider creep a possible problem unless the stresses are very large. The loading is static and is not repeated often enough to consider either low or high-cycle fatigue. Also, none of the environmental conditions would cause any deterioration of the connector.

So the structural integrity of this design is assured if the stresses in the structure are below the yield stress under all operating conditions. The tubing is also included in this consideration. It is subjected to an internal pressure of 1500 psi and a transverse moment of 450 inch lb. The hoop stress is:

$$S_2 = \frac{q\,r}{t} = 10{,}040 \text{ psi}$$

The maximum tensile stress is:

$$S_1 = \frac{qr}{2t} + \frac{M_t}{\pi R^2 t} = 15{,}100 \text{ psi.}$$

The yield stress of the tubing decreases with temperature and is approximately 23,000 psi at 700°F. Therefore, the structural integrity of the tubing is assured.

The union and flanged-section are subjected to an internal pressure of 1500 psi and a maximum axial force which occurs at 500°F and can be calculated from equation 5-15.

At 500°F; $a_n = a_u = 8.82 \times 10^{-6}$ in/in °F, $a_F = 9.48 \times 10^{-6}$ in/in °F and $E = 26 \times 10^6$ psi.

P = 2200 lb, $F_T = 0$ and $M_T = -450$ inch lb to get the greatest possible compressive force, $f_u = -3530$ lb. The weakest section is the protruding part of the flanged-section. In this part the hoop stress is:

$$S_1 = \frac{q\,r}{t} = 5360 \text{ psi.}$$

The axial compressive stress is:

$$S_3 = -9910 \text{ psi.}$$

These stresses are below the yield stress of the flanged-section. Therefore, the structural integrity of the union and flanged-section is assured.

The nut is subjected to a maximum axial force which occurs at 500°F and can be calculated from equation 5-14. At 500°F $a_N = a_u = 8.82 \times 10^{-6}$ in/in °F, $a_F = 9.48 \times 10^{-6}$ in/in °F, and $E = 26 \times 10^6$ psi.

P = 2200 lb, $F_T = 890$ lb (corresponding to an internal pressure of 1500 psi), and $M_T = 450$ in lb to get the largest possible tensile force, $f_N = 4160$ lb.

The stresses in the nut are calculated by separating the nut into four standard elastic elements as was done in Section 5.4.3 to calculate the spring constant for the nut.

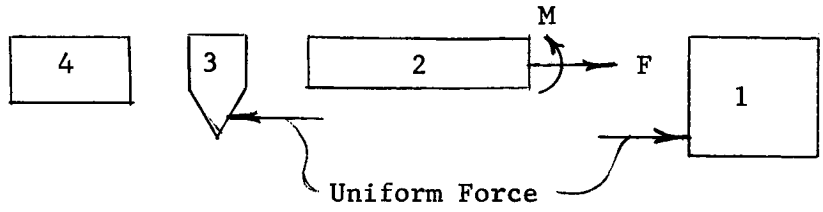

During the calculation of the spring constant the forces, moments, deflections and rotations at all of the joints were calculated for a unit axial force. From these it was determined that the maximum moment in the shell occurs at the junction of (1) to (2).

The stresses for the critical areas are calculated for the 4160 lb axial force with the aid of the results of the spring constant calculation. The maximum tensile hoop stress for the elastic ring (1) is 3660 psi. The tensile stress in the shell (2) due to the axial force, F, is 7000 psi. The tensile stress at the inner radius of shell (2) due to the moment, M, is 58,900 psi. Thus, at the inner radius of shell (2), where shell (2) joins ring (1), there is a total tensile stress of 65,900 psi. The shear stress on the threads is 3280 psi.

The minimum yield stress of the AISI 316 steel, used in the nut, for a 1/2 inch to 3/4 inch rod in the 1/4 hard condition is 70,000 psi at room temperature. Therefore, as the outside diameter of the nut is about 1-3/4 inches and the nut operating temperature is 500°F, the minimum yield stress will be somewhat below 70,000 psi. All of the calculated stresses except one are well below the yield stress. The stress at the inner radius at the junction of (1) and (2) is probably above the yield stress. However, the stress is very localized and is about 29,000 psi 180° from the point of maximum stress.

As all of the stresses in the nut are very low except for a very localized stress there will be no gross deformation of the nut nor is there any chance of a failure. Prior to use in the leakage testing the nut will be axially loaded on a tensile testing machine for a calibration of strain gages mounted on the nut. The axial load will be gradually increased to 4000 lb. This may cause localized yielding and strain hardening and will definitely reduce the possibility of localized yielding during the leakage testing. Therefore, the nut design is accepted without any changes.

5.4.1.2.7 Reliability

Reliability is built into the connector in a number of ways. The most important of which is the use of a disposable gasket. The only part of the connector that is permanently deformed during assembly or operating conditions is the gasket, and it is used only once. Therefore, at each assembly the connector is exactly the same. If the connector performs satisfactorily at the first assembly it will perform satisfactorily at each assembly.

Also, the connector design includes sufficiently close tolerances on the critical dimensions for sealing. The connector structure is sized to prevent permanent deformation or damage to any part of it under all operating conditions. The design configuration minimizes the possibility of damage to the sealing surfaces of the connector.

In addition to the design factors necessary to achieve high reliability there are other important factors. The connector must receive careful handling prior to and during assembly to prevent damage to the connector. The method of attaching the connector to the tubing must be standardized so that a good connection is assured every time. The assembly procedure must assure a proper assembly and a predetermined preload each time.

Of course the connector manufactured and tested in the laboratory received careful handling. The connection to the tubing is a weld that was tested for leakage. The preload was determined by using calibrated strain gages on the nut so that at each assembly the nut was simply tightened until the gages indicated the required preload.

5.4.2 Test Equipment

5.4.2.1 Fluid Contained

The purpose of the test equipment is to determine the leakage of the threaded connector under all of the specified operating conditions. For this purpose helium was chosen as the fluid to be contained in the connector. It is gaseous at all of the test temperatures and is therefore more difficult to contain than a liquid. Also, helium is safe to work with and the flow of helium is easily measured in the mass-spectrometer leak detector.

The helium supply is a high pressure bottle, Fig. 5.9. A pressure regulator mounted on the bottle is used to set the pressure to the connector. The pressure is measured by an independent pressure gage in the helium line to the connector. The helium line enters the back side of the bracket to which the connector is mounted, see Fig. 5.9 and 5.10, and pressurizes the inside of the tubing and connector.

5.4.2.2 Leak Detector

The helium that leaks through the connector is collected in the vacuum chamber that surrounds the connector, Fig. 5.9. This chamber slides over the tube connector and bolts to the end bracket. There is a seal between the chamber and bracket. The chamber has a small tube rising from it which is connected to the leak detector through a number of flexible hoses. It is

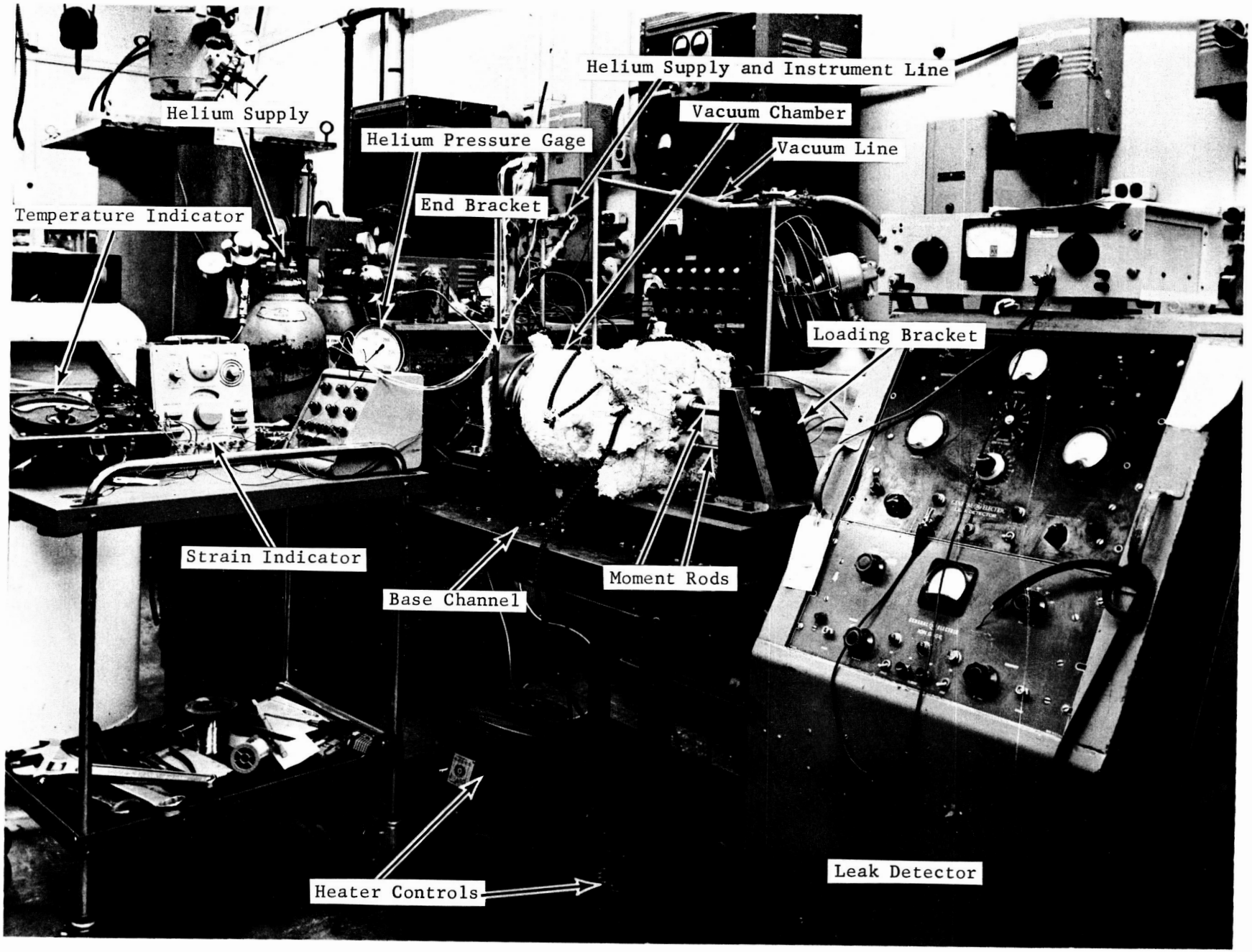

FIG. 5.9 TEST EQUIPMENT

ORIGINAL PAGE
BLACK AND WHITE PHOTOGRAPH

FIG. 5.10 MOUNTED TUBE CONNECTOR

through these hoses that a vacuum is drawn on the chamber and the leak detector draws the helium. The chamber must be evacuated in order to sense the low level of leakage set forth in the connector requirements.

Incorporated in the leak detector are vacuum pumps that evacuate the chamber and draw the helium through the leak detector. The leak detector is a mass spectrometer that will differentiate between gases and directly measure the flow of helium, Fig. 5.9.

5.4.2.3 Vacuum Chamber and End Bracket

The test connector is welded to two pieces of one-inch tubing, one of which is welded to the end bracket, Fig. 5.9 and drawing 544E540 Sheet 3. The end bracket has a hole concentric with the tube, through which the helium is introduced and the internal instrumentation wiring passes. Opposite the tube the helium supply and instrument line is welded to the end bracket. The other piece of one inch tubing is sealed off by the slotted block.

The end bracket was designed and manufactured specifically for the threaded connector tests. The vacuum chamber as well as the loading bracket and base channel were designed and manufactured for the 4 inch flanged connector tests. All of the drawings for the test fixture are in the Section 5.4.4.

5.4.2.4 Moment Rods

A moment is applied to the connector by putting equal and opposite forces on the moment rods. The rods each have a pin which engages the slotted block, one on the top and one on the bottom. The couple applied to the slotted block results in a pure transverse moment on the connector. The size of the moment is controlled by adjusting the forces in the moment rods. These forces are adjusted by tightening or loosening the nuts on the moment rods which are located on either side of the load bracket, Fig. 5.11 and drawing 544E540 Sheet 3.

5.4.2.5 Instrumentation

The instrumentation consists of strain gages and thermocouples. Strain gages are mounted on the tubing, midway between the slotted block and connector to measure the applied moment. Strain gages are also mounted on the flats of nut to measure the preload during assembly.

Thermocouples are placed inside the union, on the outside of the tubing between the mounting bracket and connector, on the outside of the nut, on the outside of the flanged-section, and on the outside of the tubing between the connector and slotted block. These accurately describe the temperature distribution in the connector so that a uniform hot or cold temperature can be achieved.

The thermocouple wires inside the connector pass out through the helium supply line. The thermocouple and strain gage wires on the outside of the connector enter the instrumentation stand-pipe just above the point on the mounting bracket where the connector is attached. All of the instrumentation wires go to switching boxes and strain and temperature indicators as shown in Fig. 5.9.

ORIGINAL PAGE
BLACK AND WHITE PHOTOGRAPH

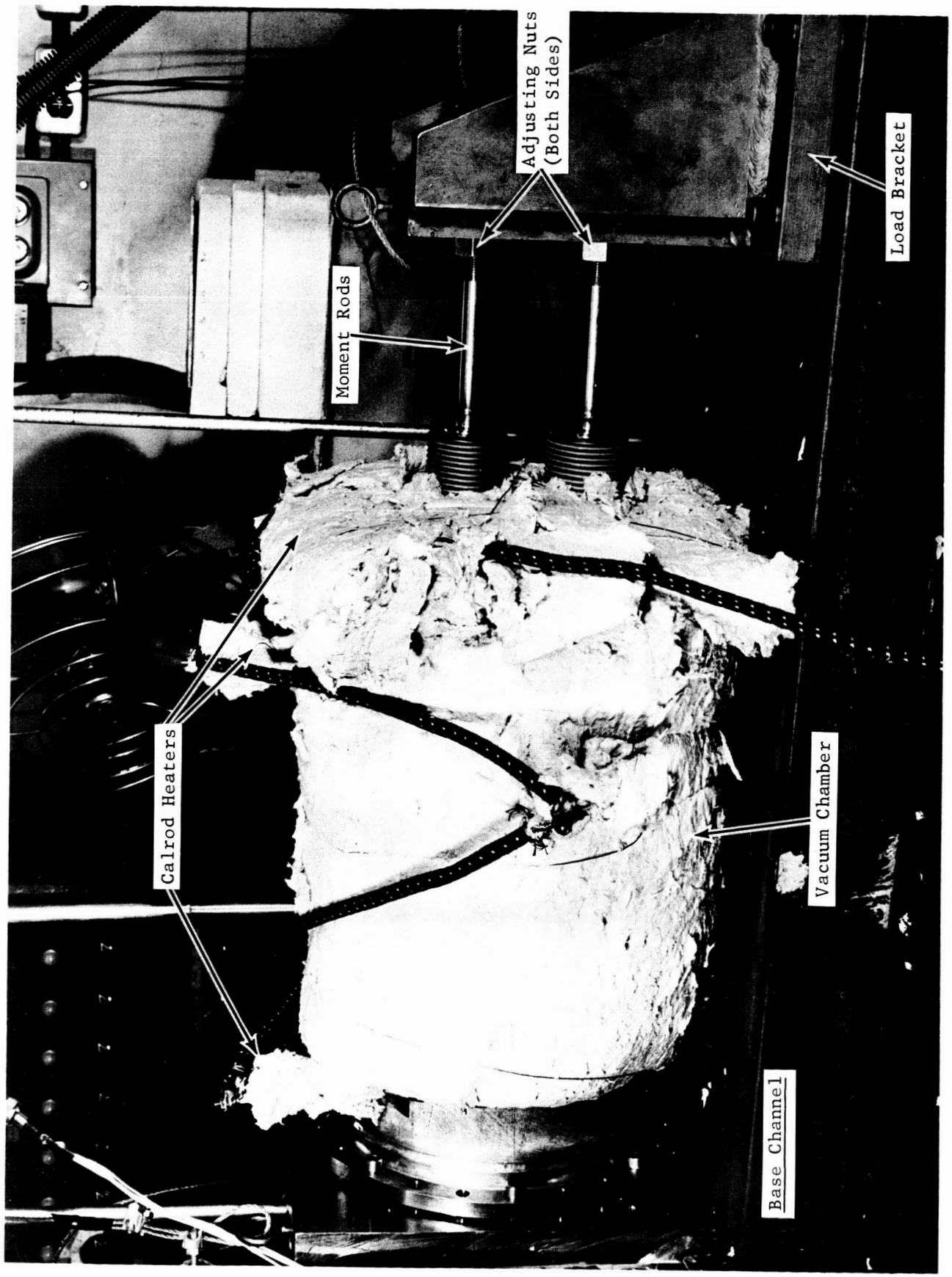

FIG. 5.11 VACUUM CHAMBER AND LOADING MECHANISM

5.4.2.6 Heating and Cooling

The connector is heated by a number of calrod heaters on the outside of the vacuum chamber and mounting bracket, Fig. 5.11 and drawing 544E540 Sheet 1. These heaters are independently controlled by a number of variacs, Fig. 5.9. The connector is cooled by submersing the base channel, brackets, and vacuum chamber assembly into a tube of liquid nitrogen.

5.4.3 Equation for Calculation of Preload

The welded-knife-edge connector may be represented by the following simplified model.

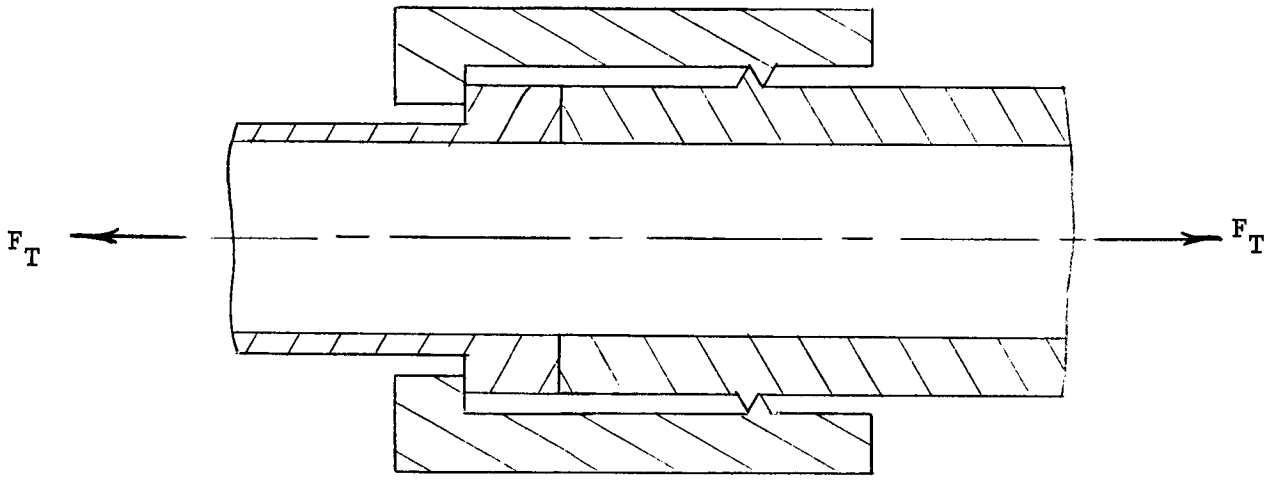

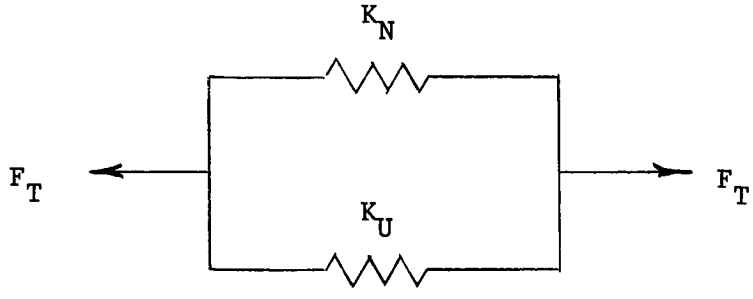

Fig. 5.12

The total force in the nut or union due to an axial force, F_T, preload, P, and the thermal growth of the connector is:

$$5\text{-}1 \qquad F_U = \frac{K_U}{K_N+K_U} F_T - \frac{K_N K_U}{K_N + K_U} (G_U - G_N) - P$$

$$5\text{-}2 \qquad F_N = \frac{K_N}{K_N+K_U} F_T + \frac{K_N K_U}{K_N + K_U} (G_U - G_N) + P$$

The effect of a transverse moment applied to the connector is to increase the tensile force in one half of the connector circumference and decrease it in the other half. For sealing, the point of maximum tensile force is of primary interest. A transverse moment, M_T, is distributed between the nut and union as follows:

$$5\text{-}3 \quad M_U = \frac{I_U}{I_U + I_N} M_T$$

$$5\text{-}4 \quad M_N = \frac{I_N}{I_U + I_N} M_T$$

The moment in the nut or union may be represented as an axial force per linear inch of mean circumference which varies linearly along the circumference and is self-equilibrating in the axial direction

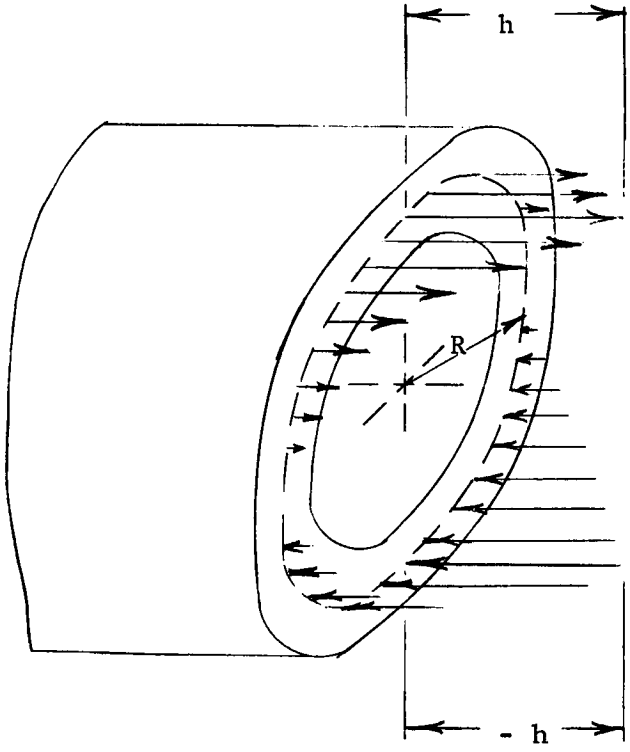

$M = \pi R^2 h$

A uniform axial force which would result in the same maximum axial force per linear inch at the mean radius would equal $2 \pi R h$.

let $H = 2 \pi R h$

5-5 $$H = \frac{2M}{R}$$

For the nut,

5-6 $$H_N = \frac{2 I_N M_T}{R_N (I_U + I_N)}$$

However, the calculation for the union requires a correction factor to account for the difference between the mean radius of the union and that of the seal. Because the mean seal radius is larger than the mean union radius the effect of an angular rotation of the union due to an applied moment is magnified on the seal.

$$h_U = \left(\frac{M_U}{\pi R_U^2}\right) \left(\frac{R_S}{R_U}\right)$$

5-7 $$H_U = \frac{2 I_U R_S M_T}{R_U^2 (I_U + I_N)}$$

Then the maximum tensile force on the nut is:

$$f_N = F_N + H_N$$

5-8 $$f_N = \frac{K_N F_T}{K_N+K_U} + \frac{K_N K_U}{K_M+K_U} (G_U - G_N) + P + \frac{2 I_N}{R_N (I_U+I_N)} M_T$$

The minimum compressive force in the union is

$$f_U = F_U + H_U$$

5-9 $$f_U = \frac{K_U}{K_N+K_U} F_T - \frac{K_N K_U}{K_N+K_U} (G_U - G_N) - P + \frac{2 I_U R_S}{R_U^2 (I_U+I_N)} M_T$$

The spring constant for the union and flanged-section, K_U, is calculated by considering the elements as a series of right circular cylinders in direct compression. The active length is taken from the shoulder of the flanged-section, where the nut applies a force, to the center of the length of thread engagement between the nut and union.

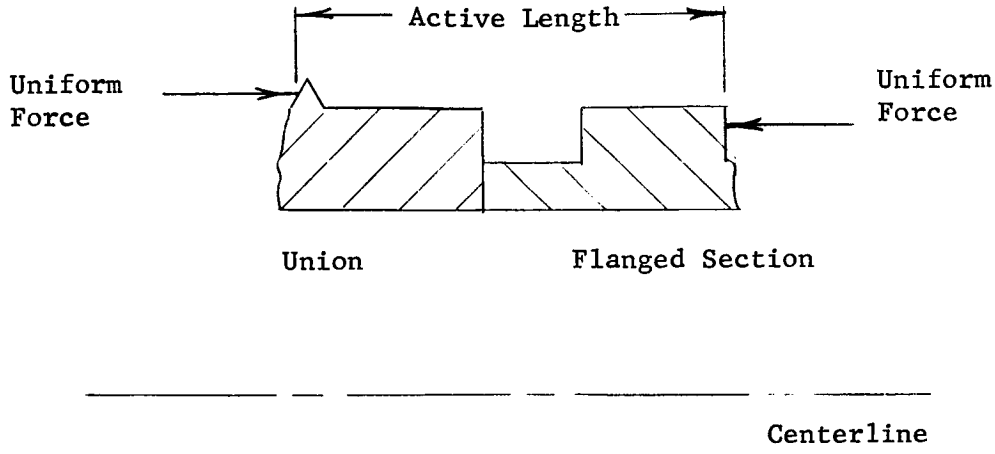

5-10 $$K_U = \frac{E}{1.573}$$

The spring constant for the nut, K_N, is calculated by considering the nut to consist of two shells and two rings. The active length is the same as that for the union and flanged-section. Also, the modulus of elasticity is the same.

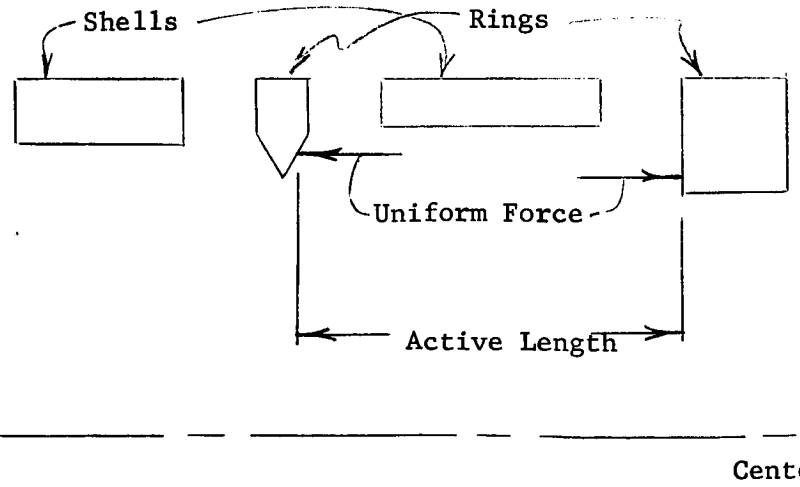

The radial and axial deflection and in plane rotation can be calculated for the four elements. Joining equation can be written. The simultaneous solution of all the equations gives the spring constant.

5-11 $$K_N = \frac{E}{4.68}$$

The axial thermal growth of the elements is due to the direct axial thermal expansion and the axial deflection due to the radial thermal expansion at the threads. Because of the thread angle a radial growth results in an axial deflection. The temperatures are assumed uniform in each element.

$$G_U = .572\ a_U T_U + .58\ a_F T_F$$

5-12

$$G_N = 1.152\ a_N\ T_N$$

The T's are the changes in temperature from a room temperature of 70^oF.

The area moments of inertia are calculated for the equivalent nut and the equivalent union and flanged-section.

$$I_N = .1562\ in^4$$

5-13

$$I_U = .0637\ in^4$$

Equations 5-10, 5-11, 5-12, and 5-13 substituted in equations 5-8 and 5-9 give:

5-14 $$f_N = .251\ F_T + E\ \left\{.0915\ a_U\ T_U + .0928\ a_F\ T_F - .1843\ a_N\ T_N\right\}$$

$$+ P + 2.34\ M_T$$

5-15 $$f_U = .749\ F_T - E\ \left\{.0915\ a_U\ T_U + .0928\ a_F\ T_F - .1843\ a_N\ T_N\right\}$$

$$- P + 1.42\ M_T$$

5.4.4 Design Drawings

FOLDOUT FRAME

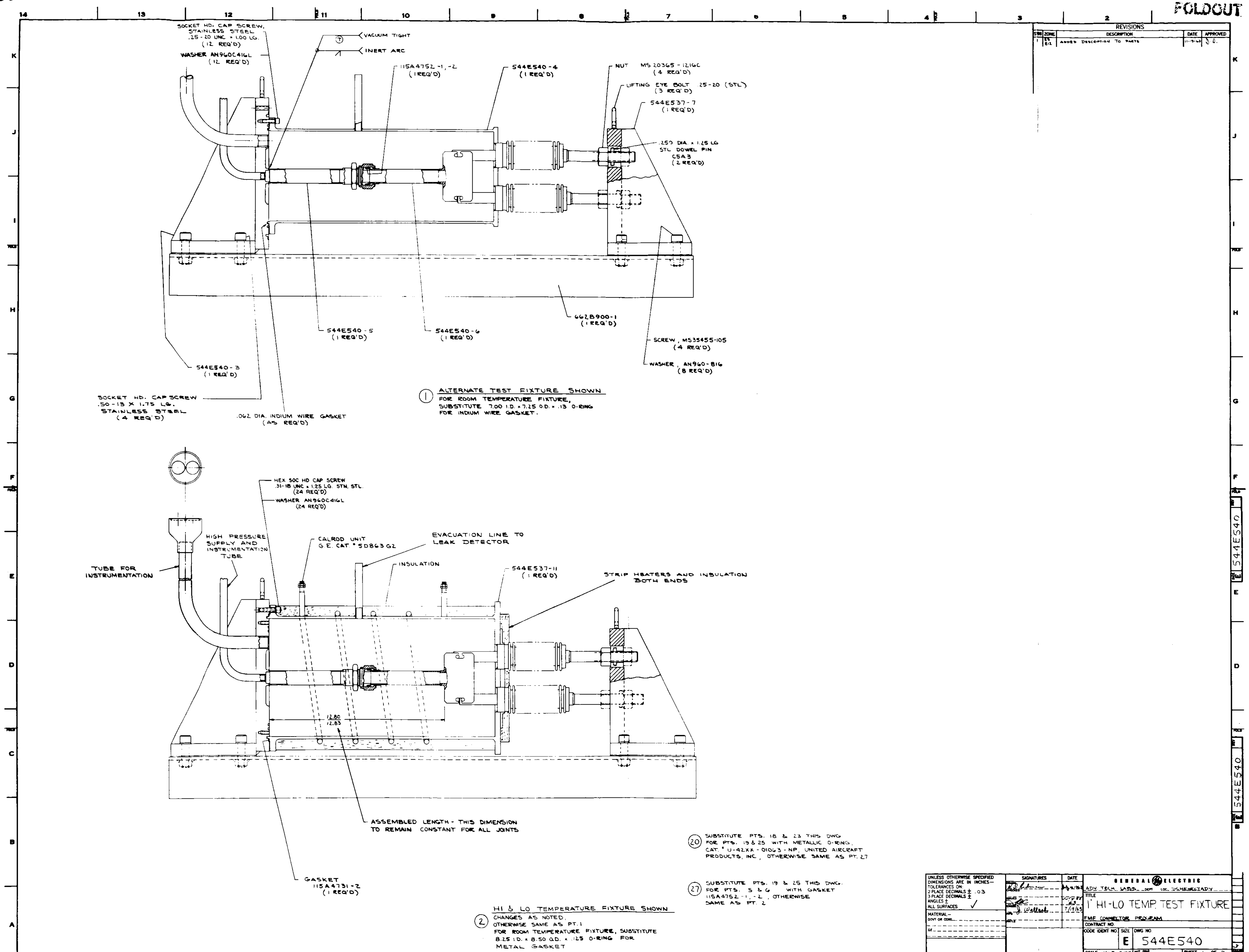

FOLDOUT FRAME 2

ORIGINAL PAGE IS OF POOR QUALITY

ORIGINAL PAGE IS OF POOR QUALITY

FOLDOUT FRAME 1.

FOLDOUT FRAME 2.

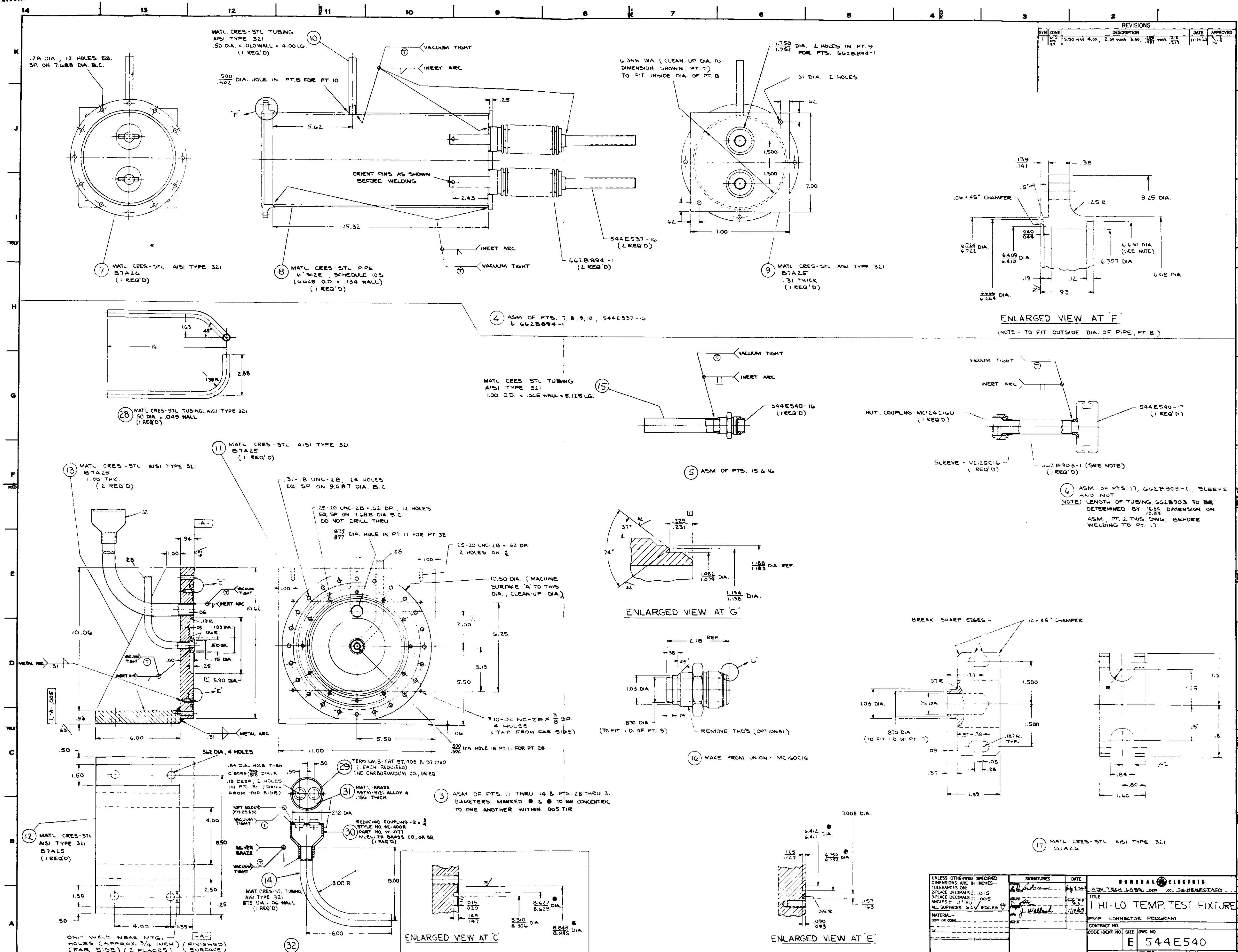

ORIGINAL PAGE IS OF POOR QUALITY

FOLDOUT FRAME

FOLDOUT FRAME 2

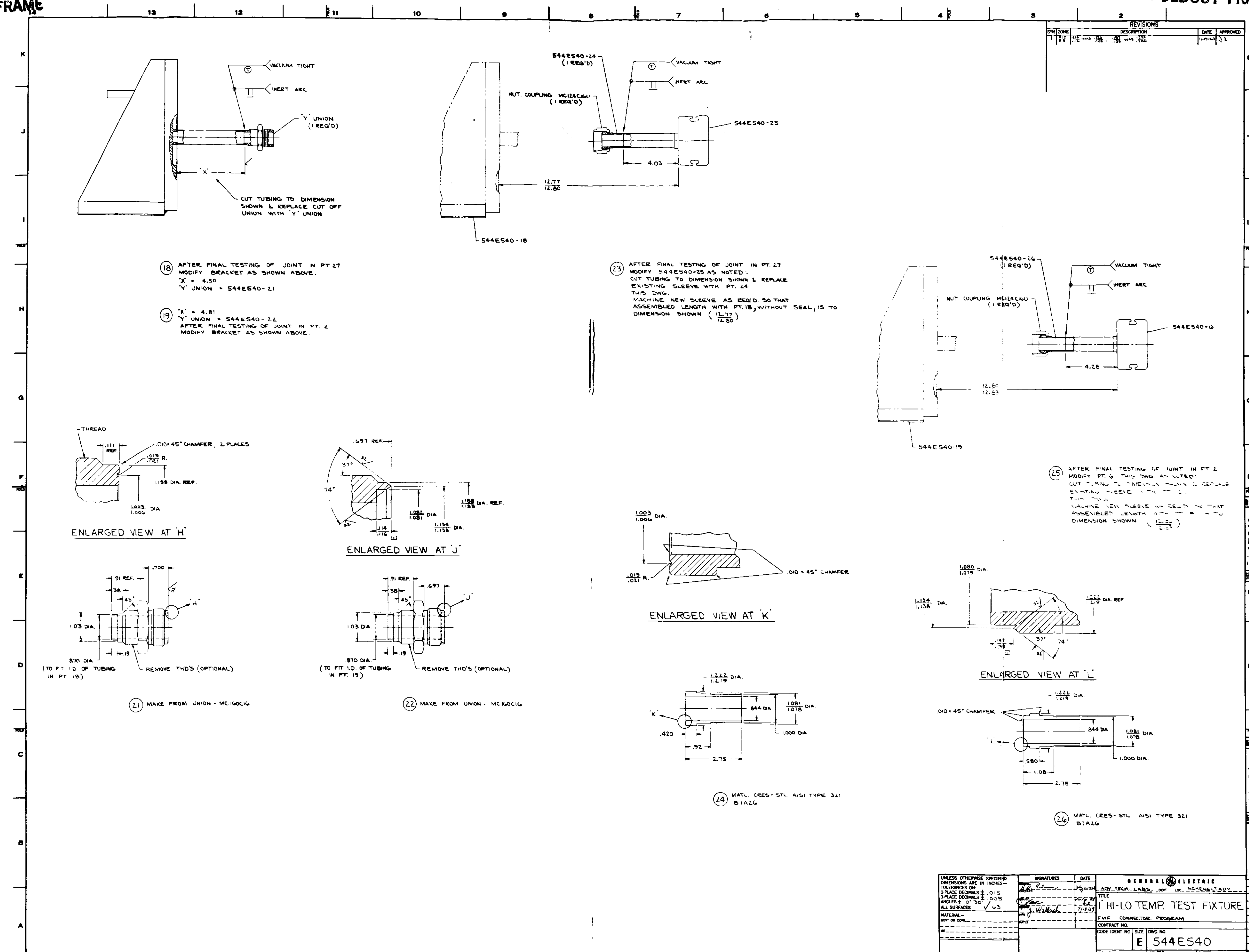

SIZE	115A4731	SHEET	REV
A			A

REVISIONS			
SYM	DESCRIPTION	DATE	APPROVED
A	CHG. INSIDE DIA., CHG. THICKNESS OF COPPER, ADDED PT. 2	7/9/63	J. Wallach

NOTES -

DIAMETERS TO BE CONCENTRIC TO ONE ANOTHER WITHIN .010 TIR.

GASKET TO BE FLAT WITHIN .06 MAX. WHEN RECEIVED (INSPECTION NOTE)

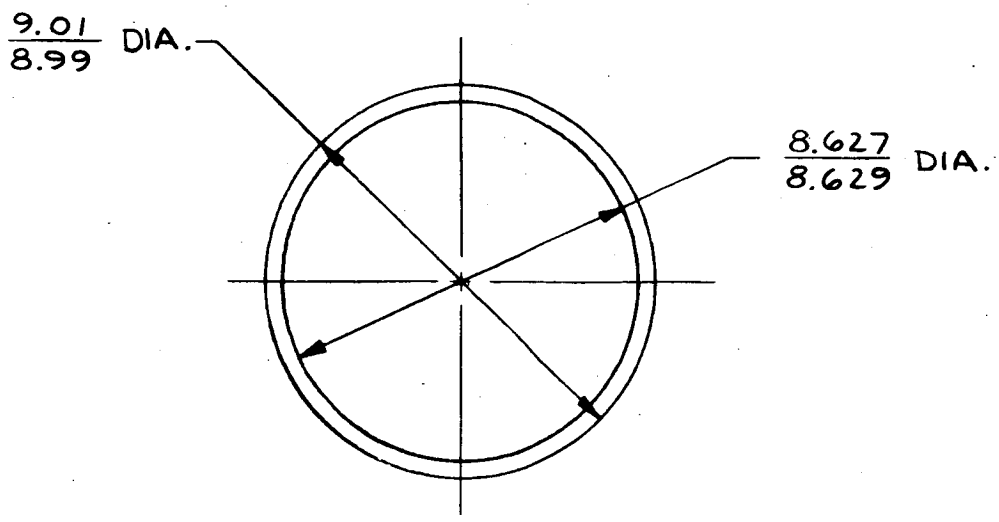

(1) MATL. CERTIFIED OFHC COPPER (OXYGEN FREE) ANACONDA ALLOY #121, ASTM SPEC. B152 TEMPER SOFT, ROCKWELL HARDNESS #F45 .065 ±.003 THICK

(2) MATL. ANNEALED ALUM. AA 1100-0 (25-0) .063 ±.003 THK.

PURCHASE PART DWG.

UNLESS OTHERWISE SPECIFIED DIMENSIONS ARE IN INCHES. TOLERANCES ON: FRACTIONS ± DECIMALS ± ANGLES ± ALL SURFACES ✓ MATL GOVT OR COML ---- GE ----	SIGNATURES	DATE
	DRAWN W. D. Rudman	June 24, 1963
	CHECKED	
	ISSUED [illegible]	24 June '63
	ENGR R. N. LaFond	6-24-63
	MFG	
	MATLS	

NEXT ASM 544E537

PRINTS TO

GENERAL ELECTRIC
ATL DEPT. LOC SCHENECTADY

TITLE GASKET
FMF CONNECTOR PROGRAM
CONTRACT NO.

CODE IDENT NO.	SIZE	DWG NO.
	A	115A4731

SCALE NONE	WT CALC ACTUAL	SHEET

FN-901-F (5-63) PRINTED IN U.S.A.

SIZE		SHEET	REV
A	115A4752		

REVISIONS

SYM	DESCRIPTION	DATE	APPROVED
1	1.080/1.081 WAS 1.088/1.083 ; .122/.120 WAS .107/.055	11-19-63	J.A.

NOTE

DIAMETERS TO BE CONCENTRIC TO ONE ANOTHER WITHIN .010 TIR.

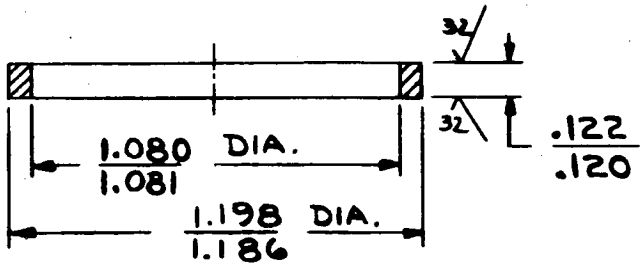

(1) MATL. CERTIFIED OFHC COPPER (OXYGEN FREE) ANACONDA COPPER #121, ASTM SPEC. B152 TEMPER SOFT, ROCKWELL HARDNESS F45 APPROX.

(2) MATL. ANNEALED ALUM. AA1100-0 (2S-0)

PURCHASE PART DWG.

UNLESS OTHERWISE SPECIFIED DIMENSIONS ARE IN INCHES. TOLERANCES ON: FRACTIONS ± DECIMALS ± ANGLES ± ALL SURFACES ✓	SIGNATURES	DATE
MATL GOVT OR COML	DRAWN L.D. Anderson	7/10/63
	CHECKED	
GE	ISSUED	July 25 '63
NEXT ASM 544E540	ENGRG	
	MFG	
	MATLS	

GENERAL ELECTRIC ATL DEPT. LOC SCHENECTADY

TITLE GASKET

FMF CONNECTOR PROGRAM

CONTRACT NO.

CODE IDENT NO.	SIZE	DWG NO.
	A	115A4752

SCALE 2/1 | WT CALC ACTUAL | SHEET

PRINTS TO

GE-N-901-F (5-63) PRINTED IN U.S.A.

3

DRAWING NO. 662B903 CONT ON SHEET SH NO.

GENERAL ELECTRIC

UNLESS OTHERWISE SPECIFIED USE THE FOLLOWING:				
APPLIED PRACTICES	SURFACES	TOLERANCES ON MACHINED DIMENSIONS		
		FRACTIONS	DECIMALS	ANGLES
	✓	±	± .005	± 0° 30'

REV NO. 1 | 662B903 CONT ON SHEET | SH NO.

TITLE FLARED TUBING END, MODIFIED

FIRST MADE FOR CONNECTOR PROGRAM

FCF ON 544E540

662B903 CONT ON SHEET SH NO.

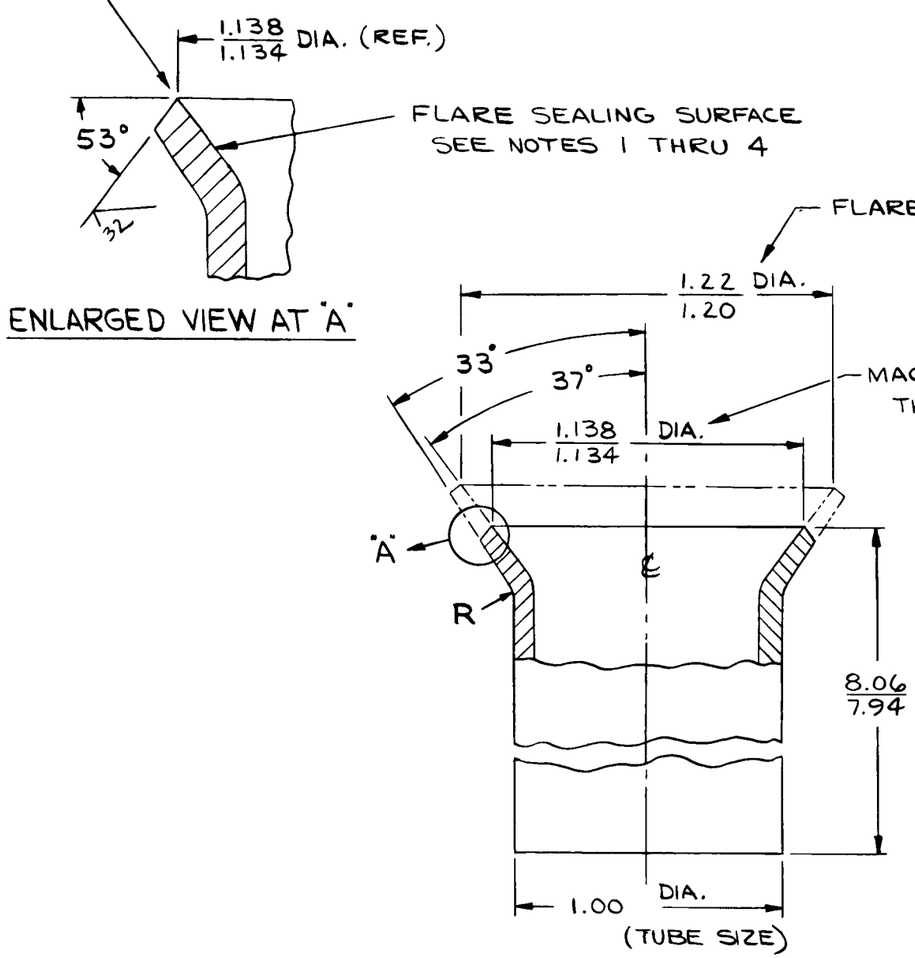

1 MATL. CRES-STL TUBING
AISI TYPE 321A (ANNEALED)
.065 WALL

NOTES –

1. FLARE SHALL BE FORMED SQUARE WITH CENTERLINE OF TUBE.
2. FLARE SEALING SURFACE SHALL BE CONCENTRIC WITH OUTSIDE DIAMETER OF TUBE.
3. THE SEALING SURFACE ROUGHNESS IN BOTH RADIAL & TANGENTIAL DIRECTIONS SHALL NOT EXCEED 32.
4. THERE SHALL BE NO RADIAL SCRATCHES ON THE FLARE.

REVISIONS		PRINTS TO	
1	NOV. 19, '63 REVISED NOTES		
			3

MADE BY H. D. Robinson June 24, 1963 | APPROVALS J. W. 7/1/63

ISSUED Jac 1 July '63

ATL DIV OR DEPT

SCHENECTADY LOCATION

662B903 CONT ON SHEET SH NO.

FOLD

FF 506-F (11-62)
PRINTED IN U.S.A.

5.4.5 Nomenclature

		Units
a_F	Coefficient of thermal expansion for flanged-section	in/in ^oF
a_N	Coefficient of thermal expansion for nut	in/in ^oF
a_U	Coefficient of thermal expansion for union	in/in ^oF
E	Modulus of elasticity	lb/in^2
F_N	Axial force on nut (plus in tension)	lb
F_T	Total axial force (plus in tension)	lb
F_U	Axial force on union (plus in tension)	lb
G_N	Thermal growth of nut (plus for elongation)	in
G_U	Thermal growth of union and flanged section (plus for elongation)	in
h	Maximum force per linear inch of circumference due to applied moment	lb/in
H	Axial force (plus in tension)	lb
H_N	Axial force on nut	lb
H_U	Axial force on union	lb
I_N	Area moment of inertia of equivalent nut	in^4
I_U	Area moment of inertia of equivalent union and flanged section	in^4
K_N	Spring constant of nut	lb/in
K_U	Spring constant of union and flanged-section	lb/in
M_N	Moment on nut	in lb
M_T	Total moment	in lb
M_U	Moment on union and flanged section	in lb
P	Preload (plus for tension in nut)	lb
q	Internal pressure	lb/in^2
r	Inside radius	in
R	Mean radius	in

R_N	Mean radius of nut	in
R_S	Mean radius of seal	in
R_U	Mean radius of union	in
t	Wall thickness	in
T_F	Temperature change in flanged-section	^oF
T_N	Temperature change in nut	^oF
T_U	Temperature change in union	^oF

5.4.6 References

1. "Design Criteria for Zero-Leakage Connectors for Launch Vehicles", Final Report for First Contract Period of NASA Contract NAS 8-4012.

2. "Design Criteria for Zero-Leakage Connectors for Launch Vehicles", Quarterly Technical Progress Report No. 4 (Report Period Ending 5/31/63), Contract NAS 8-4012.

3. P. Guthman, "Tube Connectors - A State-of-the-Art Survey", Chrysler Corporation Missile Division, Huntsville Operations.

4. G. R. Barton, "Tubular Joining by Induction Brazing and Fusion Welding Methods", presented 8 October 1962 at 25th SAE Aerospace Forum in Los Angeles.

5. "Design Criteria for Zero Leakage Connectors for Launch Vehicles -- Fundamental Seal Interface Studies and Design and Testing of Tube and Duct Separable Connectors", F. O. Rathbun (editor), December 15, 1963, Contract NAS 8-4012.

6. LEAKAGE TESTS OF MC FLARED TUBING CONNECTORS

by

G. W. Sarney

6.0 Summary

The stringent requirement in rocket propulsion systems for leak-tight fluid connections has created interest in the leakage characteristics of flared tubing connectors. Marshall Space Flight Center developed the "MC" fitting to meet rocket propulsion leakage requirements. A series of tests have been run at the A.T.L. leakage facility to determine the leakage characteristics of these "MC" fittings.

The "MC" configurations tested include the sizes 1/2", 3/4" and 1" of stainless steel and aluminum alloy materials. The main effects considered are: flare process and surface finish, external torque, internal pressure and fitting material. Other factors investigated are: repeatability of seal, torque relaxation, crush washer gaskets, plating of the union sealing surface, and antifriction bearing surfaces for the nuts.

The following conclusions may be drawn:

1. Leak-tight connections were obtained only in a few cases when gross deformations of the union resulted in a new sealing surface geometry featuring uniform contact with a small contact area. This new sealing geometry and high sealing pressure could be obtained only for stainless steel connectors with high strength sleeves.

2. Connections not showing gross deformations of the union leaked due to non-uniform sealing pressure. Also the magnitude of the sealing pressure when distributed over the whole union sealing area is below the yield stress of the connector materials. Metal gasket test results in Volume 3 of the First Contract Period (similar sealing area and internal pressure) indicate that leaks on the order of 10^{-4} to 10^{-2} cc/sec will occur when the sealing stress is slightly lower than the yield stress.

3. The general leakage level of the "MC" flared connector when pressurized with helium to 1500 psi is 10^{-4} to 10^{-2} cc/sec.

4. The high-quality, smooth sealing-surface finish is an aid in reducing the leakage area but, high sealing pressures are necessary to obtain leak-tightness.

5. The "MC" specification for union surface flatness is not necessary since the union becomes concave on the first torquing operation due to yielding in the hoop direction.

6. The special flare process gives a circumferential directional surface finish, but no improvement in crest-to-valley roughness or leakage was evident.

7. The sealing pressure was not uniform around the fitting. Each time a flared connector is assembled, leakage paths are produced by the ovality of the mating parts.

8. The leakage level increased with connect-disconnect tests of aluminum fittings, and the sealing surfaces became very rough. When the stainless steel fittings were reassembled with the same parts, the leakage level and the local surface roughness did not increase, although the sealing surfaces of the unions were grossly deformed.

9. Plating the union sealing surfaces decreased leakage, but did not seal in many cases since the sealing pressure was not uniform.

10. The leakage-pressure relation was linear.

11. Torque relaxation was not a problem.

12. Antifriction bearings on the shoulder of the nut prevented burring there.

13. The Swagelok connector exhibited very good sealing ability, especially with a soft sleeve, because the sealing pressure was several times the yield stress and was uniform.

14. Insertion of Voi-Shan crush washers improved the leak-tightness of stainless steel fittings but did not materially improve the leak-tightness of the aluminum fittings.

6.1 Introduction

A major reliability problem in the Saturn launch vehicle is the leak-tightness of the over one thousand demountable tubing connections. In an effort to improve the probability of leak-tight connections over conventional fittings, Marshall Space Flight Center has developed the "MC" flare fitting.

Basically the "MC" fitting is a high-quality version of the conventional "AN" fitting. It is schematically illustrated in Figure 6.1. The surface finish roughness and degree of ovality are rigidly controlled by the "MC" specification MSFC-SPEC-143. In particular, the union fitting must meet the following limits:

(a) The conical sealing surface must be round within the following limits:

1. In 360 degrees the maximum deviation must not exceed .0003 inch.
2. The maximum rate of deviation shall not exceed .00010 in. 15 degrees of the arc.

(b) The conical sealing surface shall not exhibit concave areas but may exhibit a convex configuration of a concentric nature but not to exceed .0005 inch.

(c) The final sealing-surface finish shall have a maximum crest-to-valley profile of 10 to 14 microinches for steel and 22 to 30 microinches for aluminum alloy.

The sealing surfaces are inspected to be free of such defects as tool chatter marks, scratches, handling marks and ridges.

The rated torques for each size fitting are also specified. There is given a minimum rated and maximum rated value with provisions for increasing the torque to 150 percent of the maximum rated torque in order to improve leaktightness during test.

A new tube flaring process has been developed at Marshall Space Flight Center in order to improve the tube sealing surface finish and ovality. This process is called the special flare process in this report.

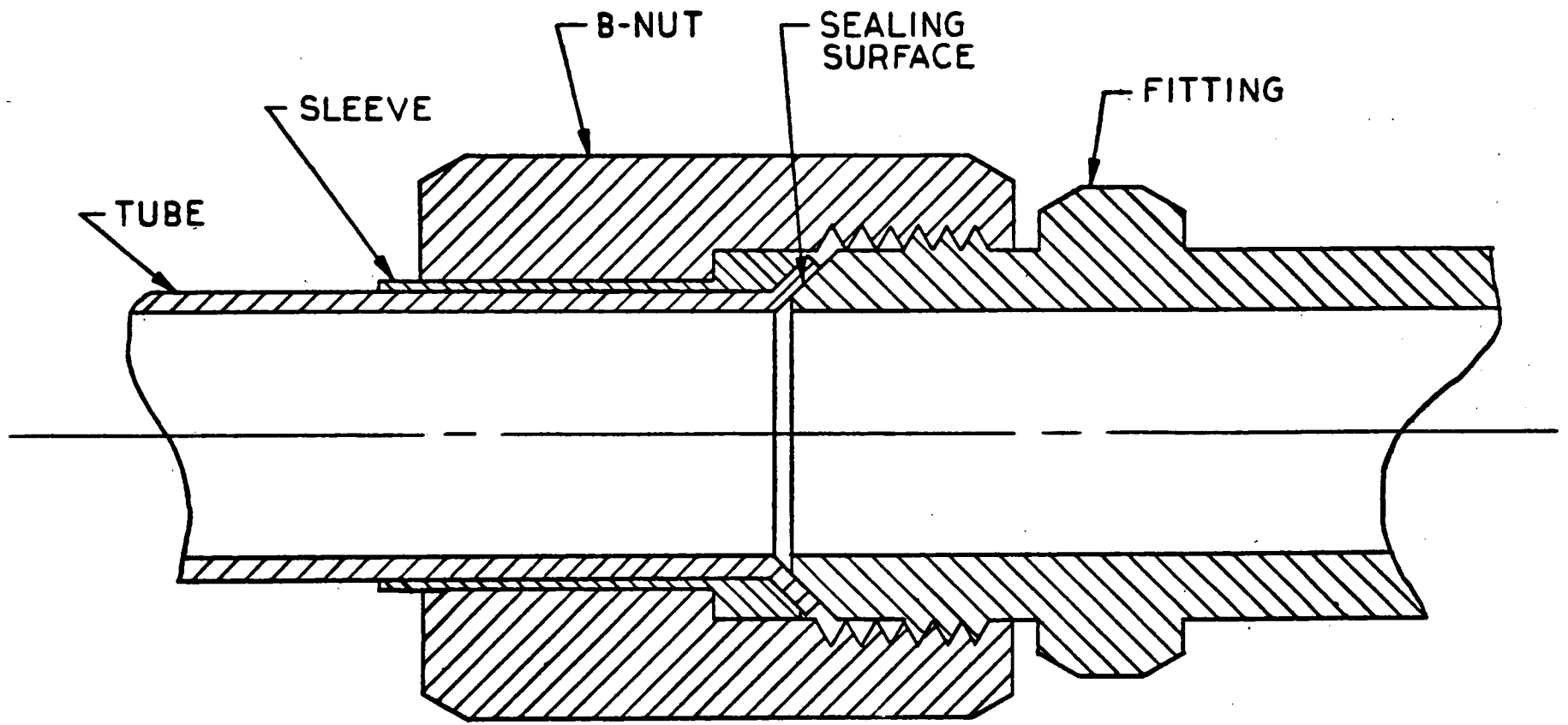

FIGURE 6.1 STANDARD FLARED "AN" CONNECTION

6.2 Test Procedure and Apparatus

Leakage tests were performed on "MC" flared fittings supplied by Huntsville using various levels of applied torque and internal pressure. The connector configurations tested are as follows:

Tube Size	Material	Flare Operation
1/2"	Aluminum	Special (A-1,A-2)
1/2"	Stainless Steel	Standard (S-3,S-4)
1/2"	Stainless Steel	Special (S-1, S-2)
3/4"	Aluminum	Standard (A-3,A-4)
3/4"	Aluminum	Special (A-1,A-2)
3/4"	Stainless Steel	Standard (S-3,S-4)
3/4"	Stainless Steel	Special (S-1, S-2)
1"	Aluminum	Standard (A-3, A-4)
1"	Aluminum	Special (A-1, A-2)
1"	Stainless Steel	Standard (S-3, S-4)
1"	Stainless Steel	Special (S-1, S-2)

The torques were applied using a calibrated torque wrench. The torque values are those specified in the "MC" specifications as minimum rated, maximum rated, 125 percent of maximum rated and 150 percent of maximum rated and are presented below for each connector.

		Aluminum		
Tube Size	Min.	Max.	125% Max.	150% Max.
1/2"	300	400	500	600
3/4"	650	800	1000	1200
1"	900	1100	1375	1650
		Stainless Steel		
1/2"	400	450	562	675
3/4"	900	1000	1250	1500
1"	1200	1400	1750	2100

Each connector was assembled and torqued to the specified values and then enclosed in a vacuum tight cylinder to permit mass spectrometer leakage measurements. This test apparatus is shown in Figure 6.2.

The internal pressure using helium gas can be regulated for readings at 300, 600, 1,000 and 1,500 psi. The resultant leakage from the connector will be sensed and measured by the calibrated mass spectrometer.

A vital part of this investigation is the observation of the effect of sealing surface finish on the leakage. This observation took three forms:

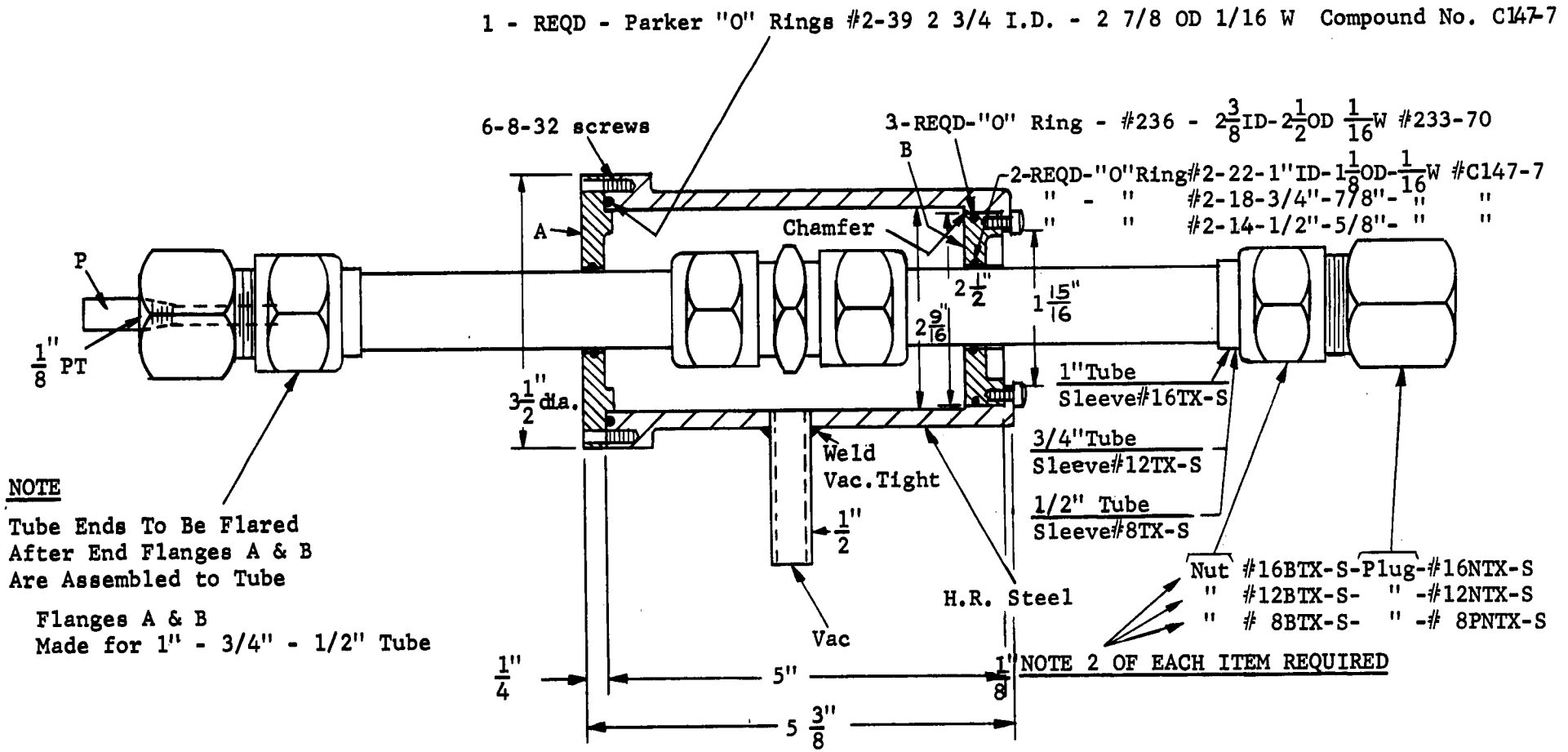

FIGURE 6.2 TEST APPARATUS

1. Visual observation to determine gross marks and deformations
2. Photomicrographs to determine the microscopic characteristics of the surface.
3. Interference microscope and profilometer examination to obtain a measure of surface roughness.

All mating surfaces were examined by microscope before test. Interference photographs of the original flared surface could not be obtained directly due to tube curvature interferences. Therefore a replication technique (Section 6.6) was used and photomicrographs taken from the replicate.

Various special tests were run to investigate the effects of repeatibility of seal, torque relaxation, crush washers as gaskets, plating of the union sealing surface, and antifriction bearing surfaces for the nuts. The repeatibility of the seal was examined by connect-disconnect operations on several connector configurations until some trend in leakage was noted. The torque relaxation was checked after each test by noting the torque necessary to tighten the nut further, which is essentially a repeat of the torque procedure before test. Voi-Shan crush washers of copper and aluminum were used in most configurations to evaluate the effect on leakage of these soft gaskets. Initial tests of the washers indicated that interference of the shoulders on the union might have adverse effects on sealing surface mating. On succeeding tests Voi-Shan washers were used both with the shoulders intact and with them cut off. After several connections of a fitting, deterioration of the nut shoulder surface was observed, causing binding of the nut during the torquing operation. On succeeding tests antifriction washers (English "DU"; teflon coated washers) were used on the nut shoulders.

A special test of a 1/2" Swagelok connector (Figure 6.3) was run under the same torque and pressure conditions as the 1/2" "MC" flared connector as a comparison. One Swagelok connector was made entirely of stainless steel and another was stainless steel with a brass sleeve. Since the sealing occurs on the sleeve, the brass sleeve acts as a built-in gasket.

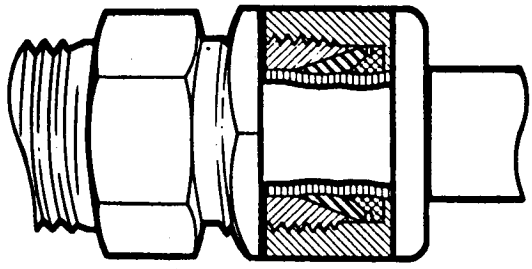

FIGURE 6.3 SWAGELOK CONNECTOR

6.3 Observations

The tests of the "MC" flared connectors involved only eleven samples - each of a different configuration. A number of variables affecting connector leakage performance were not controlled or monitored during these tests. Therefore correlation of the leakage with surface finish, sealing pressure, and internal pressure is not possible for each test; however, the tests are important to indicate general trends and problem areas. The observations and conclusions which follow are limited by the relatively small sampling.

Table 6.1 illustrates all those variables which were controlled and inspected in the tests. The variables controlled include the connector configuration, applied torque, and internal pressure. Items inspected include the sealing surface finish of the union and flares before and after test. The flare and union sealing surface concentricity and the friction of the nut shoulder and thread were not determined. These two factors are very important in determining the magnitude and distribution of the sealing pressure. It is believed that the large variations in measured leakage as shown in Table 6.2 are due to variations in the magnitude and distribtuion of the sealing pressure.

A calculation of the sealing pressure as a function of the applied torque has been carried out with an assumed uniform distribution over a nominal sealing area and with an assumed coefficient of friction on the nut shoulder and thread. The maximum sealing pressures are listed below for each size connector (using the maximum torque and a minimum friction coefficient of 0.10). The sealing pressures were calculated on the basis of elastic deformation and may not actually be achieved due to yielding of the flare in the hoop direction.

TABLE 6.4

Comparison of Aluminum and Stainless Steel MC Flared Fittings

		Aluminum	Stainless Steel
Yield strength of tubes, psi.		35,000	75,000
Yield strength of unions and nuts, psi.		56,000	70,000
Yield strength of sleeves, psi.		66,000	150,000
Sealing pressure, psi, when fitting is torqued to 150% of maximum			
3/4" dia. tube	(Friction coef. = .10)	32,000	39,900
	(Friction coef. = .13)	24,600	30,800
1" dia. tube	(Friction coef. = .10)	27,000	34,400
	(Friction coef. = .13)	21,100	26,800
Yield strength of aluminum crush washer, psi.		6,000	6,000
Yield strength of copper crush washer, psi.		10,000	10,000

NOTES:

All yield strength data are for 0.2% offset.

Yield strengths of fitting parts are minimum values given in military specifications. Aluminum unions and nuts are assumed to be made from forged aluminum 7075T73, and aluminum sleeves are assumed to be made from cold-finished aluminum QQA-282, heat treatment T6; however, Procurement Specification MSFC-SPEC-143 is not clear on this.

Yield strengths of crush washers are maximum values furnished by Voi-Shan Mfg. Co.

The sealing pressure is below the yield stress of the fitting materials even for optimum sealing conditions so that large leaks may be expected. The gasket test results in Volume 3 of the final report for the First Contract Period (similar sealing area and internal pressure) indicate that leaks on the order of 10^{-4} to 10^{-2} cc/sec will be obtained when the sealing stress is slightly lower than the yield stress. These values are typical for the "MC" fittings tested.

In two cases, sealing as low as the mass-spectrometer sensitivity (10^{-8} cc/sec) was obtained. Inspection of these fittings after test showed the unions had grossly deformed so that their concave faces formed a new sealing-surface configuration as shown in the sketch below. Only stainless steel connectors showed this characteristic due to their high strength sleeves.

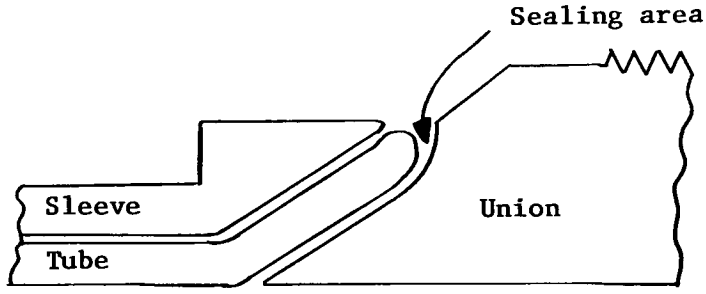

This new configuration has two advantages which make good sealing possible. Gross deformation of the union insures that the mating parts are concentric. The actual sealing area becomes a thin line so that high sealing stresses are obtained with the same axial load and torques. This type of seal was observed in tests of stainless steel fittings and was independent of flare process and tube size.

The Voi-Shan washer was developed to patch leaking flared connectors. Since the sealing pressure is below the yield stress of the fitting materials, the use of a gasket with a low yield stress should provide some improvement. The tests show that some improvement is obtained but not enough for adequate sealing. This is expected because the sealing pressure is still not several times the yield stress of the soft gasket and it is not uniform around the fitting. Inspection of the Voi-Shan washers after tests with a poor seal show that the contact pressure was not uniform. This is indicated in the comparison chart in Table 6.1. Plated union sealing surfaces using both gold and copper metals of various thicknesses from 1 mil to 10 mils produced similar results to the Voi-Shan washers. The reason again was non-uniform contact around the union. Comparing the use of the Voi-Shan washer with regard to aluminum and stainless steel fittings, the insertion of crush washers improved the leaktightness of the stainless steel fittings but did not materially improve the leaktightness of the aluminum fittings. When torqued to 150% of the maximum specified torque and pressurized with helium at 1500 psi, the stainless steel fittings with crush

washers sealed to the 10^{-8} atm cc/sec level, while aluminum fittings with crush washers had leakage values ranging from 4×10^{-5} to 2×10^{-3} atm cc/sec. In this limited series of tests, there was no significant difference in leakage between the aluminum crush washers, with a maximum compressive yield strength of 6,000 psi, and copper crush washers, with a maximum compressive yield strength of 10,000 psi.

In an effort to explain the difference in performance between the stainless steel fittings and the aluminum fittings with crush washers, the comparative yield stress data in Table 6.4 have been compiled. The indicated sealing pressures, computed on the basis of elastic deformations, are probably not actually achieved, in view of the possible deformation of the unions in hoop compression and the possible deformations of other parts in hoop tension.

The most significant difference between the stainless steel and aluminum fittings appears to be the much higher strength of the stainless steel sleeves. This suggests that the leaktightness of the aluminum fittings with crush washers might be significantly improved by using higher-strength sleeves.

Since the sealing pressure is below the yield stress of the fitting materials, the sealing surface finish is an important leakage parameter. The high-quality, very smooth "MC" surface finish is an aid in reducing leakage. In general, the crest-to-valley roughness before tests is 30 micro-inches for steel and 40 micro-inches for aluminum. These are not acceptable surface finishes with respect to the "MC" specifications. The flatness of the union sealing surface cone in the axial direction was evaluated using a Talysurf profilometer. Most unions were slightly concave and therefore did not meet the "MC" specifications. However, this is not considered critical since the unions became much more concave after torquing.

The special flare process showed pronounced circumferential directional properties in the microstructure. However, the roughness is about the same as for the standard process, and no significant differences in leakage levels of the two processes was observed.

The surface finish was inspected after test both visually and through photomicrographs to determine what deterioration had occurred. Connect-disconnect tests performed on several connectors showed that the steel fittings did not deteriorate, whereas the aluminum fittings exhibited gross scratches and roughness. The leakage level for the stainless steel connectors did not increase after several connections, but the aluminum connector leakage increased to a level too great for mass-spectrometer measurements ($> 10^{-1}$ cc/sec). This is expected from the sealing-surface finish observations.

The leakage level increased linearly with internal pressure, indicating that the mode of leakage is molecular flow rather than laminar flow. (See Section 22 of the final report for the first contract period.)

The leakage decrease with an increase in torque was usually less than linear. This is probably due to higher friction in the nut at high torques and due to deformations of the union which increase the sealing contact area. When sealing did occur with higher torques, it was caused by deformations of the union which reduced the contact area.

Torque relaxation was checked by repeating the assembly torquing operation after each test and also after long periods of time. Through all the tests, only very few isolated cases exhibited torque relaxation, and in these cases it was slight.

A problem was noted on the connect-disconnect tests when burrs appeared on the shoulder of the nut. This gave the nut undesirable friction characteristics and made the torquing operation erratic. The problem was avoided in further tests by the use of antifriction (English DU) washers on the shoulder of the nut.

The special test of the stainless steel Swagelok connector showed sealing to the limit of the mass spectrometer sensitivity (10^{-8} cc/sec) at the maximum rated torque of a similar "MC" flared connector. When a brass sleeve was used on this Swagelok connector, sealing occurred at the minimum rated torque and also upon reassembly at 25 percent below this value. The sealing ability of the Swagelok connector illustrates several points discussed previously. Gross deformations of the sleeve assure that the mating parts are concentric. The sealing area is very small so that a high sealing pressure is obtained. In the case of the soft brass sleeve, the sealing pressure is many times the yield stress of the brass at very low torques.

6.4 Results

The results of this investigation are presented in three tables. Table 6.1 is a summary of several leakage data points from all tests in chart form. Table 6.2 is a condensed leakage data presentation for all tests. Table 6.3 shows all the data and observations from test #4.

TABLE 6.1 Summary of "MC" Flared Connector Leakage Data

Size Inches	Configuration	Test No.	First Connection Min Torque - Pressure 1500 psi	First Connection Max Torque - Pressure 1500 psi	Leakage After (Max Torque - Pressure 1500)	Leakage with Voi-Shan (copper, Aluminum) Washers	Visual Inspection Union Surface Finish After Test
1/2"	A-1,2	1	1.63×10^{-4}	1.48×10^{-7}	(8th) $> 10^{-1}$	—	Slightly concave in lower middle. Sealing not uniform and sealing width - .10"
1/2"	S-1,2	2	4.5×10^{-3}	5.1×10^{-4}	—	—	Very concave-one end more than other. Sealing not uniform. Sealing width .10"
1/2"	S-3,4	3	1.3×10^{-2}	1.75×10^{-3}	(6th) 2.8×10^{-4}	—	Very concave & smooth Sealing uniform. Sealing width .10 inch
3/4"	A-1,2	4	1.4×10^{-2}	1.70×10^{-3}	(4th) $> 10^{-1}$	Copper 7.1×10^{-4} Aluminum 7.0×10^{-4}	Slightly concave in lower. Sealing not uniform & scratches. Sealing width 1/8"
3/4"	A-3,4	8	7.2×10^{-3}	7.9×10^{-4}	—	Copper 1.6×10^{-4} Aluminum 1.7×10^{-4}	Concave in lower-convex in middle. Not uniform. Sealing width - 1/8 inch
3/4"	S-1,2	7	2.2×10^{-3}	5.5×10^{-5}	(5th) 2.3×10^{-4}	Copper 1.0×10^{-8} Aluminum 1.0×10^{-8}	Slightly concave. Sealing uniform & smooth. Sealing width .10" with thin edge.
3/4"	S-3,4	6	$> 10^{-1}$	3.6×10^{-3}	—	—	Very concave-one end more than other. Sealing uniform Sealing width 1/8" on thin ridge
1"	A-1,2	11	1.6×10^{-2}	2.5×10^{-3}	—	Copper 1.6×10^{-3} Aluminum 8.8×10^{-4}	Flat-not uniform around. Sealing thin line on one-.10 width on other.
1"	A-3,4	10	1.6×10^{-3}	5.6×10^{-4}	—	Copper 4.2×10^{-5} Aluminum 3.0×10^{-4}	Union surface-flat. Not uniform around. Sealing width .10 in.
1"	S-1,2	9	8.2×10^{-3}	3.1×10^{-3}	—	Copper 1.0×10^{-8}	Union surface flat. Uniform thin line contact middle.
1"	S-3,4	5	3.3×10^{-3}	1.0×10^{-8} (only low reading of set)	(6th) $> 10^{-1}$	Copper 1.0×10^{-8}	Slightly concave in middle, one more than other. Not uniform around. Sealing width .10"

* Material noted by: S - stainless steel
A - aluminum alloy

** Flaring processes noted by: 1-2 Special Process
3-4 Standard Process

Leakage values are in atm cc/sec

TABLE 6.2 Leakage Results for Repeated Assemblies for MC Fittings

Test #1

Configuration: 1/2" O.D., aluminum; special flare (A-1,2)

Assembly	Torque (in.lb)	Pressure (psi)	Leakage Rate (cc/sec)
1	280	1500	1.63×10^{-4}
	400	1500	6.1×10^{-6}
	500	1500	3.3×10^{-7}
	600	1500	1.4×10^{-7}
2	600	1500	6.9×10^{-3}
3	600	1500	8.6×10^{-4}
4	600	1500	5.2×10^{-3}
5	600	1500	1.12×10^{-3}
6	600	1500	1.20×10^{-2}
7	600	1500	1.42×10^{-2}
8	600	1500	1.0×10^{-1}
9	700	1500	1.3×10^{-2}
10	800	1500	1.8×10^{-3}

Test #2

Configuration: 1/2" O.D.; stainless steel; special flare (S-1,2)

Assembly	Torque (in.lb)	Pressure (psi)	Leakage Rate (cc/sec)
1	400	1500	4.5×10^{-3}
	450	1500	3.2×10^{-3}
	562	1500	1.1×10^{-3}
	675	1500	5.1×10^{-4}

Test #3

Configuration: 1/2" O.D.; stainless steel; standard flare (S-3,4)

Assembly	Torque (in.lb)	Pressure (psi)	Leakage Rate (cc/sec)
1	400	1500	1.3×10^{-2}
	450	1500	1.45×10^{-2}
	562	1500	5.3×10^{-3}
	675	1500	1.75×10^{-3}
2	675	1500	1.43×10^{-3}
3	675	1500	9.1×10^{-5}
4	675	1500	4.8×10^{-4}
5	675	1500	6.5×10^{-4}
6	675	1500	2.8×10^{-4}

TABLE 6.2 (continued)

Test #5

Configuration: 1" O.D., stainless steel; standard flare (S-3,4)

Assembly	Torque (inlb)	Pressure (psi)	Leakage Rate (cc/sec)
1	1200	1500	3.3×10^{-3}
	1400	1500	1.2×10^{-3}
	1750	1500	4.0×10^{-8}
2 (with Voi-Shan copper washer)	1400	1500	1.0×10^{-8}
3	1750	1500	1.7×10^{-4}
	2100	1500	1.3×10^{-2}
4	2100	1500	1.5×10^{-2}
5	2100	1500	1.4×10^{-2}
6	2100	1500	$> 10^{-1}$
7	2100	1500	$> 10^{-1}$
9 (with gold plated union, 1 mil thick)	1200	1500	5.3×10^{-3}
	1750	1500	3.1×10^{-3}
	2100	1500	8.1×10^{-4}
9 (with gold plated union, 1 mil thick)	1750	1500	2.8×10^{-3}
	2100	1500	1.3×10^{-4}
10 (with gold plated union, 1 mil thick)	2100	1500	1.4×10^{-2}
11 (with gold plated union, 1 mil thick)	2100	1500	5.9×10^{-4}
12 (with gold plated union, 1 mil thick)	2100	1500	1.1×10^{-2}
13 (with gold plated union, 1 mil thick)	2100	1500	2.3×10^{-4}
14 (gold plated union 1 mil thick)	2100	1500	1.4×10^{-3}
15 (gold plated union 1 mil thick)	2100	1500	4.8×10^{-4}
16 (with copper plated union, 10 mil thick)	1200	1500	$> 10^{-1}$
	1750	1500	1.4×10^{-2}
	2100	1500	1.3×10^{-2}
17 (with gold plated union, 2 mil thick)	1200		

TABLE 6.2 (continued)

Test #6

Configuration: 3/4" O.D.; stainless steel; standard flare (S-3,4)

Assembly	Torque (in lb)	Pressure (psi)	Leakage Rate (cc/sec)
1	900	1500	$> 10^{-1}$
	1000	1500	$> 10^{-1}$
	1250	1500	1.2×10^{-3}
	1500	1500	3.6×10^{-3}

Test #7

Configuration: 3/4" O.D.; stainless steel; special flare (S-1,2)

Assembly	Torque (in lb)	Pressure (psi)	Leakage Rate (cc/sec)
1	900	1500	2.2×10^{-3}
	1000	1500	2.6×10^{-3}
	1250	1500	8.1×10^{-4}
	1500	1500	5.5×10^{-5}
2	1500	1500	1.0×10^{-8}
3	1500	1500	1.8×10^{-4}
4	1500	1500	7.5×10^{-6}
5	1500	1500	2.3×10^{-4}
6 (with copper Voi-Shan washers without shoulders)	1500	1500	1.0×10^{-8}
7 (with copper Voi-Shan washers without shoulders)	1500	1500	1.0×10^{-8}
8 (with copper Voi-Shan washers)	1500	1500	5.0×10^{-8}
9 (with copper Voi-Shan washers)	1500	1500	1.0×10^{-8}

TABLE 6.2 (continued)

Test #8

Configuration: 3/4" O.D.; aluminum alloy; standard flare (A-3,4)

Assembly	Torque (in.lb)	Pressure (psi)	Leakage Rate (cc/sec)
1	650	1500	7.2×10^{-3}
	800	1500	2.9×10^{-3}
	1000	1500	1.3×10^{-3}
	1200	1500	7.9×10^{-4}
2 (with copper Voi-Shan washer)	1200	1500	1.6×10^{-4}
3 (with aluminum Voi-Shan washers)	1200	1500	1.7×10^{-4}
4 (175% max rated torque)	1400	1500	2.9×10^{-4}
5 (200% max rated torque)	1600	1500	6.6×10^{-4}
6 (225% max rated torque)	1800	1500	2.6×10^{-4}
7 (250% max rated torque)	2000	1500	2.3×10^{-4}

Test #9

Configuration: 1" O.D.; stainless steel; special flare (S-1,2)

Assembly	Torque (in.lb)	Pressure (psi)	Leakage Rate (cc/sec)
1	1200	1500	8.2×10^{-3}
	1400	1500	4.9×10^{-3}
	1750	1500	4.5×10^{-3}
	2100	1500	3.1×10^{-3}
2 (with copper Voi-Shan washers)	2100	1500	1.0×10^{-8}
3 (with copper Voi-Shan washers)	2100	1500	1.0×10^{-8}

Test #10

Configuration: 1" O.D. aluminum alloy; standard flare (A-3,4)

Assembly	Torque (in.lb)	Pressure (psi)	Leakage Rate (cc/sec)
1	900	1500	$> 10^{-1}$
	1100	1500	1.6×10^{-3}
	1375	1500	7.2×10^{-4}
	1650	1500	5.6×10^{-4}
2 (with copper Voi-Shan washers)	1650	1500	4.2×10^{-5}
3 (with copper Voi-Shan washers without shoulders)	1650	1500	4.8×10^{-4}
4 (with aluminum Voi-Shan washers without shoulders)	1650	1500	3.0×10^{-4}

TABLE 6.2 (continued)

Test #11

Configuration: 1" O.D. aluminum alloy; special flare (A-1,2)

Assembly	Torque (in lb)	Pressure (psi)	Leakage Rate (cc/sec)
1	900	1500	1.6×10^{-2}
	1100	1500	7.6×10^{-3}
	1375	1500	3.7×10^{-3}
	1650	1500	2.5×10^{-3}
2 (with copper Voi-Shan washers)	1650	1500	1.6×10^{-3}
3 (with copper Voi-Shan washers without shoulders)	1650	1500	3.0×10^{-3}
4 (with aluminum Voi-Shan washers without shoulders)	1650	1500	8.8×10^{-4}

TABLE 6.3 Leakage Results and Observations for a Typical Test (Test #4)

Configuration: 3/4" O.D.; aluminum; special flare (A-1,2)

Surface finish

Figures 6.4, 6.5, 6.6 and 6.7 show typical photomicrographs of the flared surface finish. Figures 6.4, 6.5 and 6.6 point out deep scratches and pits while Figure 6.7 shows a more typical area of the sealing surface finish.

Figures 6.8 and 6.9 are interference pictures showing the roughness of the surface. These figures show a typical surface roughness of 10-20 micro-inch with scratches which go much deeper (approximately 100 micro-inch).

Figures 6.10 and 6.11 show typical axial profiles of the union sealing surface using a Talysurf prolilometer. The union surface appears slightly convex by about 100 micro-inches on end A-1 and 100 micro-inches on end A-2. The typical peak-to-valley profile is approximately 40 microinches. (Therefore neither end of this union meets the "MC" Specification.)

First Connection

Torque (in.lb)	Pressure (psi)	Leakage Rate (cc/sec)
650	300	2×10^{-3}
	600	5.2×10^{-3}
	1000	9.6×10^{-3}
	1500	1.4×10^{-2}
800	300	1.1×10^{-3}
	600	2.5×10^{-3}
	1000	4.8×10^{-3}
	1500	7.8×10^{-3}
1000	300	5.6×10^{-4}
	600	1.4×10^{-3}
	1000	2.5×10^{-3}
	1500	4.1×10^{-3}
1200	300	2.6×10^{-4}
	600	5.5×10^{-4}
	1000	1.1×10^{-3}
	1500	1.7×10^{-3}

Torque Check 1200 in.lb.

Inspection Circumferential scratches and pits

FIGURE 6.4
Photomicrograph of Flare End A-1
Magnification 168X

FIGURE 6.5
Photomicrograph of Flare End A-1
Magnification 168X

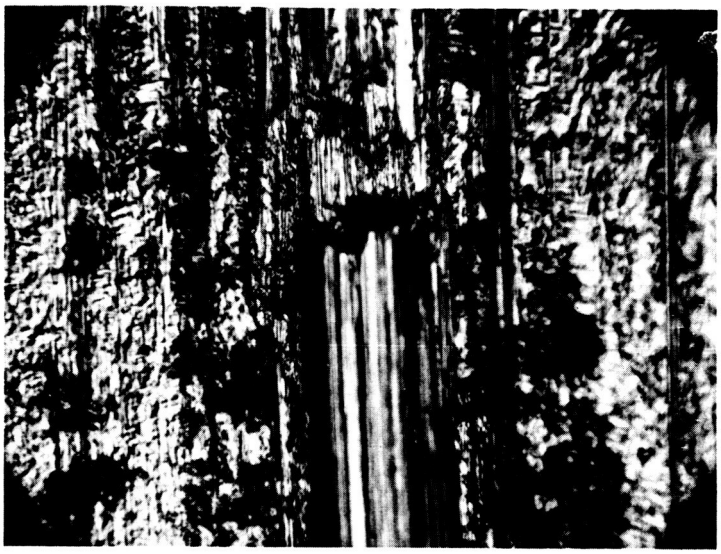

FIGURE 6.6
Photomicrograph of Flare End A-2
Magnification 168X

FIGURE 6.7
Photomicrograph of Flare End A-2
Magnification 168X

FIGURE 6.8
Interference Photomicrograph of Flare End A-1
Magnification 8 x 25
Interference lines 11.8 microinches

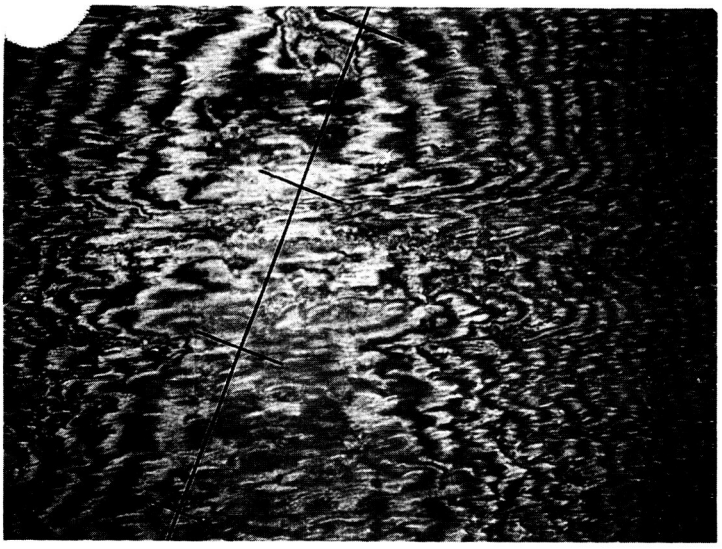

FIGURE 6.9
Interference Photomicrograph of Flare End A-2
Magnification 8 x 25
Interference lines 11.8 microinches apart

FOLDOUT FRAME 1.

FOLDOUT FRAME 2.

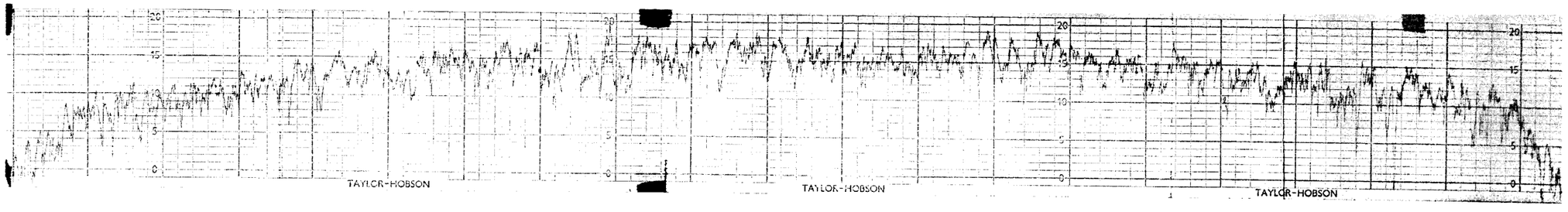

FIGURE 6.10
Typical axial profile of end A-1 union surface finish
Vertical Scale: 10 microinches between light lines
Horizontal Scale: .01 inch between heavy lines

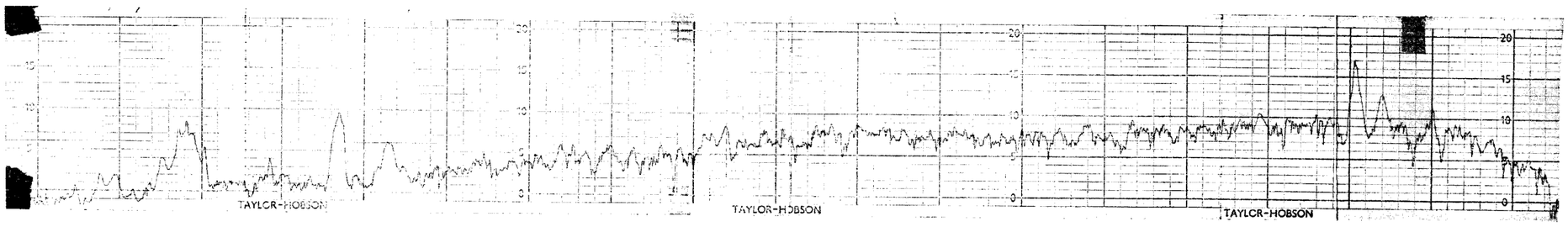

FIGURE 6.11
Typical axial profile of end A-2 union surface finish
Vertical Scale: 20 microinches between light lines
Horizontal Scale: .01 inch between heavy lines

Second Connection Torque 1200 in. lb.

Pressure	Leakage Rate cc/sec
300	1.7×10^{-3}
600	4.2×10^{-3}
1000	7.9×10^{-3}
1500	1.2×10^{-2}

Torque Check 1200 in. lb.

Inspection Circumferential scratches and pits

Third Connection Torque 1200 in. lb.

Pressure	Leakage Rate cc/sec
300	1.9×10^{-3}
600	4.3×10^{-3}
1000	8×10^{-3}
1500	1.2×10^{-2}

Torque Check 1200 in. lb.

Inspection Circumferential scratches and pits

Fourth Connection Torque 1200 in. lb.

Pressure	Leakage Rate cc/sec
300	5.7×10^{-3}
600	1.2×10^{-2}
1000	1.3×10^{-2}
1500	7.9×10^{-3}

Sensitivity of Leak Detector falls off

Torque Check 1200 in. lb.

Inspection Surface rough with circumferential scratches

Fifth Connection Copper Washer Installed (Voi-Shan) Torque 1200

Pressure	Leakage Rate (cc/sec)
300	1.1×10^{-4}
600	2.4×10^{-4}
1000	4.4×10^{-4}
1500	7.1×10^{-4}

Torque Check 1200 in. lb.

TABLE 6.3 (continued)

Sixth Connection — Aluminum Washer Installed (Voi-Shan) Torque 1200

Pressure	Leakage Rate (cc/sec)
300	1.1×10^{-4}
600	2.4×10^{-4}
1000	4.4×10^{-4}
1500	7×10^{-4}

Torque 1200 in. lb.

Inspection Surface rough with circumferential scratches

Examination of the sealing surface finish of the flares and union after test showed visible circumferential scratches. These scratches appeared even though the tube ends were held from rotating during the torquing operation. The flare surface finishes were also observed with the microscope and the scratches are again evident in Figures 6.12 and 6.13. The roughness of the union surface finish was evaluated using a profilometer as shown in Figure 6.14. The surface is grossly deformed and much rougher than before test.

FIGURE 6.12
Typical Photomicrograph of Flare End A-2 after test
Magnification 8 x 25

FIGURE 6.13
Typical Interference Photomicrograph of Flare End A-2 after test
Magnification 8 x 25
Interference Lines 11.8 microinches apart

FOLDOUT FRAME 1.

FOLDOUT FRAME 2.

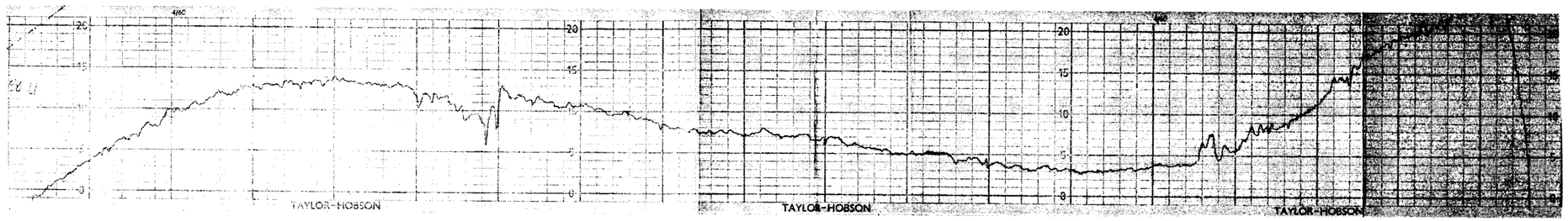

FIGURE 6.14
Typical axial profile of union surface end A-1 after test
Vertical Scale: 50 microinches between light lines
Horizontal Scale: .01 inch between heavy lines

6.5 Appendix. Replication Technique

A surface replication method supplied by the Zeiss microscope company was used to observe the flare surface finish. This was necessary due to the concave curvature of the flare which prohibited proper positioning of the microscope lenses.

The replication medium was a dark lacquer which was poured onto the flare surface finish. When the lacquer dried a back-up medium was poured on and allowed to dry. Both the replicating lacquer and the back-up medium can be pulled off together and observed under the microscope. Figures 6.15 and 6.16 show photomicrographs of a test sample and its replicate respectively. Figure 6.17 is an interference photomicrograph of the same surface area on the replicate showing replicated marks about 10 micro-inch deep.

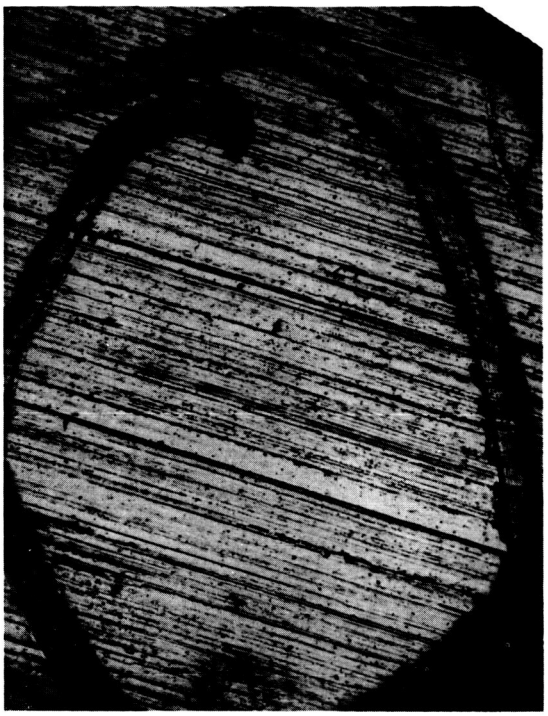

FIGURE 6.15

Test Surface
Magnification 200

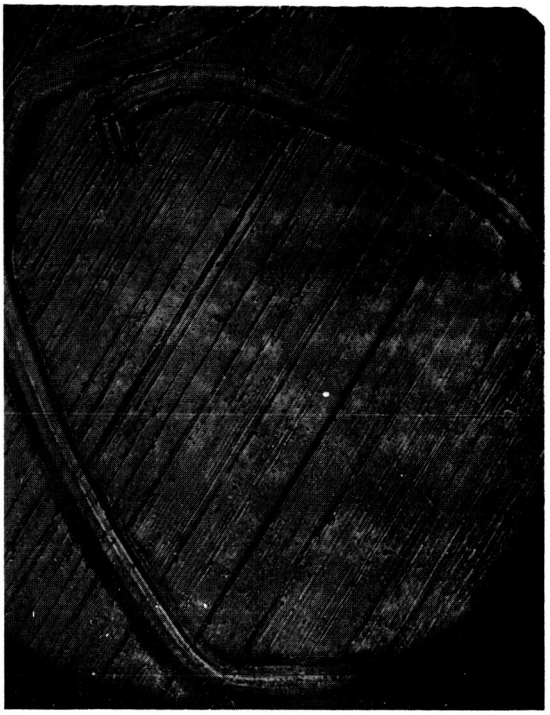

FIGURE 6.16

Replicate of Test Surface
Magnification 200

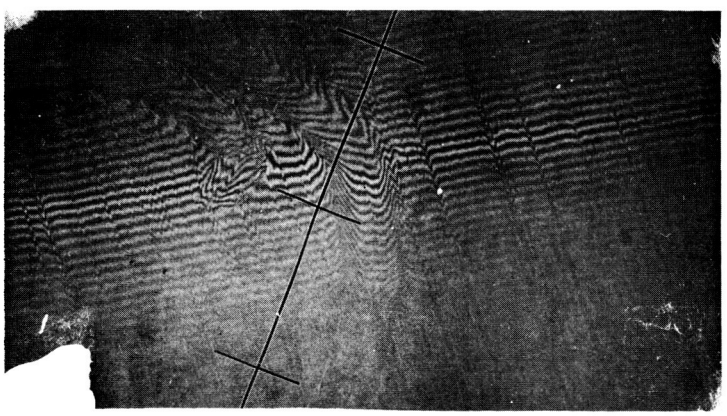

FIGURE 6.17

Replicate of test surface

Interference photomicrograph
Interference lines 11.8 microinches apart

DISTRIBUTION LIST FOR FINAL REPORT

Contract NAS8-4012

	Copies
NASA Marshall Space Flight Center Huntsville, Alabama 35812	
Office of Technical Information, M-MS-IPC	1
Purchasing Officer, Code PR-CH	1
Patent Office, M-PAT	1
Mr. Charles Wood, Technical Manager, R-P&VE	25
NASA Headquarters, Washington, D.C. 20546	
Mr. Henry Burlage, Jr., Chief, Liquid Propulsion Systems, RPL	4
Mr. Vernon E. Jaramillo, Advanced Manned Mission, MTC	1
Scientific and Technical Information Facility NASA Representative, Code CRT P. O. Box 5700 Bethesda, Maryland 20014	25
Harold Hornby Mission Analysis Division Ames Research Center Moffett Field, California 94035	2
Merland L. Moseson, Code 623 Goddard Space Flight Center Creenbelt, Maryland 20771	2
Robert F. Rose Propulsion Div., 38 Jet Propulsion Laboratory California Institute of Technology 4800 Oak Grove Drive Pasadena, California 91103	2
Floyd L. Thompson, Director Langley Research Center Langley Station Hampton, Virginia 23365	2
Dr. Abe Silverstein, Director Lewis Research Center 21000 Brookpark Road Cleveland, Ohio 44135	2
Hermann K. Weidner, Code R-P&VED Marshall Space Flight Center Huntsville, Alabama 35812	2

	Copies
Robert R. Gilruth, Director Manned Spacecraft Center Houston, Texas 77001	2
Robert W. Kamm, Director Western Operations Office 150 Pico Boulevard Santa Monica, California 90406	2
D. E. Mock Advanced Research Projects Agency Washington 25, D.C.	1
D. L. Schmidt, Code ASRCNC-2 Aeronautical Systems Division Air Force Systems Command Wright-Patterson Air Force Base Dayton, Ohio 45433	1
Maj. R. E. Bracken, Code MDGRT Air Force Missile Development Center Holloman Air Force Base, New Mexico	1
L. J. Ullian Air Force Missile Test Center Patrick Air Force Base, Florida	1
Col. Clark Technical Data Center Air Force Systems Command, Dyna-Soar Air Force Unit Post Office Los Angeles 45, California	1
Dr. H. K. Doetsch Arnold Engineering Development Center Arnold Air Force Station Tullahoma, Tennessee	1
J. Kay, Code RTMS-41 Bureau of Naval Weapons Department of the Navy Washington 25, D. C.	1
Defense Documentation Center Headquarters Cameron Station, Building 5 5010 Duke Street Alexandria, Virginia 22314 Attn: TISIA	1
Col. C. K. Stambaugh, Code AFRST Headquarters, U. S. Air Force Washington 25, D. C.	1

	Copies
I. Forsten, Chief, Liquid Propulsion Laboratory Picatinny Arsenal Dover, New Jersey 07801	1
Colonel Silk Rocket Research Laboratories Edwards Air Force Base Edwards, California 93523	1
U. S. Atomic Energy Commission Technical Information Services Box 62 Oak Ridge, Tennessee	1
Dr. Walter Wharton U. S. Army Missile Command Redstone Arsenal, Alabama 35809	1
Code 451 Chief, Missile Propulsion Division U. S. Naval Ordnance Test Station China Lake, California 93557	1
Neil Safeer Chemical Propulsion Information Agency Johns Hopkins University Applied Physics Laboratory 8621 Georgia Avenue Silver Spring, Maryland	1
L. F. Kohrs Aerojet-General Corporation P. O. Box 296 Azusa, California	1
R. Stiff Aerojet-General Corporation P. O. Box 1947 Technical Library, Bldg 2015, Dept 2410 Sacramento 9, California 95809	1
D. A. Carrison Aeronutronic A Division of Ford Motor Company Ford Road Newport Beach, California	1

	Copies
John G. Wilder MS-2293 Propulsion Dept. Aerospace Corporation 2400 East El Segundo Boulevard P. O. Box 95085 Los Angeles, California 90045	1
A. C. Tobey Arthur D. Little, Inc. Acorn Park Cambridge 40, Massachusetts	1
Dr. George Moc, Director, Research Astropower, Inc., Subsidiary of Douglas Aircraft Company 2968 Randolph Avenue Costa Mesa, California	1
A. Mendenhall Astrosystems, Inc. 1275 Bloomfield Avenue Caldwell Township, New Jersey	1
A. Scurlock Atlantic Research Corporation Edsall Road and Shirley Highway Alexandria, Virginia	1
J. H. Rodgers Beech Aircraft Corporation Boulder Facility Box 631 Boulder, Colorado	1
W. M. Smith Bell Aerosystems Company P. O. Box 1 Buffalo 5, New York	1
John M. Brueger Bendix Systems Division Bendix Corporation Ann Arbor, Michigan	1
J. D. Alexander Boeing Company P. O. Box 3707 Seattle 24, Washington	1
John Gates Chrysler Corporation Missile Division Warren, Michigan	1

	Copies
G. Kelley Curtiss-Wright Corporation Wright Aeronautical Division Wood-ridge, New Jersey	1
R. W. Hallet, Chief Engineer Advanced Space Tech. Douglas Aircraft Company, Inc. Missile and Space Systems Division 3000 Ocean Park Boulevard Santa Monica, California 90406	1
J. S. Kerr Fairchild Stratos Corporation Aircraft Missiles Division Hagerstown, Maryland	1
Frank Dore General/Dynamics/Astronautics Library & Information Services (128-00) P. O. Box 1128 San Diego, California 92112	1
F. E. Schultz General Electric Company Re-Entry Systems Department Box 8555 Philadelphia, Pennsylvania 19101	1
S. N. Suciu General Electric Company Flight Propulsion Lab Department Cincinnati 15, Ohio	1
Joseph Gavin Grumman Aircraft Engineering Corp. Bethpage, Long Island, New York	1
R.J. Hanville, Director of Research Engineering Kidde Aero-Space Division Walter Kidde and Company, Inc. 675 Main Street Belleville 9, New Jersey	1
G. D. Brewer Lockheed California Company 10445 Glen Oaks Boulevard Pacoima, California	1

	Copies
Y. C. Lee Power Systems R&D Lockheed Missiles and Space Company Attn: Technical Information Center P. O. Box 504 Sunnyvale, California	1
H. L. Thackwell Lockheed Propulsion Company P. O. Box 111 Redlands, California	1
Warren P. Boardman, Jr. The Marquardt Corporation 16555 Saticoy Street Box 2013 - South Annex Van Nuys, California 91409	1
John Calathes (3214) Martin Division Martin Marietta Corporation Baltimore 3, Maryland	1
J. D. Goodlette Mail A-241 Martin Denver Division Martin Marietta Corporation Denver, Colorado 80201	1
R. A. Herzmark McDonnell Aircraft Corporation P. O. Box 6101 Lambert Field, Missouri	1
H. Storms North American Aviation, Inc. Space & Information Systems Division Downey, California	1
W. E. Gasich Northrop Corporation 1001 East Broadway Hawthorne, California	1
R. J. Coar Pratt & Whitney Aircraft Corp. Florida Research and Development Center P. O. Box 2691 West Palm Beach, Florida 33402	1

	Copies
S. Fairweather Radio Corporation of America Astro-Electronics Division Defense Electronic Products Princeton, New Jersey	
Arthur Sherman Reaction Motors Division Thiokol Chemical Corporation Denville, New Jersey 07832	1
Dr. William O'Donnell Republic Aviation Corporation Farmingdale, Long Island, New York	1
E. B. Monteath Rocketdyne (Library Dept. 586-306) Division of North American Aviation 6633 Canoga Avenue Canoga Park, California 91304	1
C. E. Roth Space General Corporation 9200 Flair Avenue El Monte, California	1
G. W. Elverum Space Technology Laboratories Subsidiary of Thompson-Ramo-Wooldridge P. O. Box 95001 Los Angeles 45, California	1
Thor Smith Stanford Research Institute 333 Ravenswood Avenue Menlo Park, California 94025	1
P. T. Angell TAPCO Division Thompson-Ramo-Wooldridge, Inc. 23555 Euclid Avenue Cleveland 17, Ohio	1
John Coodloe Thiokol Chemical Corporation Redstone Division Huntsville, Alabama	1

m

Copies

Erle Martin
United Aircraft Corporation
Research Laboratories
400 Main Street
East Hartford 8, Connecticut 06108 — 1

B. Abelman
United Technology Center
587 Methilda Avenue
P. O. Box 358
Sunnyvale, California — 1

Warren C. Trent
Vought Astronautics
Box 5907
Dallas 22, Texas — 1